AD-A182 136 PERFORMANCE ANALYSIS OF FREQUENCY HOPPING MFSK (M-ARY FREQUENCY-SHIFT-KEY..(U) LEE (J S) ASSOCIATES INC ARLINGTON VA J S LEE ET AL. JUN 87 JC-2040-N 1/2

UNCLASSIFIED N00014-86-C-0279 F/G 9/1 NL

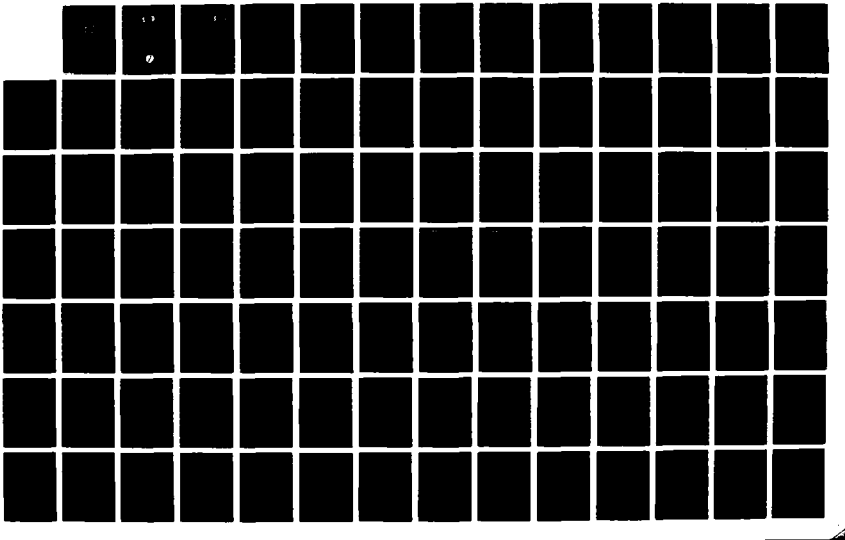

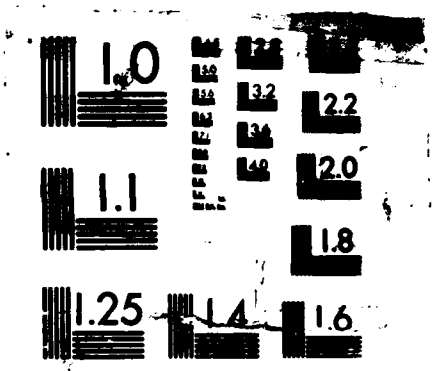

MICROCOPY RESOLUTION TEST CHART

PERFORMANCE ANALYSIS OF FREQUENCY HOPPING MFSK SYSTEMS EMPLOYING FORWARD ERROR CONTROL CODING IN THE PRESENCE OF HOSTILE INTERFERENCE

J.S. LEE ASSOCIATES INC.
2001 Jefferson Davis Hwy. Suite 601
Arlington, Virginia 22202

(12)

JC-2040-N

PERFORMANCE ANALYSIS OF FREQUENCY HOPPING MFSK SYSTEMS EMPLOYING FORWARD ERROR CONTROL CODING IN THE PRESENCE OF HOSTILE INTERFERENCE

FINAL REPORT
JUNE 1987

Prepared for

OFFICE OF NAVAL RESEARCH
800 N. QUINCY STREET
ARLINGTON, VIRGINIA 22217

CONTRACT NO.
N00014-86-C-0279
NR 411J007-01/2-21-86 (1111)

Prepared by

J. S. LEE ASSOCIATES, INC.
SUITE 601
2001 JEFFERSON DAVIS HIGHWAY
ARLINGTON, VIRGINIA 22202

REPORT DOCUMENTATION PAGE	READ INSTRUCTIONS BEFORE COMPLETING FORM
1. REPORT NUMBER	2. GOVT ACCESSION NO. AD-A182136	3. RECIPIENT'S CATALOG NUMBER
4. TITLE (and Subtitle) Performance Analysis of Frequency Hopping MFSK Systems Employing Forward Error Control Coding in the Presence of Hostile Interference	5. TYPE OF REPORT & PERIOD COVERED Final Report May 1986 - April 1987
	6. PERFORMING ORG. REPORT NUMBER JC-2040-N
7. AUTHOR(s) Jhong S. Lee, Robert H. French, Leonard E. Miller	8. CONTRACT OR GRANT NUMBER(s) N00014-86-C-0279
9. PERFORMING ORGANIZATION NAME AND ADDRESS J.S. Lee Associates, Inc. 2001 Jefferson Davis Hwy., Suite 601 Arlington, VA 22202	10. PROGRAM ELEMENT, PROJECT, TASK AREA & WORK UNIT NUMBERS NR 411J007-01/2-21-86 (1111)
11. CONTROLLING OFFICE NAME AND ADDRESS Office of Naval Rsearch 800 N. Quincy Street Arlington, VA 22217	12. REPORT DATE June 1987
	13. NUMBER OF PAGES xx + 170
14. MONITORING AGENCY NAME & ADDRESS(if different from Controlling Office)	15. SECURITY CLASS. (of this report) UNCLASSIFIED
	15a. DECLASSIFICATION/DOWNGRADING SCHEDULE

16. DISTRIBUTION STATEMENT (of this Report)

Approved for public release; distribution unlimited.

17. DISTRIBUTION STATEMENT (of the abstract entered in Block 20, if different from Report)

18. SUPPLEMENTARY NOTES

19. KEY WORDS (Continue on reverse side if necessary and identify by block number)

Frequency Hopping	Spread Spectrum Systems
M-ary Frequency Shift-Keying	Partial-Band Noise Jamming
Error Control Coding	Block Codes
Bit Error Probability	Convolutional Codes

20. ABSTRACT (Continue on reverse side if necessary and identify by block number)

Error probability analyses are performed for a coded M-ary frequency-shift-keying (MFSK) system employing L hops per M-ary word frequency-hopping (FH) spread spectrum waveforms transmitted over a partial-band Gaussian noise jamming channel. The information bit error probabilities are obtained for a square-law linear combining demodulator and for a square-law adaptive gain control (AGC) demodulator, both with forward error control (FEC) coding under conditions of worst-case partial-band noise jamming, using exact analyses of the demodulator performance

DD FORM 1 JAN 73 1473 EDITION OF 1 NOV 65 IS OBSOLETE

20. Abstract

which include both thermal noise and jamming noise. Parametric performance curves are obtained for both block codes and convolutional codes with both binary and M-ary channel modulations. The results show that thermal noise can not be neglected in the analyses if correct determinations of the optimum order of diversity and the worst-case jamming fraction are to be obtained over the whole range of signal-to-thermal noise and signal-to-jamming ratios. It is shown that the combination of non-linear combining, M-ary modulation, and forward error control coding is an effective strategy against worst-case partial-band noise jamming. However, just as was found to be the case for uncoded systems, the linear combiner is ineffective in worst-case partial-band noise jamming.

TABLE OF CONTENTS

LIST OF FIGURES

LIST OF FIGURES (Cont.)

LIST OF FIGURES (Cont.)

LIST OF FIGURES (Cont.)

LIST OF FIGURES (Cont.)

LIST OF FIGURES (Cont.)

LIST OF FIGURES (Cont.)

LIST OF FIGURES (Cont.)

LIST OF FIGURES (Cont.)

LIST OF FIGURES (Cont.)

LIST OF FIGURES (Cont.)

LIST OF FIGURES (Cont.)

LIST OF FIGURES (Cont.)

LIST OF FIGURES (Cont.)

LIST OF FIGURES (Concluded)

LIST OF TABLES

Performance Analysis of Frequency Hopping MFSK Systems Employing Forward Error Control Coding in the Presence of Hostile Interference

1.0 INTRODUCTION

One of the fundamental requirements placed on a modern military radio communications network is reliable transmission of information over channels that are subjected to hostile interference or jamming. Network radios designed to operate in such an electronic warfare environment must possess both low probability of intercept (LPI) and anti-jam qualities; this naturally leads to the choice of spread-spectrum waveforms plus error control coding for use by electronic counter-countermeasures (ECCM) network radio equipments.

As shown in Figure 1-1, the overall architecture of each link in an ECCM network encompasses the waveform design, the transmission channel, and the receiver structure. The system designer must take into account all of these aspects to design an effective ECCM link in the communications network. Briefly summarizing the link architecture, an ECCM network link encompasses an LPI waveform, the information modulation, forward error control (FEC) coding, jamming, thermal noise, the receiver type, and FEC decoding.

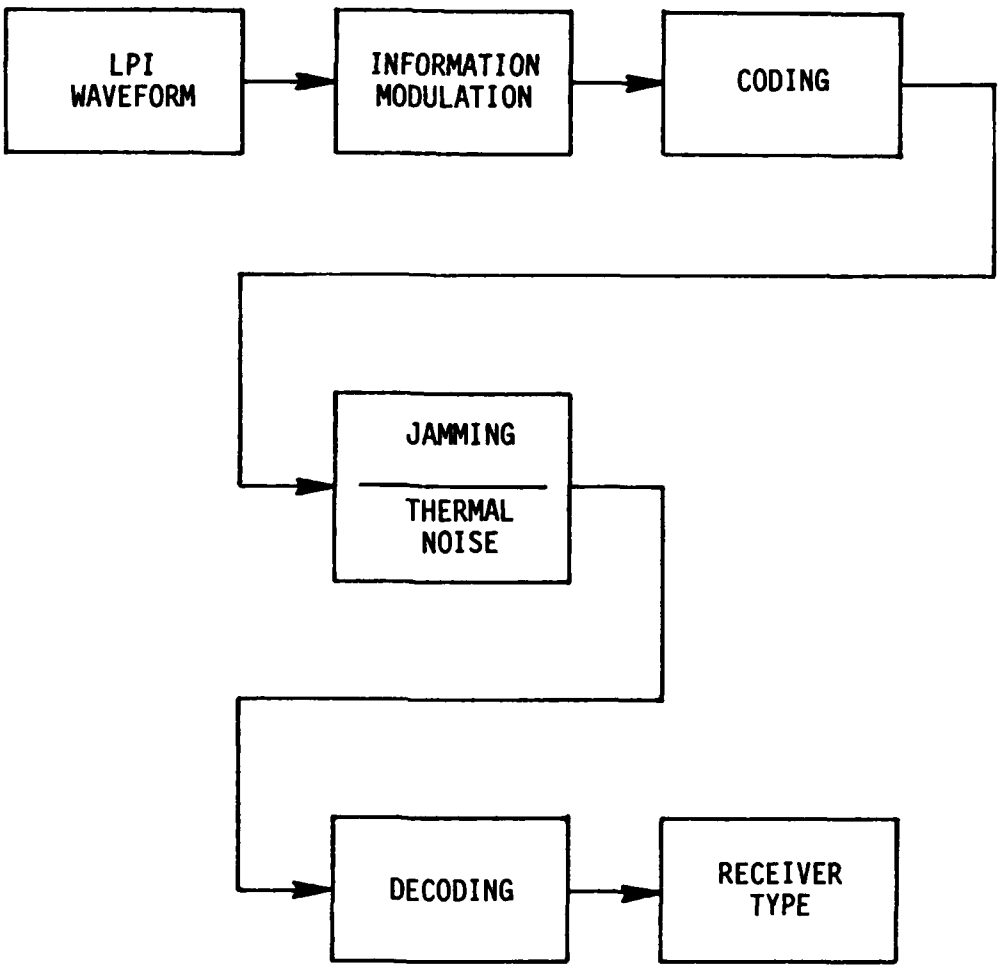

FIGURE 1-1 ARCHITECTURE OF AN ECCM LINK IN A COMMUNICATION NETWORK

A common choice of LPI waveform for an ECCM system is a frequency hopping (FH) waveform. The use of frequency hopping permits very large spread bandwidths for a high processing gain (for anti-jam) and a low energy density (for LPI). By dividing each information symbol into L hops, the energy per hop is further reduced, thereby enhancing the LPI qualities of the signal. Thus, the desirable waveform may be described as a multiple hops per symbol frequency-hopping waveform.

The modulation used in the ECCM network must be compatible with the FH waveform and L hops per symbol. These requirements are easily met through use of frequency-shift keying. It is well known that the use of higher-order signal alphabets (M-ary source coding) gives an improvement over binary FSK in the Gaussian noise channel. Therefore, it is natural to consider the use of MFSK in conjunction with the FH spread-spectrum waveform for ECCM networks in order to try to improve performance. This yields an FH/MFSK waveform. The validity of this choice of waveform is demonstrated by its use in the MILSTAR system operating at EHF.

The EW environment places a severe stress on each communications link of the network. Therefore, the designer must use every available technique to obtain the best link performance possible under a given level of jamming. Forward error control (FEC) coding will be used in the ECCM network to reduce the bit error rate experienced by the recipients of the traffic. The system designer has available many forms of FEC codes from which to choose, including both block codes (which operate on fixed-length blocks of input symbols to produce fixed-length blocks

of output symbols) and convolutional codes (which operate on a continuous input symbol stream to produce a continuous output symbol stream). Depending upon the choice of code, the system designer may also have a choice between several alternative decoding techniques at the receiving terminal of the link.

The jammer with a limited power resource will strive to inflict the worst possible degradation on the communicators using the available jamming power. Therefore, the communications system designer must assume that the jammer will be able to optimize his jamming strategy and the communications network will be operating in the presence of worst-case jamming. To account for this, the bit error probability analysis must maximize the result over the adjustable parameters of the jammer. For partial-band noise jamming, which is known to be effective against FH/MFSK [1]-[3], this amounts to optimizing the fraction of the band jammed.

The receiver unavoidably operates in the presence of thermal noise in addition to the jamming. Prior work by the authors [4]-[7] analyzed the performance of uncoded systems using both linear [4] and nonlinear [5]-[7] combining soft decision receivers in the presence of both thermal noise and worst-case partial-band noise jamming. This work showed clearly that the bit error probability analyses for FH/MFSK in the partial-band noise jamming channel must not neglect thermal noise if misleading results are to be avoided. Furthermore, it was shown therein

that the linear combining receiver does not exhibit any diversity improvement as L, the number of hops per bit, is increased beyond L=1. However, nonlinear combining receivers can realize a diversity gain, provided that the noncoherent combining loss is less dominant than the jamming power reduction realized by the nonlinear weighting.

The final element of the ECCM link architecture is the choice of the type of receiver used to process the MFSK/FH waveform. The designer's choices here are linear-law or square-law envelope detectors, plus the choice between linear combining or one of several nonlinear combining schemes for detecting the L hops/symbol waveform. Typical receiver structures are the conventional square-law linear combining receiver, the adaptive gain control receiver, and a self-normalizing receiver. The receiver issue will be addressed more fully in Chapter 2 of this report.

The intent of the present report is to furnish to the system designer an examination of a coded system in the partial-band noise jamming environment, including the important considerations of thermal noise effects and exact analysis of the demodulation performance. To this end, we extend our prior analyses [4]-[7] to the case of a coded M-ary system employing forward error control (FEC) coding (both block and convolutional codes are considered) and using a nonlinear combining receiver. Numerous previous works [2], [8]-[13] have addressed the problem of coded systems employing FH/MFSK modulations. However, the prior works have ignored thermal noise [2], [8]-[11] or have employed union-Chernoff bounds for the

channel symbol error probabilities [9]-[12]. In the case of [12] and [13], hop-by-hop hard decisions were assumed for the L hops per channel digit. The cases of slow hopping (L=1) with a hard-decision receiver including thermal noise and a soft-decision receiver with side information and no thermal noise are treated in [19].

2.0 SYSTEM DESCRIPTION

We assume that information from a binary source is presented to the transmitter and that the receiver must deliver a binary information stream to the user. However, neither FEC coding nor channel modulation need be restricted to a binary alphabet.

2.1 Generic Coded FH/MFSK System

Figure 2-1 shows the transmitter for the system under consideration. Information bits {x} from a binary source at rate R_b are mapped to Q-ary symbols {y} where $Q = 2^q$ at rate $R_q = R_b/q$ and applied to the coder's input. The FEC coder then operates over symbols from $GF(2^q)$. Note that if the coder is a binary coder, then q = 1 and the binary-to-Q-ary conversion is a straight-through connection. The FEC coder outputs n coded Q-ary symbols {ξ} (q-bit bytes) for every k Q-ary information symbols inputted to it; thus the code rate is r = k/n and the output coded symbols are generated at $R_c = nR_q/k = nR_b/kq$. The channel modulation is FH/MFSK with $M = 2^K$. The coded Q-ary symbols are converted to M-ary words {z} at rate $R_d = qR_c/K = nR_b/kK$ for input to the MFSK modulator. If M = Q, this conversion is a straight-through connection. The M-ary words are applied to an MFSK modulator which selects one of M baseband frequencies $f_1, f_2, \ldots, f_M$ based on the M-ary input at rate

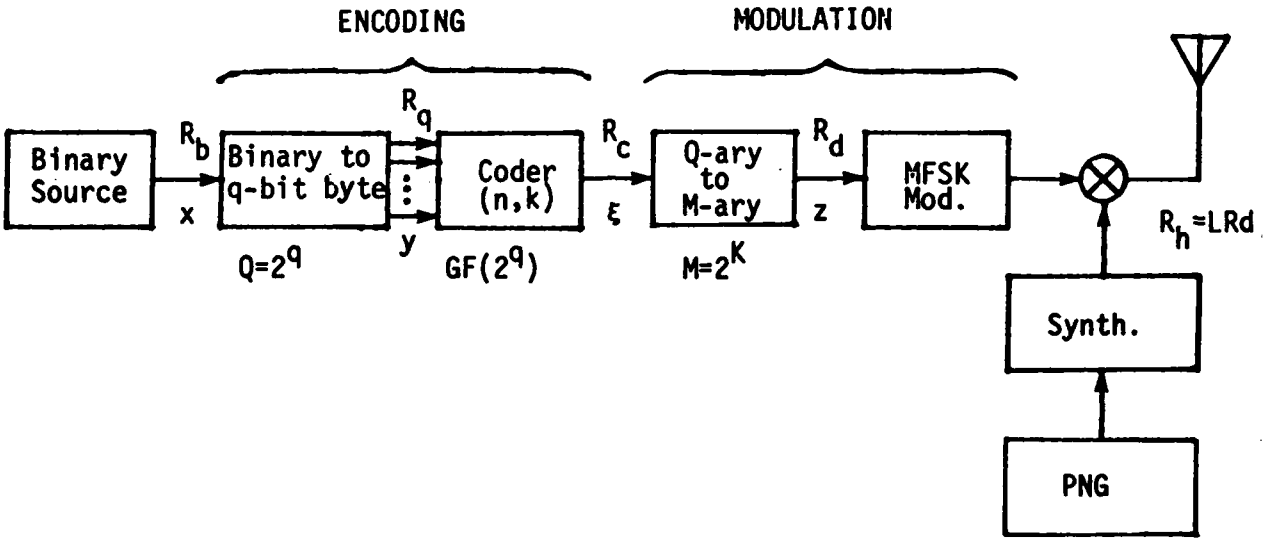

FIGURE 2-1 BLOCK DIAGRAM OF TRANSMITTER

$R_d = 1/T_d$. The M frequencies are spaced at intervals of B Hz where $B = R_h = L/T_d$, with L being the number of hops per M-ary word and R_h being the hopping rate. Thus the total bandwidth of the M-ary cluster is $MB = ML/T_d$ Hz. The selected baseband signal is broken into the L hops, each of duration T_d/L, by mixing with the output of a synthesizer which is controlled by a pseudo-random sequence generator. The synthesizer selects a new frequency f_H every T_d/L seconds, and thus $R_h = LR_d = nLR_b/kK$. The synthesizer can select from a set of N_h possible frequencies spaced B Hz apart; thus the total system bandwidth is $W = N_hB$ Hz. The output of the mixer is passed through a filter of width W Hz, translated to RF, amplified, and radiated from the transmit antenna.

A block diagram of the receiver is shown in Figure 2-2. The composite received waveform consisting of the sum of signal, thermal noise, and jamming is dehopped by mixing with the output of a frequency synthesizer controlled by a pseudorandom sequence generator operating in synchronism with the one in the transmitter. The dehopped signal r(t) is applied to an MFSK demodulator*, which decides which of M frequencies was transmitted and outputs the M-ary word decision $\hat{z}$. The M-ary words $\{\hat{z}\}$ are converted to Q-ary symbols $\{\hat{\xi}\}$ and applied to the decoder input (if M = Q, the conversion is a straight-through connection). The decoder performs error correction and outputs Q-ary information symbols $\{\hat{y}\}$, which are

*The system component which we call the demodulator in the context of a coded system corresponds to the receiver in the context of an uncoded system.

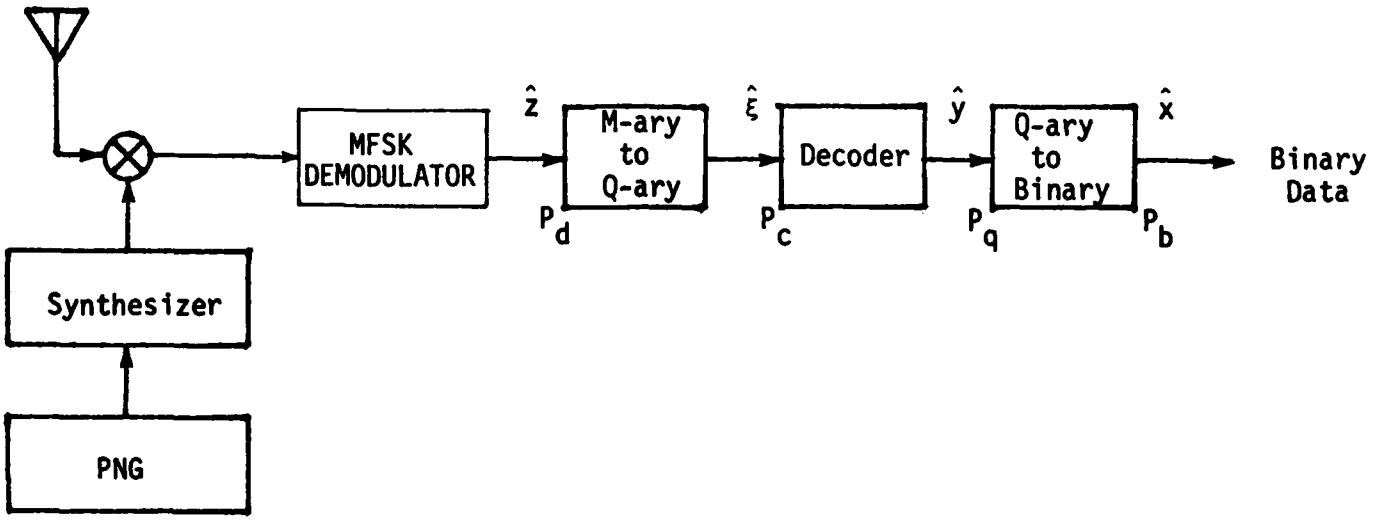

FIGURE 2-2 BLOCK DIAGRAM OF RECEIVER

converted to binary to reconstruct the received estimate $\{\hat{x}\}$ of the original binary data sequence.

The choice of the type of MFSK demodulator is a critical factor in determining the system performance. Figure 2-3 shows a generic demodulator structure for MFSK/FH with L hops/symbol. The structure shows a μ-law envelope detector. If we set μ=1, the demodulator is a linear-law demodulator, i.e. it forms the envelope of the filter output. If, on the other hand, we set μ=2, the demodulator then is a square-law demodulator which forms the squared envelope of the filter output. The weight function $f_k(\cdot)$ is specified in Table 2-1 for several different types of demodulators.

We have analyzed and computed the performance of the coded FH/MFSK system using two types of demodulators: the square-law linear combiner and the square-law adaptive gain control (AGC) demodulator.

2.2 Square-Law Linear Combining Demodulator

The square-law linear combining demodulator is presented as a baseline for comparison of other more complicated demodulator structures. Although the square-law linear combining demodulator is a reasonably close, practically implementable approximation to the optimum receiver for the Gaussian channel, we would expect that some other structure may provide better performance on a non-Gaussian channnel such as the partial-band jamming channel.

A block diagram of the square-law linear combining demodulator is shown in Figure 2-4. The dehopped signal (plus noise and jamming) is applied to a bank of M bandpass filters, each of width B, centered at the M possible signalling frequencies. The output of each filter is

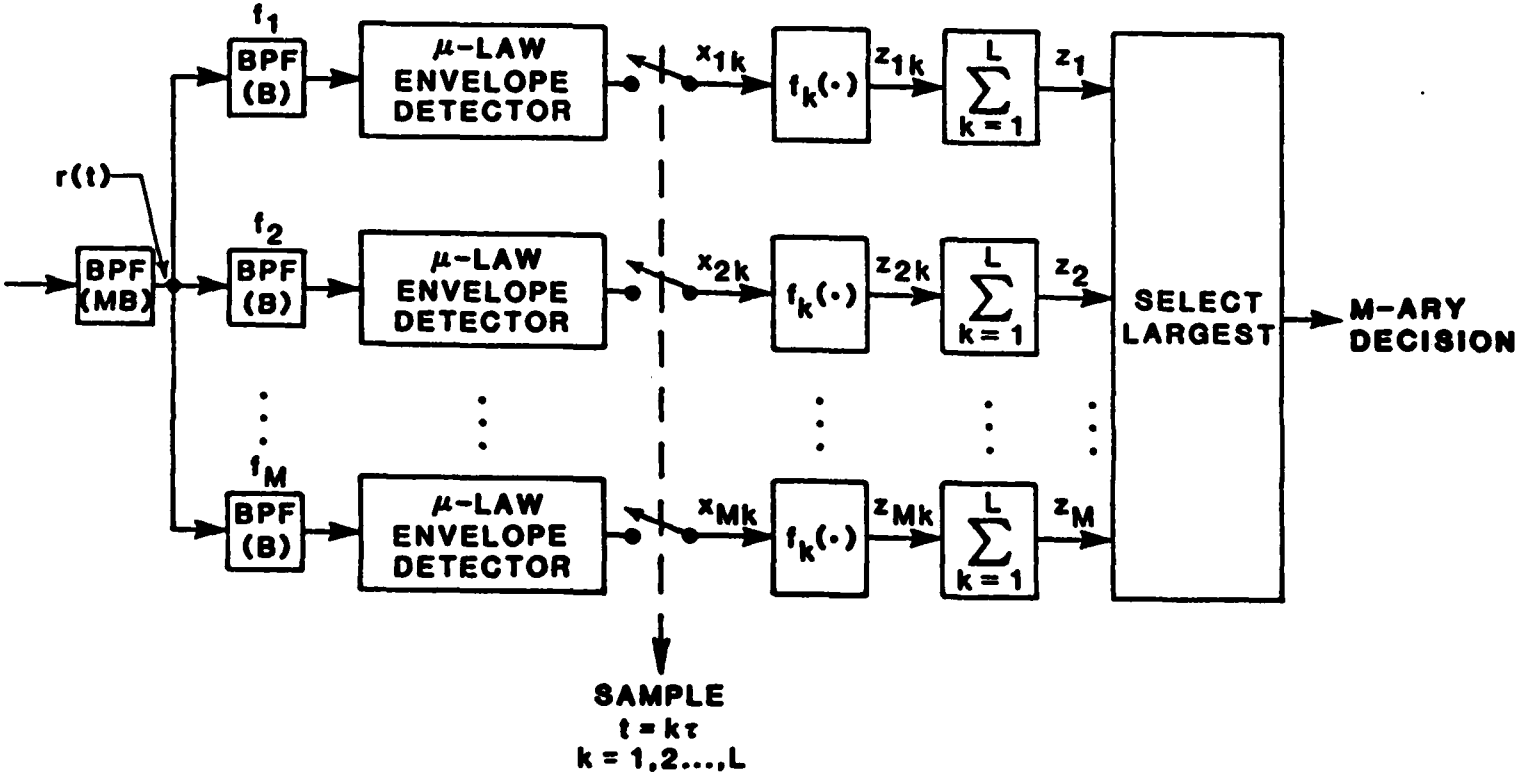

FIGURE 2-3 GENERIC FH/MFSK DEMODULATOR STRUCTURE

TABLE 2-1

DESCRIPTIONS OF FH/MFSK DEMODULATORS

RECEIVER TYPE	SPECIFICATION OF $z_{ik} = f_k(x_{ik})$, i=1,2,...,M	REMARKS
LINEAR COMBINING RECEIVER	$z_{ik} = x_{ik}$	Direct Connection (Linear Combining)
AGC RECEIVER	$z_{ik} = x_{ik}/\sigma_k^2$ $\sigma_k^2 = \begin{cases} \sigma_N^2, & \text{if not jammed} \\ \sigma_N^2 + \sigma_J^2, & \text{if jammed} \end{cases}$ (σ_k^2 = measured)	Adaptive Gain Control (Nonlinear Combining)
SELF-NORMALIZING RECEIVER	$z_{ik} = \dfrac{x_{ik}}{\sum_{i=1}^{M} x_{ik}}$	Practical Realization of AGC Using In-Band Measurements

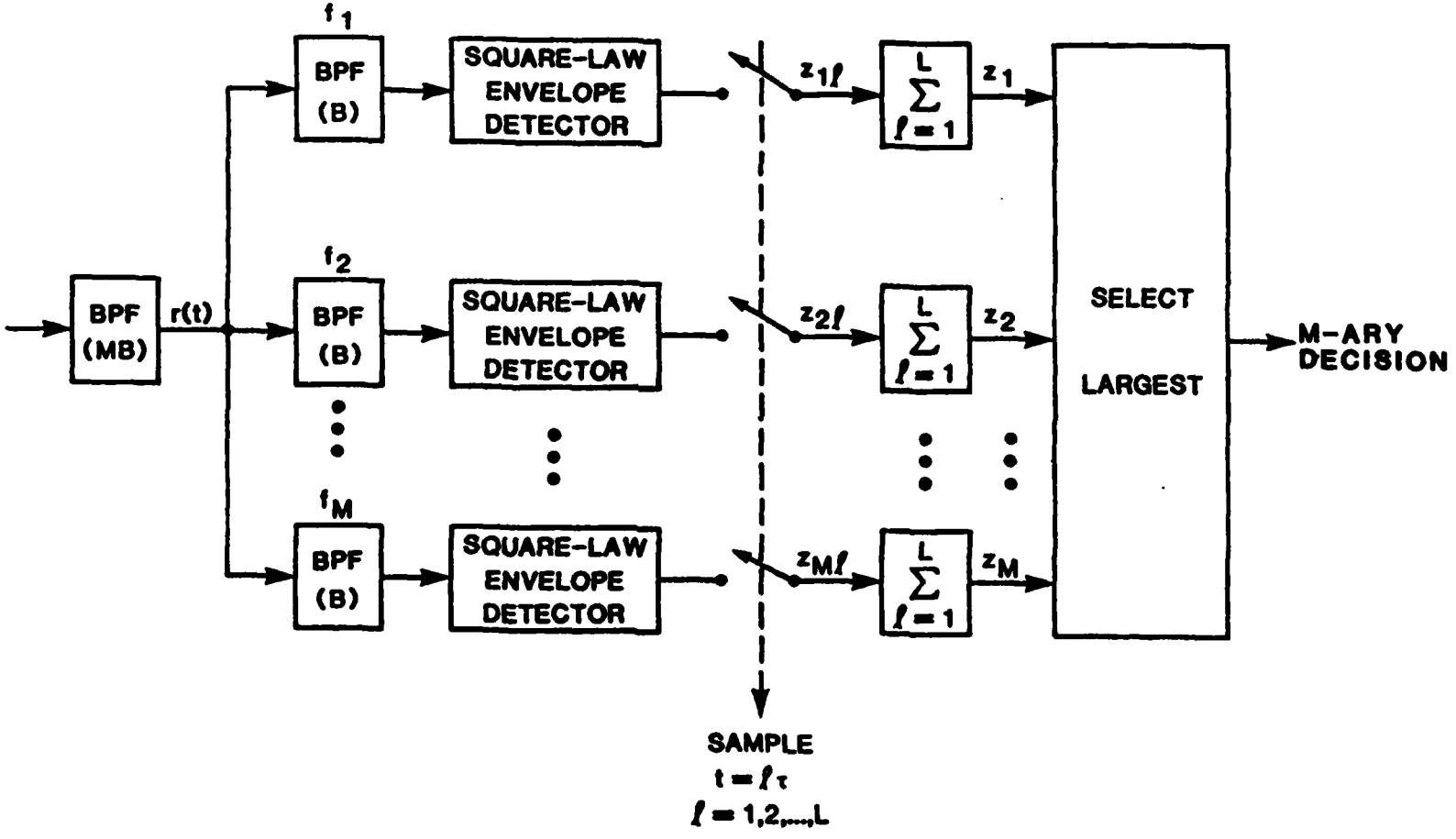

FIGURE 2-4 SQUARE-LAW LINEAR COMBININB DEMODULATOR

processed by a square-law envelope detector (i.e. a device whose output voltage is proportional to the square of the envelope of the input signal). Each squared envelope is sampled once every τ seconds. The L samples from the L hops in one M-ary word are summed for each channel of the receiver. At the end of L hops the sums are compared, the largest sum is selected, and the M-ary word decision $\hat{z}$ is made on the basis of which channel has this largest sum.

2.3 The Adaptive Gain Control Demodulator

A block diagram of the adaptive gain control (AGC) demodulator is shown in Figure 2-5. The dehopped signal is applied to a bank of M+1 filters. The first M of these filters are centered at the M signalling frequencies $f_1, f_2, \ldots, f_M$. The (M+1)-st filter provides a noise-only channel in which the noise power or noise plus jamming power σ_ℓ^2 is measured. Alternatively, a look-ahead scheme could be used for the noise power measurement, assuming the jammer itself is not hopping. The design is idealized in that it is predicated on the assumptions that the noise power or noise plus jamming power σ_ℓ^2 on the ℓth hop is measured perfectly and that σ_ℓ^2 is the same for all dehopped channels [5]. The noise measurement σ_ℓ^2 is used to form the weights $1/\sigma_\ell^2$ which are applied, hop by hop, to each of the square-law envelope detector outputs. The effect of the normalization is to prevent jammed hops from dominating in the decision process which involves choosing the largest of the sums over L hops of the normalized detector outputs. The identity of the channel having the

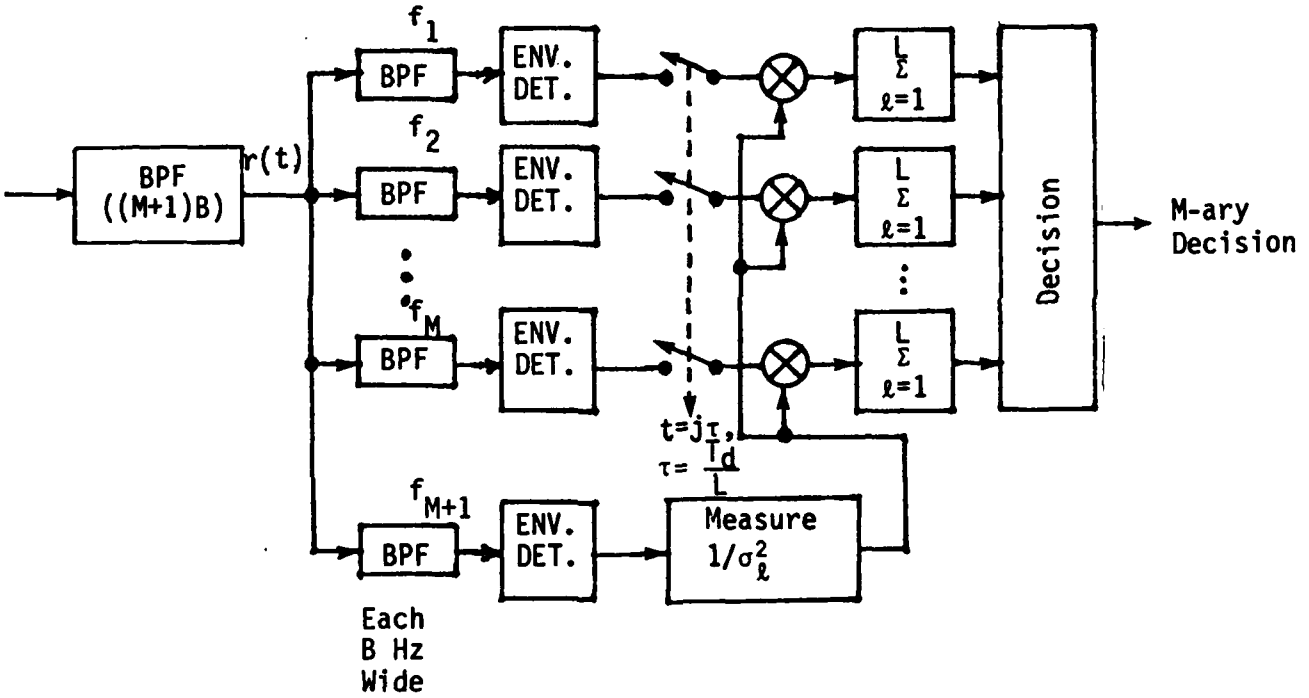

FIGURE 2-5 ADAPTIVE GAIN CONTROL DEMODULATOR

largest decision variable is outputted as the M-ary word decision $\hat{z}$.

We have selected the adaptive gain control (AGC) receiver for our present analysis. The analysis is idealized in that the per-hop noise variance is assumed to be known exactly, as discussed in [5]. Because of this ideal AGC normalization, the performance measures obtained are useful as lower bounds on what may be realized in practice. This is borne out by comparison to a self-normalizing receiver which does not require any noise-power measurements. As shown in [6], the AGC receiver and the more practical self-normalizing receiver differ by only about 1 to 2 dB in performance under partial-band noise jamming. Since the performance difference is not great, we have chosen to consider the AGC receiver for its analytical tractibility (see, for example, [20, Chap. 5] for the analytical and computational challenges presented by the self-normalizing demodulator).

3.0 DECODER ANALYSIS

The performance analysis of the demodulators, which output hard decisions, is available from prior work of the authors [20]. The major new piece of the system which requires analysis is the FEC decoder which operates on these hard decisions. We are considering both block codes and convolutional codes. Since there are profound differences between these two classes of codes, the error performance of the two kinds of decoders must be considered separately.

3.1 Analysis of Block-Code Decoders

The theory of block codes is well documented in the literature, e.g. [18], [21], and [22]. We will not discuss the details of block codes beyond that which is necessary to define the quantities involved in expressing the output uncorrected symbol error rate in terms of the input symbol error rate at the decoder.

The coder accepts a block of k information symbols and outputs a group of n>k coded symbols; the code is described as an (n,k) code. The structure of the code is such that the minimum distance between code words (n-tuples of coded digits) is d. The term distance in this context most commonly is the Hamming distance, which is defined as the number of places in which two code words differ. A code with minimum distance d can correctly decode a received code word if the number of errors in the n-tuple is not greater than

$$t = \left[\frac{d-1}{2}\right] \qquad (3\text{-}1)$$

where [x] denotes the greatest integer less than or equal to x.

The exact computation of the uncorrected error rate at the output of the decoder for a block code requires knowledge of the complete weight structure of the code and the decoding algorithm. Since the complete weight structure of most codes is unknown, an approximate analysis is required.

For an (n,k) block decoder which accepts an n-tuple of Q-ary coded symbols and outputs a k-tuple of decoded Q-ary information symbols, the probability of error P_q in a decoded Q-ary symbol is well approximated by [14]

$$P_q \simeq \frac{d}{n} \sum_{i=t+1}^{d} \binom{n}{i} P_c^i (1-P_c)^{n-i} + \frac{1}{n} \sum_{i=d+1}^{n} i \binom{n}{i} P_c^i (1-P_c)^{n-i} \qquad (3\text{-}2)$$

where d is the minimum distance between code words and t is given by (3-1).

It should be noted that other authors, e.g. [11], have used approximations other than (3-2) for the function $P_q(P_c)$. One commonly used form may be obtained from (3-2) by omitting the first summation and replacing the lower limit of the second summation by t+1 in lieu of d+1. However, this alternative form may substantially underestimate P_q for small values of P_c [14]. We shall use (3-2) for our analyses of block codes. The input-output error rate relation (3-2) is plotted in Figures 3-1 through 3-5 for several typical block codes.

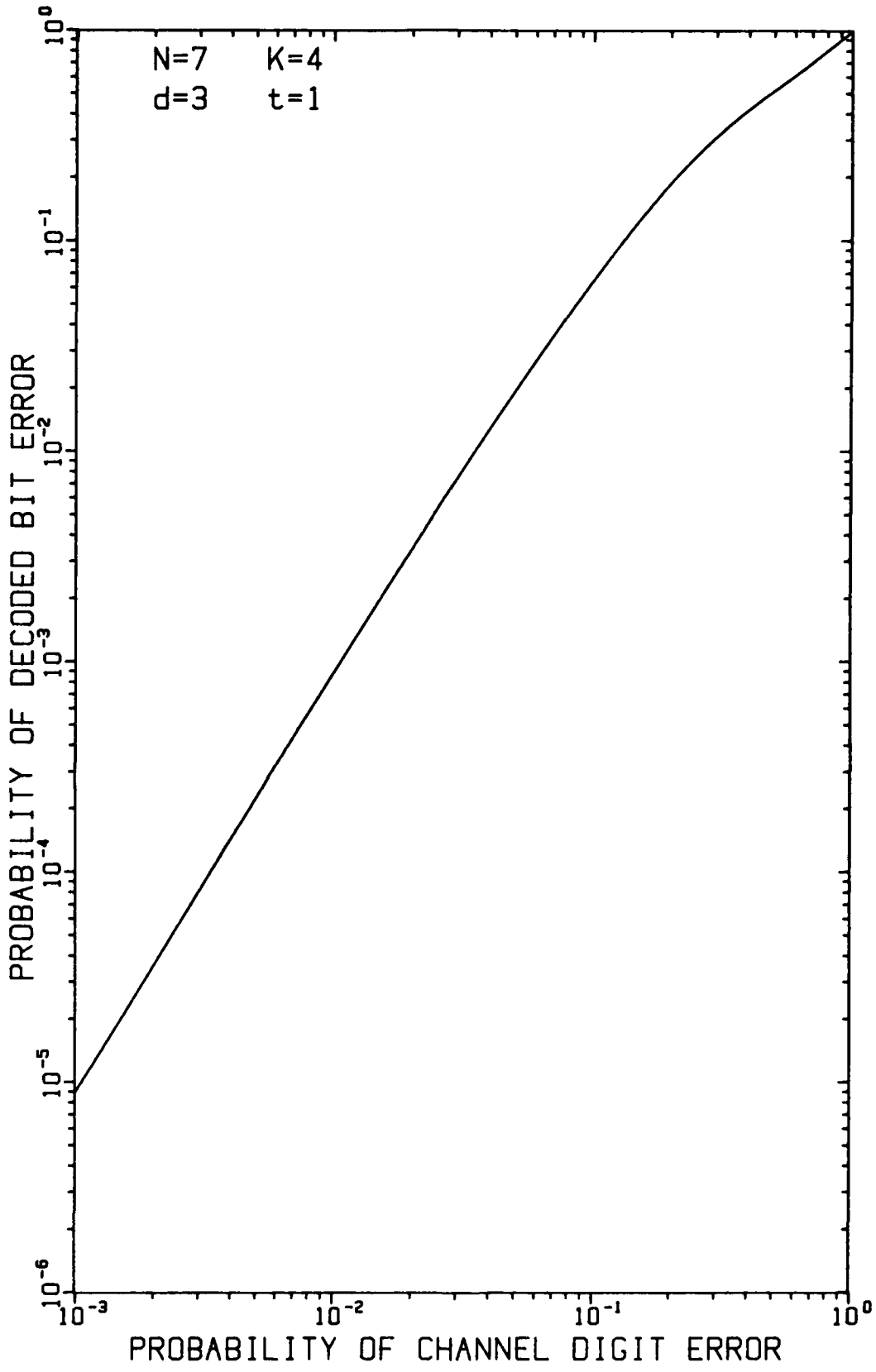

FIGURE 3-1 DECODER PERFORMANCE FOR HAMMING (7,4) CODE

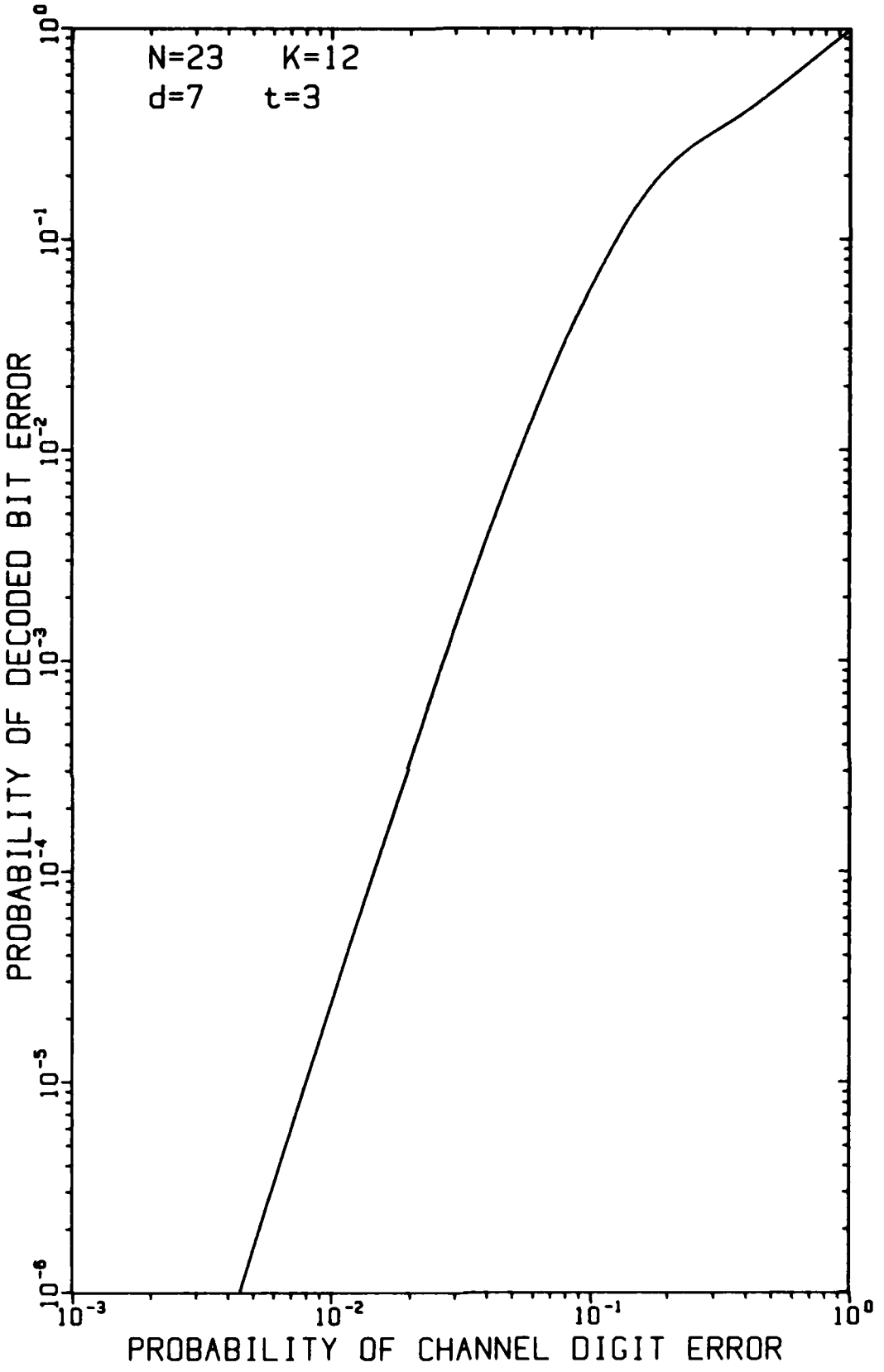

FIGURE 3-2 DECODER PERFORMANCE FOR GOLAY (23,12) CODE

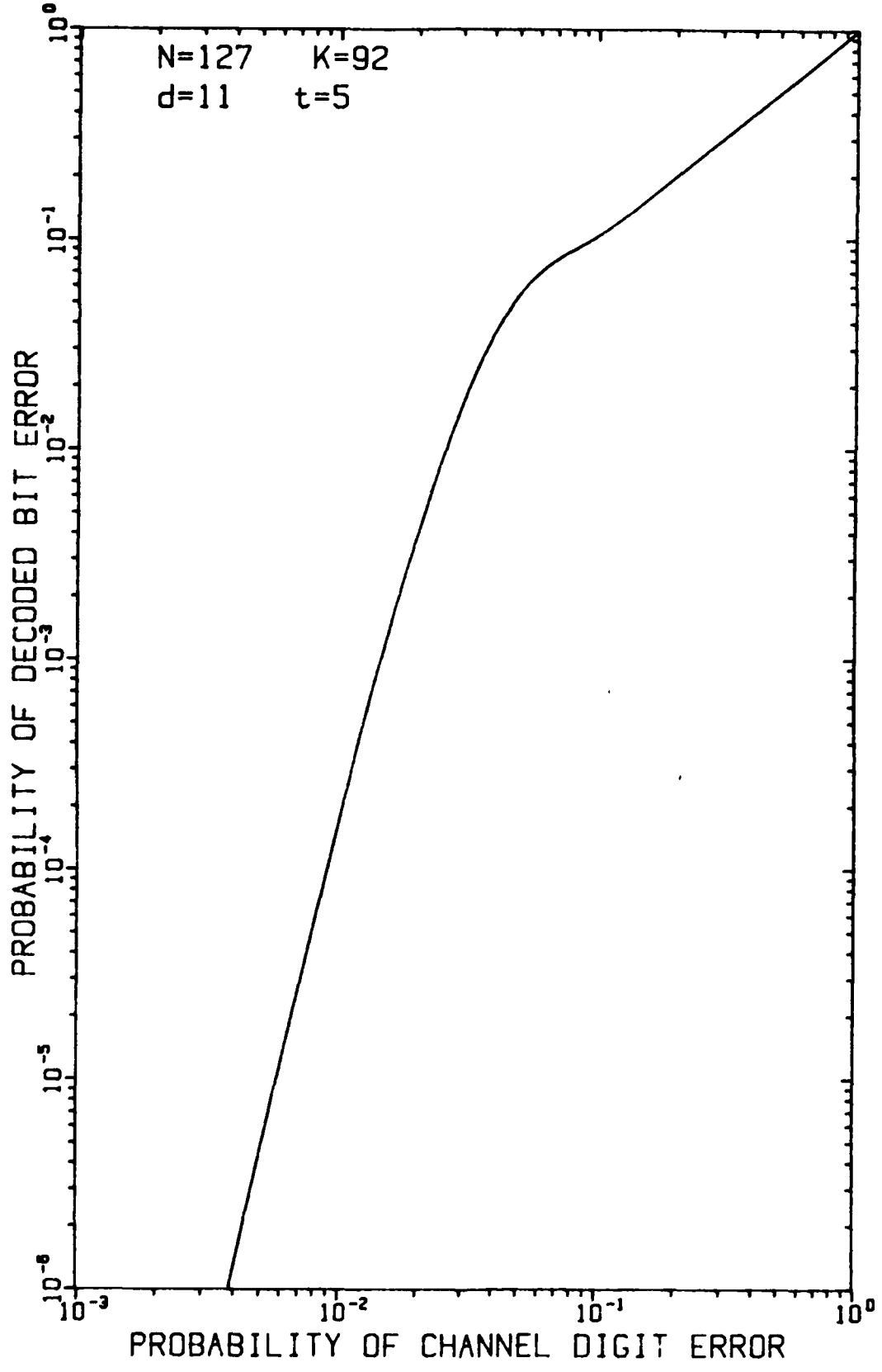

FIGURE 3-3 DECODER PERFORMANCE FOR BCH (127,92) CODE

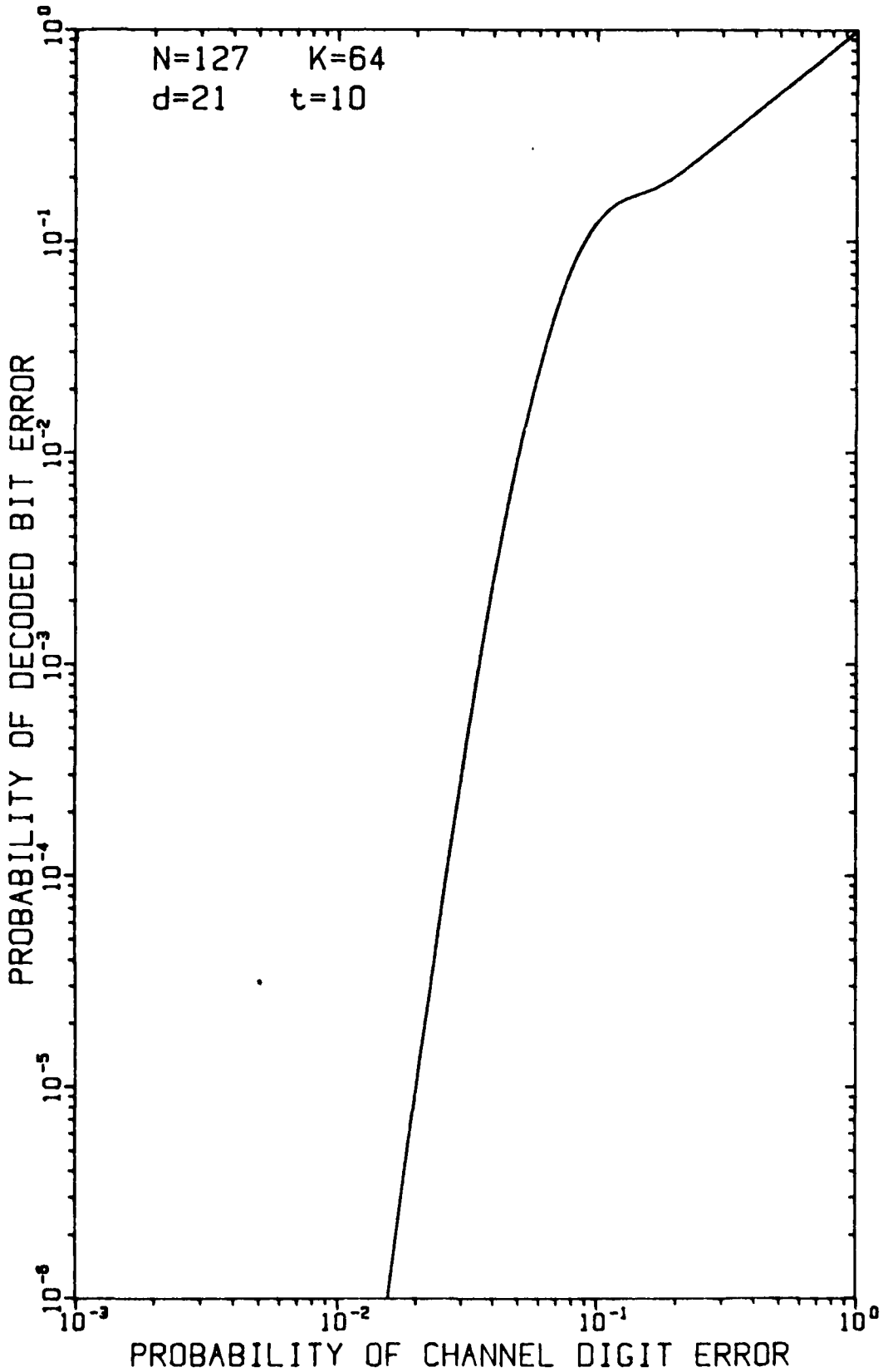

FIGURE 3-4 DECODER PERFORMANCE FOR BCH (127,64) CODE

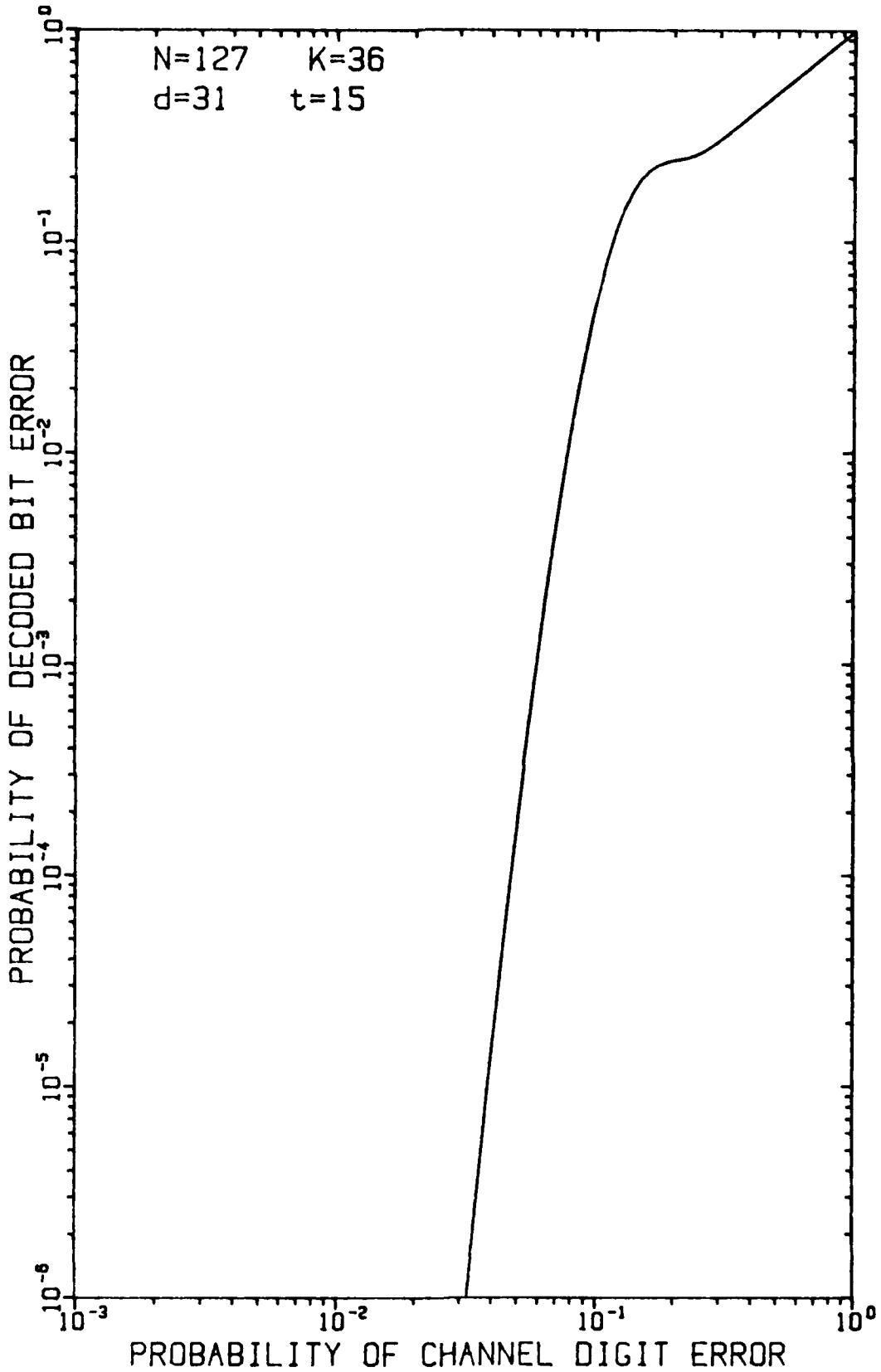

FIGURE 3-5 DECODER PERFORMANCE FOR BCH (127,36) CODE

3.2 Analysis of Convolutional Codes

Unlike block codes, the output of a convolutional coder depends not only upon the current group of input symbols, but also upon the previous k-1 groups of input symbols. The parameter k is called the constraint length of the code [22]. The code rate r is the ratio of number of input symbols per output symbol. For example, a rate-1/2 code produces two output symbols for each input symbol.

All of the convolutional codes which we consider are binary codes with constraint length 7. For the best rate-1/2, constraint-length-7 binary convolutional code with Viterbi decoding, the information-bit error rate may be bounded by [15]

$$P_b \leq \frac{1}{2}\,(36D^{10} + 211D^{12} + 1404D^{14} + \ldots), \tag{3-3}$$

where the probability p_m that an incorrect path differing in m symbols is chosen by the decoder is bounded by [12]

$$P_m \leq \frac{1}{2}\,D^m \tag{3-4}$$

with

$$D = 2\sqrt{P_c(1-P_c)}\ , \tag{3-5}$$

and P_c is the probability of error in a demodulated symbol.

The number of terms used in evaluating (3-3) and other similar expressions affects the accuracy for $P_c > 10^{-3}$. We used in our computations the terms given in [11]. Trial computations using additional terms given by [15] showed little difference in regions where the coded systems show useful coding gain.

The relation (3-5) is actually an approximation to D in the sense that is uses the Bhattacharyya bound for the probability of choosing an incorrect path [18, p. 247]. This approximation is independent of the distance between the correct and the incorrect paths. A more complicated, but more nearly exact, form for D^m may be found using the exact pair-wise error probabilities; see, for example, [16, p. 393], [17, p. 465], or [18, p. 247]. However, we will use (3-5) in order to compare our analysis of the performance including thermal noise on an equal basis with prior analyses which have neglected thermal noise [11].

For the best rate-1/3, constraint-length-7 convolutional code [15]

$$P_b \leq \frac{1}{2}\left(D^{14} + 20D^{16} + 53D^{18} + \ldots\right) \tag{3-6}$$

and for rate-1/4 and rate-1/8 codes obtained by repeating the tap connections of a rate-1/2 code, the decoded information-bit error probabilities are bounded by [11]

$$P_b \leq \frac{1}{2}\left(36D^{20} + 211D^{24} + 1404D^{28} + \ldots\right) \tag{3-7}$$

and

$$P_b \leq \frac{1}{2}\left(36D^{40} + 211D^{48} + 1404D^{56} + \ldots\right), \tag{3-8}$$

respectively. The rate-1/4 and rate-1/8 codes obtained by repeating the taps of a rate-1/2 code are not the best codes of these constraint lengths; weights for better codes are known [23]. However, we have again chosen to analyze codes for which no-thermal-noise results are available in the literature.

4.0 SYSTEM PERFORMANCE ANALYSES INCLUDING NUMERICAL RESULTS

Except for the decoder input-output error performance as discussed in Section 3.0, the system analysis is the same for both block codes and convolutional codes. Similarly, the only influence of the demodulator type (linear combiner or AGC) is the form of the equation for the channel error probability. Therefore, we present one unified analysis to cover all cases, followed by numerical results.

4.1 Mathematical Analysis

Referring back to Figure 2-2, we desire to obtain the probability of received bit error, P_b, for the binary sequence $\{\hat{x}\}$. To do this, we first find the probability of M-ary word error, P_d, at the demodulator output. This is then transformed to the probability of error in a Q-ary digit at the decoder input. Then one of the decoder relations (3-2), (3-3), (3-6), (3-7), or (3-8), as appropriate to the code under consideration, is used to obtain the probability of an uncorrected error in a decoded Q-ary symbol, P_q. Finally, P_b is obtained from P_q.

4.1.1 Probability of M-ary Word Error

The jammer is assumed to have available J watts of power which is distributed uniformly over a fraction γ, $0 \leq \gamma \leq 1$, of the total spread-spectrum system bandwidth W. Each hopped transmission is subjected to jamming with probability γ; and the probability that a given hop is not jammed is $1-\gamma$. The jamming power in the jammed cell of bandwidth B is

$$\sigma_J^2 = \frac{JB}{\gamma W} = \frac{N_J B}{\gamma} \tag{4-1}$$

where $N_J \triangleq J/W$ is the average jamming noise spectral density for the system bandwidth W. As in [4]-[7], we assume that the M adjacent frequency cells of the MFSK modulation band are either all jammed or all unjammed on any given hop.

Let the received energy per information bit be $E_b = ST_b$ where S is the received signal power and $T_b = 1/R_b$ is the information bit duration. Then the energy per coded M-ary word is

$$E_d = \frac{kKE_b}{n} \tag{4-2}$$

and the energy per hop is

$$E_h = \frac{E_d}{L} = \frac{kKE_b}{nL} \quad . \tag{4-3}$$

Further, let N_0 denote the thermal noise density at the receiver.

Let $\hat{z}$ denote a word of the received sequence of coded M-ary words $\{\hat{z}\}$. If we define $P_d(e|\ell)$ to be the conditional probability of error, given that ℓ of the L hops per M-ary word are jammed, then the probability that $\hat{z}$ is in error is given by

$$P_d(e) = \sum_{\ell=0}^{L} \binom{L}{\ell} \gamma^{\ell}(1-\gamma)^{L-\ell} P_d(e|\ell) \, .$$

For the square-law linear combining demodulator, the conditional error probability is [20]

$$P_d(e|\ell) = \sum_{m=1}^{M-1} \binom{M-1}{m} \frac{(-1)^{m+1}}{(m+1)^{L-\ell}(\delta m+1)^{\ell}} \sum_{n=0}^{\infty} \frac{c_{nm}}{(m+1)^n n!} e^{-\lambda_\ell/2}$$

$$\cdot \sum_{k=0}^{\infty} \sum_{r=0}^{k} \frac{1}{(k-r)!r!} \left[\frac{\lambda_{0,\ell}}{2(m+1)}\right]^{k-r} \left[\frac{\lambda_{1,\ell}}{2(\delta m+1)}\right]^{r} (k+L)_n \, d_{nrk} \qquad (4\text{-}5)$$

where the coefficients c_{nm} are defined as

$$c_{nm} = \begin{cases} 1, & n=0 \\ \frac{1}{n} \sum_{q=1}^{n} \binom{n}{q} [(m+1)q-n] c_{n-q,m} \beta_q, & n \neq 0; \end{cases} \qquad (4\text{-}6)$$

the terms d_{nrk} are given by

$$d_{nrk} = \sum_{j=0}^{n} \binom{n}{j} \left(\frac{\delta-1}{\delta m+1}\right)^j \frac{(r+\ell)_j}{(k+L)_j}; \qquad (4\text{-}7)$$

the parameters $\lambda_{0,\ell}$, $\lambda_{1,\ell}$ and λ_ℓ are given by

$$\lambda_{0,\ell} = 2(L-\ell)\rho_N, \qquad (4\text{-}8)$$

$$\lambda_{1,\ell} = 2\ell\rho_T, \qquad (4\text{-}9)$$

and

$$\lambda_\ell = \lambda_{0,\ell} + \lambda_{1,\ell}; \qquad (4\text{-}10)$$

the ratio δ is defined as

$$\delta \triangleq \sigma_T^2/\sigma_N^2 = \rho_N/\rho_T; \tag{4-11}$$

the signal-to-noise ratios ρ_N and ρ_T are given by

$$\rho_N = \frac{kK}{nL}\frac{E_b}{N_0} \tag{4-12}$$

and

$$\rho_T = \frac{kK}{nL}\frac{E_b}{N_T} \tag{4-13}$$

with

$$N_T = N_0 + N_J/\gamma; \tag{4-14}$$

and the Pochhammer symbol is defined [24, eq. 6.1.22] by

$$(a)_0 = 1 \tag{4-15a}$$

$$(a)_n = \Gamma(a+n)/\Gamma(n). \tag{4-15b}$$

For the AGC demodulator, the conditional error probability is [7]

$$P_d(e|\ell) = \sum_{m=1}^{M-1} \binom{M-1}{m} \frac{(-1)^{m+1}}{(m+1)^L} \cdot \exp\left(-\frac{m}{m+1}\rho_\ell\right) \sum_{r=0}^{m(L-1)} \frac{C_r(m,L)}{(m+1)^r} \cdot \mathcal{L}_r^{(L-1)}\left(-\frac{\rho_\ell}{m+1}\right) \tag{4-16}$$

in which $\mathcal{L}_n^m(x)$ is the generalized Laguerre polynomial;

$$C_r(m,L) \triangleq \begin{cases} m^r, & 0 \le r \le L-1; \\ \frac{1}{r} \sum_{n=1}^{L-1} \binom{r}{n} [(m+1)n-r] C_{r-n}(m,L), & r > L-1; \end{cases} \tag{4-17}$$

and the parameter ρ_ℓ is given by

$$\rho_\ell = \frac{kK}{nL} \left[\ell \frac{E_b}{N_T} + (L-\ell) \frac{E_b}{N_0} \right] \tag{4-18}$$

with N_T given by (4-14).

4.1.2 Probability of Error at Decoder Input

In the general case, the demodulated M-ary words must be mapped to Q-ary symbols prior to being presented to the decoder. Hence we must be able to relate the M-ary word error probability P_d at the demodulator output to the Q-ary symbol error probability P_c at the decoder input. We assume that

$$\frac{\max(K,q)}{\min(K,q)} = \text{integer}, \tag{4-19}$$

i.e. an integer number of M-ary words map to one Q-ary symbol, or vice versa.

Case 1: $q > K$. If $q > K$, then q/K M-ary words are mapped to one Q-ary symbol. A practical example of this case is use of, say, 8-ary FSK ($K = 3$) to transmit the output of a Reed-Solomon (63,32) code for which $Q = 64$ ($q = 6$). In this

example, each coded 64-ary symbol would be mapped to two 8-ary words for transmission by 8-ary FSK. At the receiver, the Q-ary symbol will be in error if one or more of the q/K M-ary words are in error. Therefore,

$$P_c = 1 - (1-P_d)^{q/K}, \quad q/K = \text{integer}. \tag{4-20}$$

Case 2: $q < K$. If $q < K$, then $r \triangleq K/q$ coded Q-ary symbols are grouped to form one M-ary word for transmission. In this case, it will be necessary to employ interleaving to maintain the independence of symbol errors within a code word (n-tuple of Q-ary symbols). Whenever this case arises, we assume the presence of the necessary interleaver and de-interleaver, even though they are not shown explicitly in Figure 2-2. In general, at the receiver, for $M = Q^r$, of the M words consisting of r Q-ary symbols, $Q^{r-1} = M/Q$ of them have the same Q-ary symbol in a given position. Therefore, given that a word error occurs, the probability of a symbol error in a given position is

$$\Pr\{\text{symbol error} \mid \text{word error}\} = \frac{M-1-\left(\frac{M}{Q}-1\right)}{M-1} = \frac{M}{M-1}\left(1-\frac{1}{Q}\right) \tag{4-21}$$

Thus the average symbol error probability is

$$P_c = \frac{M}{M-1}\left(1-2^{-q}\right) P_d, \quad K/q = \text{integer}. \tag{4-22}$$

In the special case q = 1 (binary coder), (4-22) becomes the familiar M-ary-to-binary error probability relation for orthogonal signals,

$$P_c = \frac{M/2}{M-1} P_d. \tag{4-23}$$

4.1.3 Error Probability at Decoder Output

The decoder is presented hard symbol decisions upon which to operate; no soft-decision (or quality) information is available to the decoder. Thus the function $P_q(P_c)$ for block codes is given by (3-2) and for convolutional codes by (3-3)-(3-8), as appropriate for the code rate under consideration.

4.1.4 Probability of Bit Error

The mapping from Q-ary symbols with $Q=2^q$ to binary bits is analogous to case 2 discussed in Secton 4.1.2. We may obtain the relation between P_b and P_q by relabeling the quantities in (4-23):

$$P_b = \frac{Q/2}{Q-1} P_q. \tag{4-24}$$

4.1.5 Worst-Case Jamming

The worst-case jamming performance, given a code, demodulator type, and values of E_b/N_0, E_b/N_J, M, and L, is found by taking

$$\max_{\gamma} [P_b(e;E_b/N_0,E_b/N_J,M,L,\gamma)]. \tag{4-25}$$

The form of $P_b(e)$ is too complicated to solve (4-25) by setting $(\partial P_b/\partial\gamma)|_{\gamma=\gamma_0}=0$ and solving for the worst-case (jammer's optimum) fraction γ_0. Therefore, we solved (4-25) by numerical search for γ_0.

4.2 Numerical Results

For our numerical computations, we have selected a representative selection of block and convolutional codes. The selected block codes are listed in Table 4-1, which also shows the pertinent parameters of the codes. The values of the parameters d and t given in the table are from [22]. The convolutional codes which we have studied are the best constraint-length-7 rate-1/2 and rate-1/3 codes found by Odenwalder [15] and rate-1/4 and rate-1/8 codes derived by repeating the taps for the rate-1/2 code [11].

We have computed coded system performance for both the linear combining demodulator and the AGC demodulator. We will discuss each type of demodulator separately.

4.2.1 Numerical Results for Square-Law Linear Combining Demodulator

We have computed the performance of the system for a variety of codes used in conjunction with the square-law linear combining demodulator. To provide a reference for evaluating the effects of the coding, we have also computed the performance of an uncoded binary system, as shown in Figures* 4-1 through 4-4 for L=1, 2, 3, and 4 hops/bit, respectively. These figures show $P_b(e)$ vs. E_b/N_0 with E_b/N_J as a parameter. For comparison, the unjammed performance of ideal BFSK is also shown on the curves. This set of 4 curves shows that increasing L with a linear combiner uniformly degrades the performance of an uncoded system in optimum** partial-band noise jamming [4].

---

*The numerous figures for this section are all placed at the end of the section.

**The term "optimum" is used here in the sense of optimum for the jammer's viewpoint; from the communicator's viewpoint it corresponds to worst-case jamming.

TABLE 4-1

BLOCK CODES STUDIED

Code Name	Output Block Size n	Information Symbols/Block k	Minimum Distance Between Code Words d	Error Correcting Capability t
Hamming	7	4	3	1
Golay	23	12	7	3
BCH	127	92	$\geq$11	5
BCH	127	64	$\geq$21	10
BCH	127	36	$\geq$31	15
Reed-Solomon	7	3	5	2
Reed-Solomon	15	9	7	3
Reed-Solomon	31	15	17	8

The first code we consider is the Hamming (7,4) code, which is a single-error-correcting code. Figures 4-5 through 4-8 show the performance as a function of E_b/N_0 with E_b/N_J as a parameter. As with the uncoded system, increasing L is seen to degrade performance uniformly. This is also evident from Figures 4-9 through 4-12 which compare the performances of the coded and uncoded systems as a function of E_b/N_J when E_b/N_0 = 13.35247 dB (which corresponds to $P_b(e) = 10^{-5}$ for ideal BFSK without jamming. The ideal BFSK curve is also shown for comparison. For this curve the abscissa is to be construed as E_b/N_0 rather than E_b/N_J. (This comment applies to all such plots of $P_b(e)$ vs. E_b/N_J.)

In Figures 4-10 through 4-12, we see a somewhat surprising cross-over of the coded and uncoded performance curves for high E_b/N_J and L>1. This phenomenon arises as a result of the noncoherent combining loss incurred when L>1. The comparisons are done on the basis of equal energy per <u>information bit</u> for both the uncoded and the coded systems; therefore the energy per <u>channel digit</u> for the coded system is 4/7 that of the uncoded system. The noncoherent combining loss is inversely related to the ratio E_d/N_T. Therefore, the coded system incurs a higher noncoherent combining loss than does the uncoded system. Additionally, the jammer can be somewhat more effective at a lower E_d/N_0. Taken together, these degradations are greater than the coding gain, and the uncoded system performs better. It is only in a region where the jammer's effects dominate over noncoherent combining loss that the coded system performs better.

We now turn our attention to the Golay (23,12) code, which is a triple-error-correcting code. Figures 4-13 through 4-16 show the performance as a function of E_b/N_0 with E_b/N_J as a parameter for L=1, 2, 3, and 4 hops/digit, respectively. Compared to the Hamming (7,4) code of Figures 4-5 through 4-8, the Golay (23,12) code performs much better for E_b/N_J of 10 dB and greater; but we still see a uniform degradation of performance as L increases from 1 to 4 hops/digit.

Figures 4-17 through 4-20 show the performance of the Golay code as a function of E_b/N_J when E_b/N_0 = 13.35247 dB (corresponding to $P_b(e) = 10^{-5}$ for ideal BFSK without jamming). Again, performance is only degraded by increasing the number of hops per digit. But unlike the Hamming code of Figures 4-9 through 4-12, the Golay code of Figures 4-17 through 4-20 does not exhibit a second cross-over at high E_b/N_J. The code rates of the two codes are nearly the same (for the Hamming code, the rate = 4/7 ≈ 0.57 and for the Golay code, the rate = 12/23 ≈ 0.52) but the Golay code has considerably greater error correcting capability, and hence greater coding gain. In this case the loss in E_d/N_0 to the coding is more than offset by the coding gain, and a net improvement in performance results.

We next consider the family of BCH codes*. We have examined three such codes: the BCH (127,92), the BCH (127,64), and the BCH (127,36) codes. Figures 4-21 through 4-24 show the performance of the BCH (127,92) code as a function of E_b/N_0 with L=1, 2, 3, and 4 hops/digit, respectively, and with E_b/N_J as a parameter; Figures 4-25 through 4-28 show the performance as a function of E_b/N_J when E_b/N_0 = 13.35247 dB for the same set of values of L.

*Bose-Chaudhuri-Hocquenghem codes

There is, again, only degradation of performance when L increases. Comparing Figures 4-21 through 4-24 with Figures 4-13 through 4-16 shows that the BCH (127,92) code outperforms the Golay (23,12) code for weak jamming but not for strong jamming, and that the cross-over point moves to higher E_b/N_J as L increases. The BCH (127,92) code has the advantage of a higher rate ($r = 92/127 \simeq 0.72$) in comparison to the Golay code (rate $r = 12/23 \simeq 0.52$), but it has a much larger block size. The BCH (127,92) code can correct 5 errors in a block of size 127 digits; the Golay (23,12) code can correct 3 errors in a block of size 23 digits. In going from the Golay (23,12) to the BCH (127,92) code, the error correcting capability has increased by only about 1.7 times as many errors/block, while the number of digits per block has increased by 5.5 times. The results is a net increase, on the average, in the number of blocks with uncorrectably many errors and a net loss of performance, except at very low digit error rates.

Performance curves for the BCH (127,64) code as a function of E_b/N_0 with E_b/N_J as a parameter and L=1, 2, 3, and 4 are shown in Figures 4-29 through 4-32, respectively. Performance curves as a function of E_b/N_J when $E_b/N_0 = 13.35247$ dB are shown in Figures 4-33 through 4-36 for the four values of L. As before, increasing L only degrades performance.

Relative to the BCH (127,92) code, the BCH (127,64) code shows better performance for E_b/N_J greater than about 15 dB, but the amount of improvement diminishes as L increases. The lower rate of the BCH (127,64) code takes its toll on performance as noncoherent combining loss increases with increasing L.

The performance of the BCH (127,36) code is given as a function of E_b/N_0 with E_b/N_J as a parameter and L=1, 2, 3, and 4 in Figures 4-37 through 4-40, respectively; and as a function of E_b/N_J when E_b/N_0 = 13.35247 dB in Figures 4-41 through 4-44. Comparing Figures 4-37 through 4-40 with Figures 4-29 through 4-32, we see that there is only a small region of E_b/N_0 and E_b/N_J for which the BCH (127,36) code performs better than the BCH (127,64) code, and that as L increases the E_b/N_J region moves to higher values of E_b/N_J. For example, when L=2 the region lies between E_b/N_J = 15 dB and E_b/N_J = 20 dB; but for L=4 the region is around E_b/N_J = 20 dB to E_b/N_J = 25 dB. The loss due to the low code rate shows quite clearly in Figures 4-41 through 4-44. Indeed, in Figures 4-43 and 4-44 the loss is so great that was the 15-error-correcting capability of the code does not offset the loss, and the coded system performs more poorly than the uncoded system in partial-band noise jamming.

4.2.1.2 Binary Convolutional Codes

We now turn our attention to the constraint-length-7 convolutional codes with Viterbi decoding. The available performance bounds for such codes, as presented in Section 3.2, are very loose bounds under high error

rates at the decoder input. Therefore, for our numerical work, we have added an additional step to the final results:

$$P_b = \min\{ [P_b \text{ given by eq. (4-24)}], 1\} . \qquad (4\text{-}26)$$

Thus, the results obtained for convolutional codes are not of use for very strong jamming.

We first consider the rate-1/2 convolutional code. The performance as a function of E_b/N_0 with E_b/N_J as a parameter is shown in Figures 4-45 through 4-48 for L=1, 2, 3, and 4, respectively. Figures 4-49 through 4-52 show the performance as a function of E_b/N_J when E_b/N_0 = 13.35247 dB, for L=1, 2, 3, and 4, respectively. As was the case with all of the block codes previously studied, increasing L results in degraded performance.

For the other convolutional codes we have considered, we present results only as a function of E_b/N_J when E_b/N_0 = 13.35247 dB (for $P_b(e) = 10^{-5}$ for ideal BFSK without jamming). The results for the constraint-length-7, rate-1/3 convolutional code are given in Figures 4-53 through 4-56, for L=1, 2, 3, and 4, respectively. The corresponding results for the rate-1/4 code are shown in Figures 4-57 through 4-60 for L=1, 2, 3, and 4, respectively; results for the rate-1/8 code are shown in Figures 4-61 through 4-64. This series of figures shows that the convolutional codes suffer from the same losses due to low rate as do the

block codes. The rate-1/3 code is better than the rate-1/2 code only for $L \leq 2$; the rate-1/4 and rate-1/8 codes are poorer than the rate-1/3 code even for L=1. For the rate-1/8 code, the loss is so great that even an uncoded system performs better for $L \geq 2$.

4.2.1.3 M-ary Block Codes

We have also computed performance curves for a few M-ary systems employing Reed-Solomon codes. Because the numerical calculations of the channel symbol error rate for the linear combining demodulator are very slow [20], the results presented here are more limited than those given for binary codes. Figures 4-65 and 4-66 show the performance of a Reed-Solomon (7,3) code with 8-ary FSK transmission as a function of E_b/N_J when E_b/N_0 = 9.09401 dB (corresponding to $P_b(e) = 10^{-5}$ for ideal 8-ary FSK without jamming) for L=1 and L=2, respectively. This is a double-error-correcting code. We observe from these figures that the 8-ary code suffers the same rate effects as the binary codes, and that increasing L degrades performance.

Figures 4-67 and 4-68 show the performance of the Reed-Solomon (15,9) and (31,15) codes, respectively, for L=1 and E_b/N_0 such that $P_b(e) = 10^{-5}$ for ideal MFSK without jamming. We have computed only L=1 results because of the computer time required for higher alphabet sizes. We observe that these more powerful codes exhibit considerable gain relative to an uncoded system in partial-band noise jamming. However, there is no reason to believe that these codes would behave any differently with increasing L

than all of the other codes studied in conjunction with the square-law linear combining demodulator.

4.2.2 Numerical Results for Adaptive Gain Control Demodulator

Before considering the combined performance of the AGC demodulator and FEC coding, it is of interest to examine briefly the performance of an L-hop/symbol AGC receiver by itself. The L-hop diversity is analogous to a repetition code with the nonlinear combining AGC receiver constituting a soft-decision decoder. In Figure 4-69, we compare the uncoded binary AGC receiver's performance [20] with the performance of a binary repetition code and hard decision receiver given by Stark [19] for the case of L=7 and E_b/N_0 = 30 dB. The AGC receiver is uniformly about 1.4 dB better than the hard decision receiver with side information, while the performance difference between the hard decision receiver without side information and the AGC receiver increases as E_b/N_0 increases. This indicates that the L-hop/symbol AGC receiver is in the class of receivers which use "side information." This "side information" is used in the AGC receiver in the form of the adaptive weighting of each hop.

Turning now to the performance of the AGC demodulator plus FEC coding, we have numerically computed performance curves for a representative selection of block and convolutional codes, using both binary and M-ary modulations.

4.2.2.1 Binary Block Codes

Figures 4-70 through 4-73 show the performance of the Hamming (7,4) code as a function of E_b/N_0 with E_b/N_J as a parameter for L=1, 2, 3, and

4, respectively. The performance of an uncoded system is also shown in dashed lines for comparison. Here we see that the performance of the AGC demodulator is much different from that of the linear combiner; performance of the AGC demodulator improves as L increases. With the nonlinear combining of the L hops, a diversity gain is achieved. However, we still see the loss due to code rate, as discussed above under the results for the linear combiner, dominating for strong jamming and higher L. As L increases, the value of E_b/N_0 required for the coded system to be better than the uncoded system increases. For example, when E_b/N_J = 15 dB and L=1 the coded system is better for E_b/N_0 > 10.7 dB, but for L= 4 the coded system is better for E_b/N_0 > 18.7 dB.

A similar set of performance curves for the Golay (23,12) code is given in Figures 7-74 through 4-77. We observe that the Golay code is much better than the Hamming code under these conditions: the Golay code at E_b/N_J = 15 dB performs nearly as well as the Hamming code at E_b/N_J = 20 dB. Under stronger jamming (E_b/N_J = 15 dB) we see improving performance with L as high as L=3; but under weak jamming (E_b/N_J = 30 dB) L=1 is best.

The performance of the BCH (127,92) code as a function of E_b/N_0 with E_b/N_J as a parameter is shown in Figures 4-78 through 4-81 for L=1 through 4, respectively. The trends are the same as observed for the Golay code, but we see greater coding gain being achieved by the 5-error-correcting BCH (127,92) code.

Performance curves for the BCH (127,64) code as a function of E_b/N_0 with E_b/N_J as a parameter are given in Figures 4-82 through 4-85 for

L=1, 2, 3, and 4, respectively. Performance trends are as observed for the other block codes with AGC demodulation. We do see increased coding gain relative to the BCH (127,92) code for L=1 when E_b/N_0 is sufficiently high; however the losses due to lower code rate are apparent even when L=1 for weak jamming (E_b/N_J = 30 dB). As L increases, the losses due to lower rate become more significant. By the time L=4 is reached, even for E_b/N_J = 15 dB the rate effect is quite noticeable. The noncoherent combining loss is also important, with L=2 being the highest optimum diversity for the range of E_b/N_0 and E_b/N_J shown in the figures.

Concluding the binary block codes that we are considering, Figures 4-86 through 4-89 show the performance of the BCH (127,36) code as a function of E_b/N_0 with E_b/N_J as a parameter for L=1, 2, 3, and 4, respectively. Here the effects of too low a code rate again show up clearly. Except at the combination of low E_b/N_J and high E_b/N_0, the BCH (127,36) code performs worse than the BCH (127,64) code. Diversity gain is realized only under strong jamming, and the optimum order of diversity does not exceed L=2.

To summarize the results for block codes, Figure 4-90 shows the information-bit error probabilities as a function of E_b/N_0 for the binary block codes we have considered, using FH/BFSK with optimum diversity in worst-case partial-band noise jamming when E_b/N_J = 15 dB. The scalloped appearance of these curves arises from the discrete values of the optimum diversity, which is necessarily an integer. Each curve in Figure 4-90 is the under-envelope of a set of curves for discrete values of L, such

as those shown in Figures 4-70 through 4-73 for the case of the Hamming (7,4) code. As E_b/N_0 increases, the optimum order of diversity increases. This is related to the effects of noncoherent combining loss, which increases as L increases and which is more severe at lower E_b/N_0 values.

It is also of value to consider plots of the performance as a function of E_b/N_J with E_b/N_0 as a parameter. Figures 4-91 thorugh 4-93 show the decoded information-bit error probability as a function of E_b/N_J for the several block codes using FH/BFSK with optimum diversity in worst-case partial-band noise jamming for E_b/N_0 = 15 dB, 30 dB, and ∞ (no thermal noise), respectively. In all three cases, we note the somewhat surprising result that the code with the greatest error correction capability, the 15-error-correcting BCH (127,36) code, exhibits poorer performance than codes with less error correction capability. As discussed in conjunction with the linear combining demodulator, this arises because our comparisons are on the basis of equal energy per <u>information bit</u>, E_b. The energy per <u>coded symbol</u> is $E_d = 36E_b/127$ for the BCH (127,36) code and $E_d = 64E_b/127$ for the BCH (127,64) code. This reduction in E_d/N_0 causes the channel error rate to rise more rapidly than the error correction capability, thus resulting in degraded performance. If we were to compare codes on the basis of equal E_d rather than equal E_b, as done for example in [13], we would obviously see much better performance for the lower rate codes because E_b would increase in proportion to 1/r. However, our approach of comparing codes on the basis of equal energy per information bit is

more appropriate for the system designer who confronts the task of selecting a code while faced with constraints of required information throughput and an average power limit for the transmitter.*

4.2.2.2 Binary Convolutional Codes

We now turn our attention to performance of binary convolutional codes used in conjunction with an AGC demodulator. We consider constraint-length-7 codes of rates 1/2, 1/3, 1/4, and 1/8 where the rate-1/4 and rate-1/8 codes are derived from the rate-1/2 code by repeating taps on the encoder [11]. We assume Viterbi (maximum likelihood) decoding with hard decisions as the input to the decoder. Because the bounds on decoder performance given in Section 3.2 are loose for high input symbol error probabilities, the results are not useful at low E_b/N_0.

Figures 4-94 through 4-97 show the performance of the best (in the sense of Odenwalder [15]) constraint-length-7, rate-1/2, convolutional codes as a function of E_b/N_0 with E_b/N_J as a parameter for L=1, 2, 3, and 4, respectively. Comparison of these figures shows optimum diversity as high as L=3 for E_b/N_J = 15 dB. We note that considerable coding gain is achieved by this code.

Results for the best rate-1/3 code are shown in Figures 4-98 through 4-101 as functions of E_b/N_0 with E_b/N_J as a parameter for L=1 through 4,

*A specified throughput requirement fixes $T_b=1/R_b$. Other system specifications (such as size, weight, prime power, cooling, etc.) will limit the average RF power output of the transmitter to some maximum, P_{max}, and the transmitter antenna gain to some maximum, $T_{TA,max}$. Then the radiated energy per bit is limited to $E_b \leq T_b P_{max} T_{TA,max}$ joules/bit, regardless of how coding and modulation split it up into hopped symbols. We, therefore, let the hop rate vary as L changes.

respectively. We see again that some diversity improvement is attainable under stronger jamming (E_b/N_J = 15 dB), but the optimum diversity is low (L=2). In comparison to the rate-1/2 code, the rate-1/3 code offers significant improvement under strong jamming.

Repeating the encoder taps of the best rate-1/2 code gives a rate-1/4 code whose performance is shown in Figures 4-102 through 4-105 for L=1 through 4, respectively. Repeating the taps twice gives a rate-1/8 code whose performance is shown in Figures 4-106 through 4-109. Although small performance gains are attained at L=1 and E_b/N_J = 15 dB when E_b/N_0 is large, for the most part these codes suffer from too low a rate. The effect is particularly striking for the case of L=4 and rate-1/8 (Figure 4-109) where the uncoded system is better than the coded system with E_b/N_J = 15 dB.

To summarize the results for convolutional codes, Figure 4-110 shows the information-bit error probabilities as a function of E_b/N_0 for the four convolutional codes we have considered, using FH/BFSK with optimum diversity in worst-case partial-band noise jamming when E_b/N_J = 15 dB. As discussed in conjunction with block codes and Figure 4-90, the scalloped appearance of the curves in Figure 4-110 is due to L being quantized to integer values only. As E_b/N_0 increases, the optimum order of diversity increases for convolutional codes, as is also the case for block codes.

It is also of interest to consider performance plots as a function of E_b/N_J with E_b/N_0 as the parameter. To show this, the performances of

binary convolutional codes using FH/BFSK with optimum diversity in worst-case partial-band noise jamming are shown in Figures 4-111, 4-112, and 4-113 for E_b/N_0 = 15 dB, 30 dB, and ∞, respectively. Just as is the case for block codes, the reduction in E_d for low rate codes results in an increase in channel error rate that overwhelms the increased error correcting ability with the result being a net loss in performance.

4.2.2.3 Summary of Binary Code Performance

Table 4-2 summarizes results obtained for binary transmission of binary coded signals using optimum diversity. The table shows the required E_b/N_J for $P_b = 10^{-5}$, the optimum diversity (L), and the worst-case jamming fraction (γ_0), for E_b/N_0 = 15 dB, 30 dB, and infinity (no thermal noise). Results for no thermal noise and perfect side information as given by Ma and Poole [11] are also included for comparison. We observe that when E_b/N_0 = 15 dB, which is a realistically attainable value, the required E_b/N_J for $P_b(e) = 10^{-5}$ is about 1 to 7 dB higher than the requirement based on bounds and no thermal noise from [11], depending upon the code. When E_b/N_0 = 30 dB (which corresponds to a negligible* $P_b(e)$ for ideal BFSK without jamming), we observe that the required E_b/N_J is within 0.1 dB of the case of no thermal noise ($E_b/N_0 = \infty$) based on our above analysis. However, for the receiver which uses side information [11], the required E_b/N_J for $E_b/N_0 = \infty$ is about 1 to 1.5 dB higher than that obtained for E_b/N_0 = 30 dB through our use of exact

*For ideal BFSK, $P_b(e) < 7 \times 10^{-218}$.

TABLE 4-2

Performance of Binary Codes Using FH/BFSK With Optimum Diversity When $P_b(e)=10^{-5}$

Code	Maximum Number of Correctable Errors	E_b/N_0=15 dB			E_b/N_0=30 dB			E_b/N_0= ∞			E_b/N_0 = ∞ with side information (Ma and Poole [11])		
		Required E_b/N_J (dB)	Optimum Diversity	Worst-Case Jamming Fraction	Required E_b/N_J (dB)	Optimum Diversity	Worst-Case Jamming Fraction	Required E_b/N_J (dB)	Optimum Diversity	Worst-Case Jamming Fraction	Required E_b/N_J (dB)	Optimum Diversity	Worst-Case Jamming Fraction
Hamming (7,4)	1	22.28	2	0.11	15.40	5	0.71	15.31	5	0.70	16.21	5.97	0.75
Golay (23,12)	3	16.97	2	0.47	13.71	3	0.64	13.61	3	0.64	14.85	3.99	0.75
BCH (127,92)	5	15.04	2	0.37	12.65	4	0.81	12.62	4	0.80	13.77	4.31	0.75
BCH (127,64)	10	14.80	2	0.85	12.53	3	0.87	12.45	3	0.86	13.95	3.13	0.75
BCH (127,36)	15	17.02	1	0.28	13.71	2	0.74	13.65	2	0.72	15.35	2.43	0.75
Convolutional,r=1/2,k=7	-	16.00	2	0.66	13.17	3	0.76	13.13	3	0.74	10.88	1.53	0.75
Convolutional,r=1/3,k=7	-	15.31	1	0.31	12.76	2	0.77	12.70	2	0.77	10.40	0.91	0.75
Convolutional,r=1/4,k=7	-	15.85	1	0.48	13.30	2	0.92	13.22	2	0.90	10.88	0.77	0.75
Convolutional,r=1/8,k=7	-	17.66	1	1.00	13.34	1	0.77	13.29	1	0.75	10.88	0.39	0.75

*r = rate, k = constraint length

analysis including thermal noise. This much greater difference results from the use of a Chernoff bound in [11] to approximate the channel error probability $P_s(e)$. For convolutional codes, the situation is reversed -- the analysis in [11] predicts a requirement about 2.5 dB less than that obtained by our more nearly exact treatment. This is attributable to the assumption in [11] of a soft-decision Viterbi decoder.

With regard to the optimum diversity, the no-thermal-noise analysis of [11] often calls for too high a level of diversity when E_b/N_0 = 15 dB. But when $E_b/N_0 = \infty$, the results from [11] when rounded to the nearest positive interger are within ± 1 of the actual optimum diversity. The worst-case jamming fraction from [11] is a constant 3/4 regardless of code or diversity level. We see from Table 4-2 that as E_b/N_0 decreases, the difference between the true worst-case jamming fraction and this value increases significantly. Clearly, the effects of thermal noise can not be neglected at practical values of E_b/N_0.

4.2.2.4 M-ary Block Codes

Some numerical results for M-ary systems using FH/MFSK are shown in Figure 4-114, which plots the information-bit error probability as a function of E_b/N_J for 8-ary FSK with optimum diversity under worst-case partial-band noise jamming when E_b/N_0 = 15 dB. The codes examined are the Hamming (7,4) and Golay (23,12) binary block codes, the Reed-Solomon (7,3) 8-ary block code, and the best (as the term is used in [15]) constraint-length-7 rate-1/2 binary convolutional code. Comparison of

Figure 4-114 with Figures 4-91 and 4-111 shows that the 8-ary system outperforms the binary system by about 7 to 8 dB in E_b/N_J at $P_b(e) = 10^{-7}$. This is a marked contrast to the uncoded systems which show, at most, a difference of about 3 dB between M=2 and M=8 [7, Fig. 10]. The greater improvement for coded systems is attributable to the fact that a small decrease in error rate at the input to the decoder results in a large decrease in error rate at the decoder output.

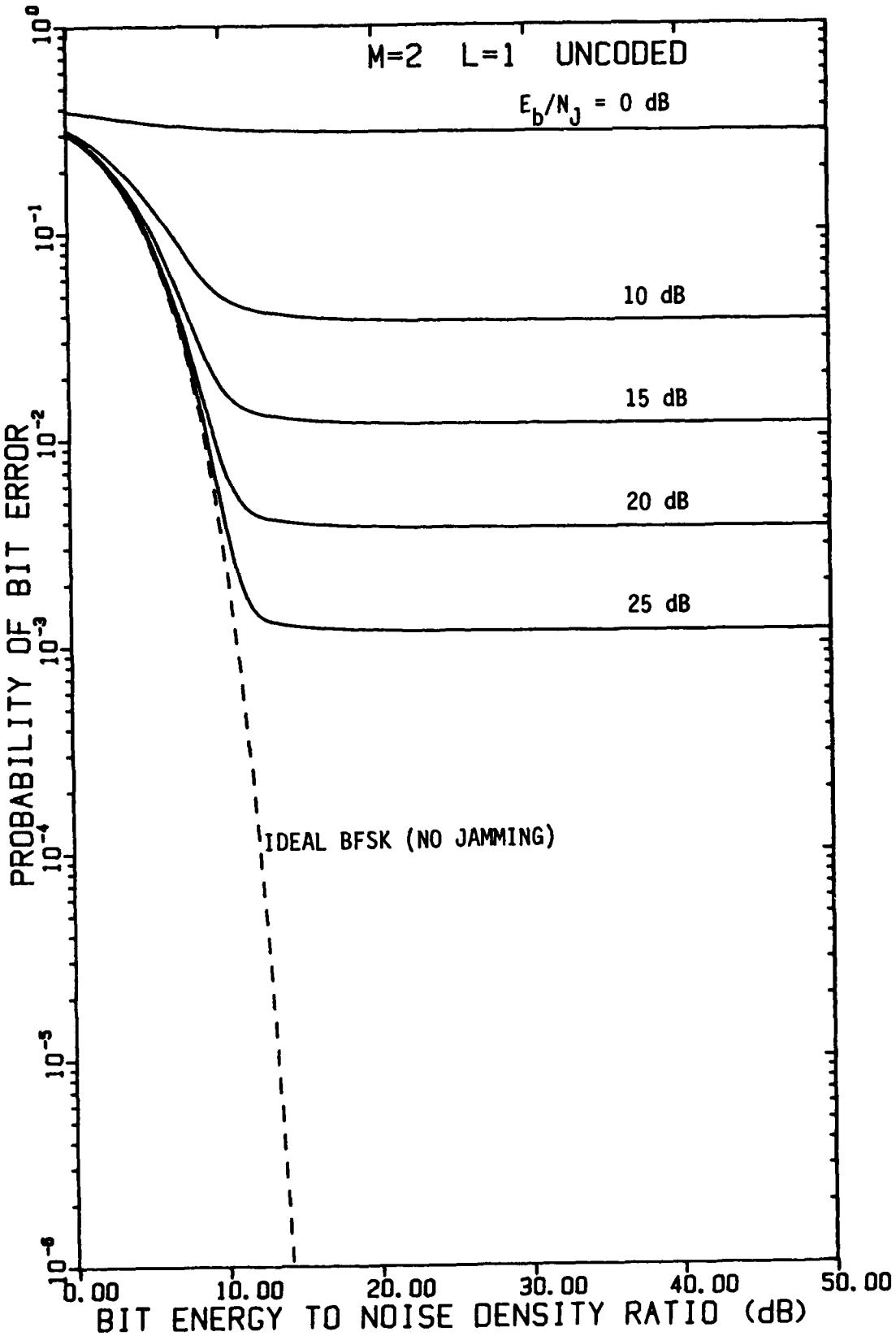

FIGURE 4-1 PERFORMANCE OF UNCODED BFSK WITH L=1 HOP/BIT AS A FUNCTION OF E_b/N_0 WITH E_b/N_J AS A PARAMETER, USING A LINEAR COMBINING DEMODULATOR, IN OPTIMUM PARTIAL-BAND NOISE JAMMING

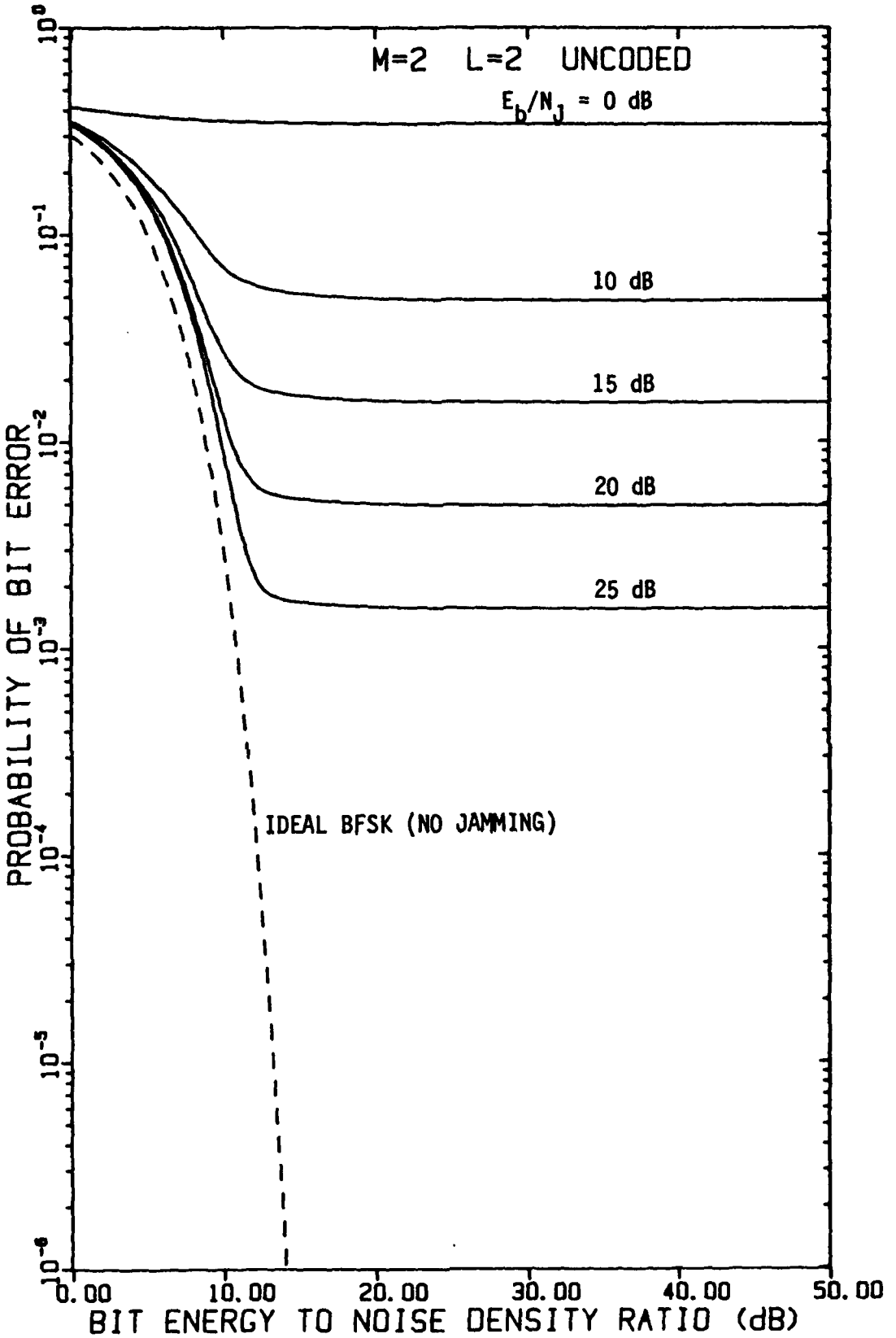

FIGURE 4-2 PERFORMANCE OF UNCODED BFSK WITH L=2 HOPS/BIT AS A FUNCTION OF E_b/N_0 WITH E_b/N_J AS A PARAMETER, USING A LINEAR COMBINING DEMODULATOR, IN OPTIMUM PARTIAL-BAND NOISE JAMMING

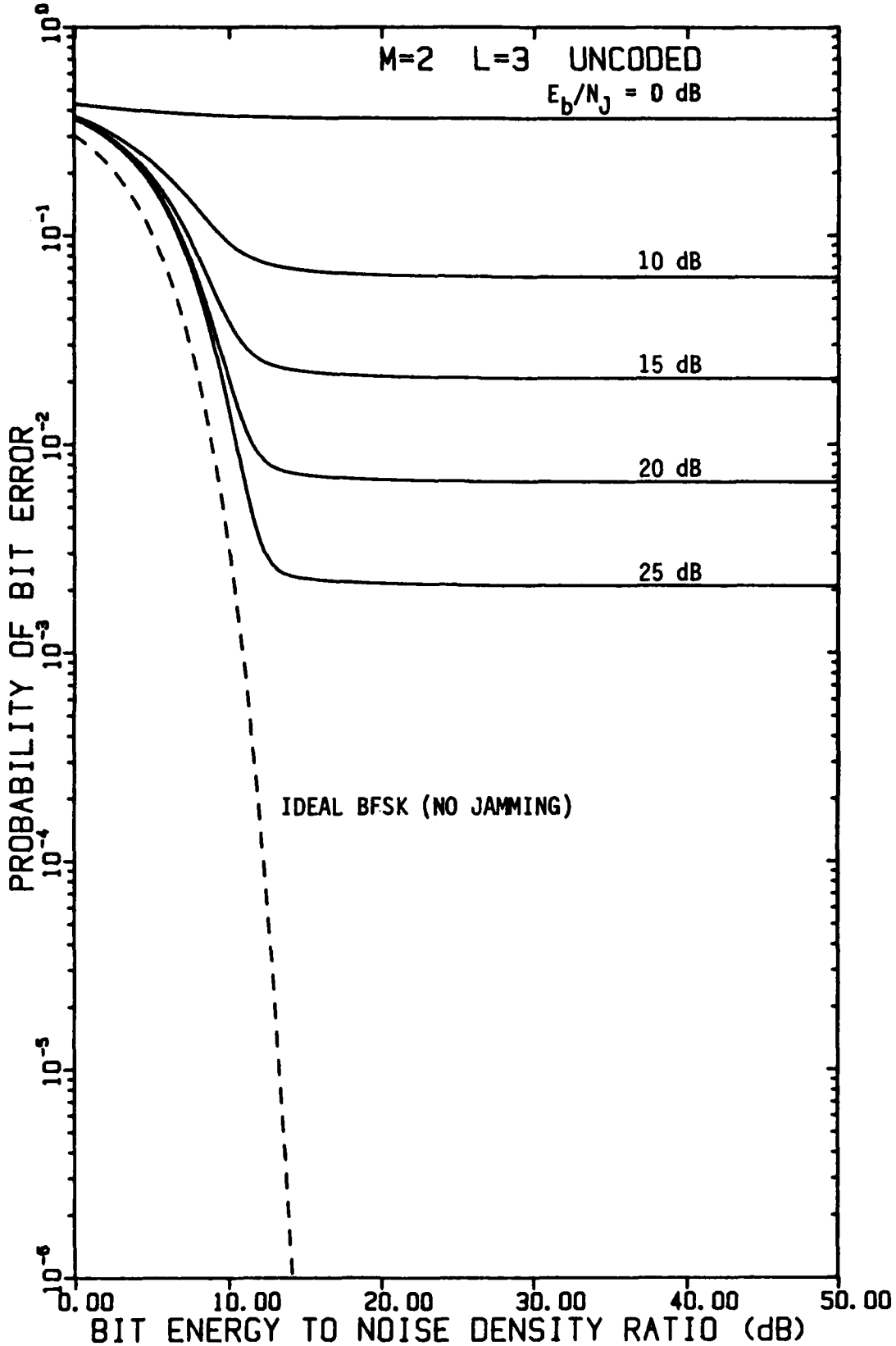

FIGURE 4-3 PERFORMANCE OF UNCODED BFSK WITH L=3 HOPS/BIT AS A FUNCTION OF E_b/N_0 WITH E_b/N_J AS A PARAMETER, USING A LINEAR COMBINING DEMODULATOR, IN OPTIMUM PARTIAL-BAND NOISE JAMMING

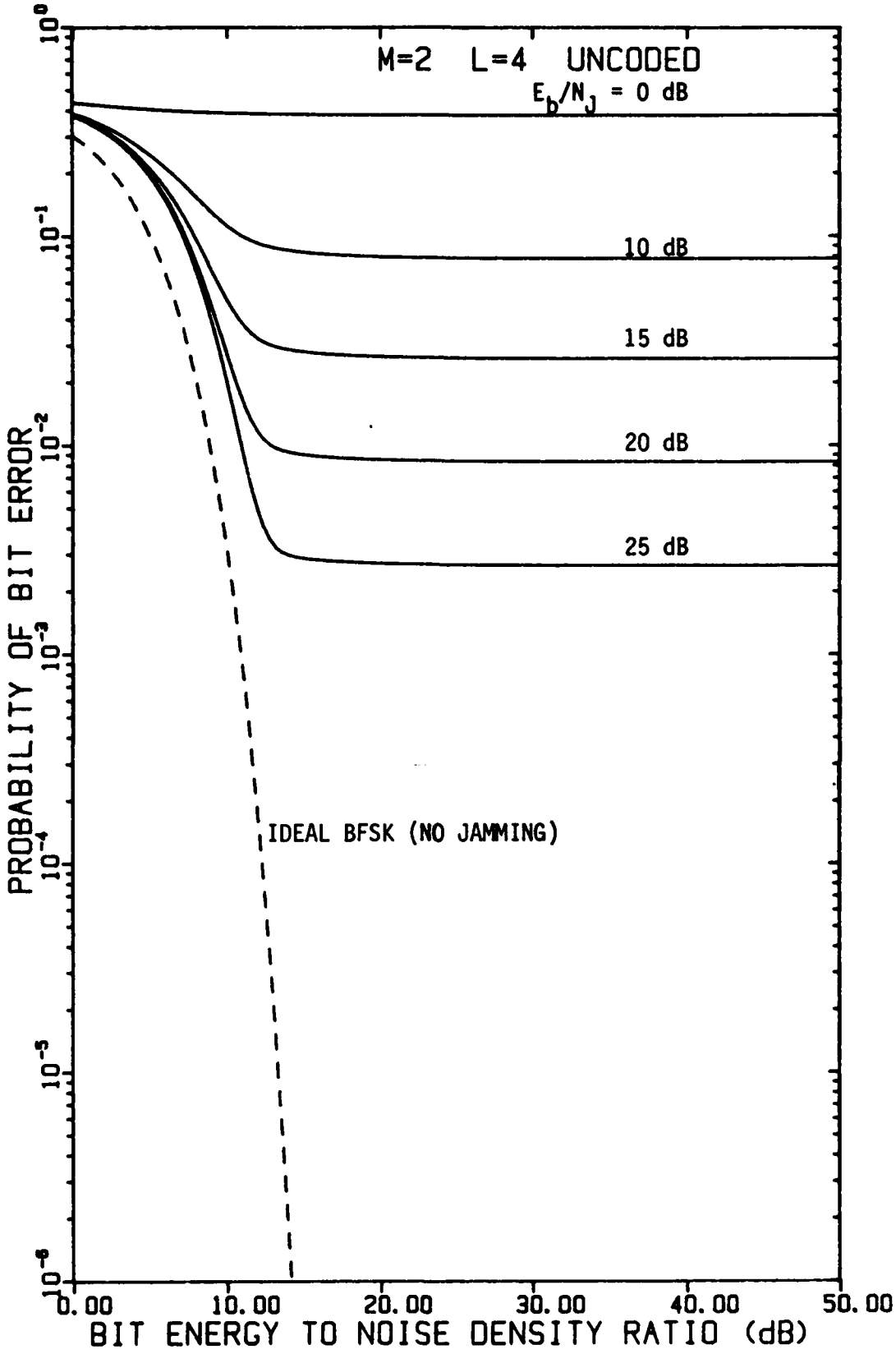

FIGURE 4-4 PERFORMANCE OF UNCODED BFSK WITH L=4 HOPS/BIT AS A FUNCTION OF E_b/N_0 WITH E_b/N_J AS A PARAMETER, USING A LINEAR COMBINING DEMODULATOR, IN OPTIMUM PARTIAL-BAND NOISE JAMMING

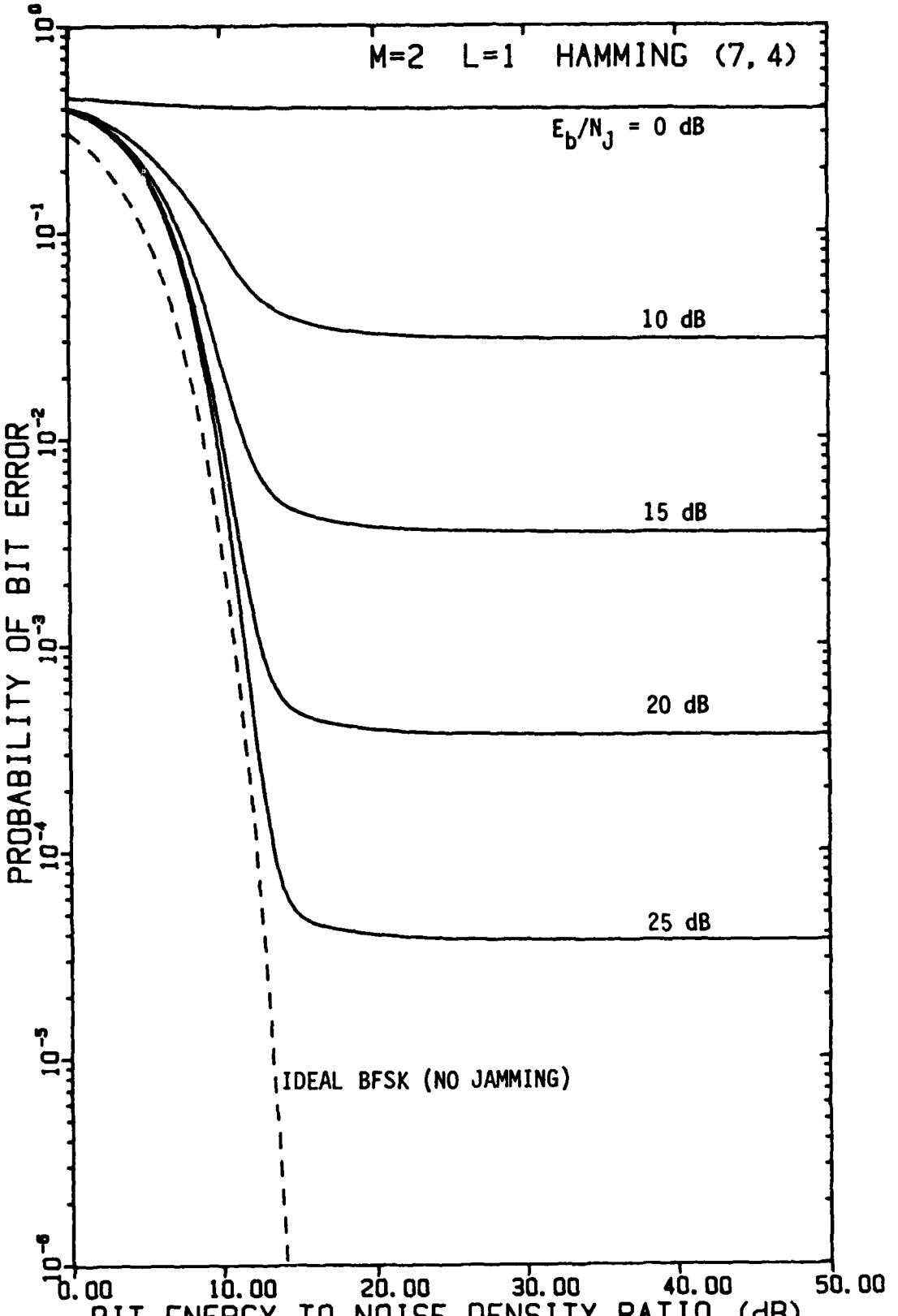

FIGURE 4-5 PERFORMANCE OF FH/BFSK WITH HAMMING (7,4) CODE AND L=1 HOPS/DIGIT AS A FUNCTION OF E_b/N_0 WITH E_b/N_J AS A PARAMETER, USING A LINEAR COMBINING DEMODULATOR, IN OPTIMUM PARTIAL-BAND NOISE JAMMING

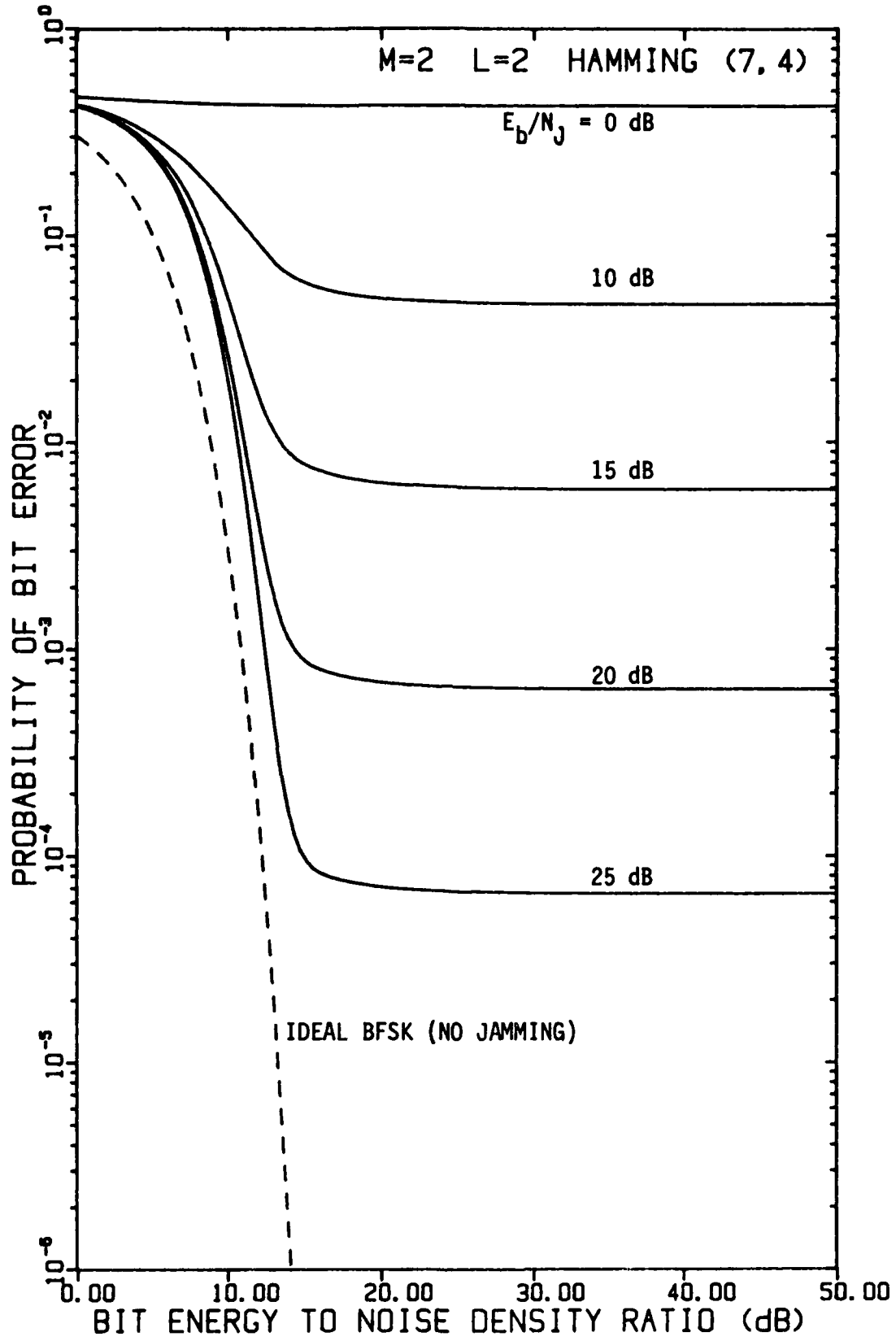

FIGURE 4-6 PERFORMANCE OF FH/BFSK WITH HAMMING (7,4) CODE AND L=2 HOPS/DIGIT AS A FUNCTION OF E_b/N_0 WITH E_b/N_J AS A PARAMETER, USING A LINEAR COMBINING DEMODULATOR, IN OPTIMUM PARTIAL-BAND NOISE JAMMING

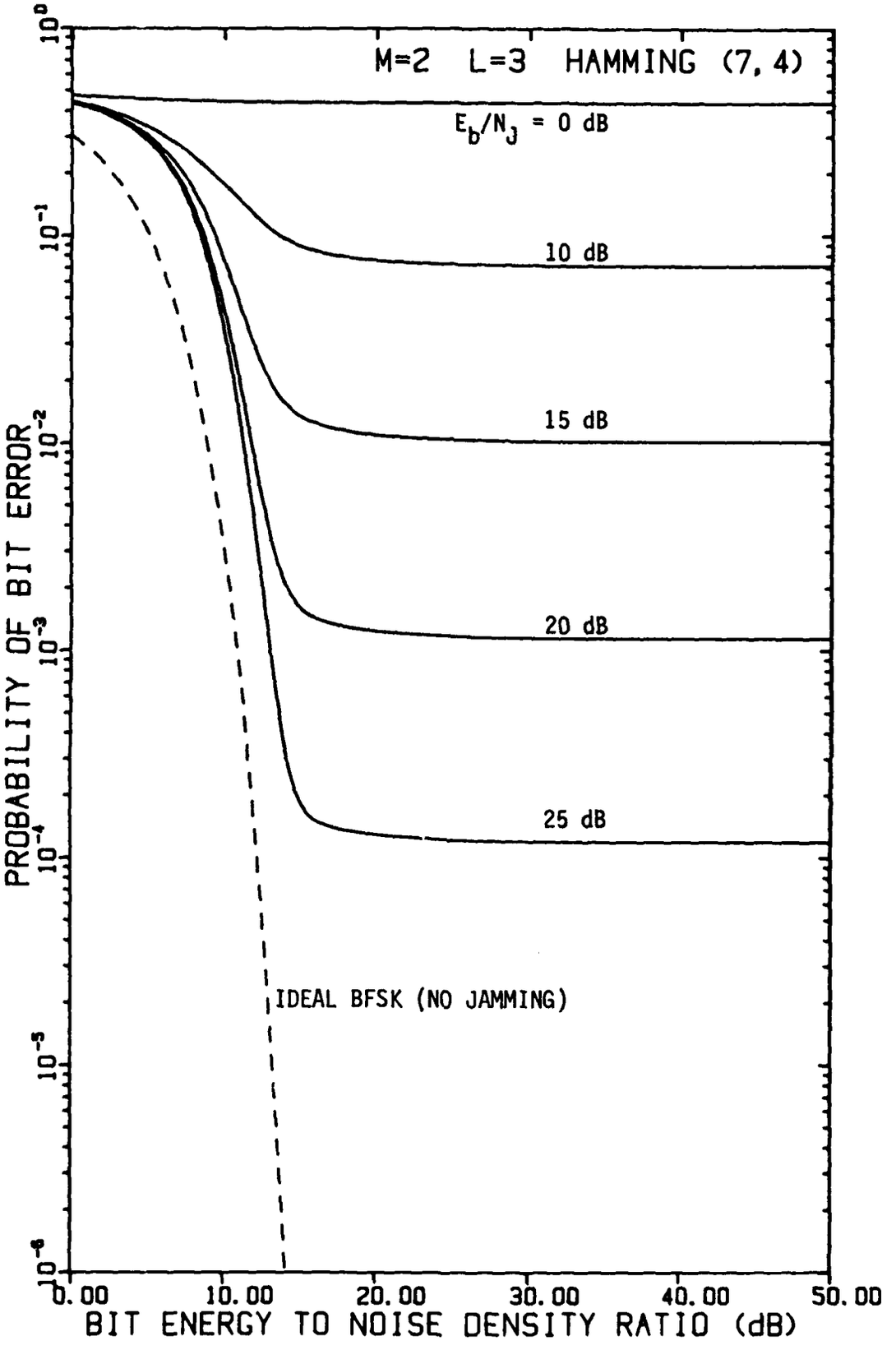

FIGURE 4-7 PERFORMANCE OF FH/BFSK WITH HAMMING (7,4) CODE AND L=3 HOPS/DIGIT AS A FUNCTION OF E_b/N_0 WITH E_b/N_J AS A PARAMETER, USING A LINEAR COMBINING DEMODULATOR, IN OPTIMUM PARTIAL-BAND NOISE JAMMING

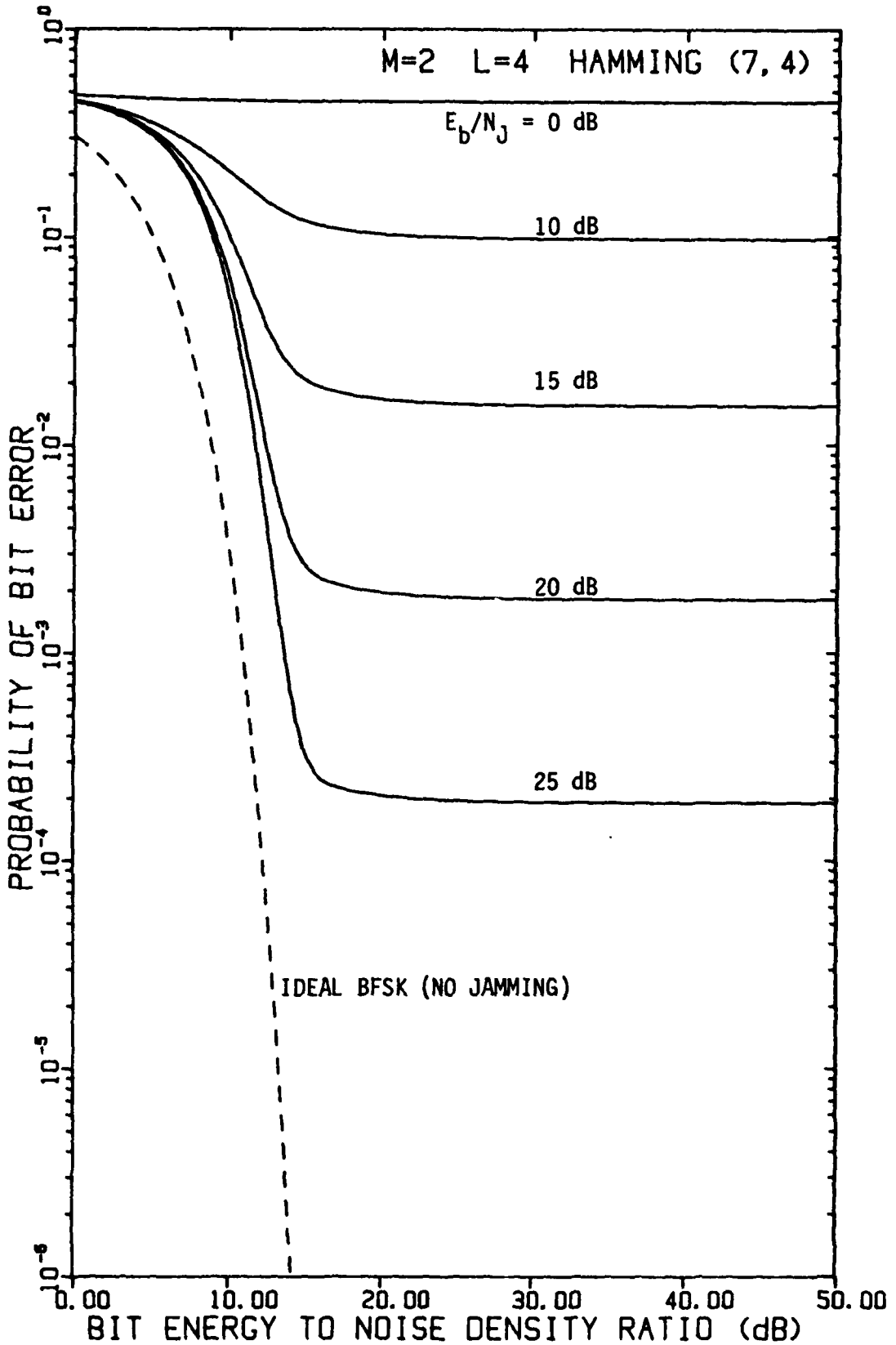

FIGURE 4-8 PERFORMANCE OF FH/BFSK WITH HAMMING (7,4) CODE AND L=4 HOPS/DIGIT AS A FUNCTION OF E_b/N_0 WITH E_b/N_J AS A PARAMETER, USING A LINEAR COMBINING DEMODULATOR, IN OPTIMUM PARTIAL-BAND NOISE JAMMING

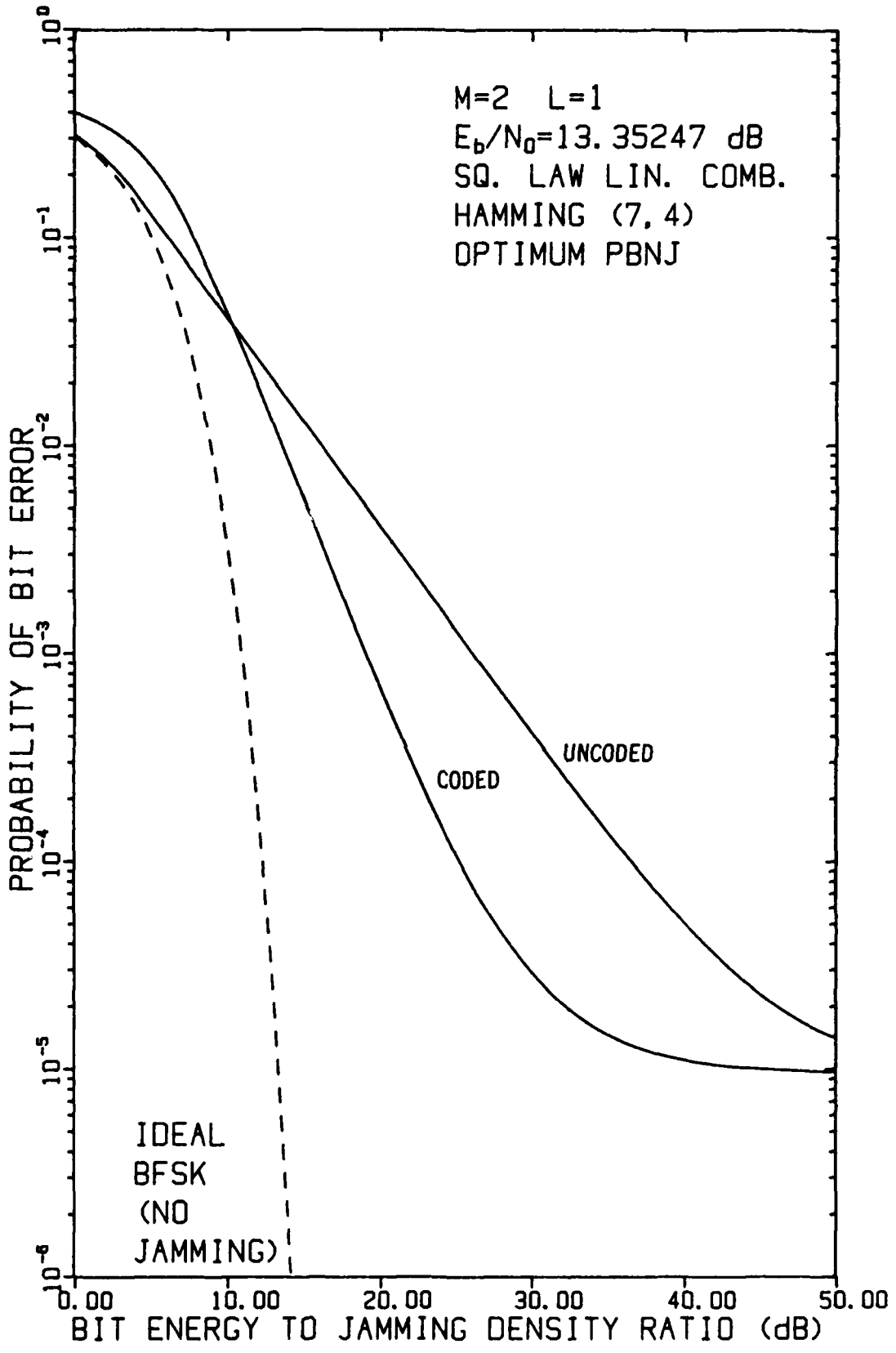

FIGURE 4-9 PERFORMANCE OF FH/BFSK WITH HAMMING (7,4) CODE AND L=1 HOP/DIGIT AS A FUNCTION OF E_b/N_J WHEN E_b/N_0 = 13.35247 dB, USING A LINEAR COMBINING DEMODULATOR, IN OPTIMUM PARTIAL-BAND NOISE JAMMING

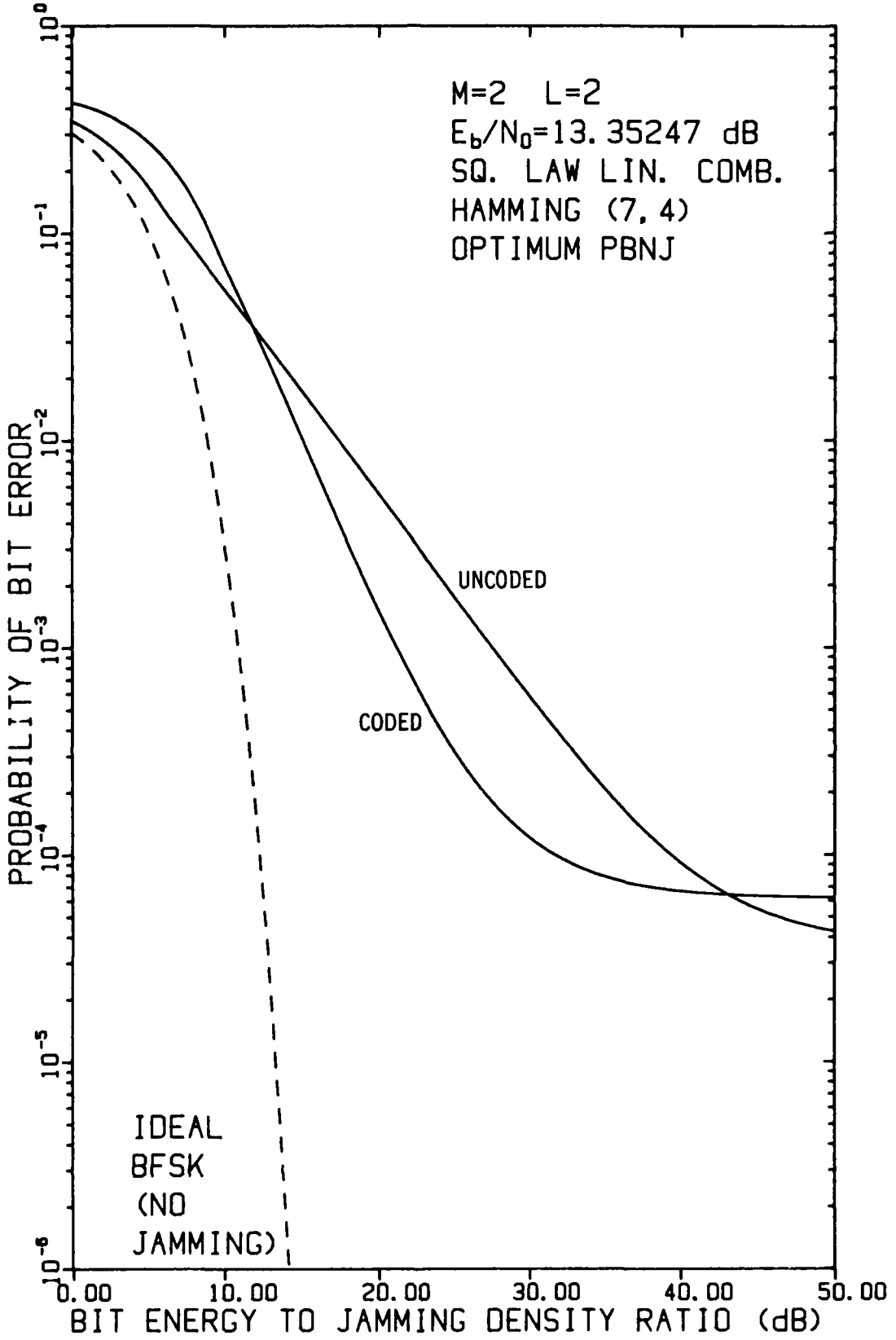

FIGURE 4-10 PERFORMANCE OF FH/BFSK WITH HAMMING (7,4) CODE AND L=2 HOPS/DIGIT AS A FUNCTION OF E_b/N_J WHEN E_b/N_0 = 13.35247 dB, USING A LINEAR COMBINING DEMODULATOR, IN OPTIMUM PARTIAL-BAND NOISE JAMMING

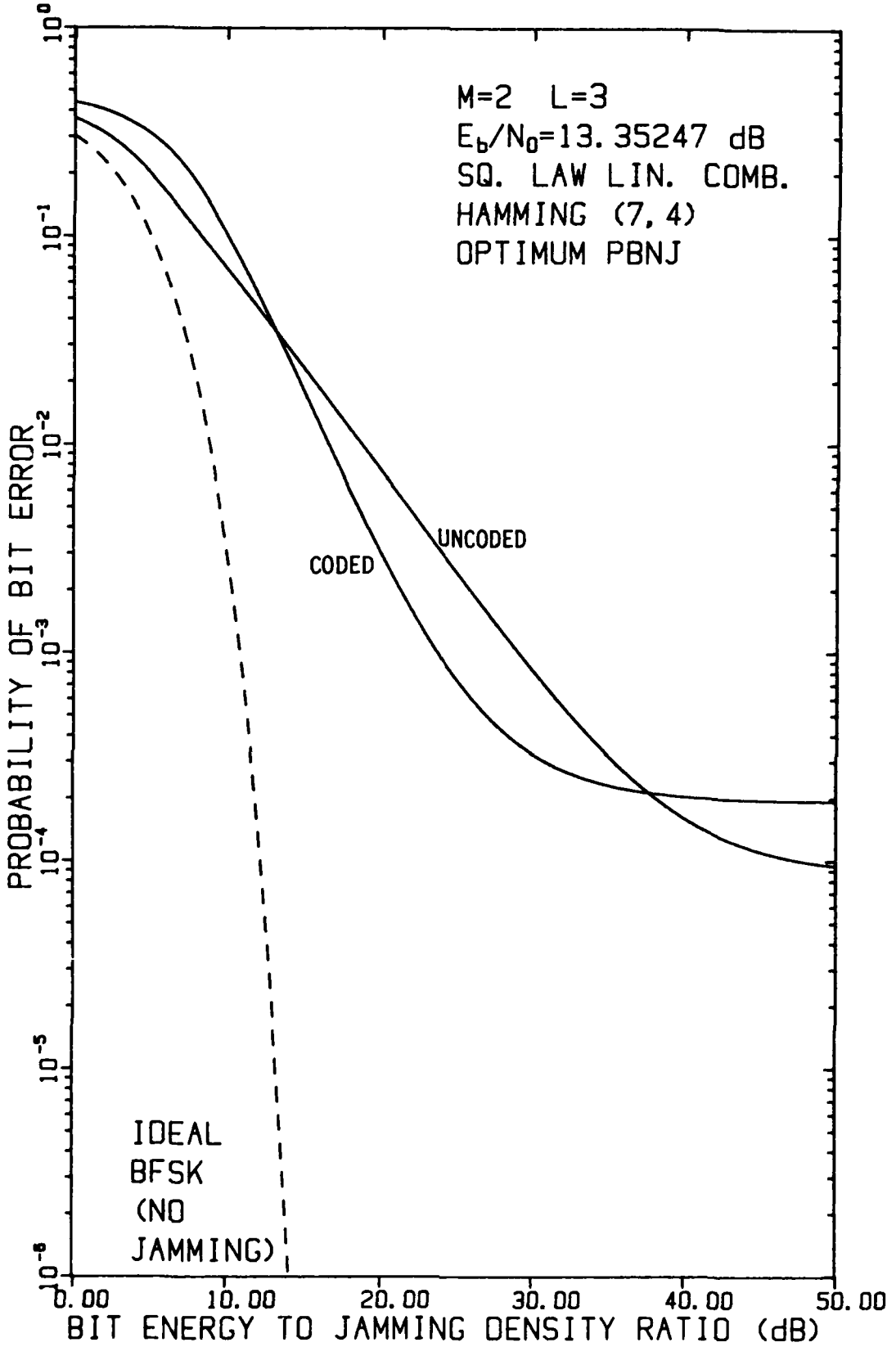

FIGURE 4-11 PERFORMANCE OF FH/BFSK WITH HAMMING (7,4) CODE AND L=3 HOPS/DIGIT AS A FUNCTION OF E_b/N_J WHEN E_b/N_0 = 13.35247 dB, USING A LINEAR COMBINING DEMODULATOR, IN OPTIMUM PARTIAL-BAND NOISE JAMMING

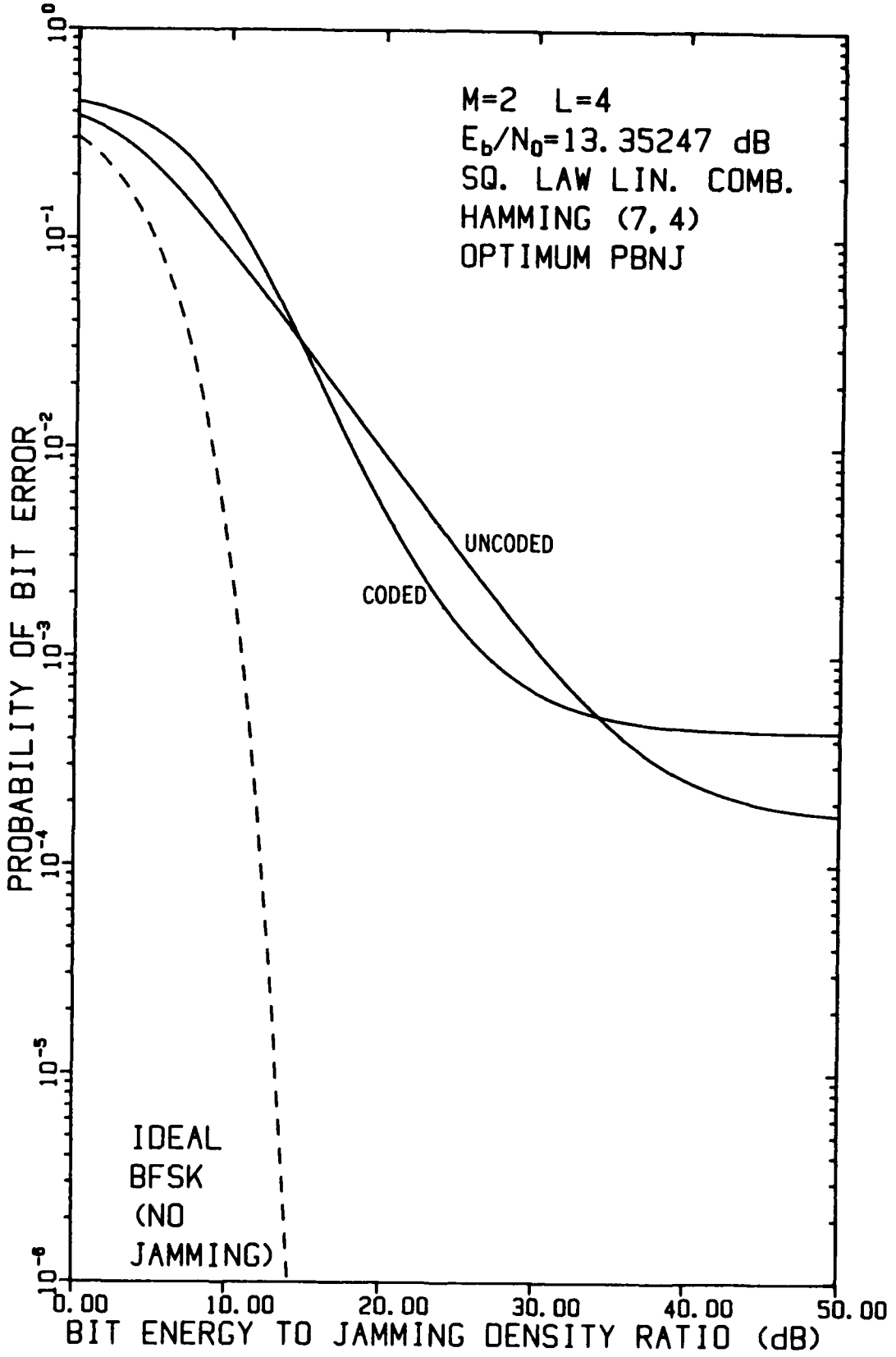

FIGURE 4-12 PERFORMANCE OF FH/BFSK WITH HAMMING (7,4) CODE AND L=4 HOPS/DIGIT AS A FUNCTION OF E_b/N_J WHEN E_b/N_0 = 13.35247 dB, USING A LINEAR COMBINING DEMODULATOR, IN OPTIMUM PARTIAL-BAND NOISE JAMMING

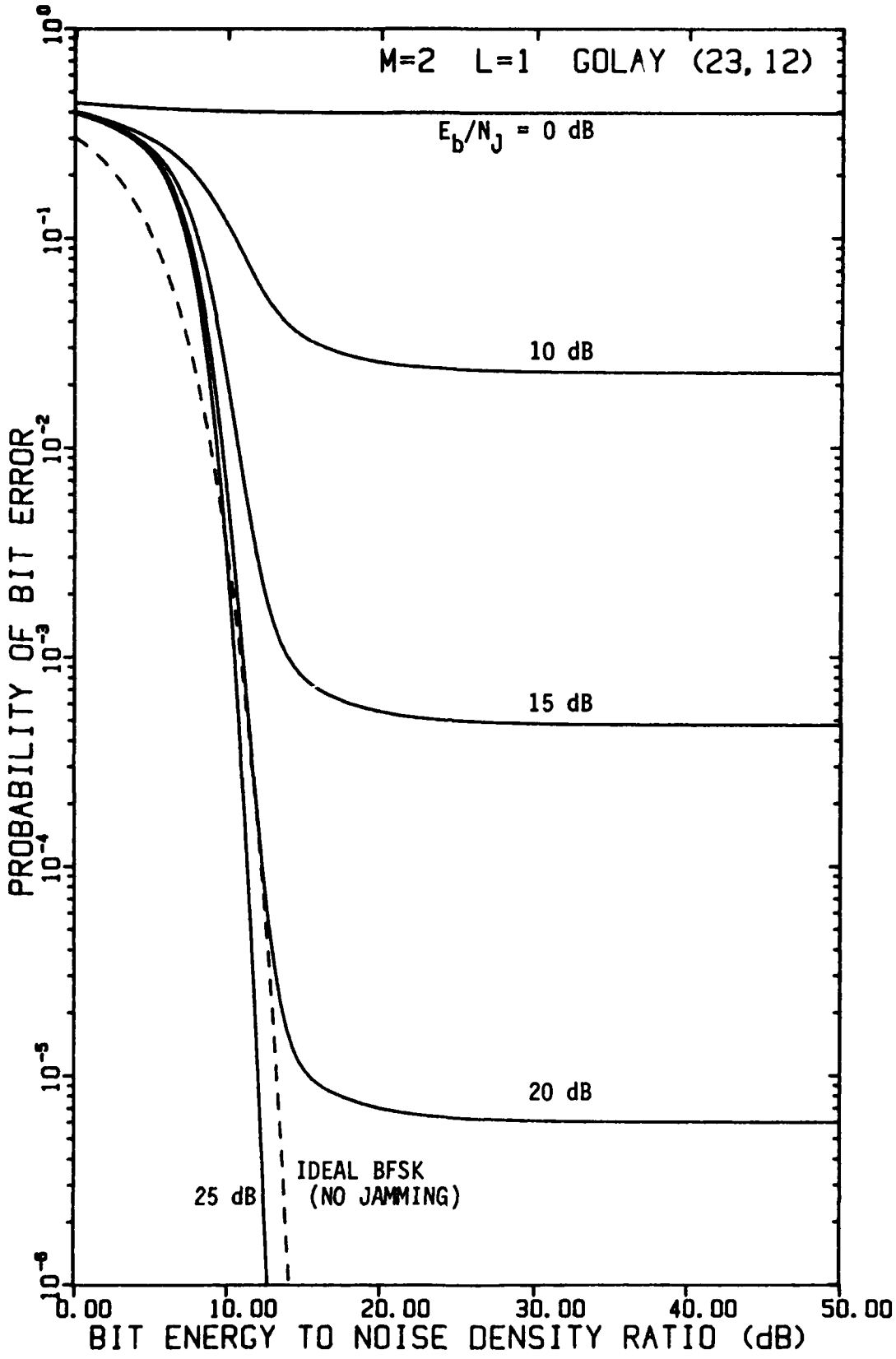

FIGURE 4-13 PERFORMANCE OF FH/BFSK WITH GOLAY (23,12) CODE AND L=1 HOP/DIGIT AS A FUNCTION OF E_b/N_0 WITH E_b/N_J AS A PARAMETER, USING A LINEAR COMBINING DEMODULATOR, IN OPTIMUM PARTIAL-BAND NOISE JAMMING

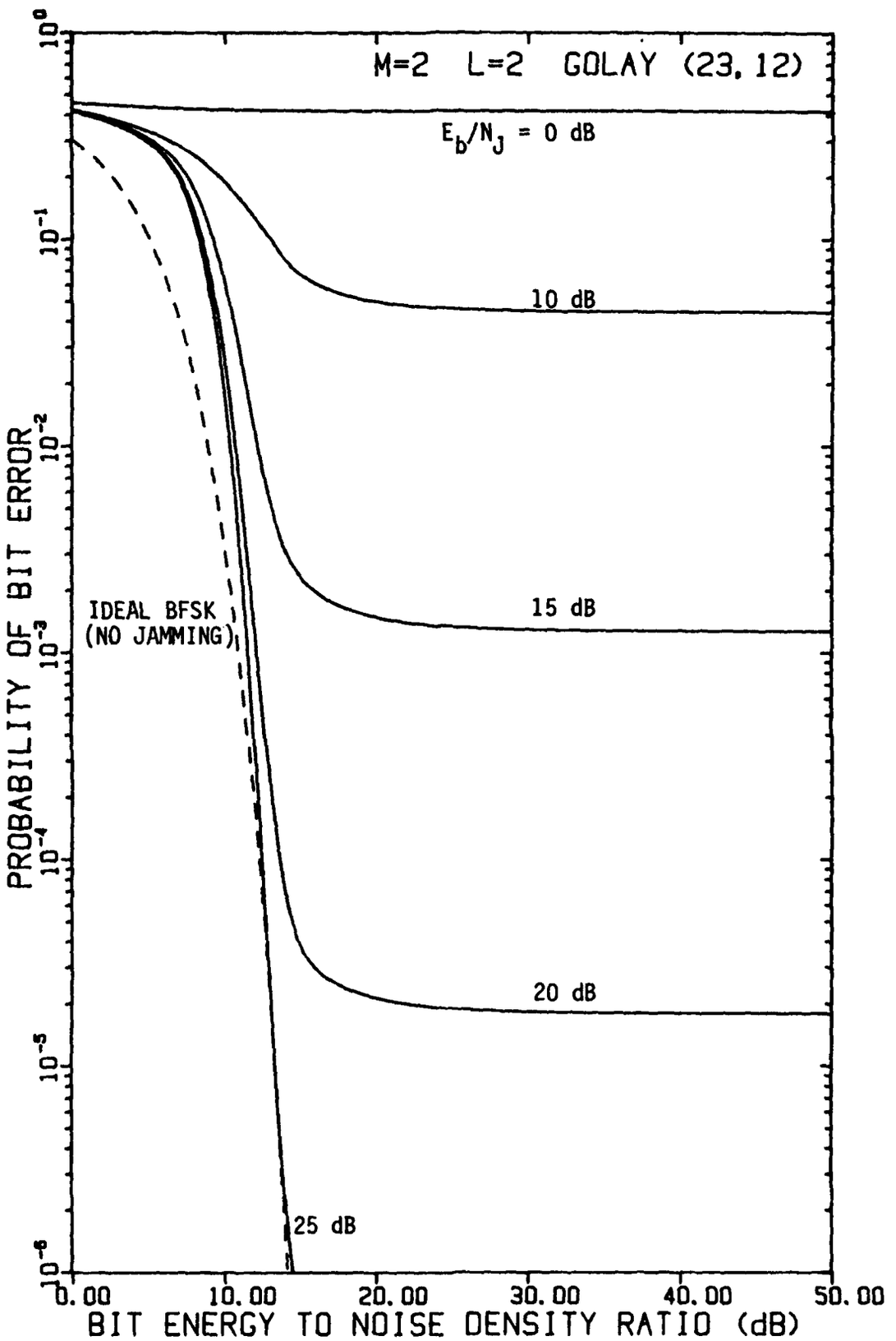

FIGURE 4-14 PERFORMANCE OF FH/BFSK WITH GOLAY (23,12) CODE AND L=2 HOPS/DIGIT AS A FUNCTION OF E_b/N_0 WITH E_b/N_J AS A PARAMETER, USING A LINEAR COMBINING DEMODULATOR, IN OPTIMUM PARTIAL-BAND NOISE JAMMING

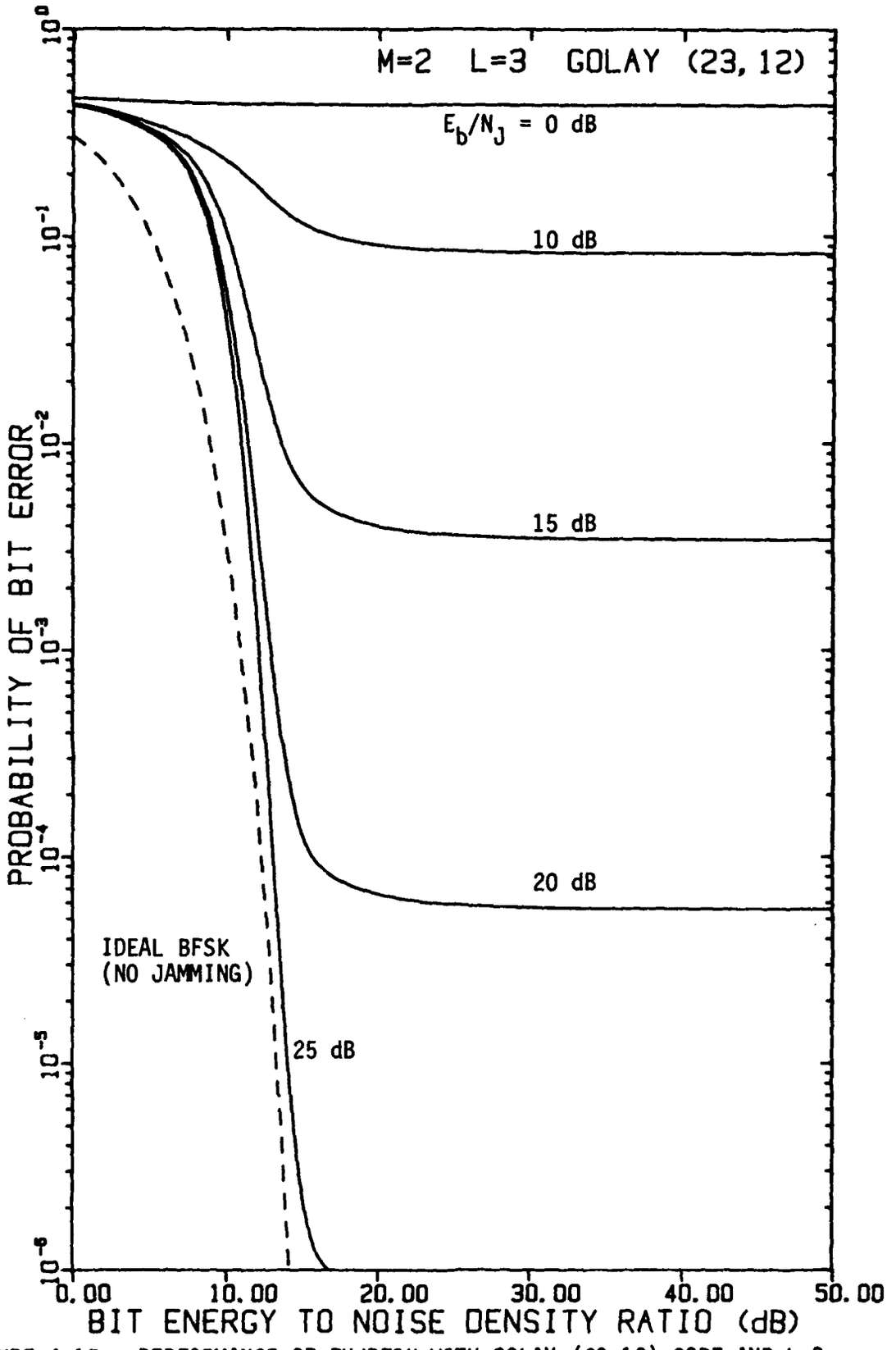

FIGURE 4-15 PERFORMANCE OF FH/BFSK WITH GOLAY (23,12) CODE AND L=3 HOPS/DIGIT AS A FUNCTION OF E_b/N_0 WITH E_b/N_J AS A PARAMETER, USING A LINEAR COMBINING DEMODULATOR, IN OPTIMUM PARTIAL-BAND NOISE JAMMING

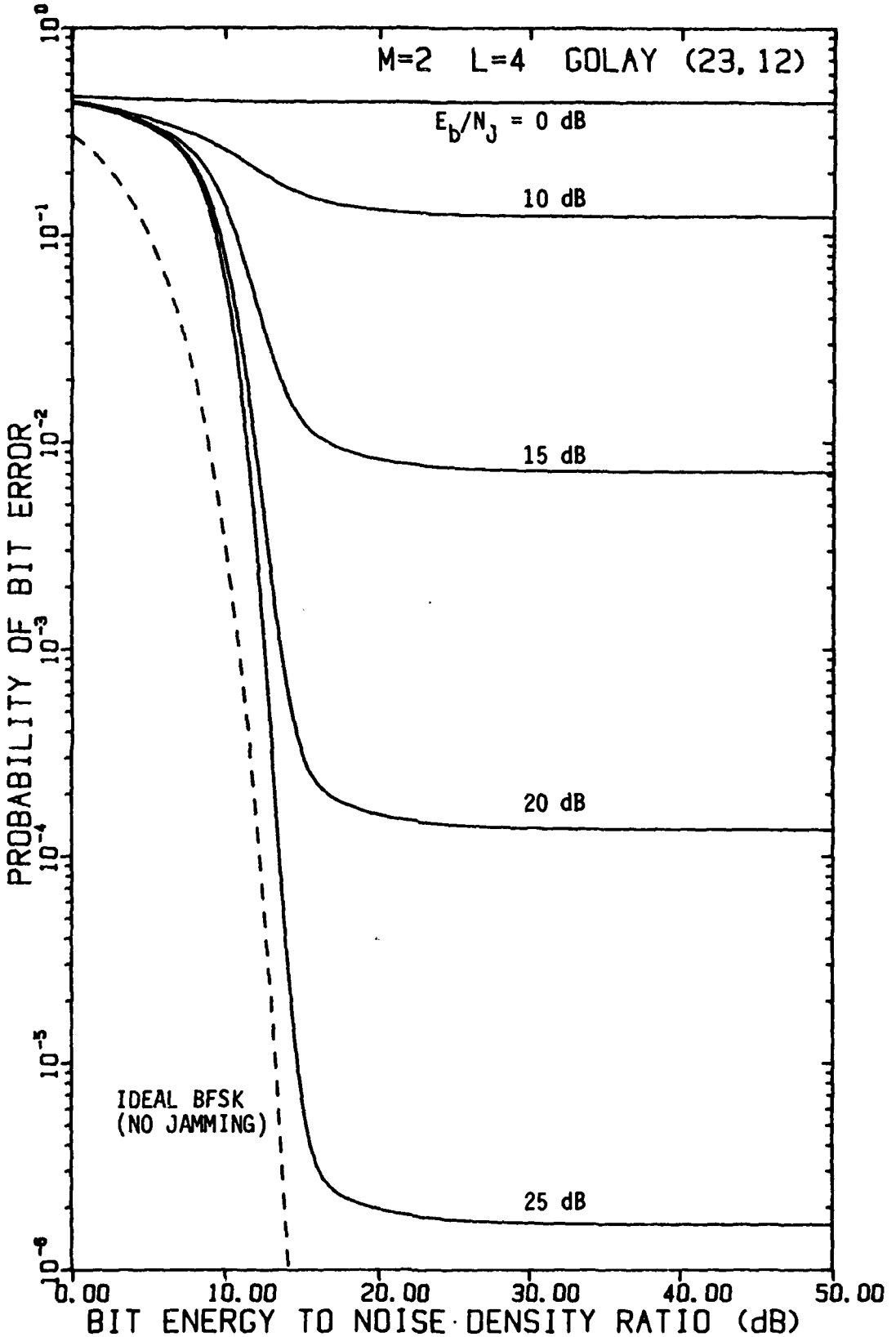

FIGURE 4-16 PERFORMANCE OF FH/BFSK WITH GOLAY (23,12) CODE AND L=4 HOPS/DIGIT AS A FUNCTION OF E_b/N_0 WITH E_b/N_J AS A PARAMETER, USING A LINEAR COMBINING DEMODULATOR, IN OPTIMUM PARTIAL-BAND NOISE JAMMING

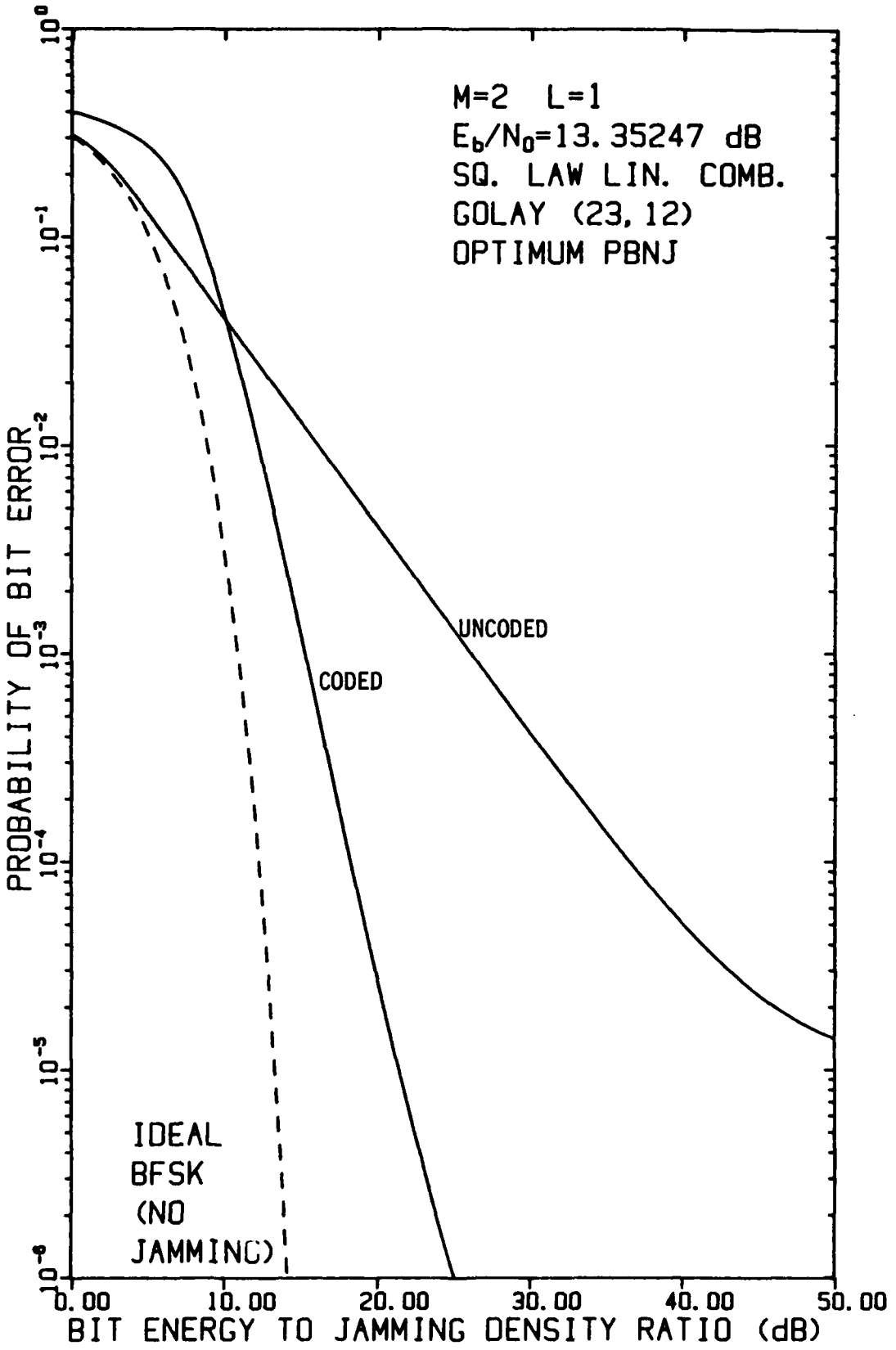

FIGURE 4-17 PERFORMANCE OF FH/BFSK WITH GOLAY (23,12) CODE AND L=1 HOP/DIGIT AS A FUNCTION OF E_b/N_J WHEN E_b/N_0 = 13.35247 dB, USING A LINEAR COMBINING DEMODULATOR, IN OPTIMUM PARTIAL-BAND NOISE JAMMING

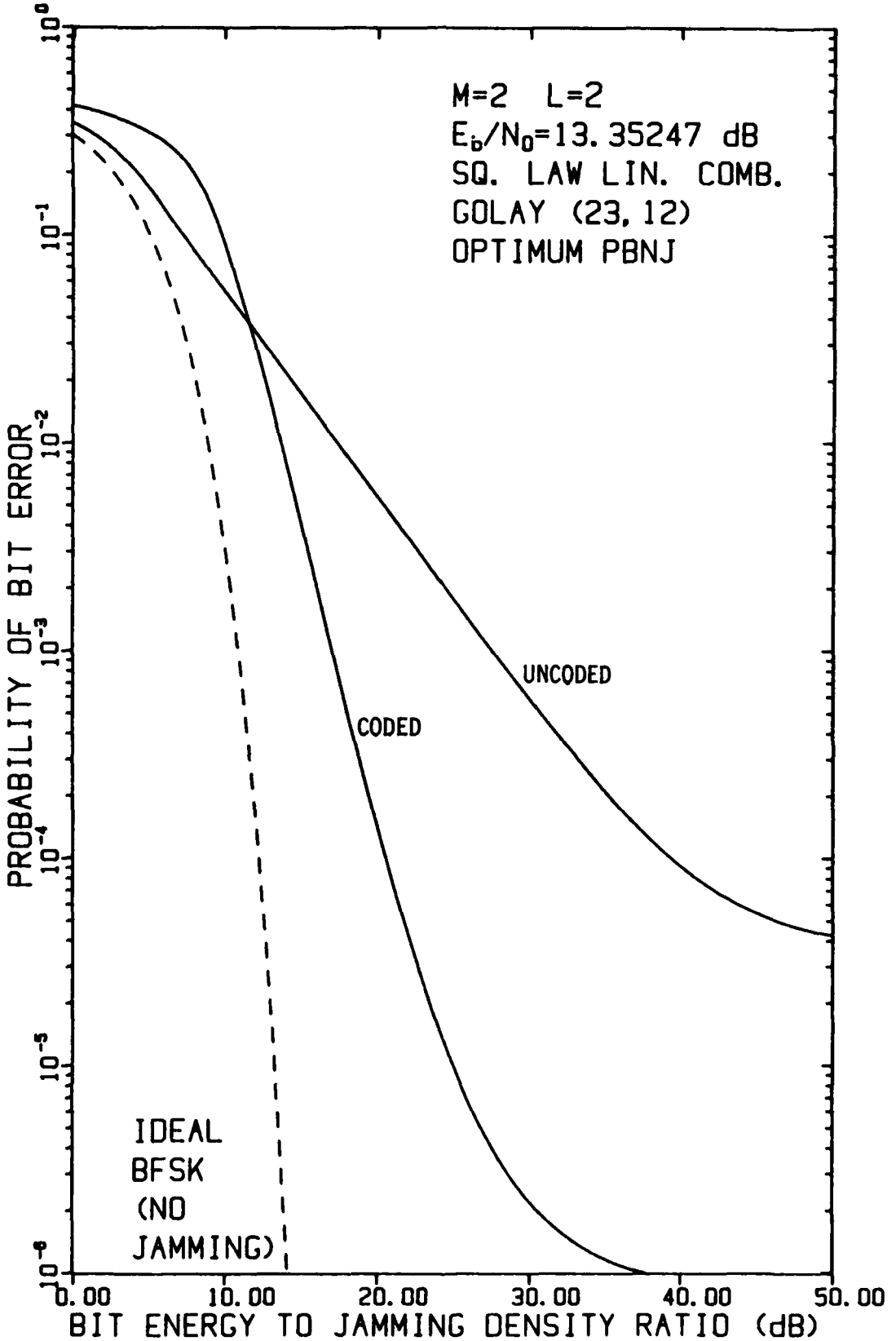

FIGURE 4-18 PERFORMANCE OF FH/BFSK WITH GOLAY (23,12) CODE AND L=2 HOPS/DIGIT AS A FUNCTION OF E_b/N_J WHEN E_b/N_0 = 13.35247 dB, USING A LINEAR COMBINING DEMODULATOR, IN OPTIMUM PARTIAL-BAND NOISE JAMMING

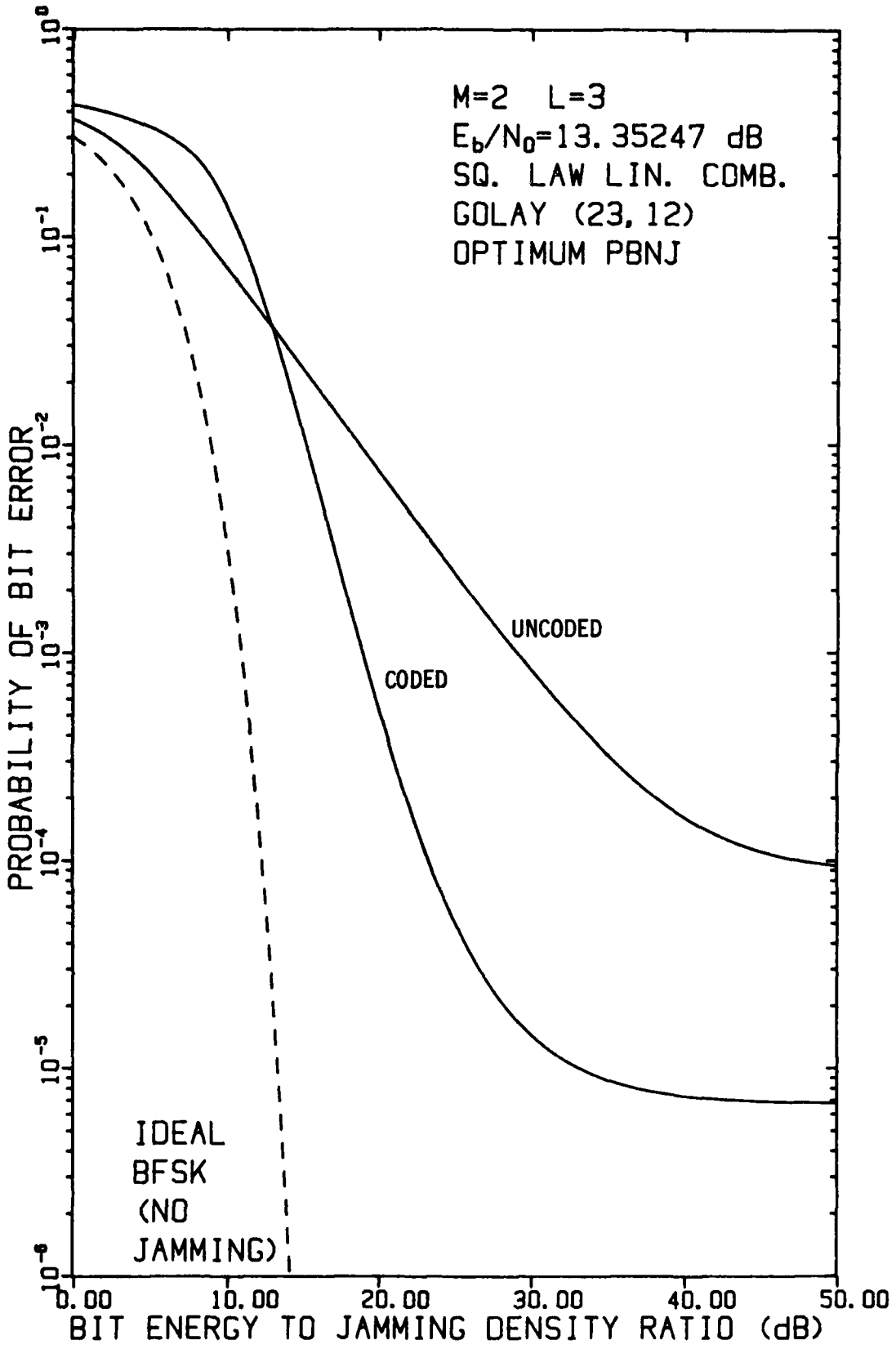

FIGURE 4-19 PERFORMANCE OF FH/BFSK WITH GOLAY (23,12) CODE AND L=3 HOPS/DIGIT AS A FUNCTION OF E_b/N_J WHEN E_b/N_0 = 13.35247 dB, USING A LINEAR COMBINING DEMODULATOR, IN OPTIMUM PARTIAL-BAND NOISE JAMMING

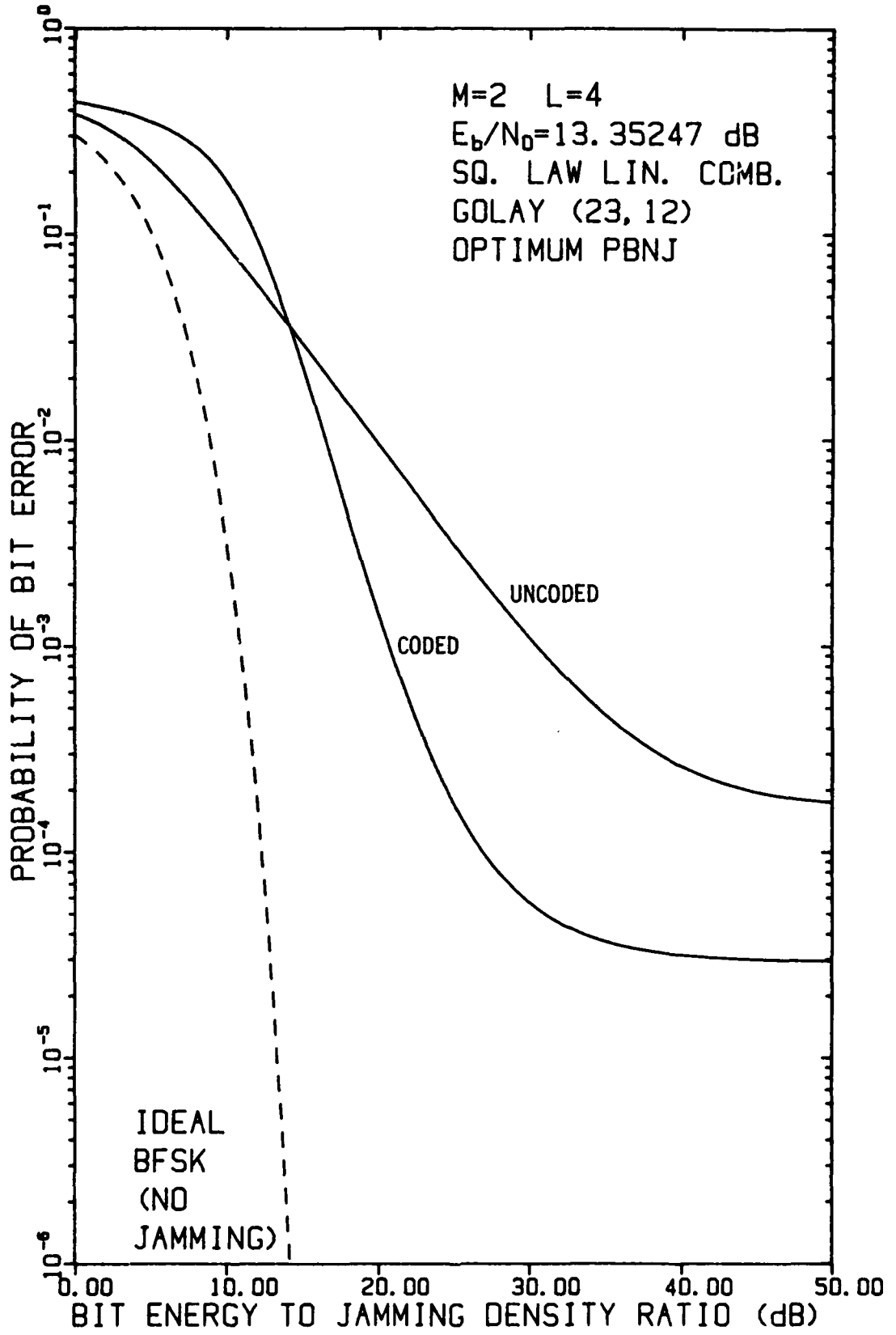

FIGURE 4-20 PERFORMANCE OF FH/BFSK WITH GOLAY (23,12) CODE AND L=4 HOPS/DIGIT AS A FUNCTION OF E_b/N_J WHEN E_b/N_0 = 13.35247 dB, USING A LINEAR COMBINING DEMODULATOR, IN OPTIMUM PARTIAL-BAND NOISE JAMMING

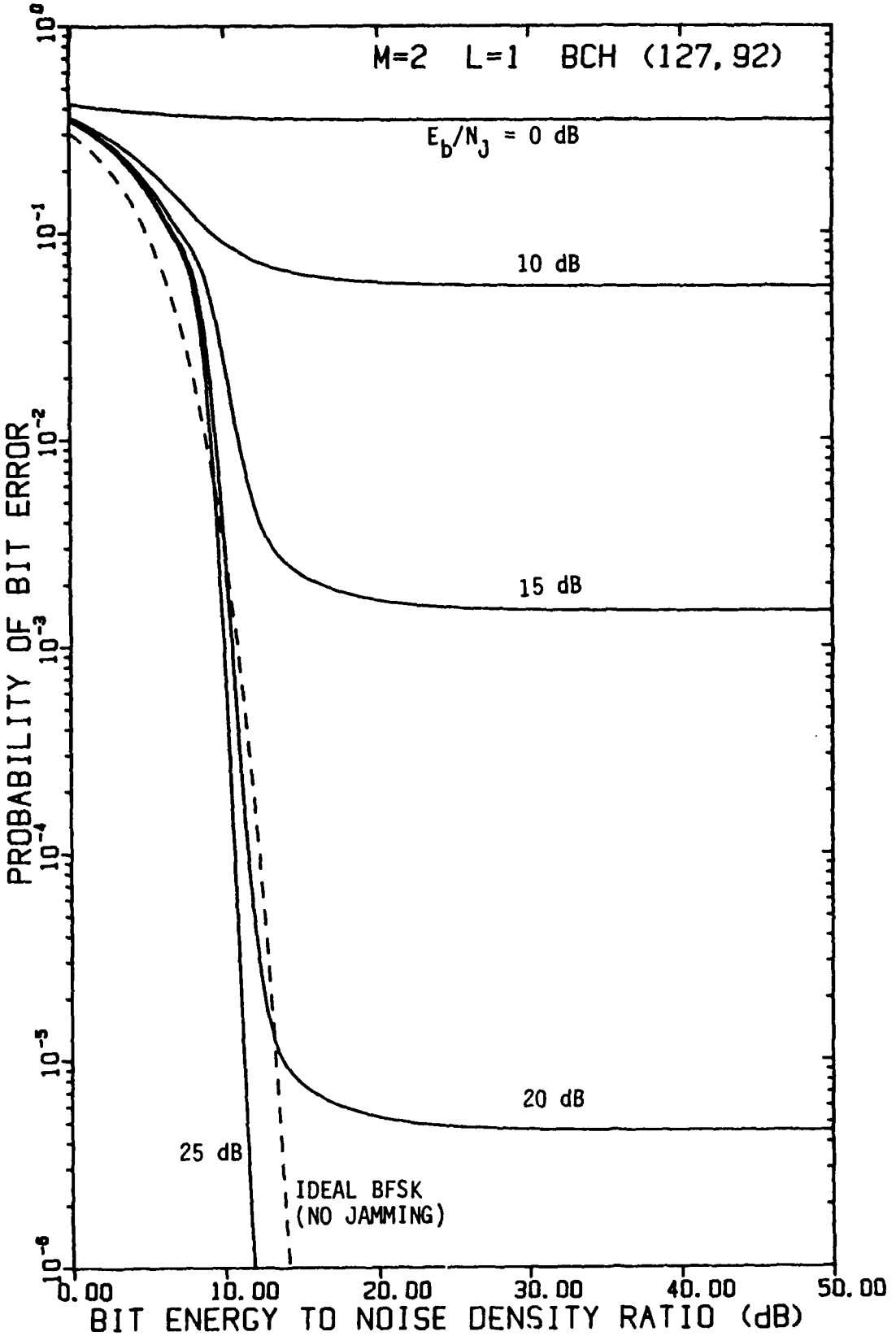

FIGURE 4-21 PERFORMANCE OF FH/BFSK WITH BCH (127,92) CODE AND L=1 HOP/DIGIT AS A FUNCTION OF E_b/N_0 WITH E_b/N_J AS A PARAMETER, USING A LINEAR COMBINING DEMODULATOR, IN OPTIMUM PARTIAL-BAND NOISE JAMMING

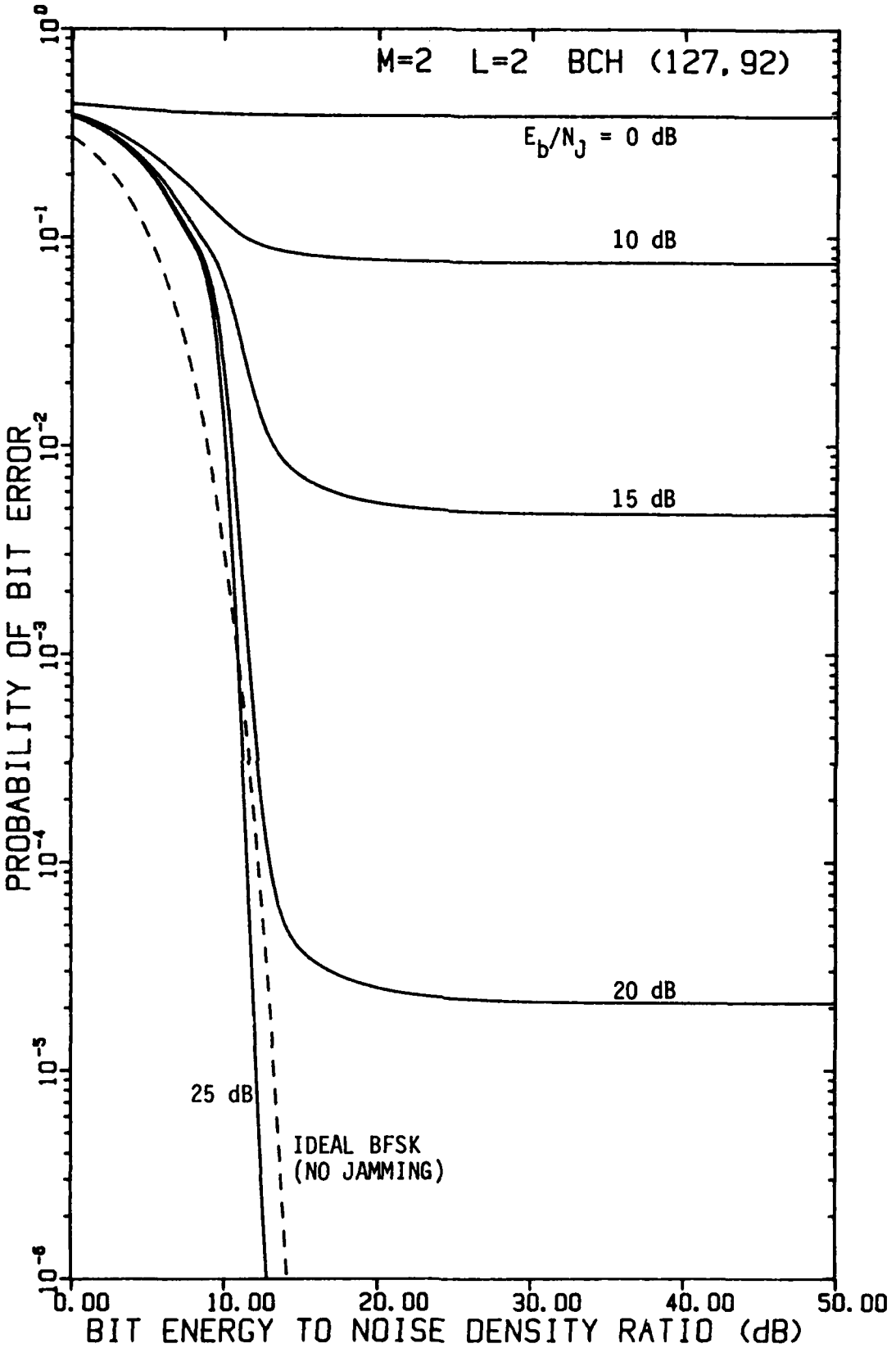

FIGURE 4-22 PERFORMANCE OF FH/BFSK WITH BCH (127,92) CODE AND L=2 HOPS/DIGIT AS A FUNCTION OF E_b/N_0 WITH E_b/N_J AS A PARAMETER, USING A LINEAR COMBINING DEMODULATOR, IN OPTIMUM PARTIAL-BAND NOISE JAMMING

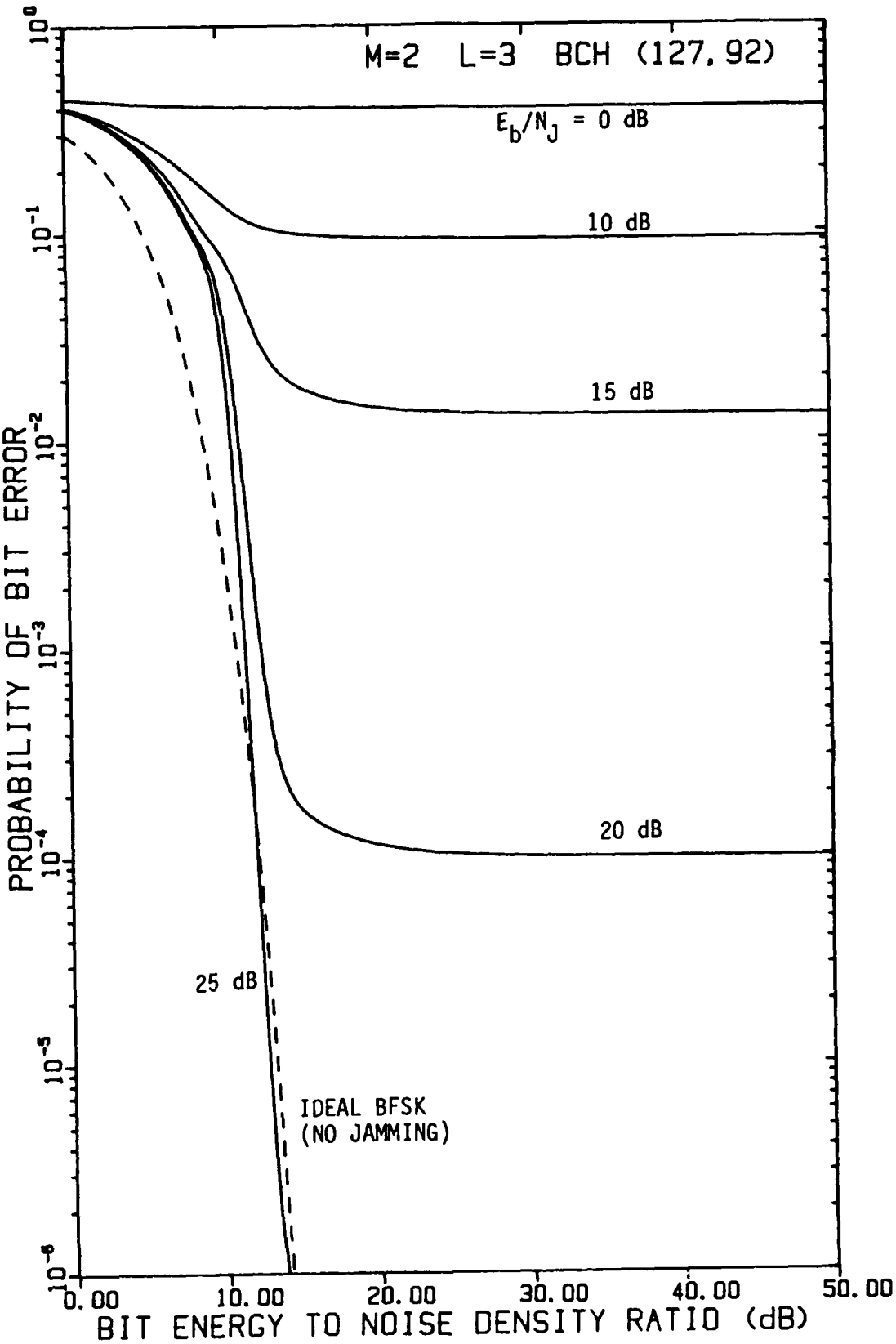

FIGURE 4-23 PERFORMANCE OF FH/BFSK WITH BCH (127,92) CODE AND L=3 HOPS/DIGIT AS A FUNCTION OF E_b/N_0 WITH E_b/N_J AS A PARAMETER, USING A LINEAR COMBINING DEMODULATOR, IN OPTIMUM PARTIAL-BAND NOISE JAMMING

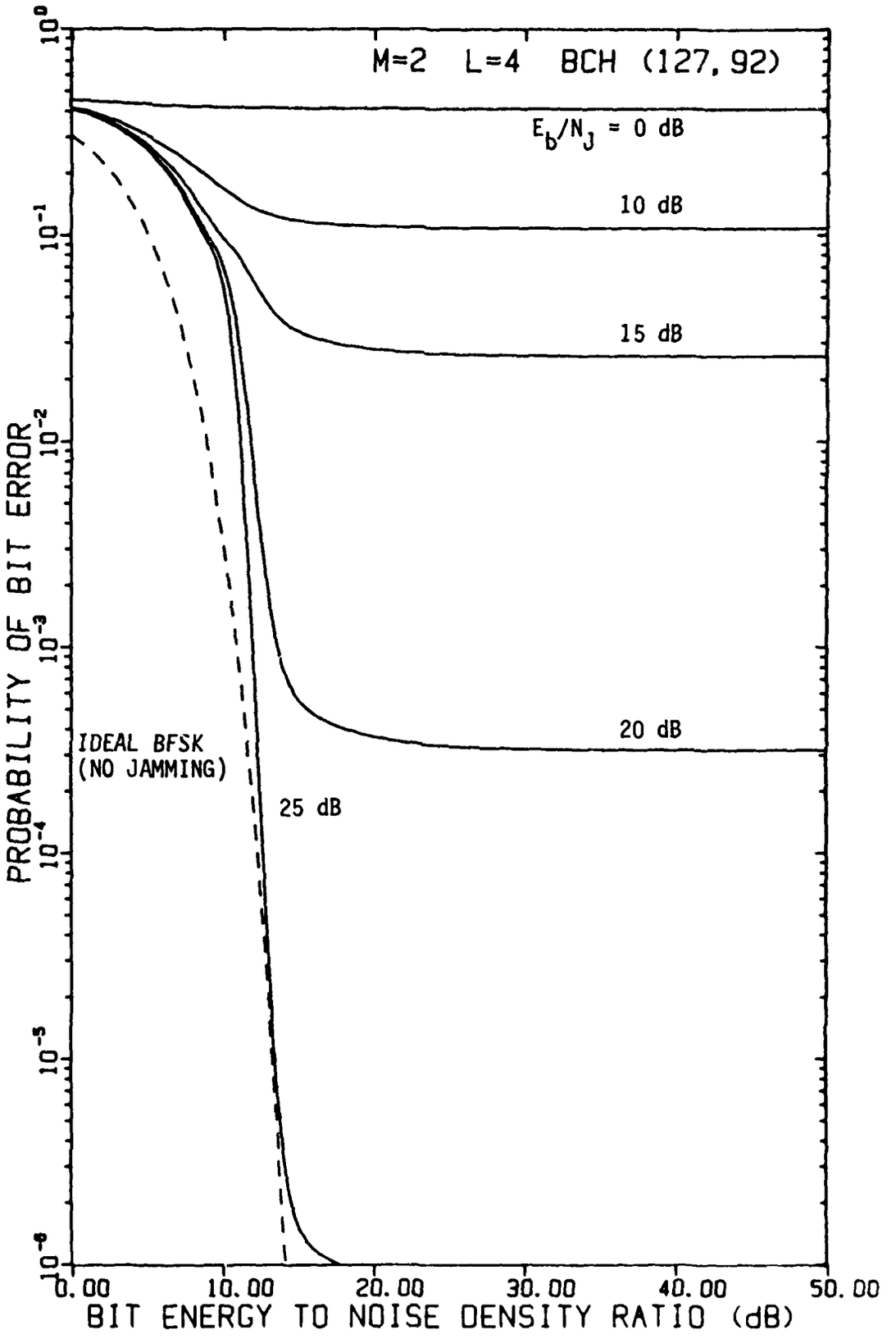

FIGURE 4-24 PERFORMANCE OF FH/BFSK WITH BCH (127,92) CODE AND L=4 HOPS/DIGIT AS A FUNCTION OF E_b/N_0 WITH E_b/N_J AS A PARAMETER, USING A LINEAR COMBINING DEMODULATOR, IN OPTIMUM PARTIAL-BAND NOISE JAMMING

AD-A182 136 PERFORMANCE ANALYSIS OF FREQUENCY HOPPING MFSK (M-ARY FREQUENCY-SHIFT-KEY..(U) LEE (J S) ASSOCIATES INC ARLINGTON VA J S LEE ET AL. JUN 87 JC-2040-N 2/2

UNCLASSIFIED N00014-86-C-0279 F/G 9/1 NL

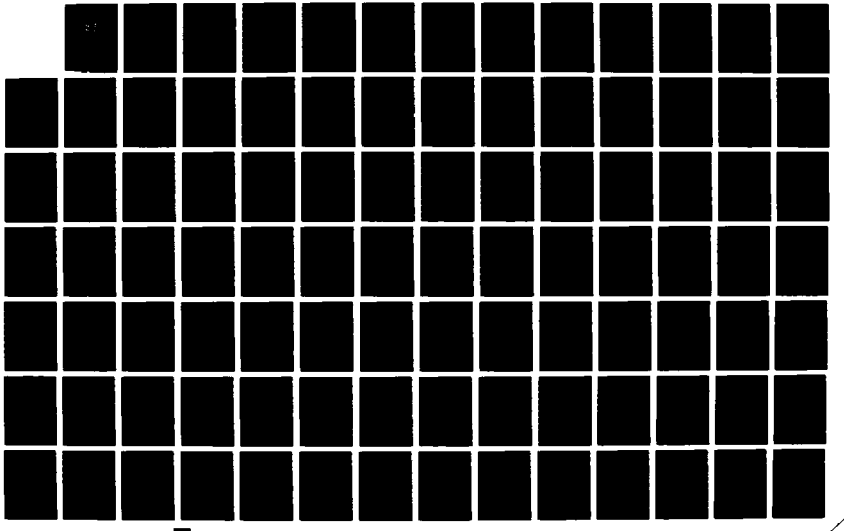

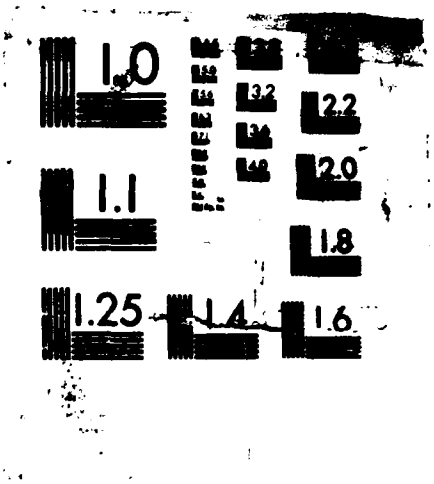

MICROCOPY RESOLUTION TEST CHART

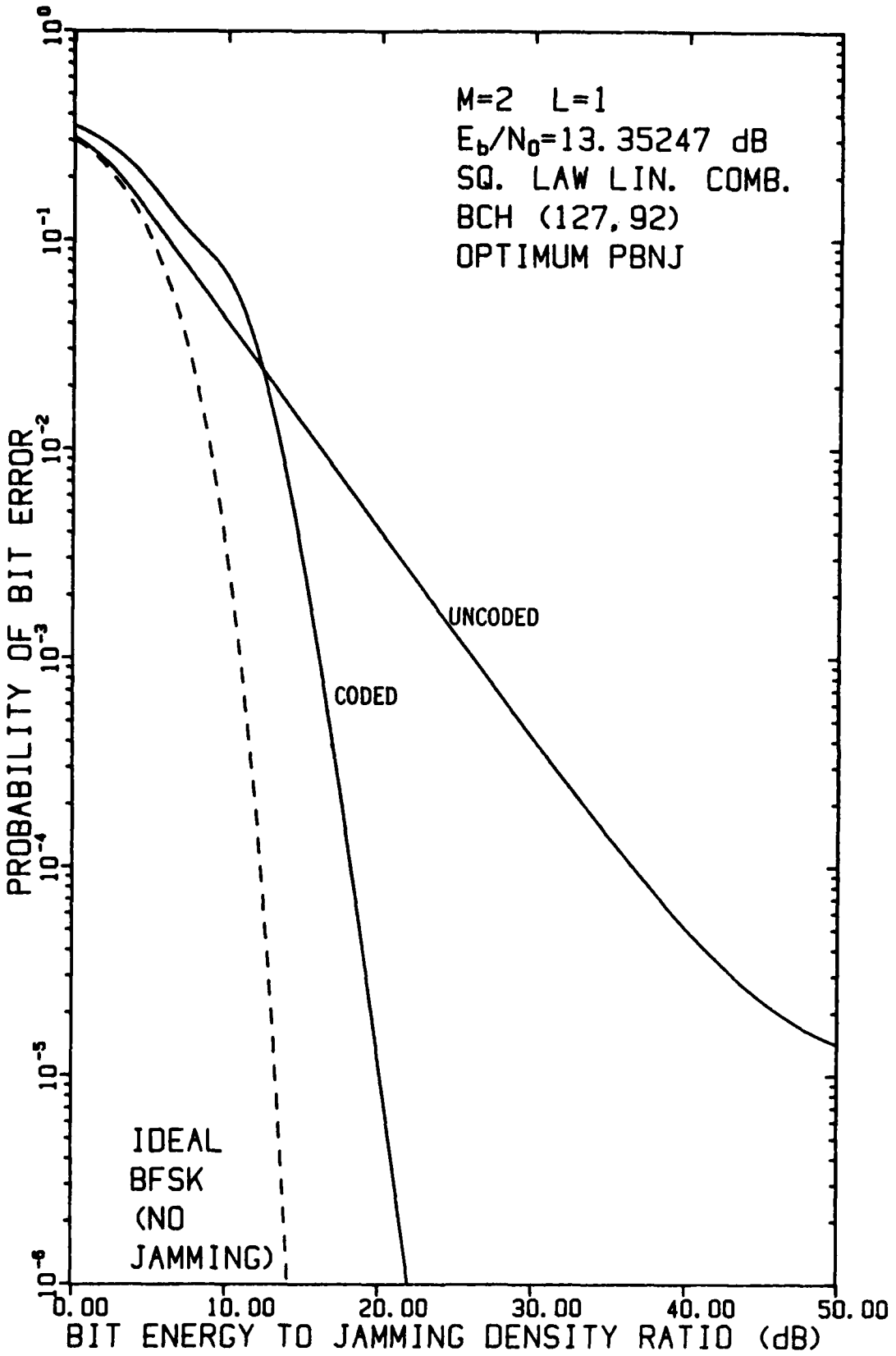

FIGURE 4-25 PERFORMANCE OF FH/BFSK WITH BCH (127,92) CODE AND L=1 HOP/DIGIT AS A FUNCTION OF E_b/N_J WHEN E_b/N_0 = 13.35247 dB, USING A LINEAR COMBINING DEMODULATOR, IN OPTIMUM PARTIAL-BAND NOISE JAMMING

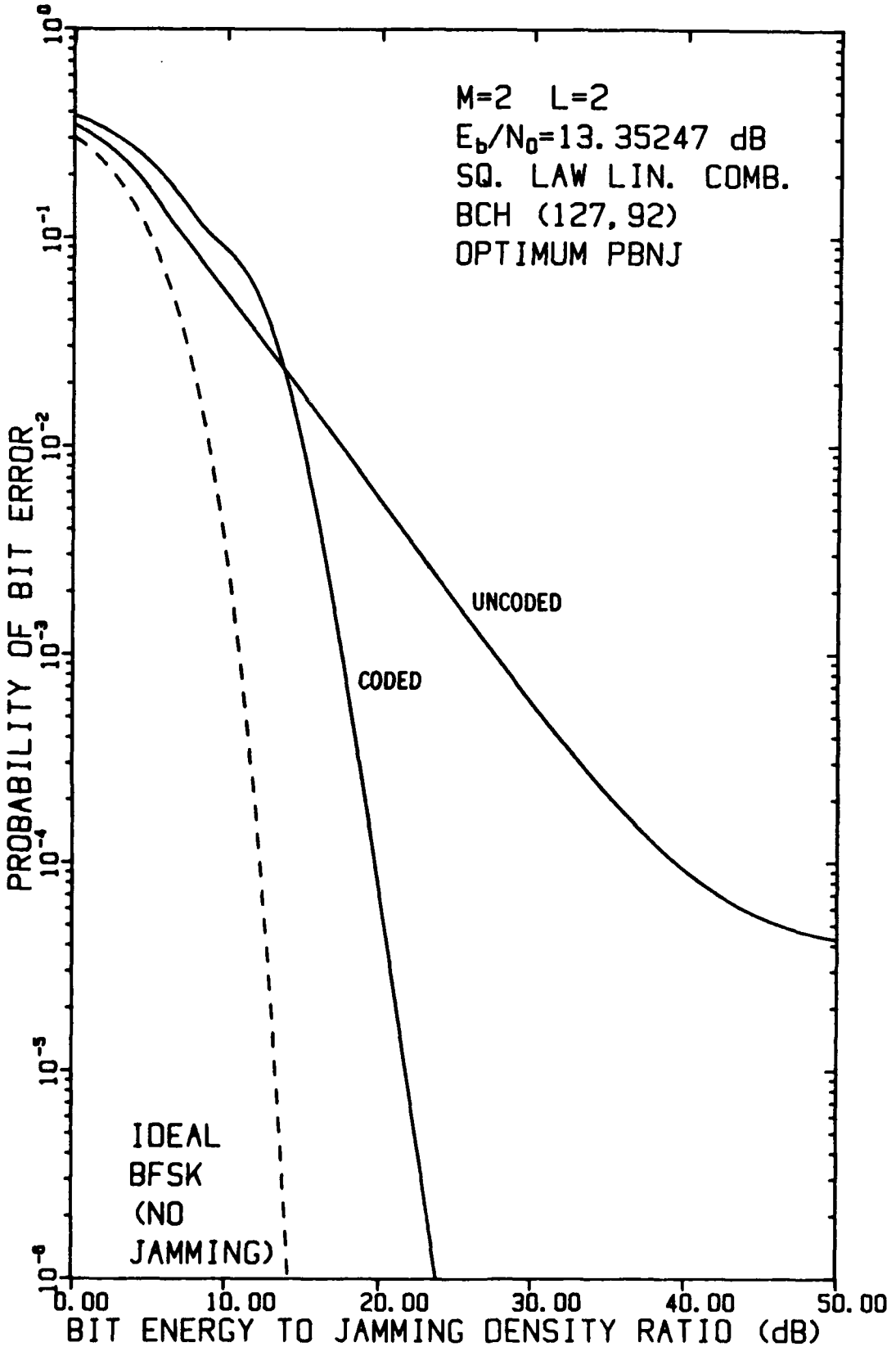

FIGURE 4-26 PERFORMANCE OF FH/BFSK WITH BCH (127,92) CODE AND L=2 HOPS/DIGIT AS A FUNCTION OF E_b/N_J WHEN E_b/N_0 = 13.35247 dB, USING A LINEAR COMBINING DEMODULATOR, IN OPTIMUM PARTIAL-BAND NOISE JAMMING

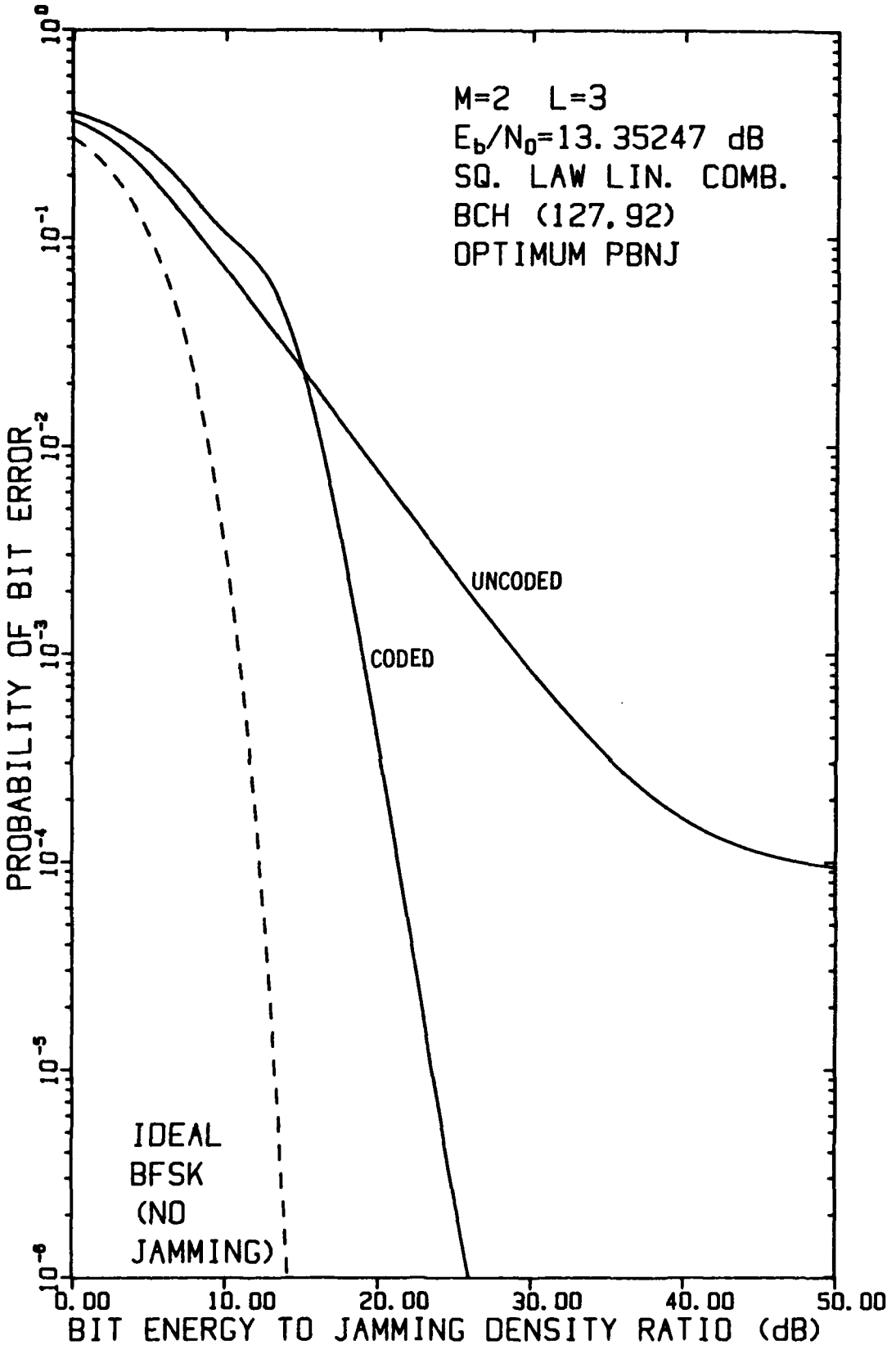

FIGURE 4-27 PERFORMANCE OF FH/BFSK WITH BCH (127,92) CODE AND L=3 HOPS/DIGIT AS A FUNCTION OF E_b/N_J WHEN E_b/N_0 = 13.35247 dB, USING A LINEAR COMBINING DEMODULATOR, IN OPTIMUM PARTIAL-BAND NOISE JAMMING

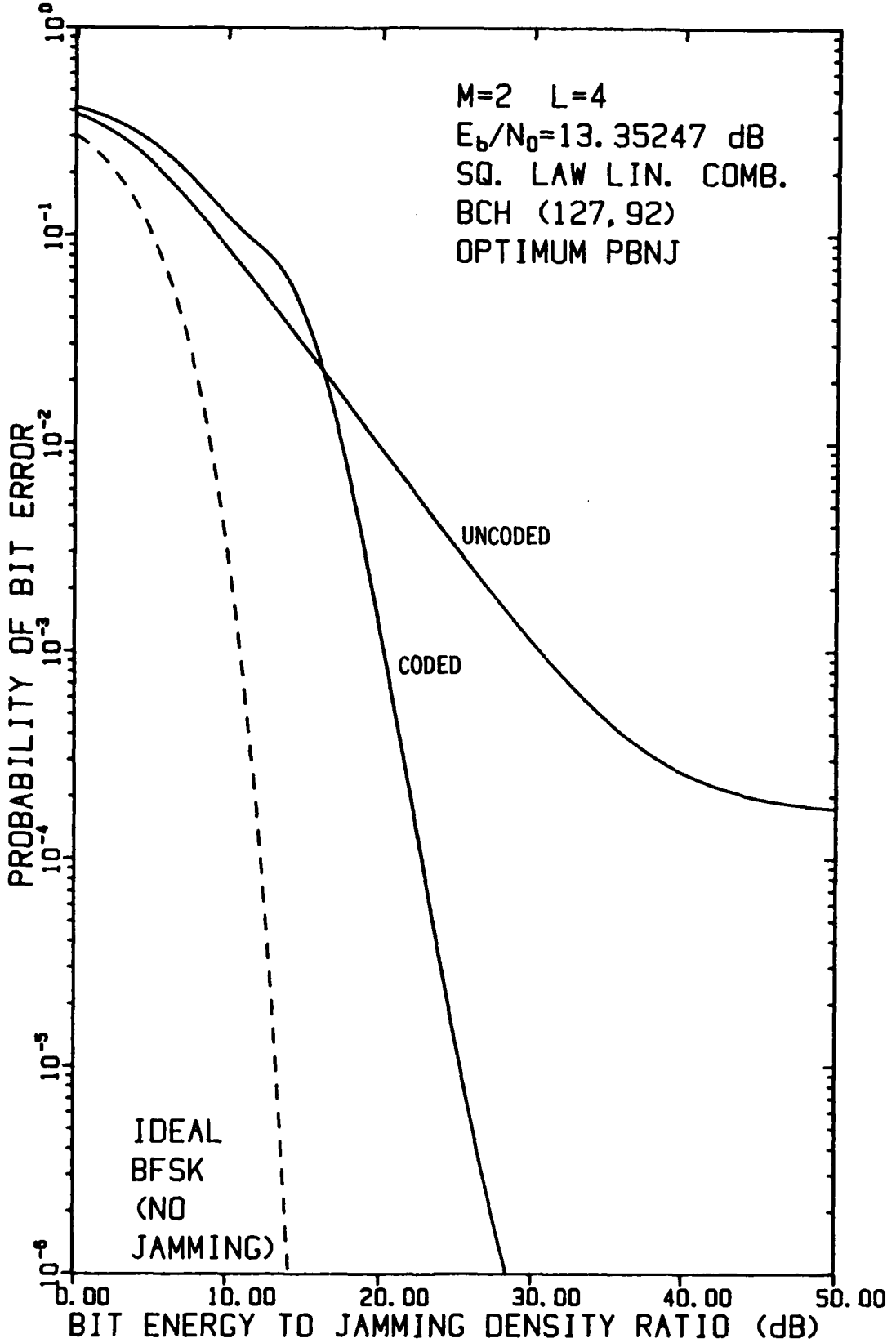

FIGURE 4-28 PERFORMANCE OF FH/BFSK WITH BCH (127,92) CODE AND L=4 HOPS/DIGIT AS A FUNCTION OF E_b/N_J WHEN E_b/N_0 = 13.35247 dB, USING A LINEAR COMBINING DEMODULATOR, IN OPTIMUM PARTIAL-BAND NOISE JAMMING

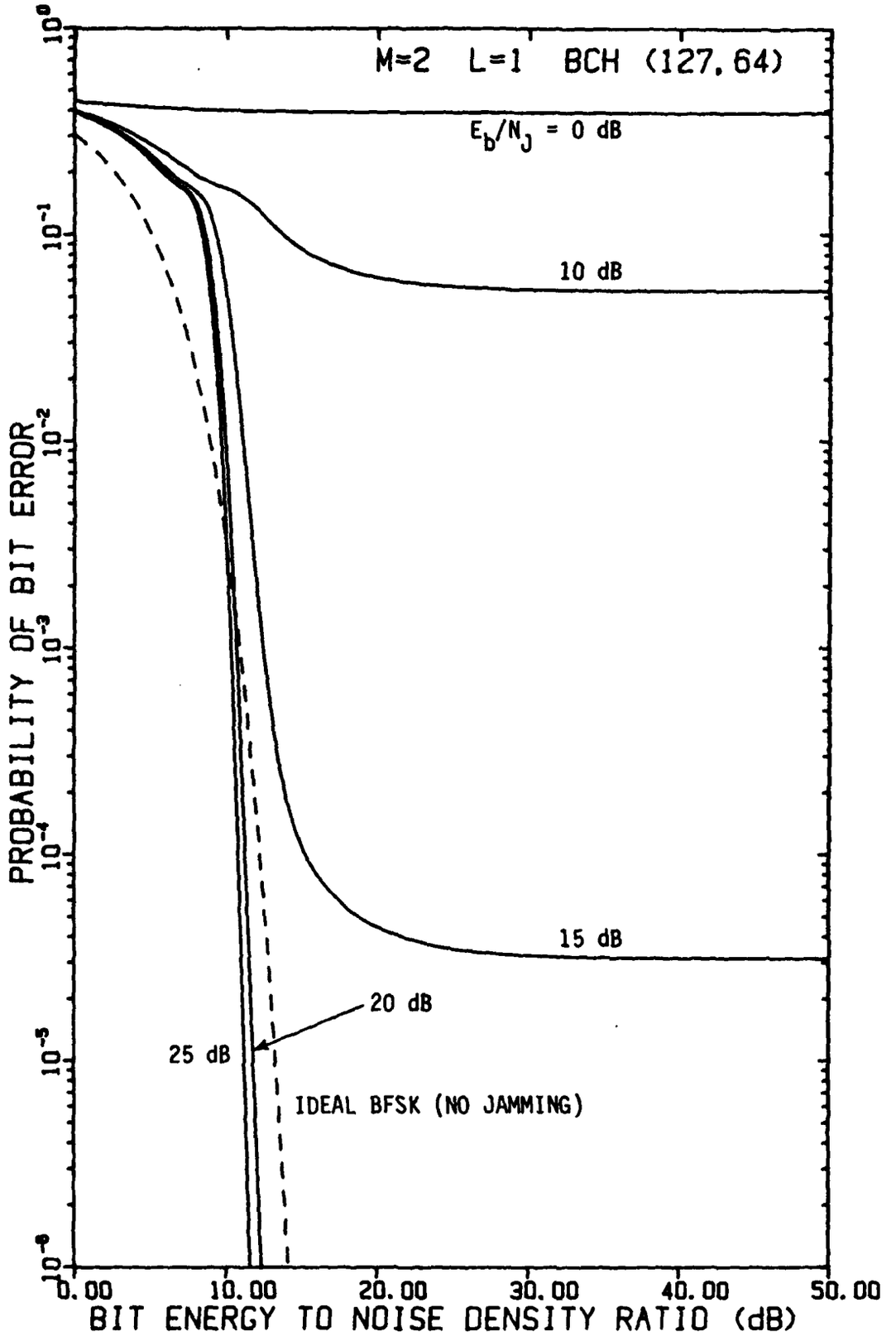

FIGURE 4-29 PERFORMANCE OF FH/BFSK WITH BCH (127,64) CODE AND L=1 HOP/DIGIT AS A FUNCTION OF E_b/N_0 WITH E_b/N_J AS A PARAMETER, USING A LINEAR COMBINING DEMODULATOR, IN OPTIMUM PARTIAL-BAND NOISE JAMMING

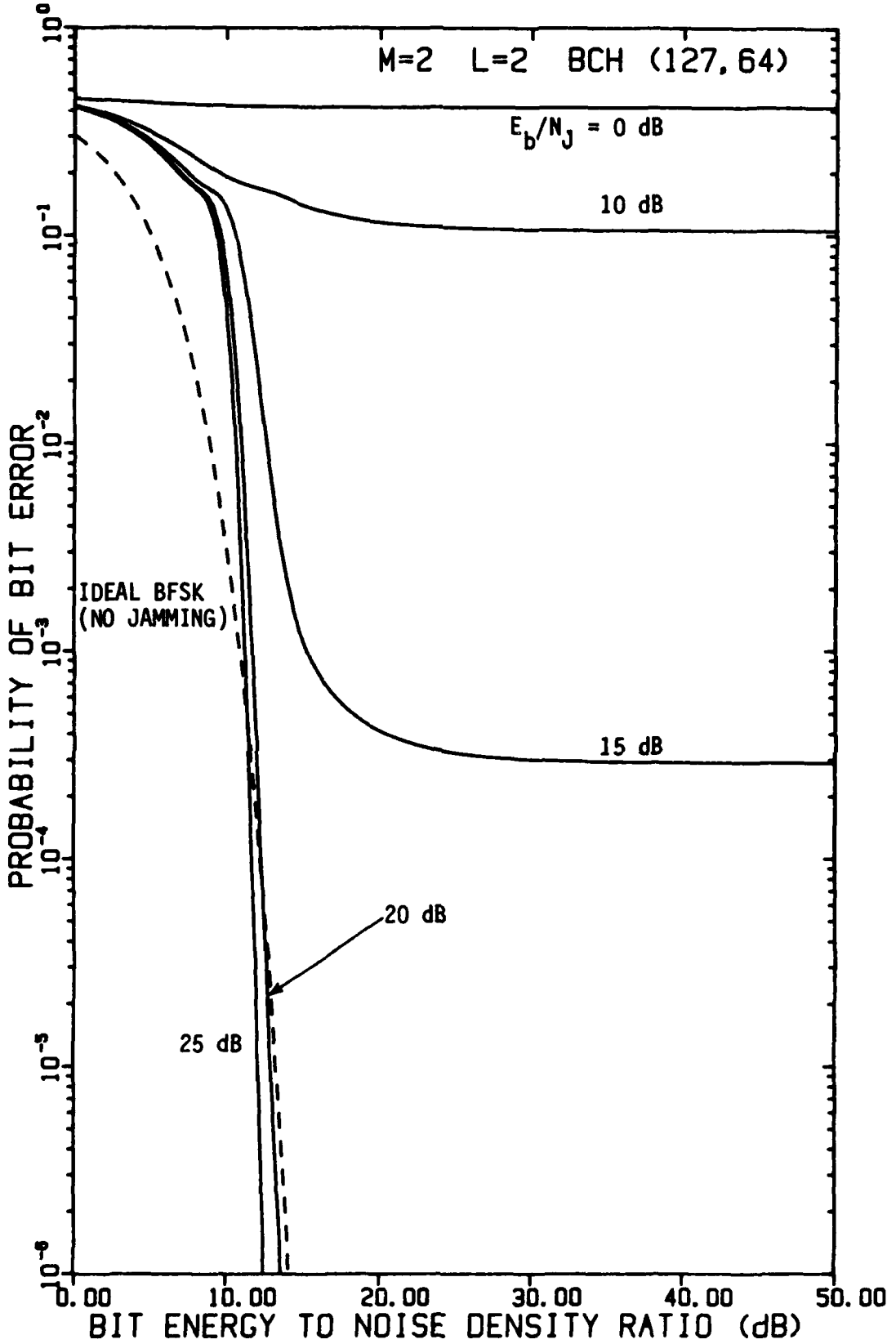

FIGURE 4-30 PERFORMANCE OF FH/BFSK WITH BCH (127,64) CODE AND L=2 HOPS/DIGIT AS A FUNCTION OF E_b/N_0 WITH E_b/N_J AS A PARAMETER, USING A LINEAR COMBINING DEMODULATOR, IN OPTIMUM PARTIAL-BAND NOISE JAMMING

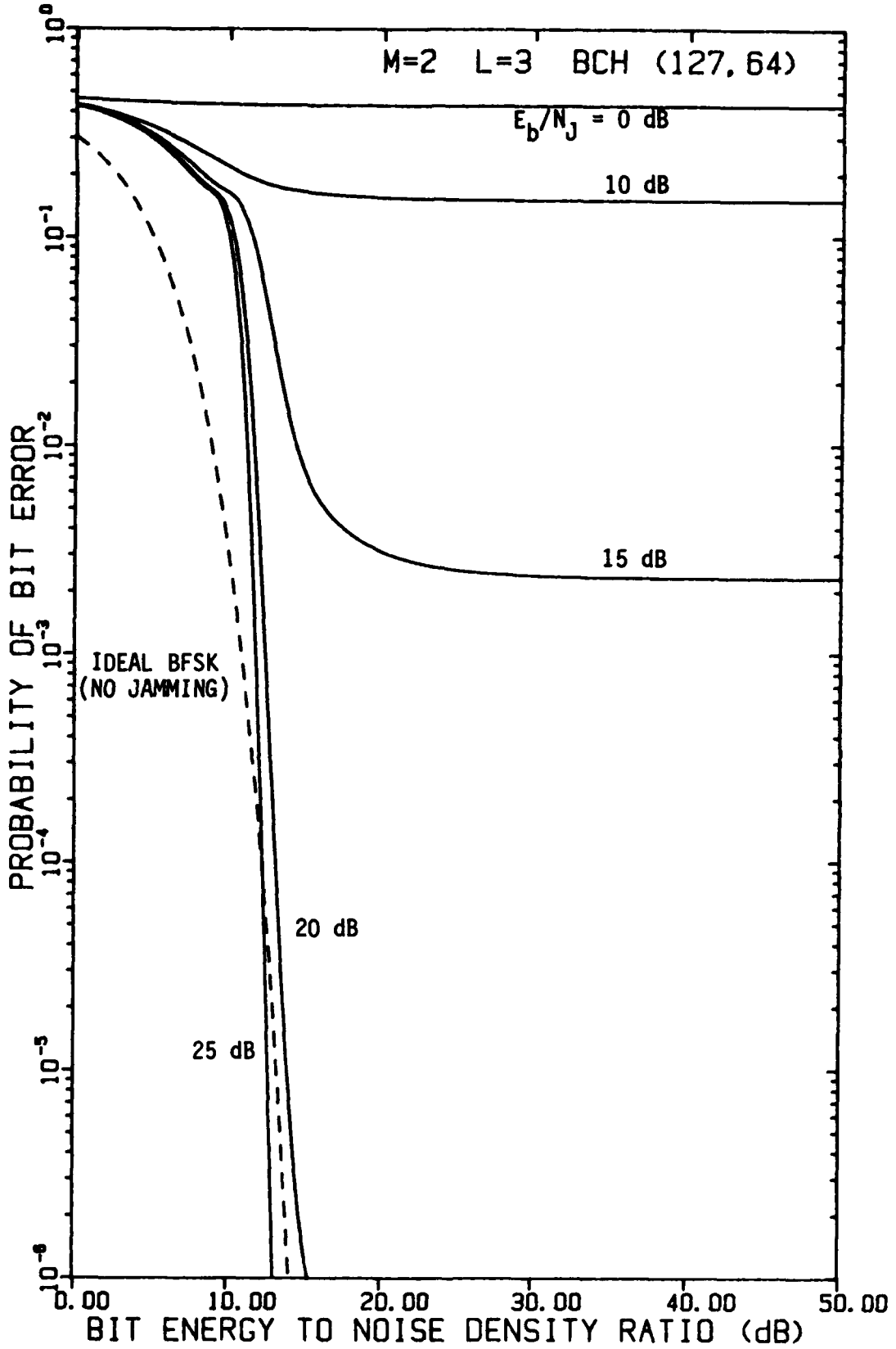

FIGURE 4-31 PERFORMANCE OF FH/BFSK WITH BCH (127,64) CODE AND L=3 HOPS/DIGIT AS A FUNCTION OF E_b/N_0 WITH E_b/N_J AS A PARAMETER, USING A LINEAR COMBINING DEMODULATOR, IN OPTIMUM PARTIAL-BAND NOISE JAMMING

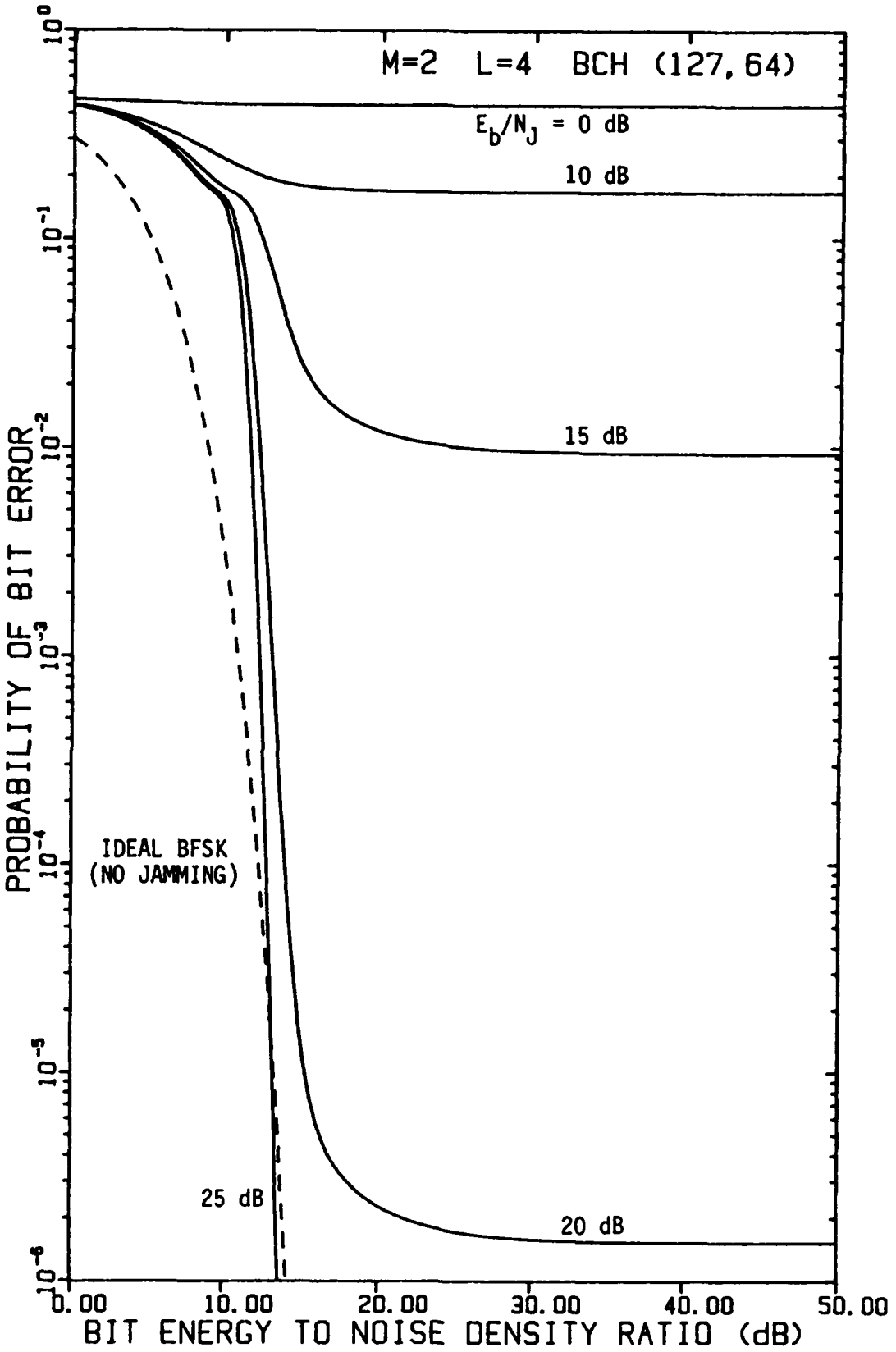

FIGURE 4-32 PERFORMANCE OF FH/BFSK WITH BCH (127,64) CODE AND L=4 HOPS/DIGIT AS A FUNCTION OF E_b/N_0 WITH E_b/N_J AS A PARAMETER, USING A LINEAR COMBINING DEMODULATOR, IN OPTIMUM PARTIAL-BAND NOISE JAMMING

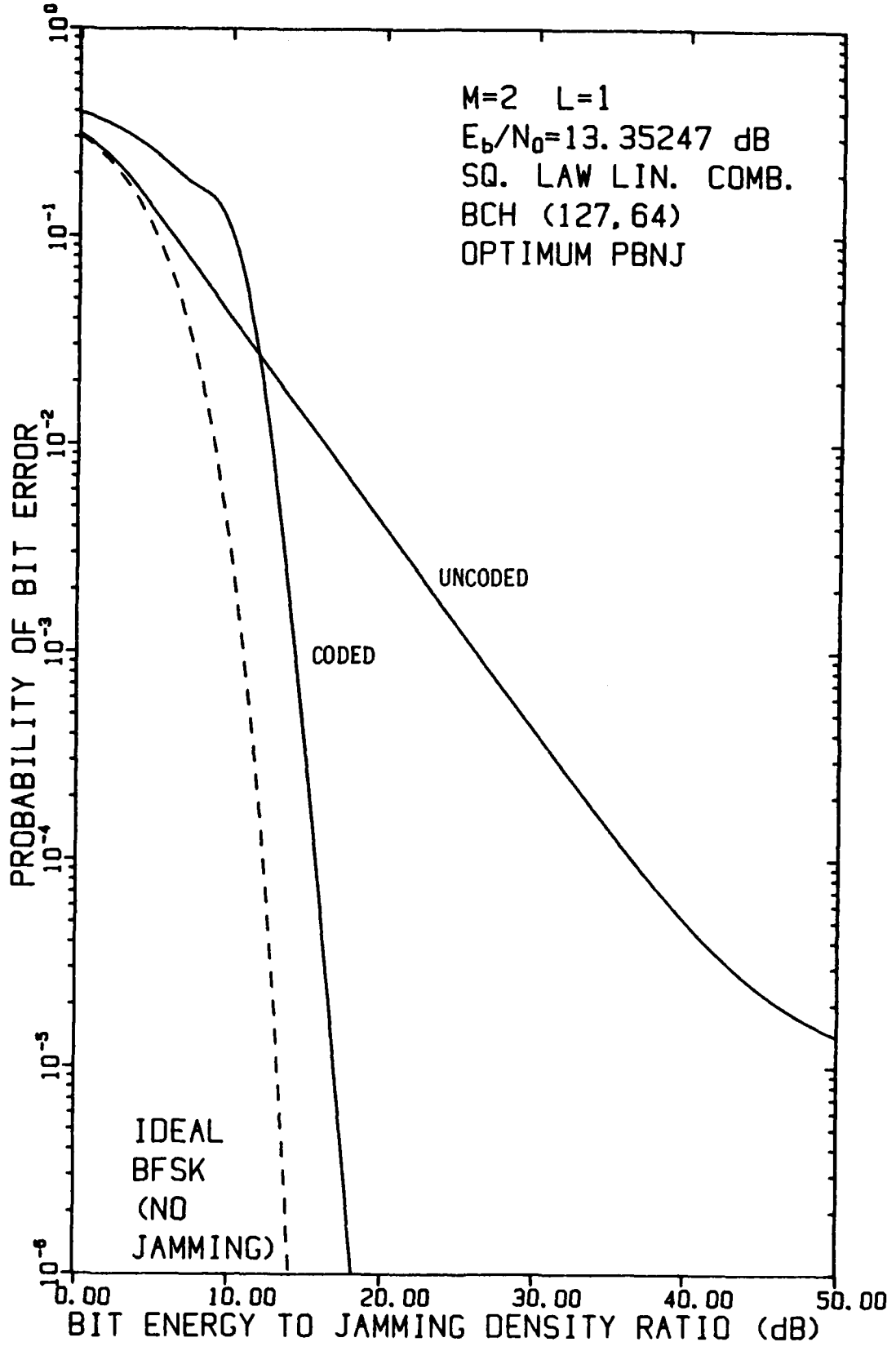

FIGURE 4-33 PERFORMANCE OF FH/BFSK WITH BCH (127,64) CODE AND L=1 HOP/DIGIT AS A FUNCTION OF E_b/N_J WHEN E_b/N_0 = 13.35247 dB, USING A LINEAR COMBINING DEMODULATOR, IN OPTIMUM PARTIAL-BAND NOISE JAMMING

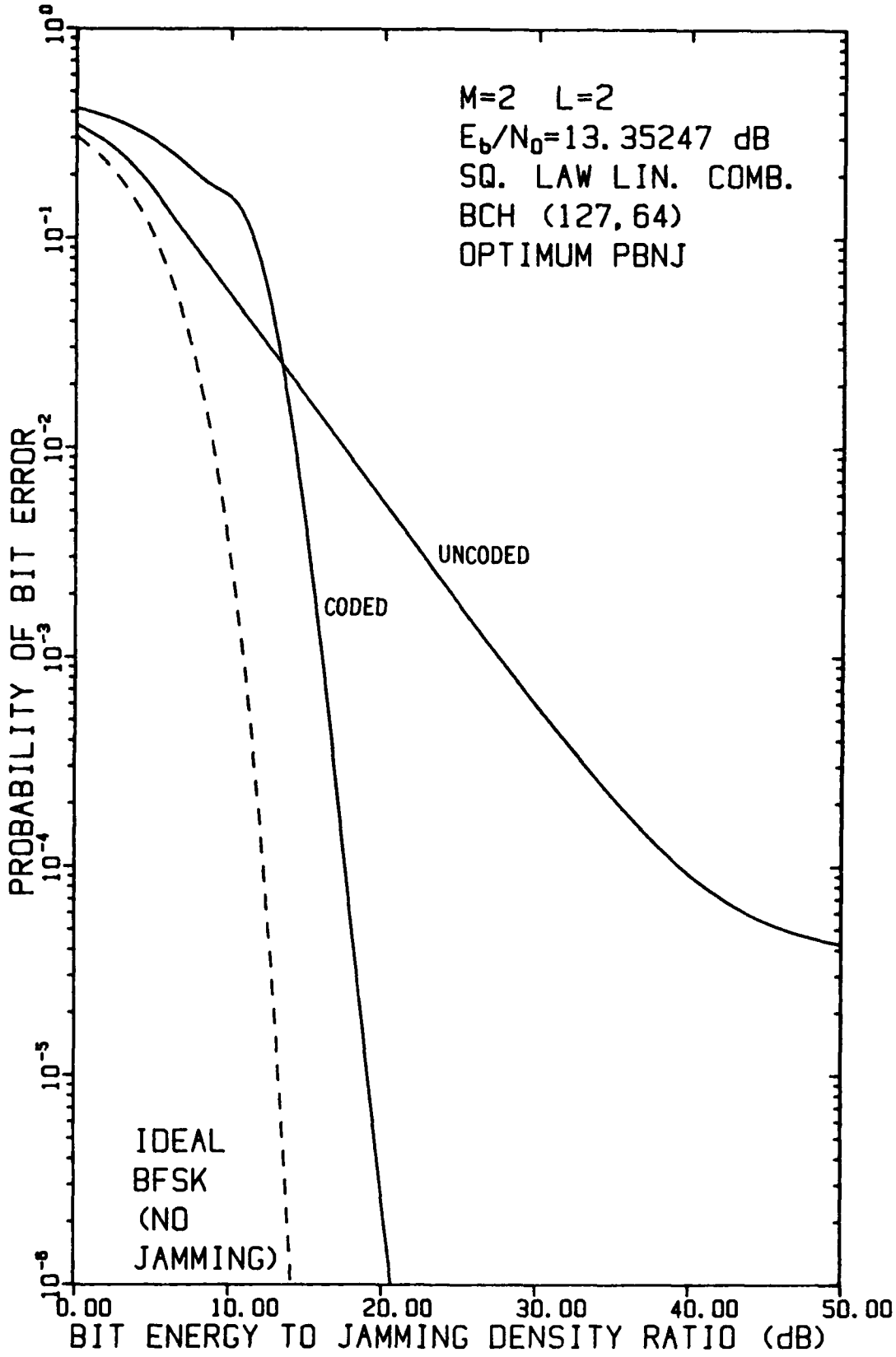

FIGURE 4-34 PERFORMANCE OF FH/BFSK WITH BCH (127,64) CODE AND L=2 HOPS/DIGIT AS A FUNCTION OF E_b/N_J WHEN E_b/N_0 = 13.35247 dB, USING A LINEAR COMBINING DEMODULATOR, IN OPTIMUM PARTIAL-BAND NOISE JAMMING

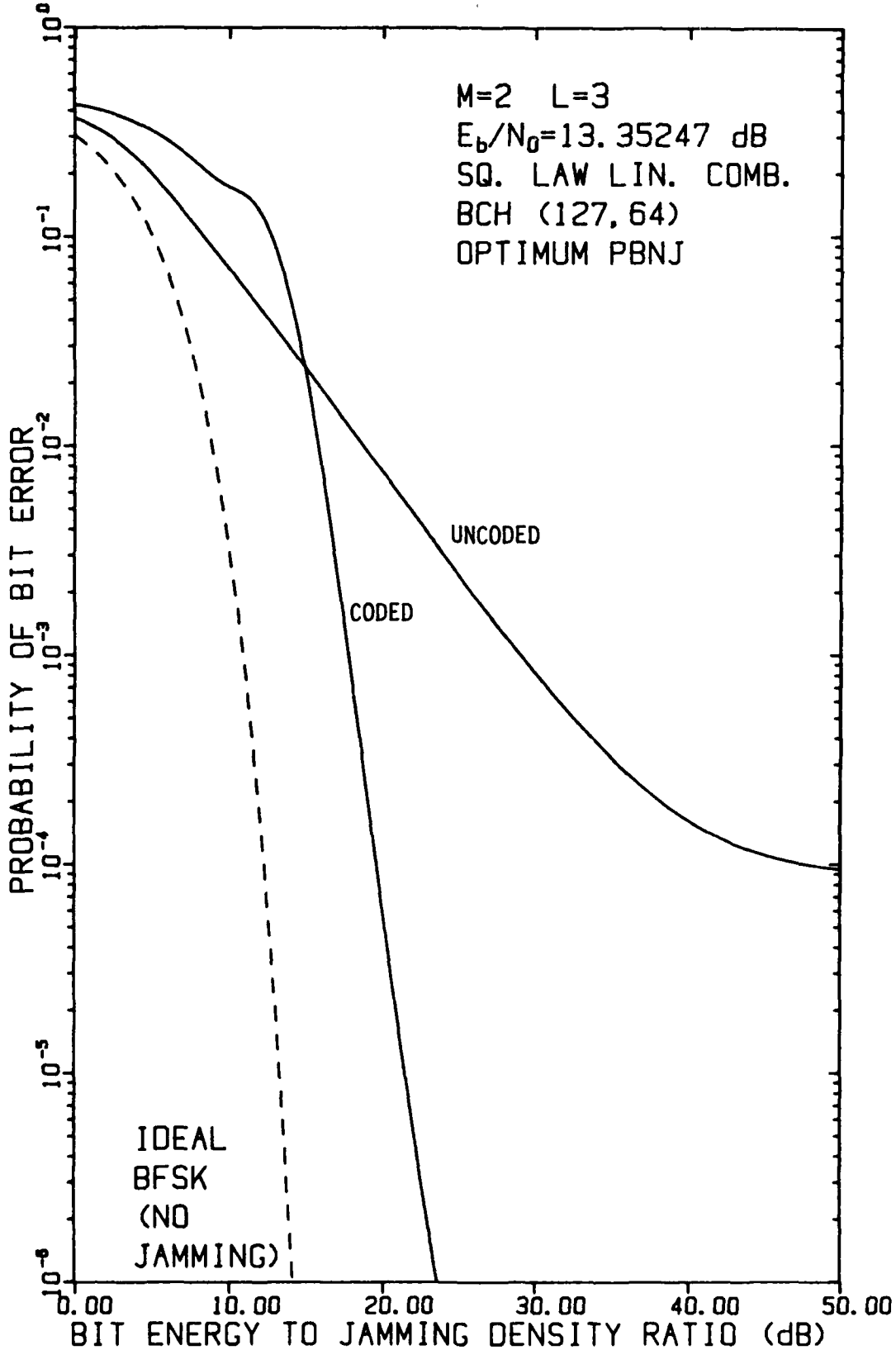

FIGURE 4-35 PERFORMANCE OF FH/BFSK WITH BCH (127,64) CODE AND L=3 HOPS/DIGIT AS A FUNCTION OF E_b/N_J WHEN E_b/N_0 = 13.35247 dB, USING A LINEAR COMBINING DEMODULATOR, IN OPTIMUM PARTIAL-BAND NOISE JAMMING

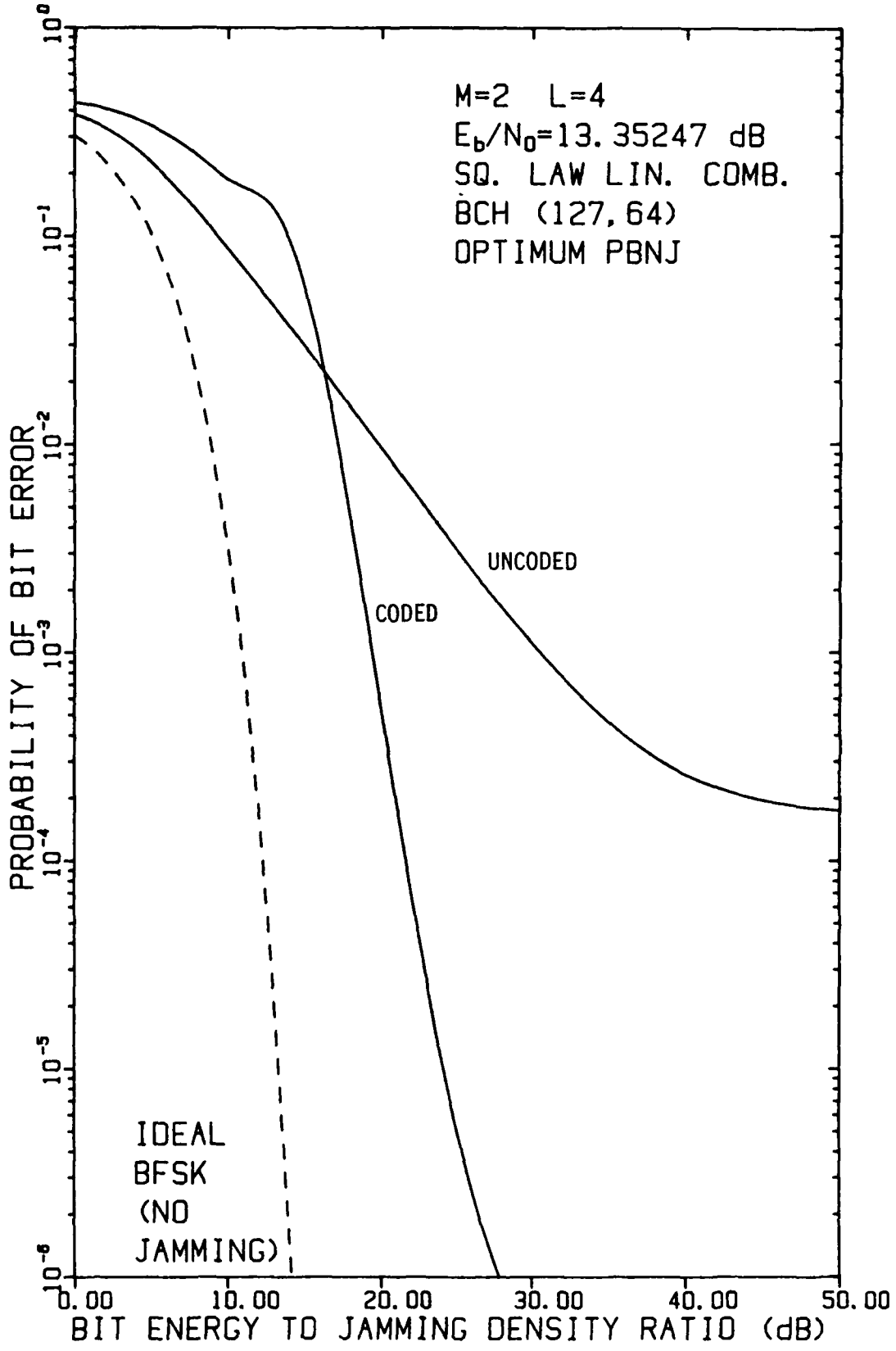

FIGURE 4-36 PERFORMANCE OF FH/BFSK WITH BCH (127,64) CODE AND L=4 HOPS/DIGIT AS A FUNCTION OF E_b/N_J WHEN E_b/N_0 = 13.35247 dB, USING A LINEAR COMBINING DEMODULATOR, IN OPTIMUM PARTIAL-BAND NOISE JAMMING

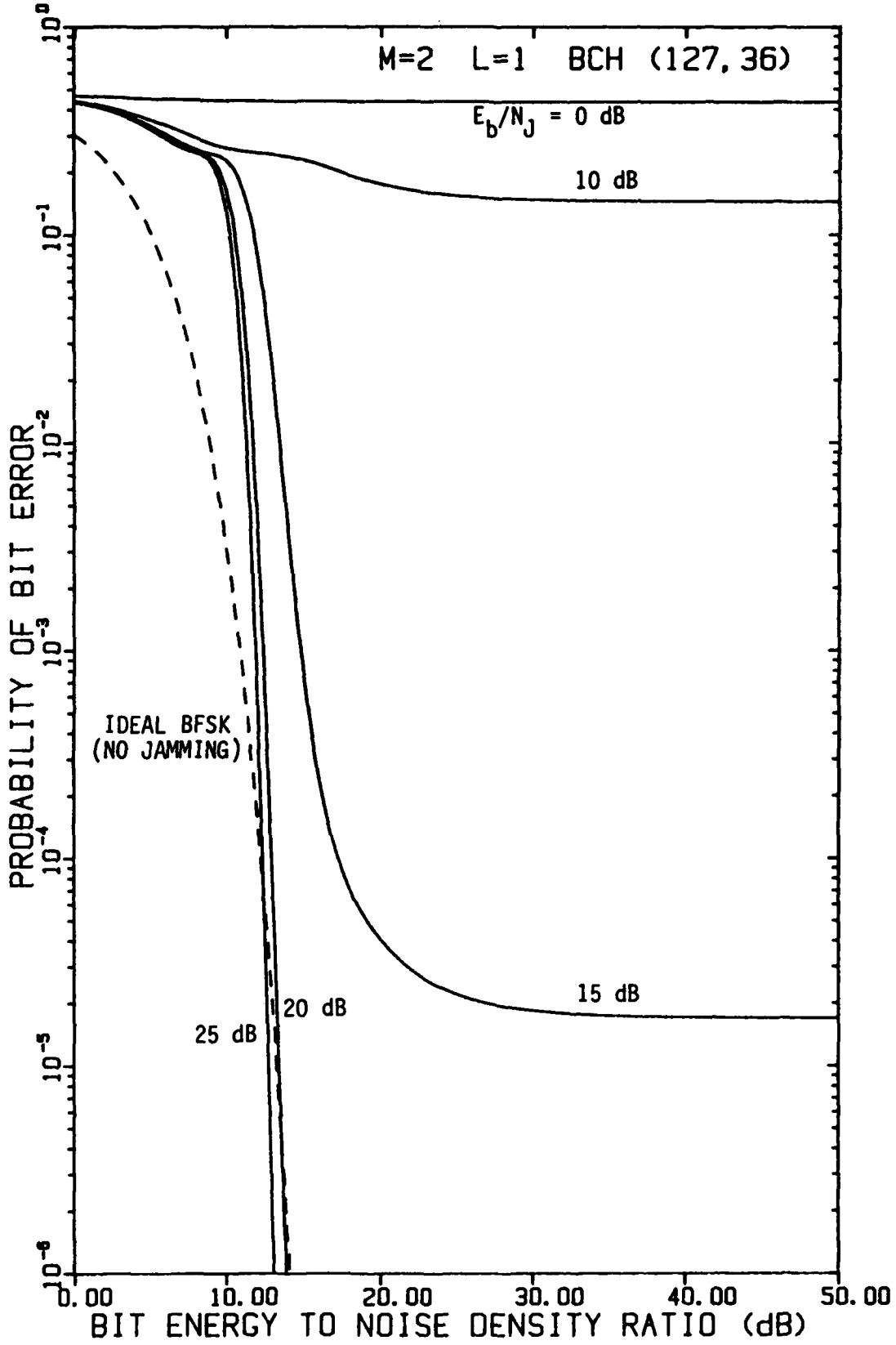

FIGURE 4-37 PERFORMANCE OF FH/BFSK WITH BCH (127,36) CODE AND L=1 HOP/DIGIT AS A FUNCTION OF E_b/N_0 WITH E_b/N_J AS A PARAMETER, USING A LINEAR COMBINING DEMODULATOR, IN OPTIMUM PARTIAL-BAND NOISE JAMMING

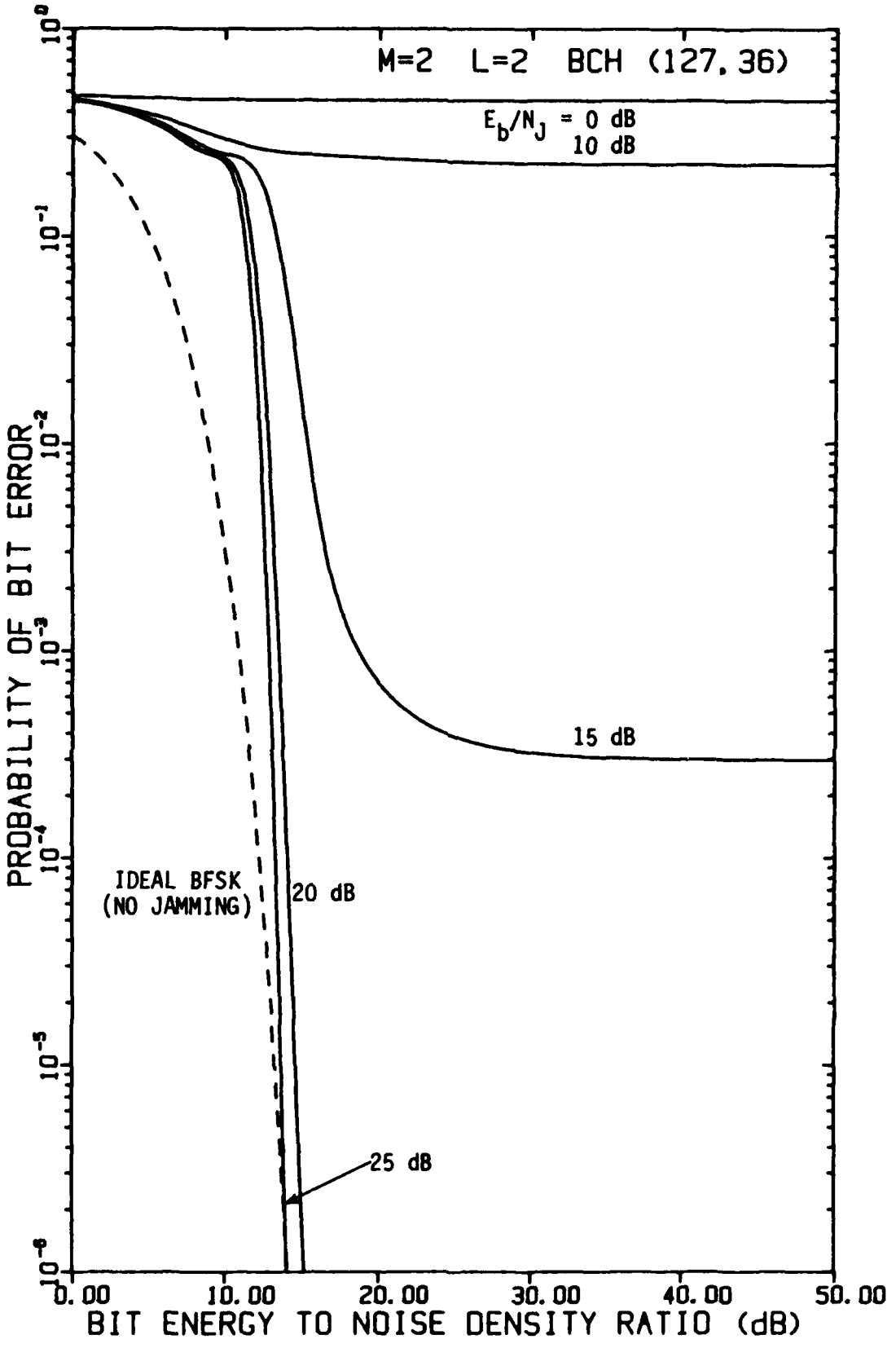

FIGURE 4-38 PERFORMANCE OF FH/BFSK WITH BCH (127,36) CODE AND L=2 HOPS/DIGIT AS A FUNCTION OF E_b/N_0 WITH E_b/N_J AS A PARAMETER, USING A LINEAR COMBINING DEMODULATOR, IN OPTIMUM PARTIAL-BAND NOISE JAMMING

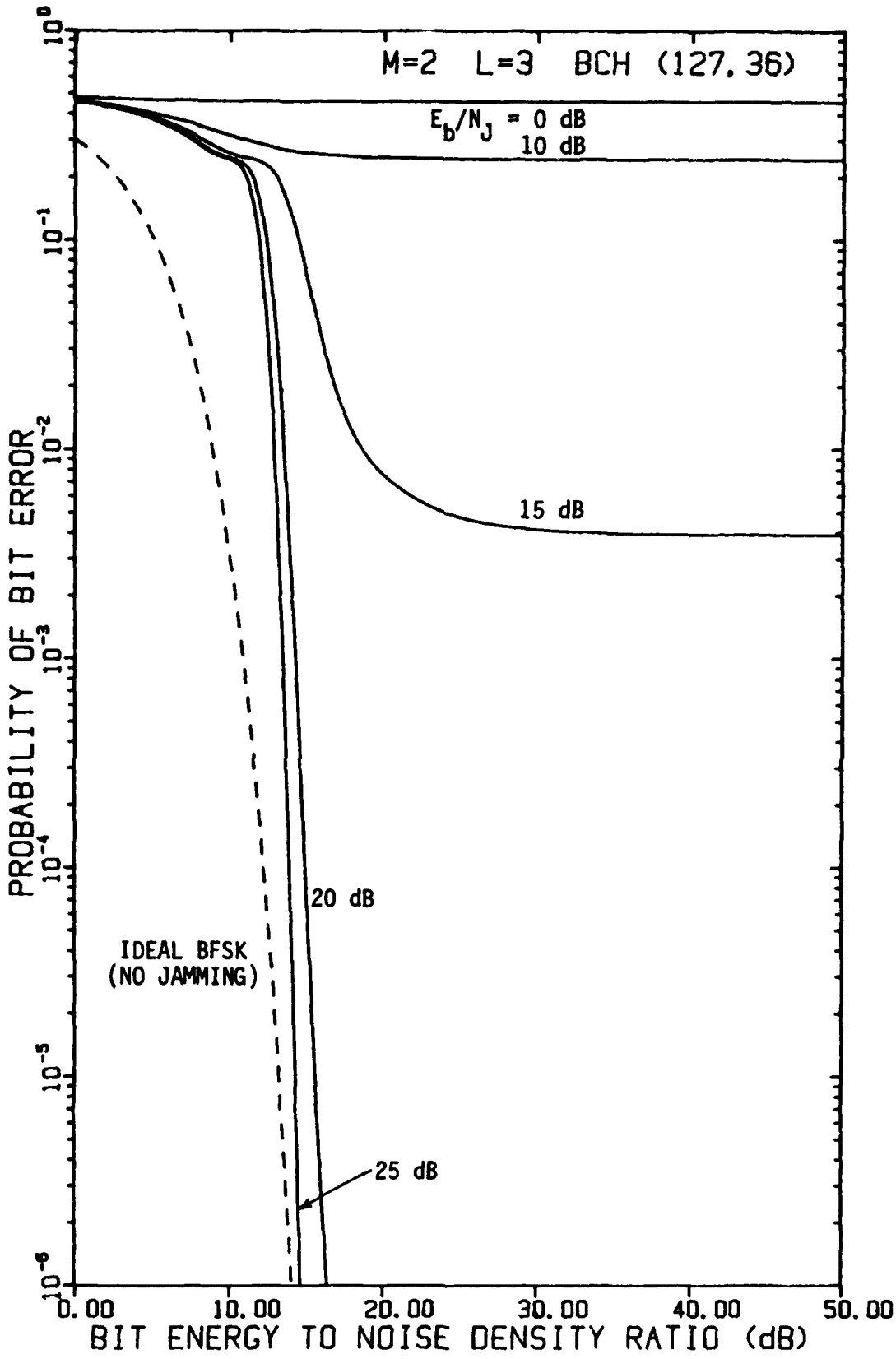

FIGURE 4-39 PERFORMANCE OF FH/BFSK WITH BCH (127,36) CODE AND L=3 HOPS/DIGIT AS A FUNCTION OF E_b/N_0 WITH E_b/N_J AS A PARAMETER, USING A LINEAR COMBINING DEMODULATOR, IN OPTIMUM PARTIAL-BAND NOISE JAMMING

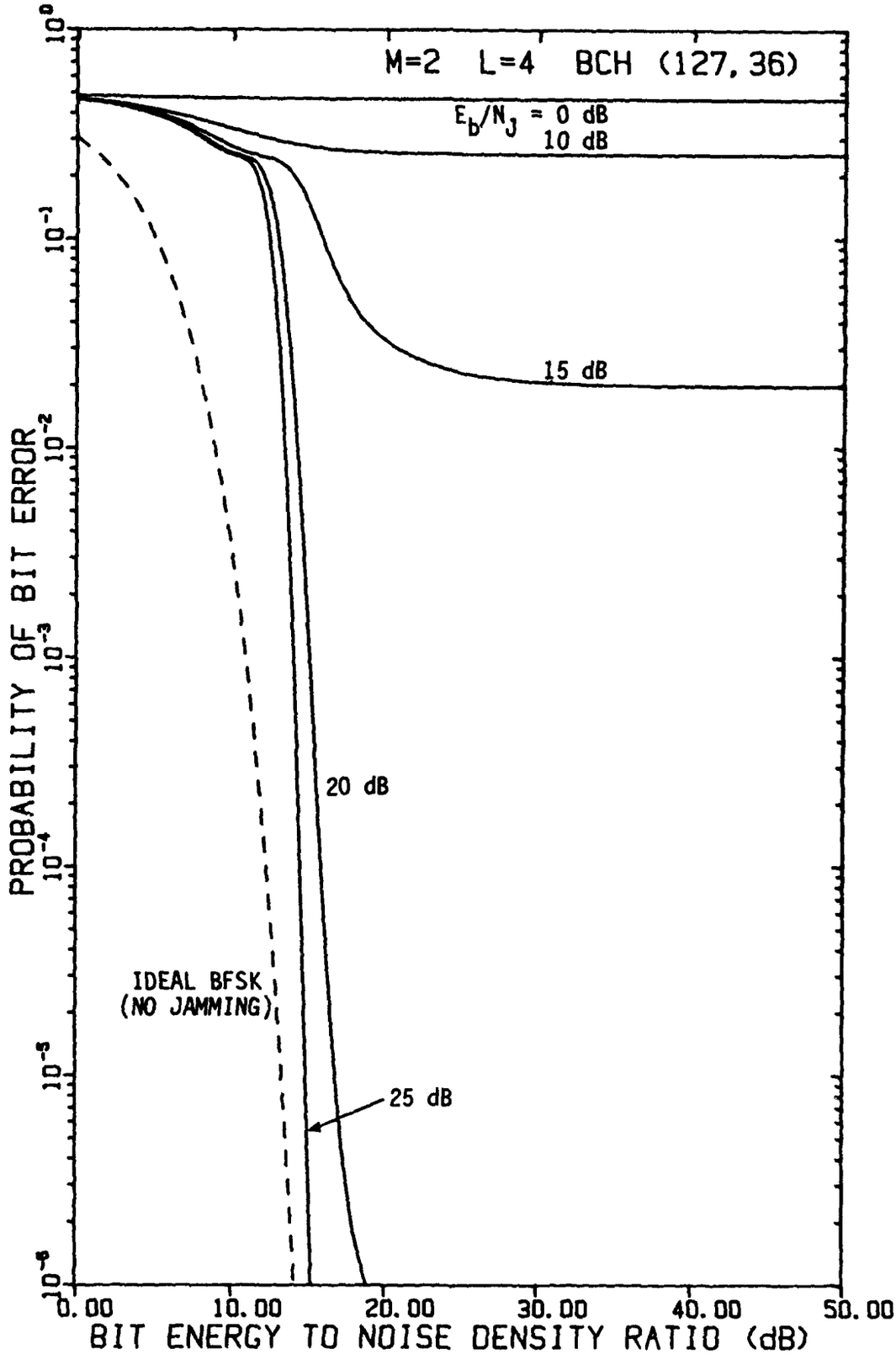

FIGURE 4-40 PERFORMANCE OF FH/BFSK WITH BCH (127,36) CODE AND L=4 HOPS/DIGIT AS A FUNCTION OF E_b/N_0 WITH E_b/N_J AS A PARAMETER, USING A LINEAR COMBINING DEMODULATOR, IN OPTIMUM PARTIAL-BAND NOISE JAMMING

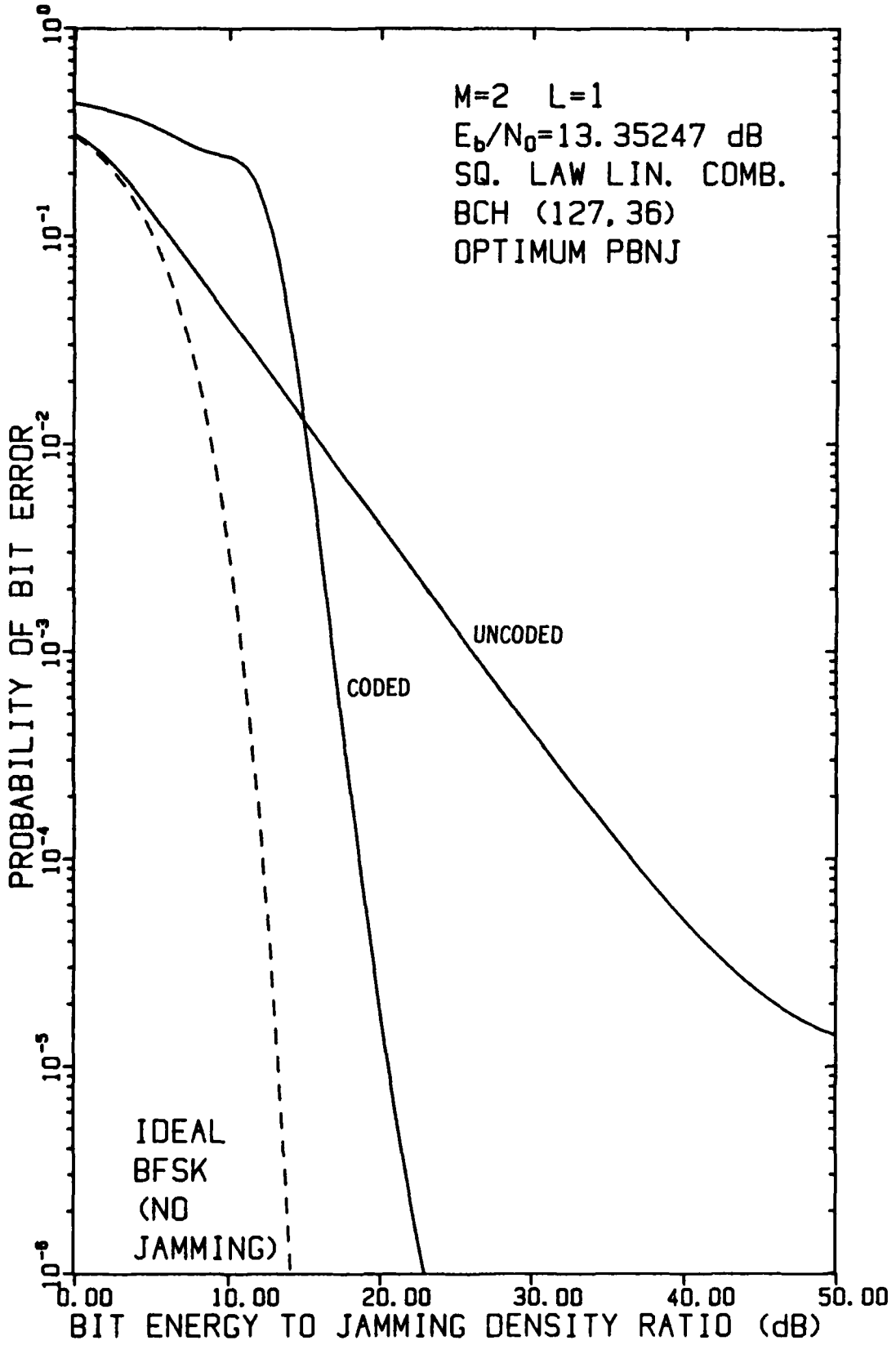

FIGURE 4-41 PERFORMANCE OF FH/BFSK WITH BCH (127,36) CODE AND L=1 HOP/DIGIT AS A FUNCTION OF E_b/N_J WHEN E_b/N_0 = 13.35247 dB, USING A LINEAR COMBINING DEMODULATOR, IN OPTIMUM PARTIAL-BAND NOISE JAMMING

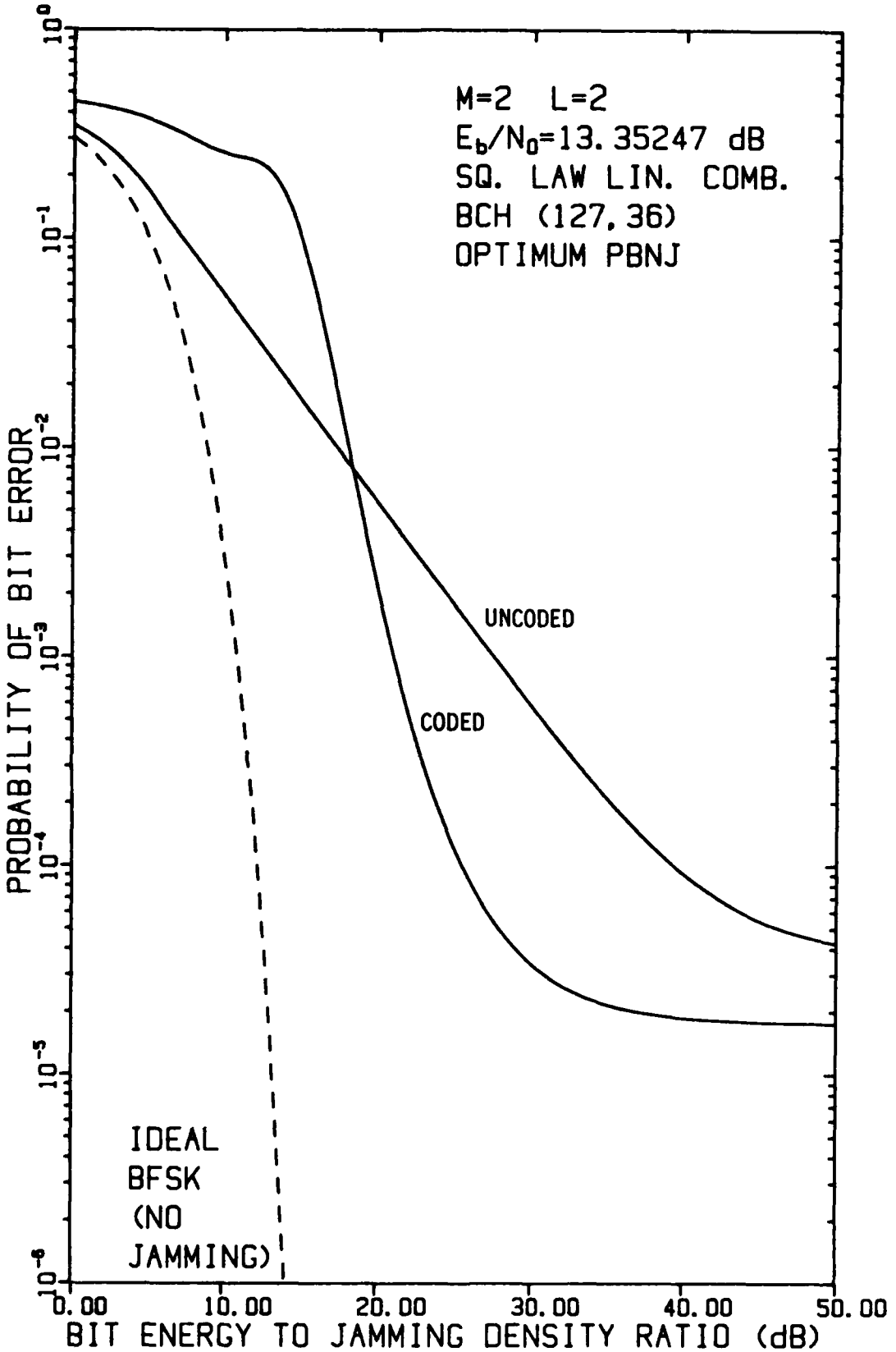

FIGURE 4-42 PERFORMANCE OF FH/BFSK WITH BCH (127,36) CODE AND L=2 HOPS/DIGIT AS A FUNCTION OF E_b/N_J WHEN E_b/N_0 = 13.35247 dB, USING A LINEAR COMBINING DEMODULATOR, IN OPTIMUM PARTIAL-BAND NOISE JAMMING

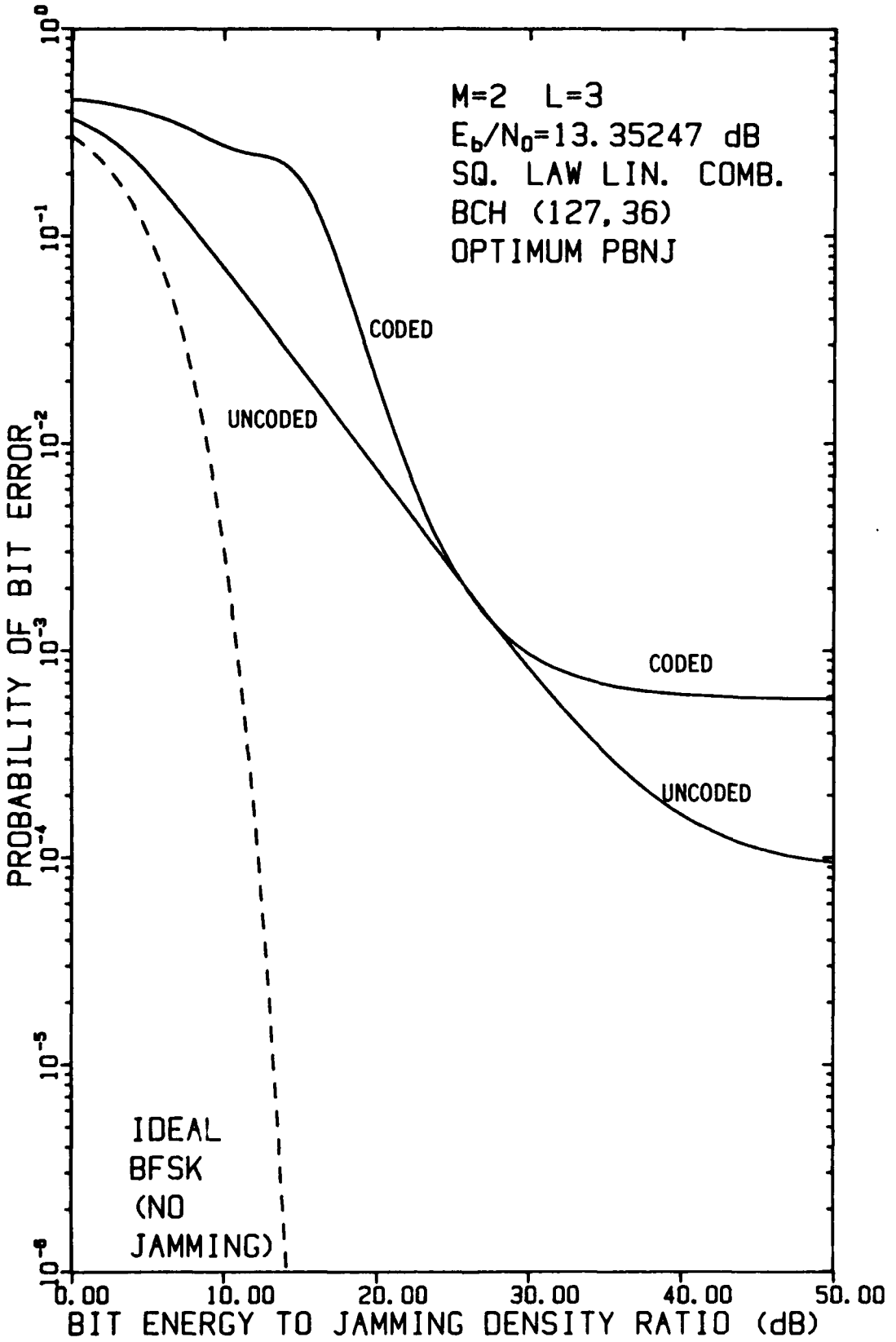

FIGURE 4-43 PERFORMANCE OF FH/BFSK WITH BCH (127,36) CODE AND L=3 HOPS/DIGIT AS A FUNCTION OF E_b/N_J WHEN E_b/N_0 = 13.35247 dB, USING A LINEAR COMBINING DEMODULATOR, IN OPTIMUM PARTIAL-BAND NOISE JAMMING

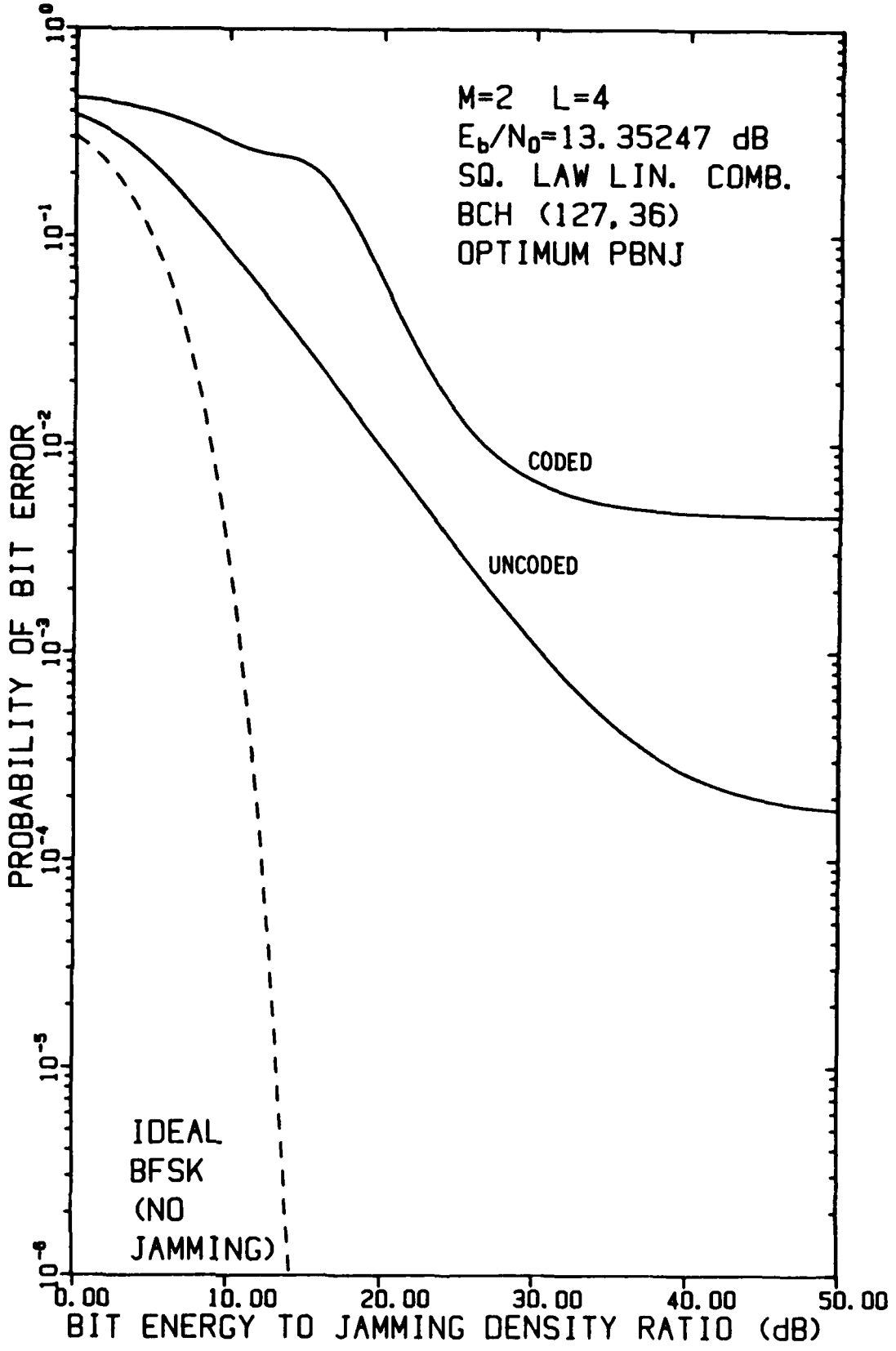

FIGURE 4-44 PERFORMANCE OF FH/BFSK WITH BCH (127,36) CODE AND L=4 HOPS/DIGIT AS A FUNCTION OF E_b/N_J WHEN E_b/N_0 = 13.35247 dB, USING A LINEAR COMBINING DEMODULATOR, IN OPTIMUM PARTIAL-BAND NOISE JAMMING

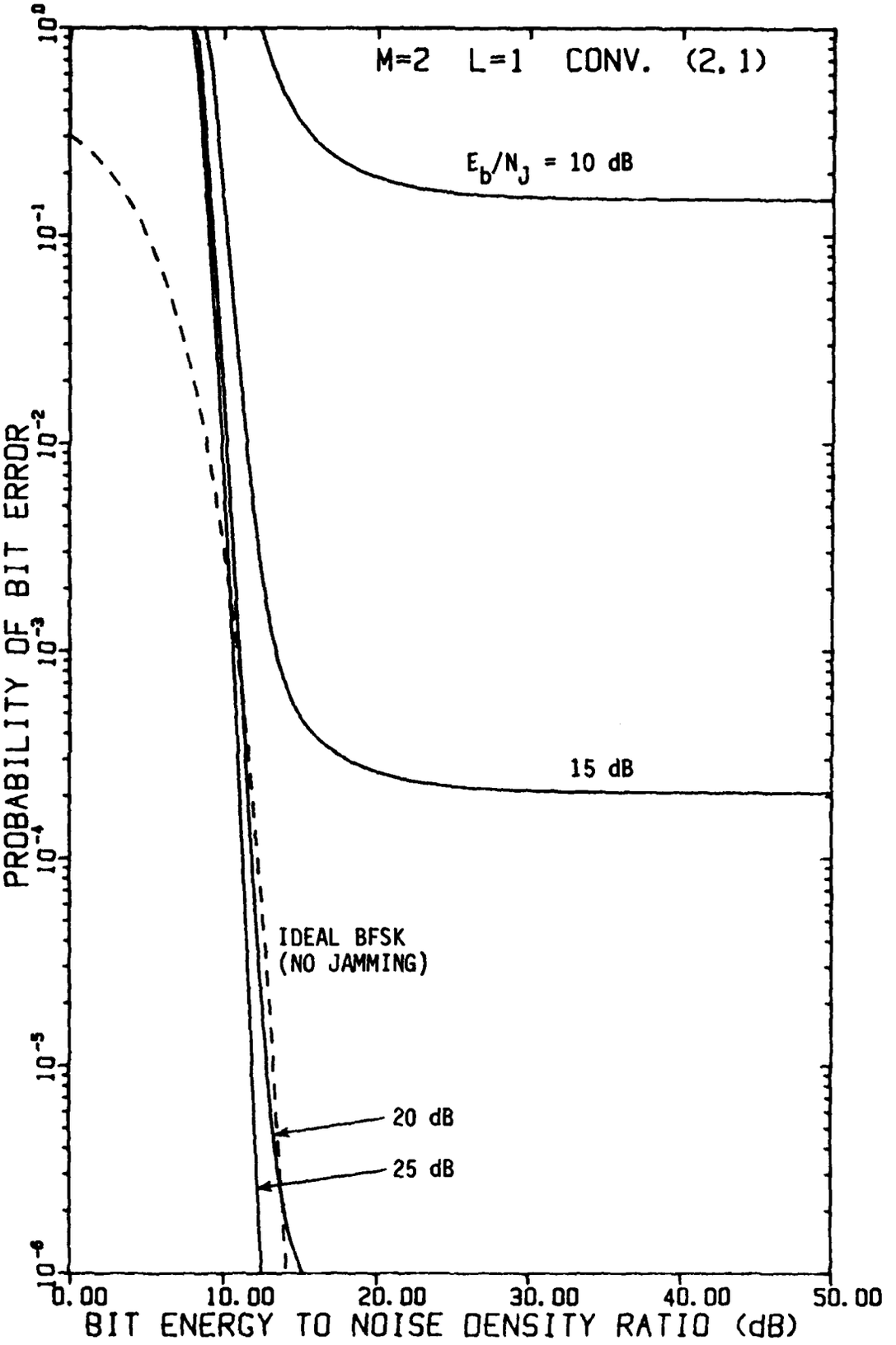

FIGURE 4-45 PERFORMANCE OF FH/BFSK WITH CONVOLUTIONAL RATE-1/2 CODE AND L=1 HOP/DIGIT AS A FUNCTION OF E_b/N_0 WITH E_b/N_J AS A PARAMETER, USING A LINEAR COMBINING DEMODULATOR, IN OPTIMUM PARTIAL-BAND NOISE JAMMING

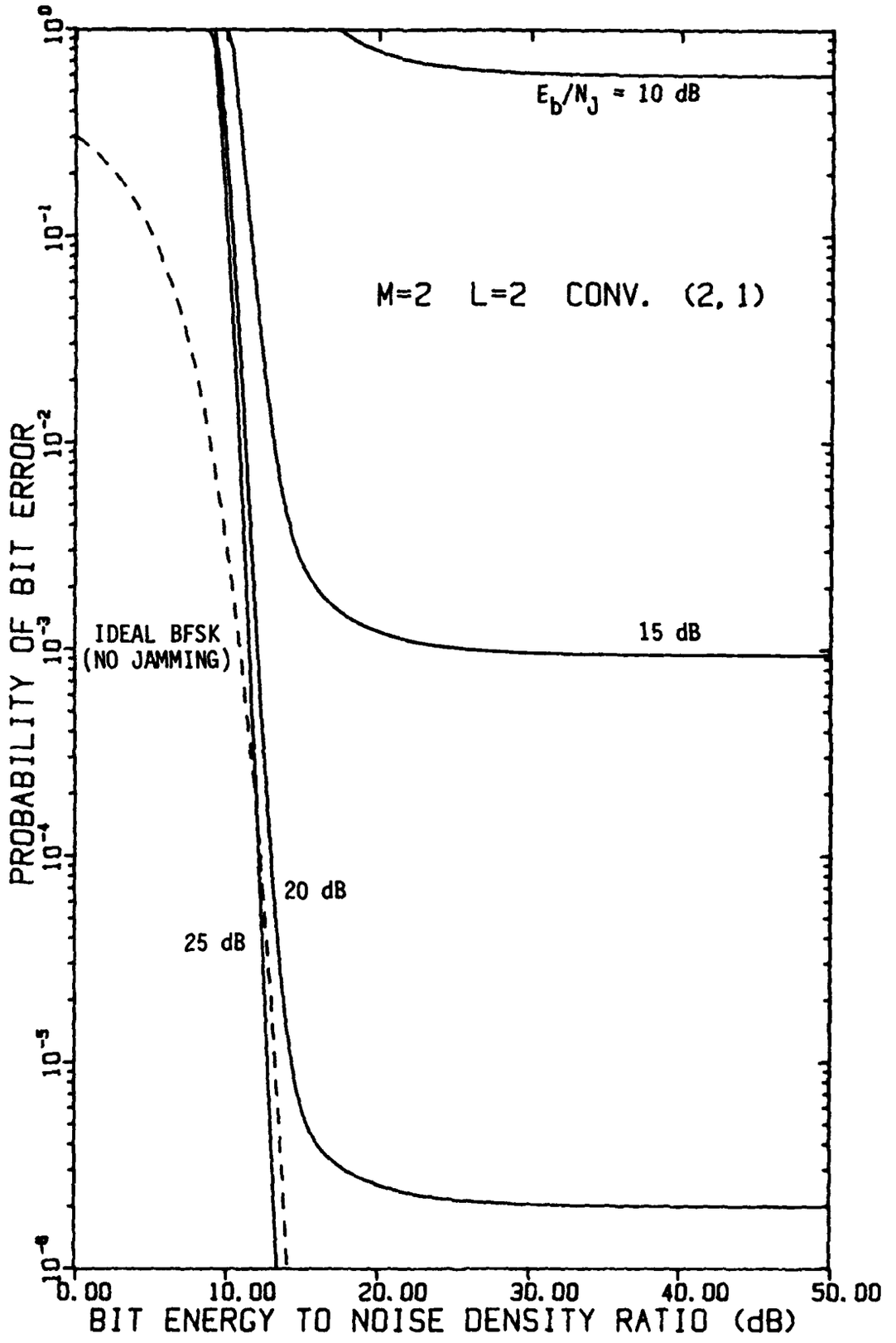

FIGURE 4-46 PERFORMANCE OF FH/BFSK WITH CONVOLUTIONAL RATE-1/2 CODE AND L=2 HOPS/DIGIT AS A FUNCTION OF E_b/N_0 WITH E_b/N_J AS A PARAMETER, USING A LINEAR COMBINING DEMODULATOR, IN OPTIMUM PARTIAL-BAND NOISE JAMMING

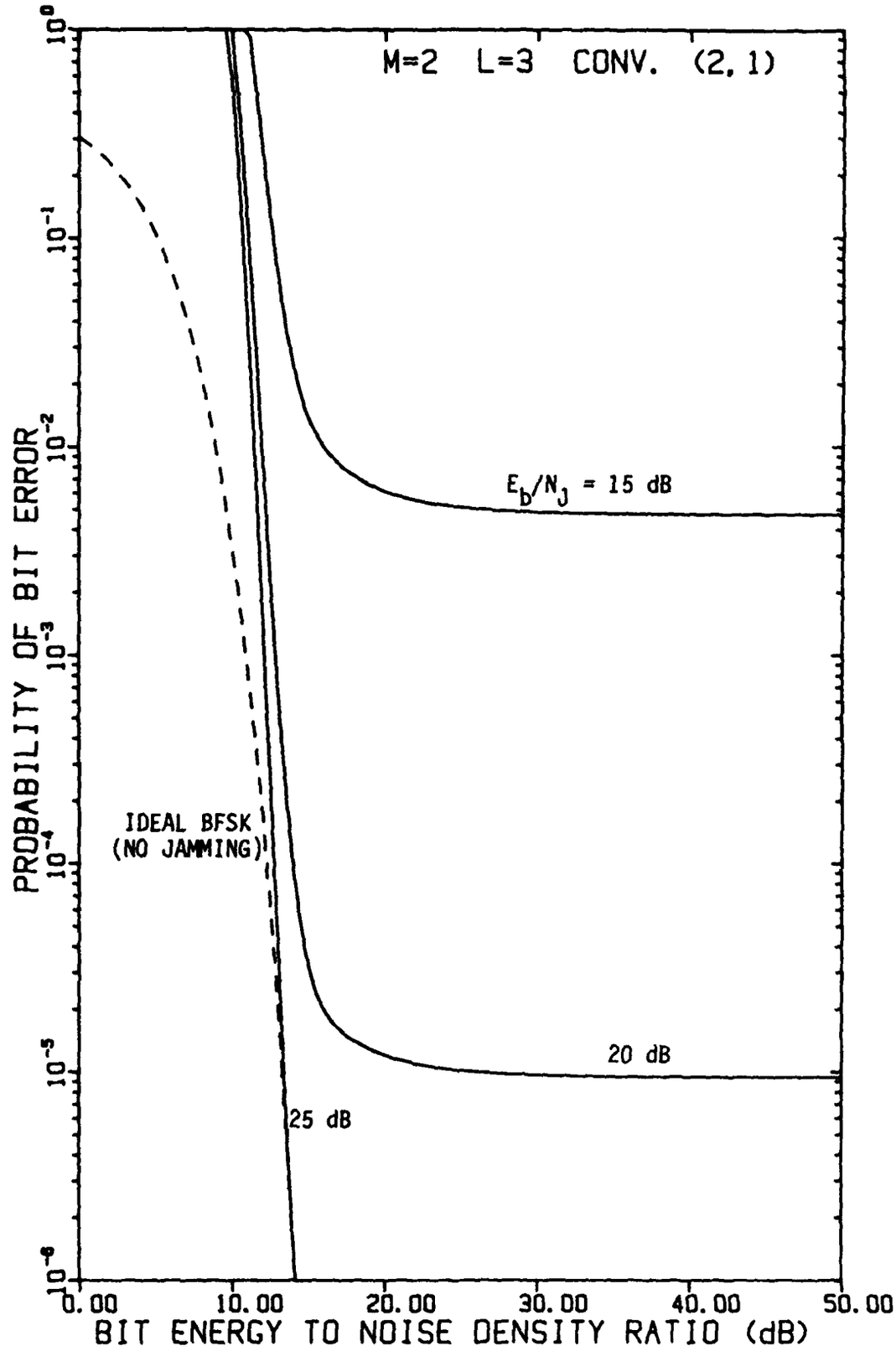

FIGURE 4-47 PERFORMANCE OF FH/BFSK WITH CONVOLUTIONAL RATE-1/2 CODE AND L=3 HOPS/DIGIT AS A FUNCTION OF E_b/N_0 WITH E_b/N_J AS A PARAMETER, USING A LINEAR COMBINING DEMODULATOR, IN OPTIMUM PARTIAL-BAND NOISE JAMMING

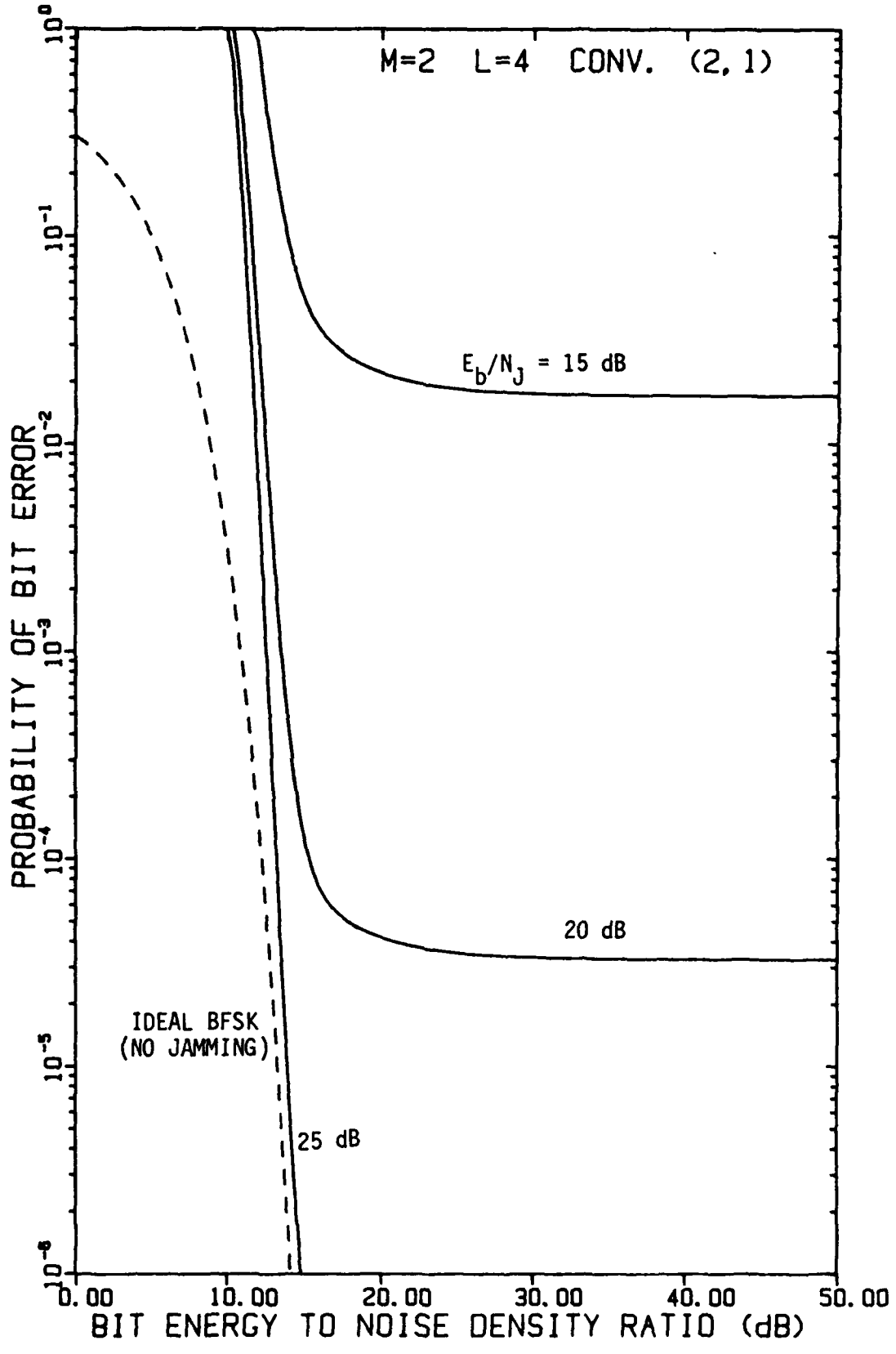

FIGURE 4-48 PERFORMANCE OF FH/BFSK WITH CONVOLUTIONAL RATE-1/2 CODE AND L=4 HOPS/DIGIT AS A FUNCTION OF E_b/N_0 WITH E_b/N_J AS A PARAMETER, USING A LINEAR COMBINING DEMODULATOR, IN OPTIMUM PARTIAL-BAND NOISE JAMMING

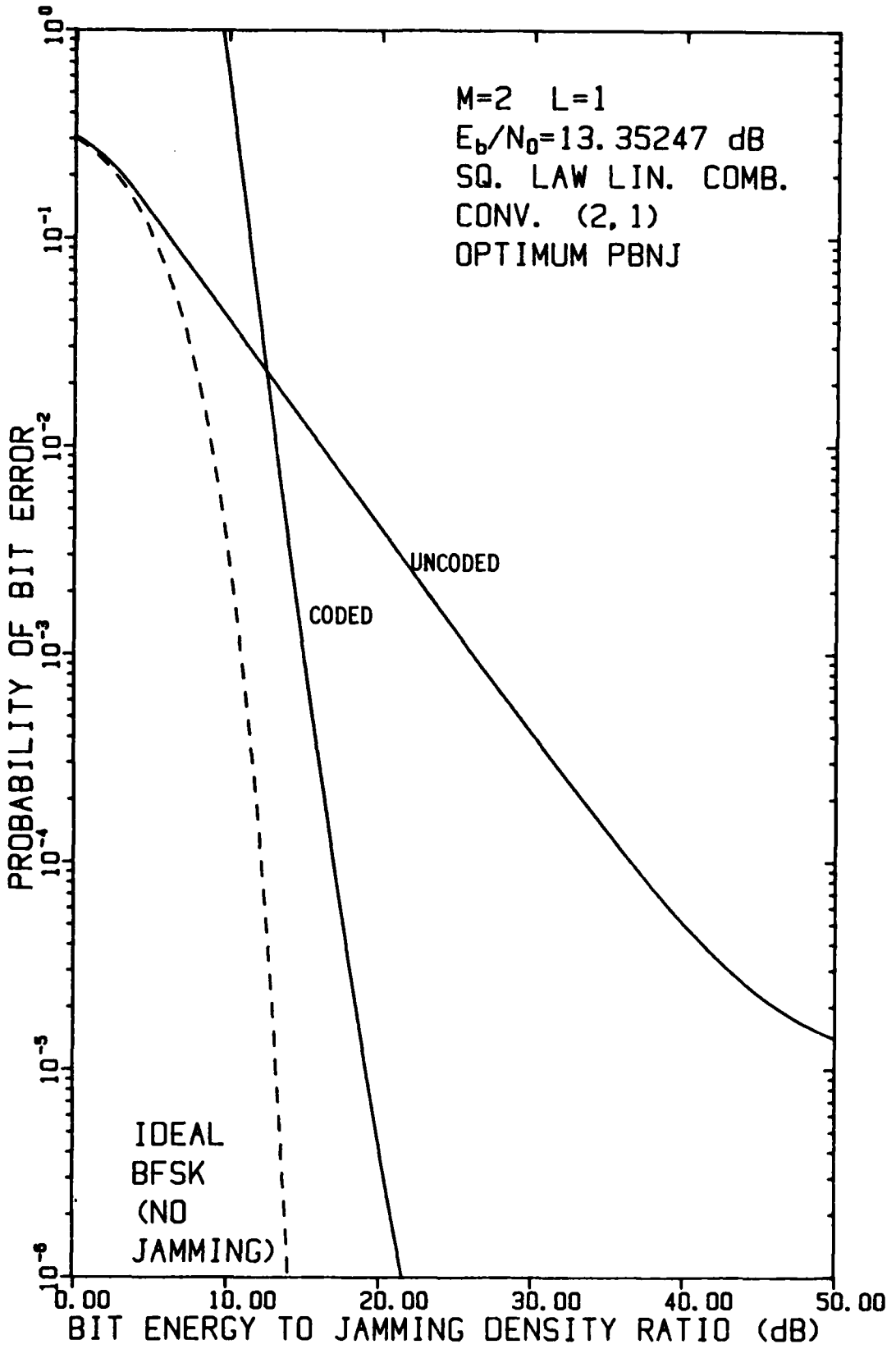

FIGURE 4-49 PERFORMANCE OF FH/BFSK WITH CONVOLUTIONAL RATE-1/2 CODE AND L=1 HOP/DIGIT AS A FUNCTION OF E_b/N_J WHEN E_b/N_0 = 13.35247 dB, USING A LINEAR COMBINING DEMODULATOR, IN OPTIMUM PARTIAL-BAND NOISE JAMMING

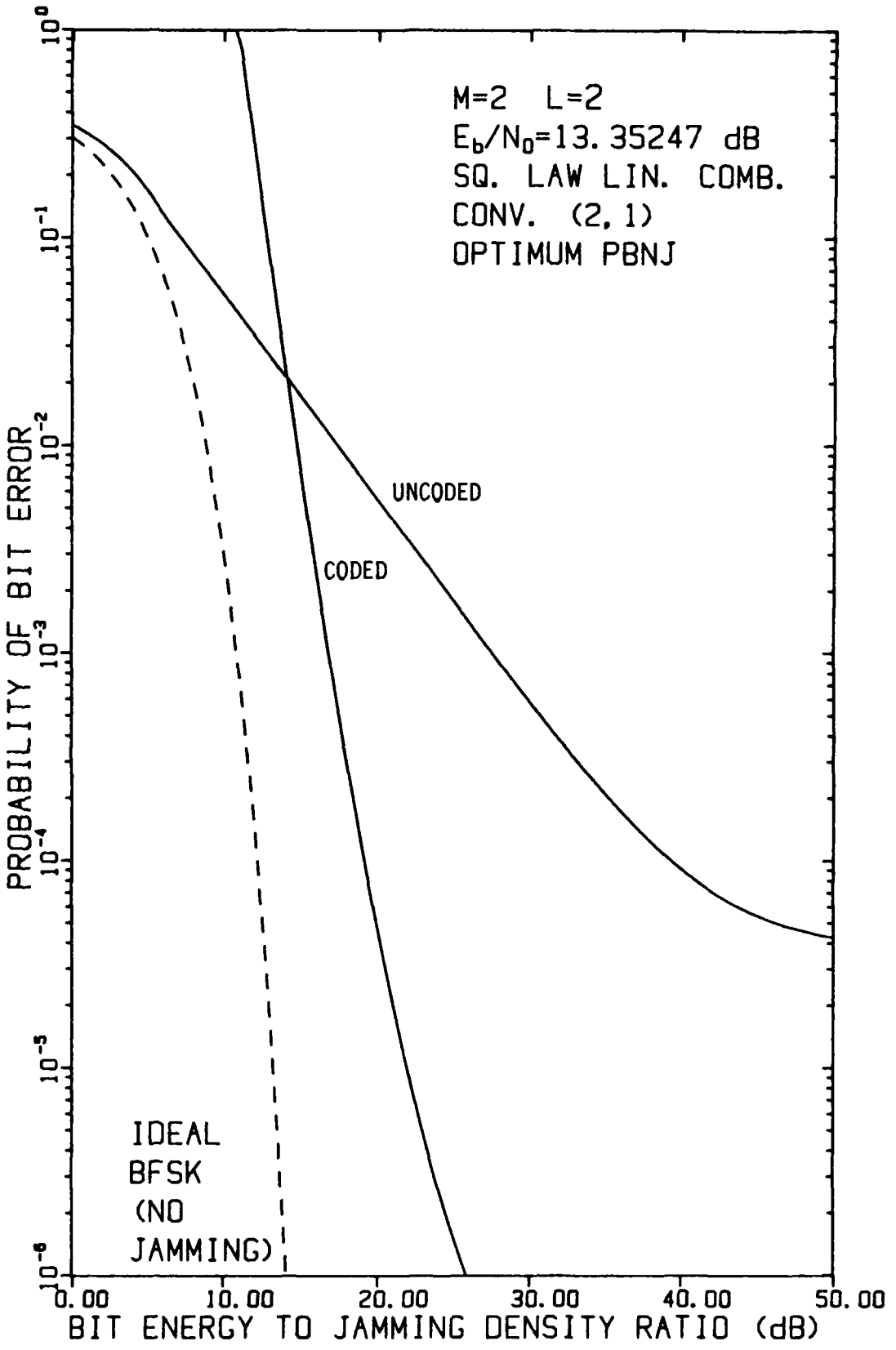

FIGURE 4-50 PERFORMANCE OF FH/BFSK WITH CONVOLUTIONAL RATE-1/2 CODE AND L=2 HOPS/DIGIT AS A FUNCTION OF E_b/N_J WHEN E_b/N_0 = 13.35247 dB, USING A LINEAR COMBINING DEMODULATOR, IN OPTIMUM PARTIAL-BAND NOISE JAMMING

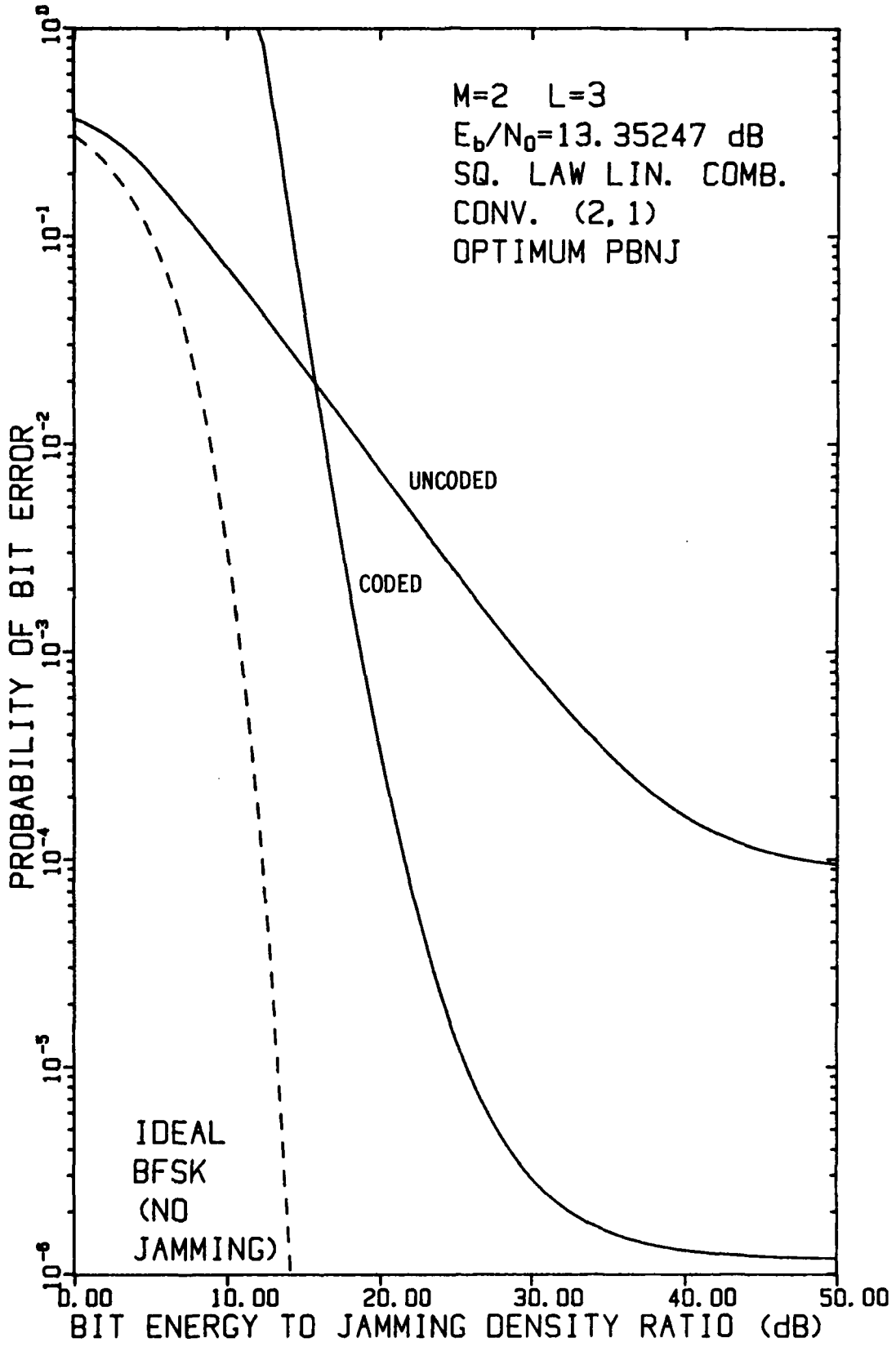

FIGURE 4-51 PERFORMANCE OF FH/BFSK WITH CONVOLUTIONAL RATE-1/2 CODE AND L=3 HOPS/DIGIT AS A FUNCTION OF E_b/N_J WHEN E_b/N_0 = 13.35247 dB, USING A LINEAR COMBINING DEMODULATOR, IN OPTIMUM PARTIAL-BAND NOISE JAMMING

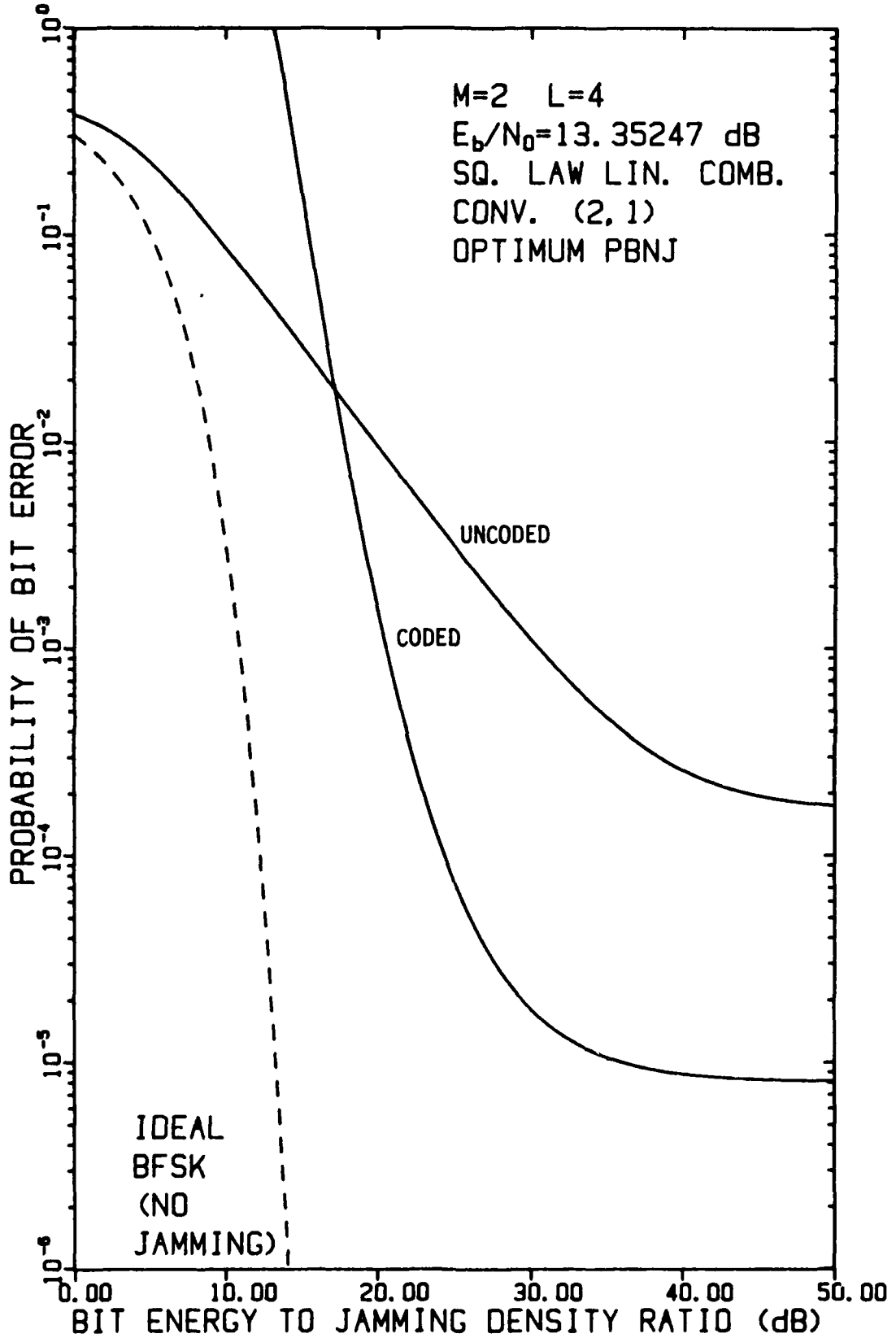

FIGURE 4-52 PERFORMANCE OF FH/BFSK WITH CONVOLUTIONAL RATE-1/2 CODE AND L=4 HOPS/DIGIT AS A FUNCTION OF E_b/N_J WHEN E_b/N_0 = 13.35247 dB, USING A LINEAR COMBINING DEMODULATOR, IN OPTIMUM PARTIAL-BAND NOISE JAMMING

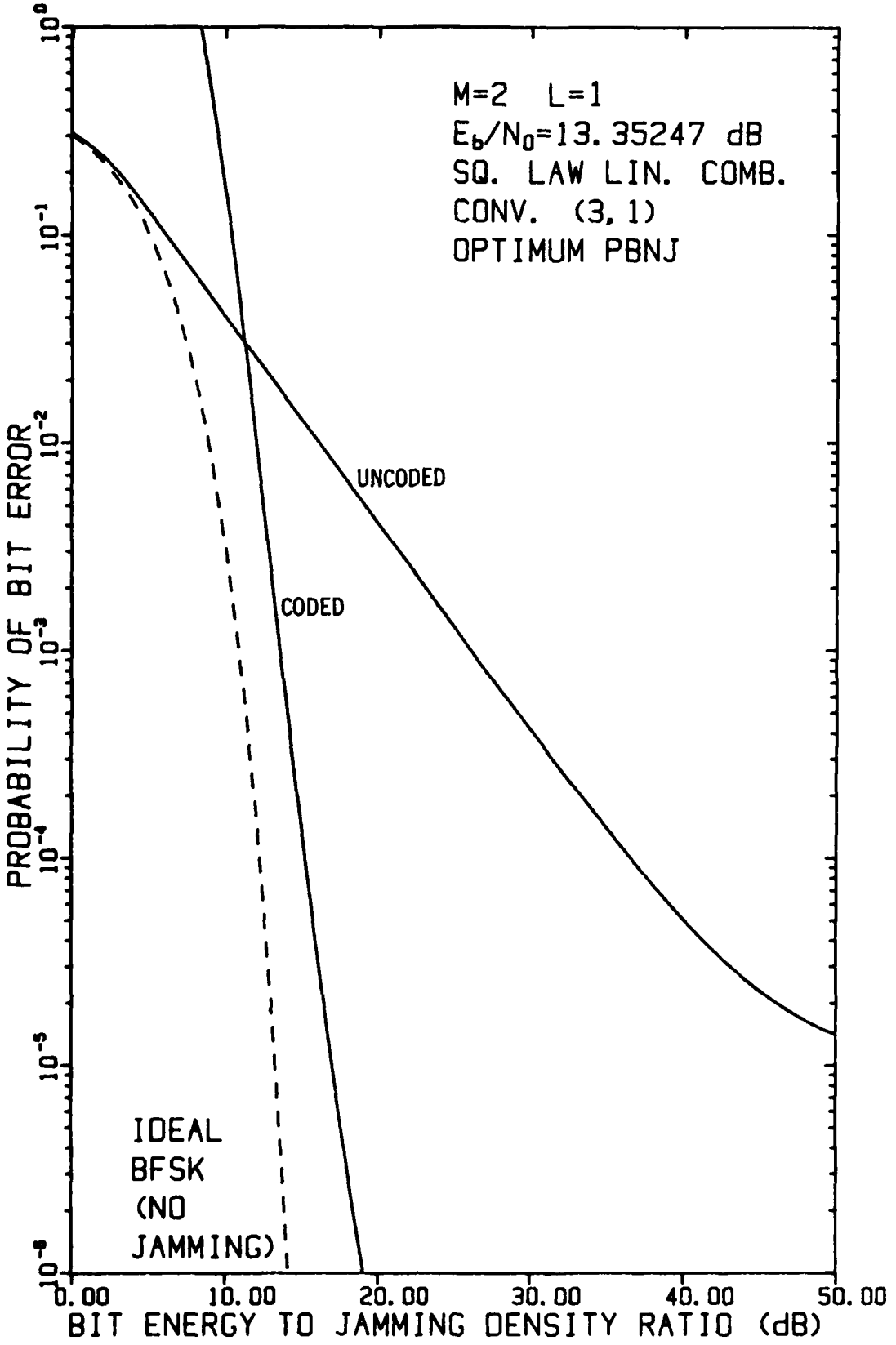

FIGURE 4-53 PERFORMANCE OF FH/BFSK WITH CONVOLUTIONAL RATE-1/3 CODE AND L=1 HOP/DIGIT AS A FUNCTION OF E_b/N_J WHEN E_b/N_0 = 13.35247 dB, USING A LINEAR COMBINING DEMODULATOR, IN OPTIMUM PARTIAL-BAND NOISE JAMMING

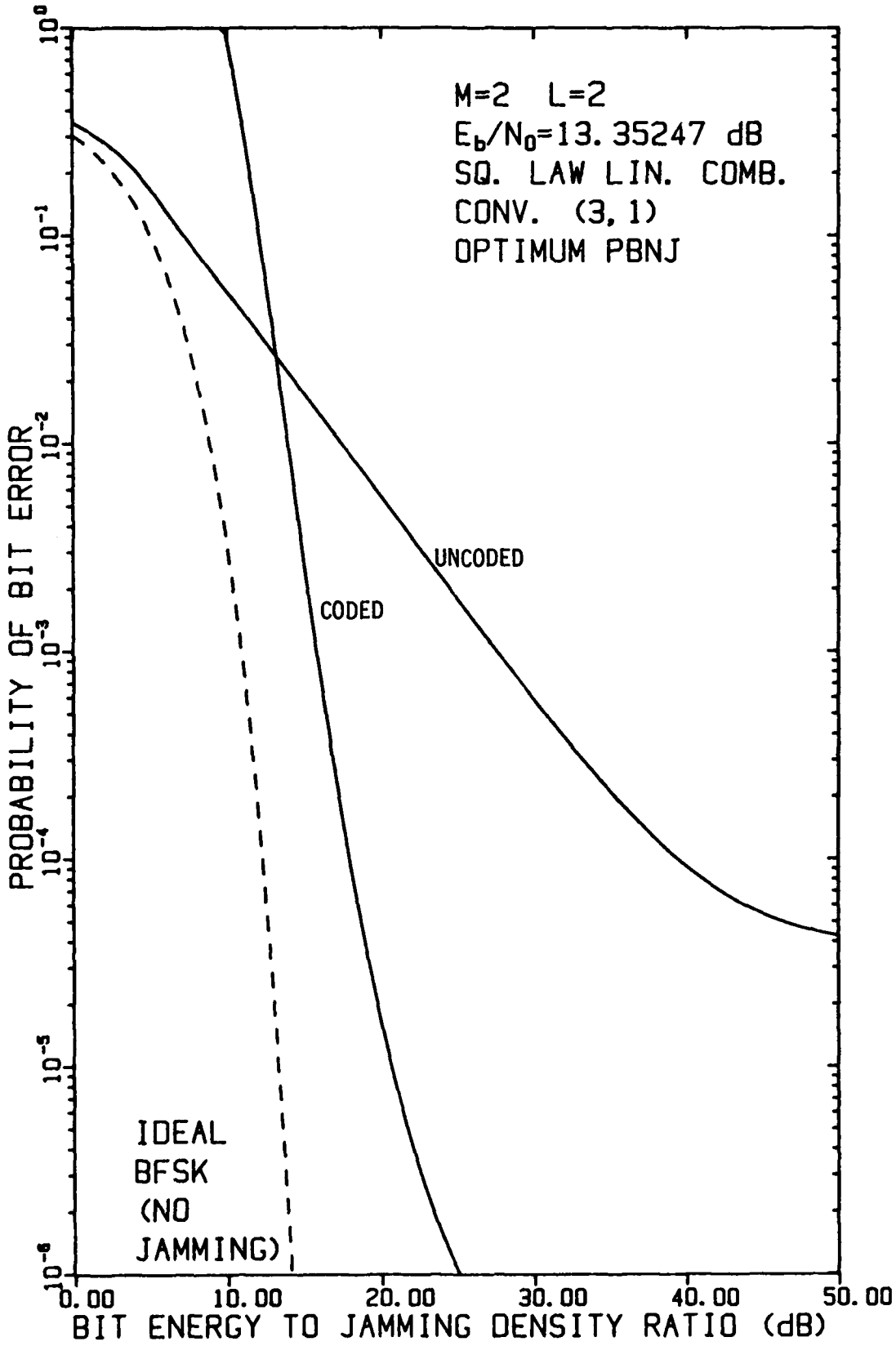

FIGURE 4-54 PERFORMANCE OF FH/BFSK WITH CONVOLUTIONAL RATE-1/3 CODE AND L=2 HOPS/DIGIT AS A FUNCTION OF E_b/N_J WHEN E_b/N_0 = 13.35247 dB, USING A LINEAR COMBINING DEMODULATOR, IN OPTIMUM PARTIAL-BAND NOISE JAMMING

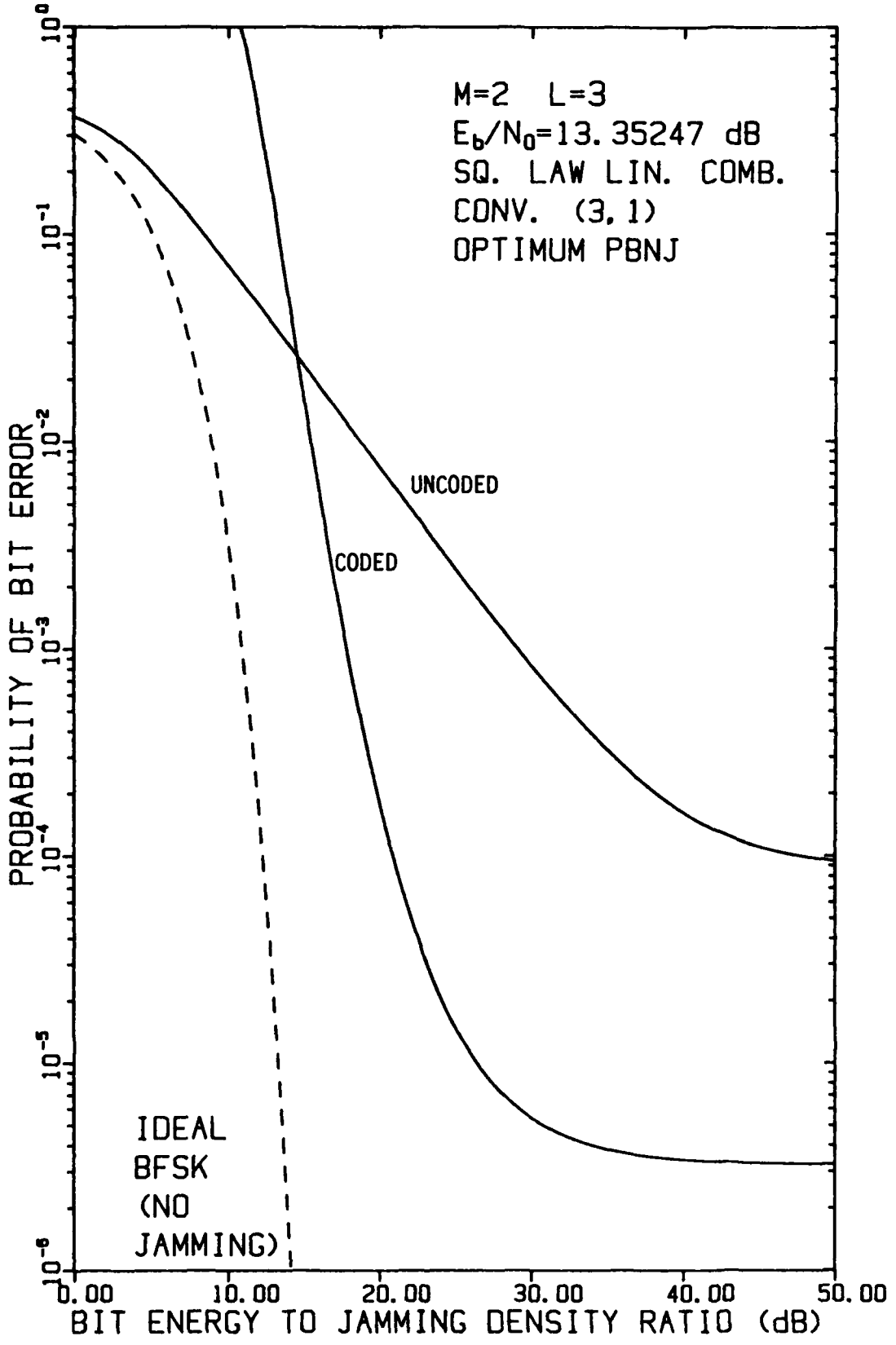

FIGURE 4-55 PERFORMANCE OF FH/BFSK WITH CONVOLUTIONAL RATE-1/3 CODE AND L=3 HOPS/DIGIT AS A FUNCTION OF E_b/N_J WHEN E_b/N_0 = 13.35247 dB, USING A LINEAR COMBINING DEMODULATOR, IN OPTIMUM PARTIAL-BAND NOISE JAMMING

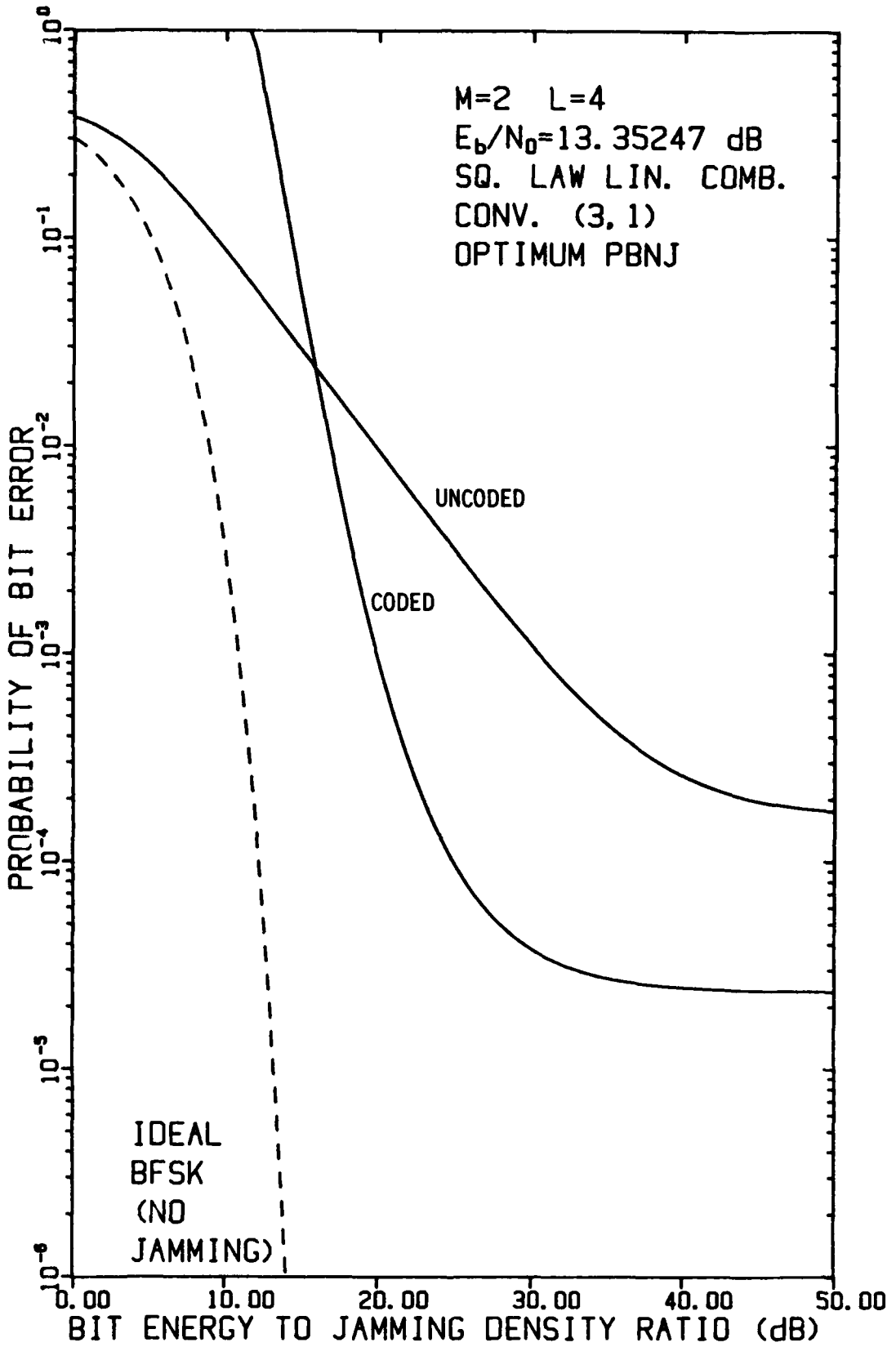

FIGURE 4-56 PERFORMANCE OF FH/BFSK WITH CONVOLUTIONAL RATE-1/3 CODE AND L=4 HOPS/DIGIT AS A FUNCTION OF E_b/N_J WHEN E_b/N_0 = 13.35247 dB, USING A LINEAR COMBINING DEMODULATOR, IN OPTIMUM PARTIAL-BAND NOISE JAMMING

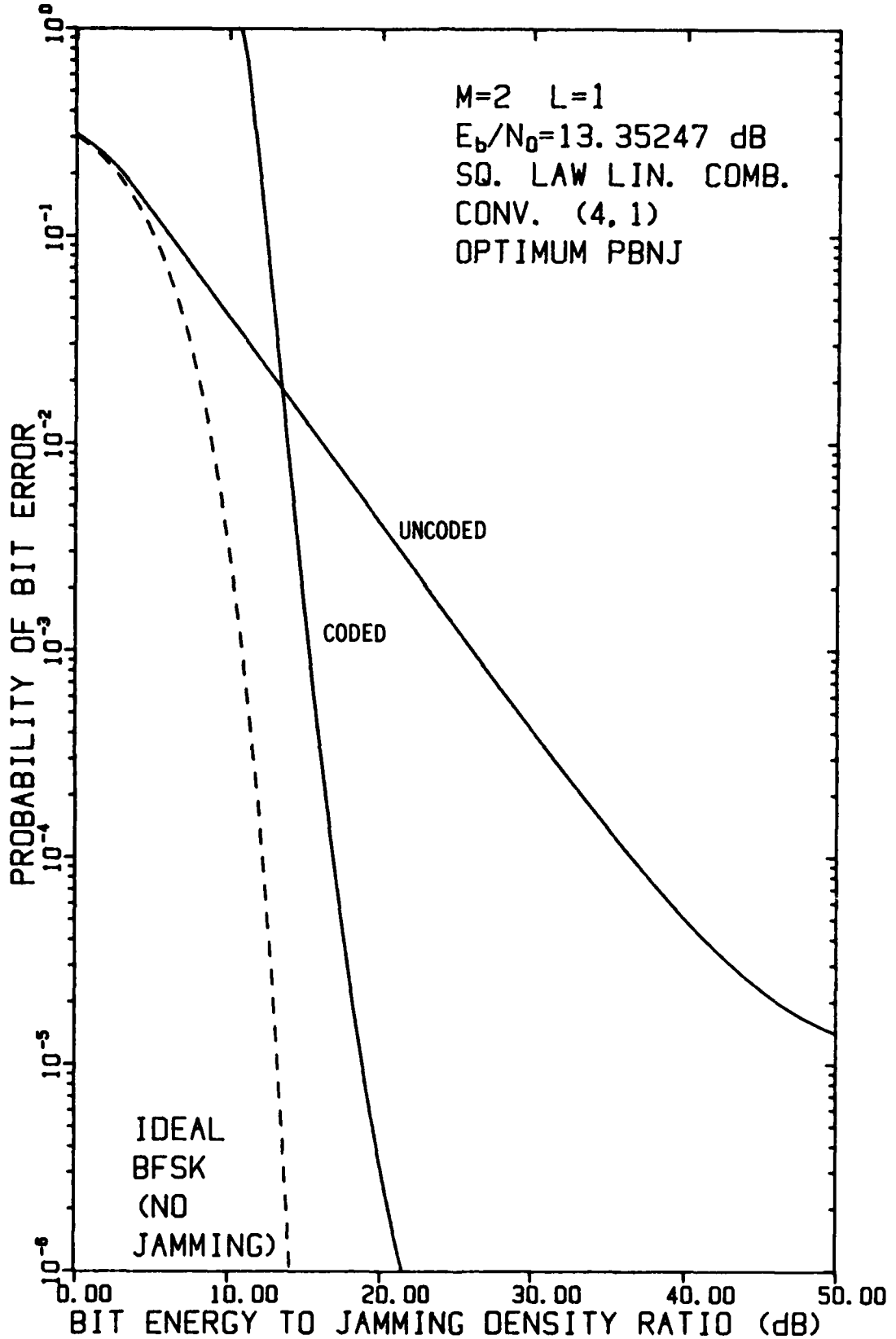

FIGURE 4-57 PERFORMANCE OF FH/BFSK WITH CONVOLUTIONAL RATE-1/4 CODE AND L=1 HOP/DIGIT AS A FUNCTION OF E_b/N_J WHEN E_b/N_0 = 13.35247 dB, USING A LINEAR COMBINING DEMODULATOR, IN OPTIMUM PARTIAL-BAND NOISE JAMMING

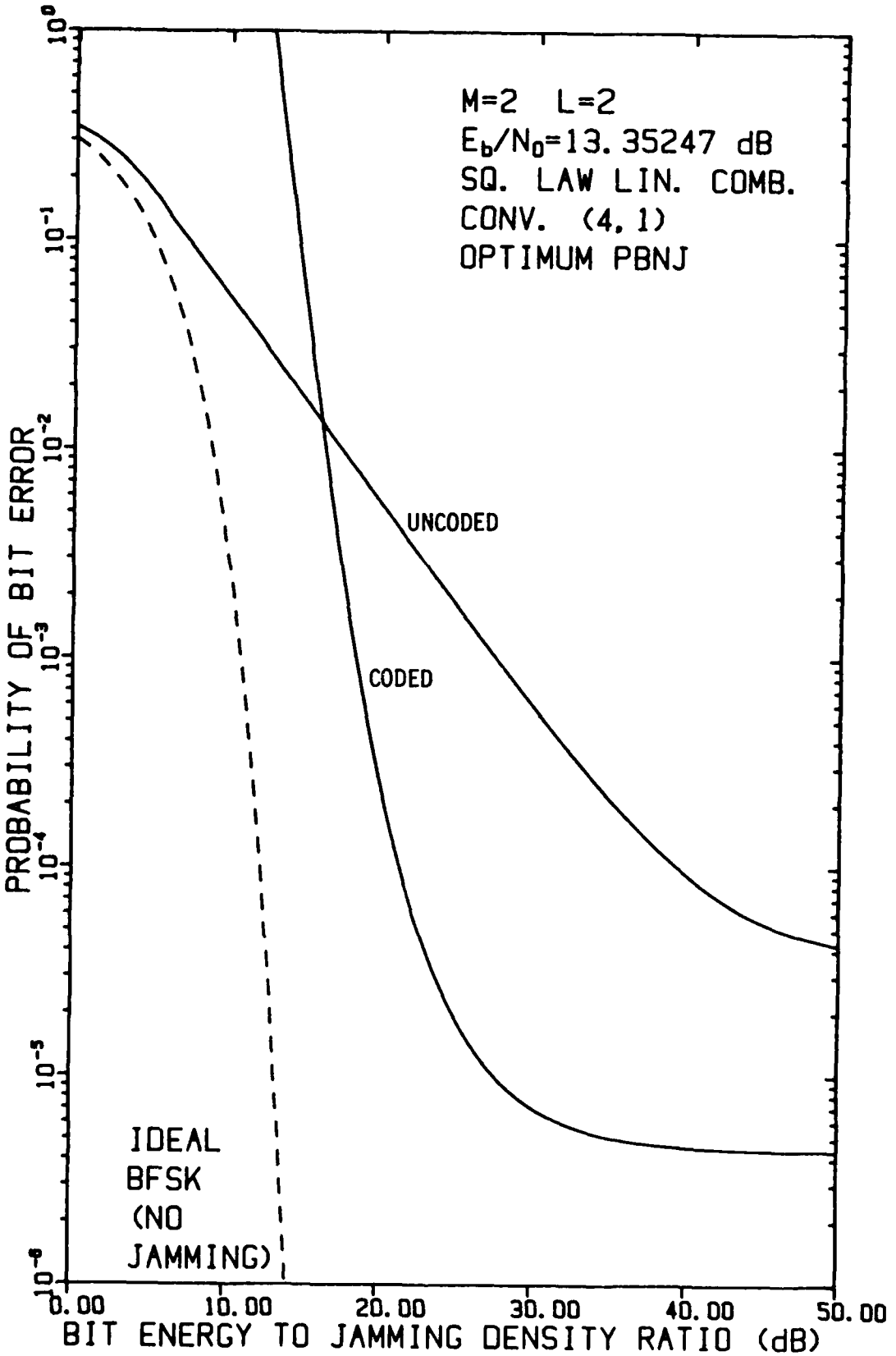

FIGURE 4-58 PERFORMANCE OF FH/BFSK WITH CONVOLUTIONAL RATE-1/4 CODE AND L=2 HOPS/DIGIT AS A FUNCTION OF E_b/N_J WHEN E_b/N_0 = 13.35247 dB, USING A LINEAR COMBINING DEMODULATOR, IN OPTIMUM PARTIAL-BAND NOISE JAMMING

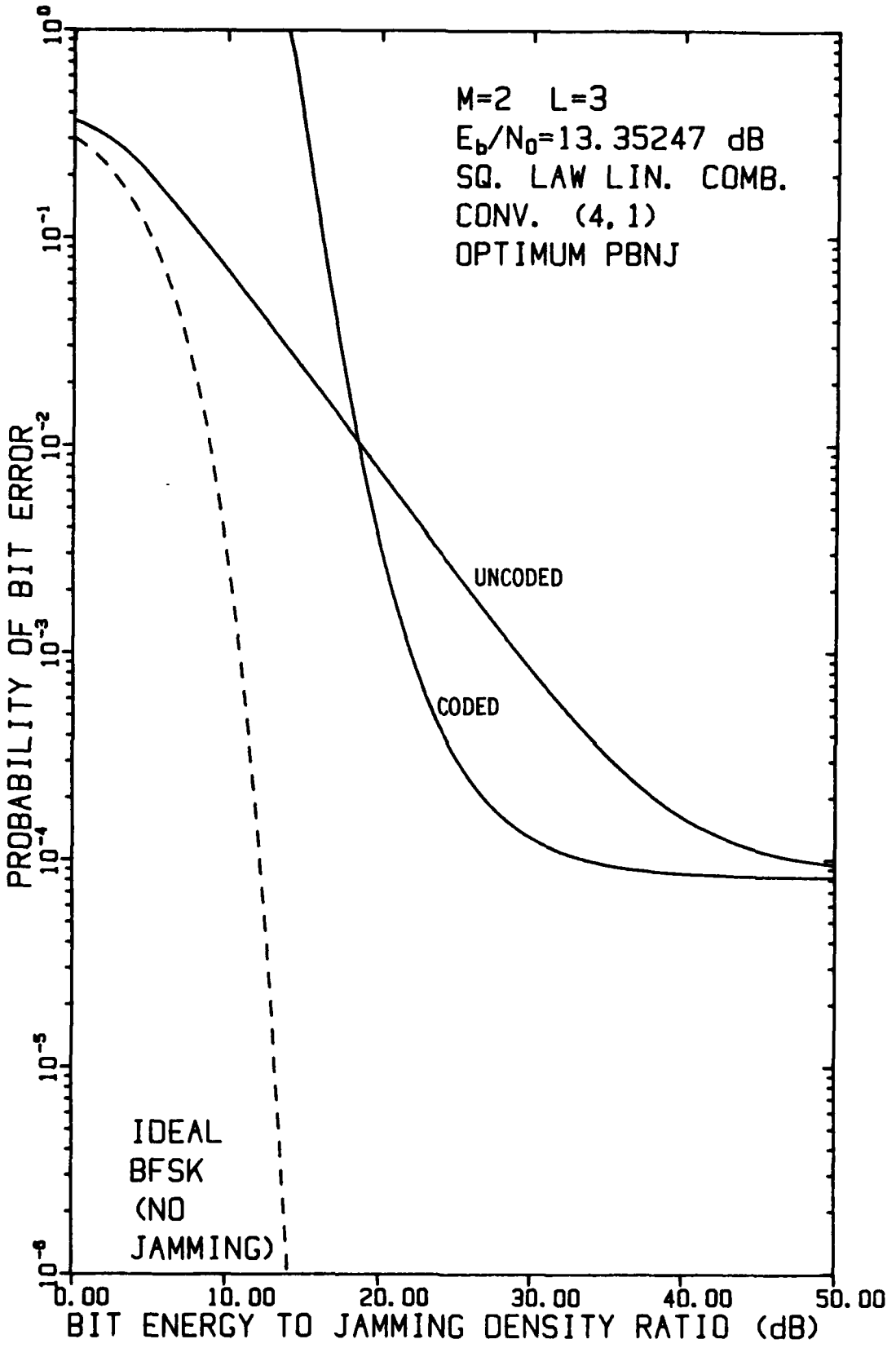

FIGURE 4-59 PERFORMANCE OF FH/BFSK WITH CONVOLUTIONAL RATE-1/4 CODE AND L=3 HOPS/DIGIT AS A FUNCTION OF E_b/N_J WITH E_b/N_0 = 13.35247 dB, USING A LINEAR COMBINING DEMODULATOR, IN OPTIMUM PARTIAL-BAND NOISE JAMMING

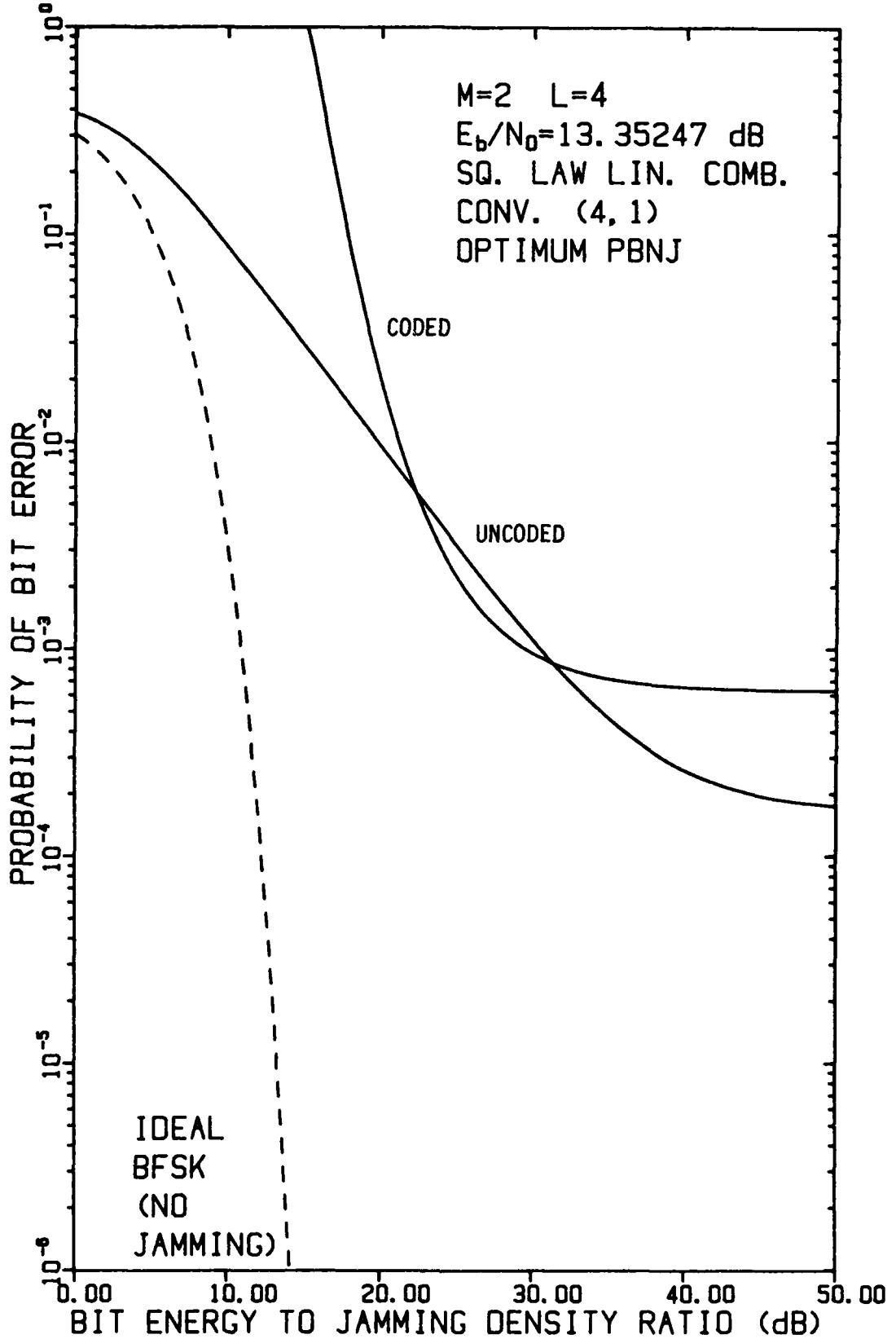

FIGURE 4-60 PERFORMANCE OF FH/BFSK WITH CONVOLUTIONAL RATE-1/4 CODE AND L=4 HOPS/DIGIT AS A FUNCTION OF E_b/N_J WHEN E_b/N_0 = 13.35247 dB, USING A LINEAR COMBINING DEMODULATOR, IN OPTIMUM PARTIAL-BAND NOISE JAMMING

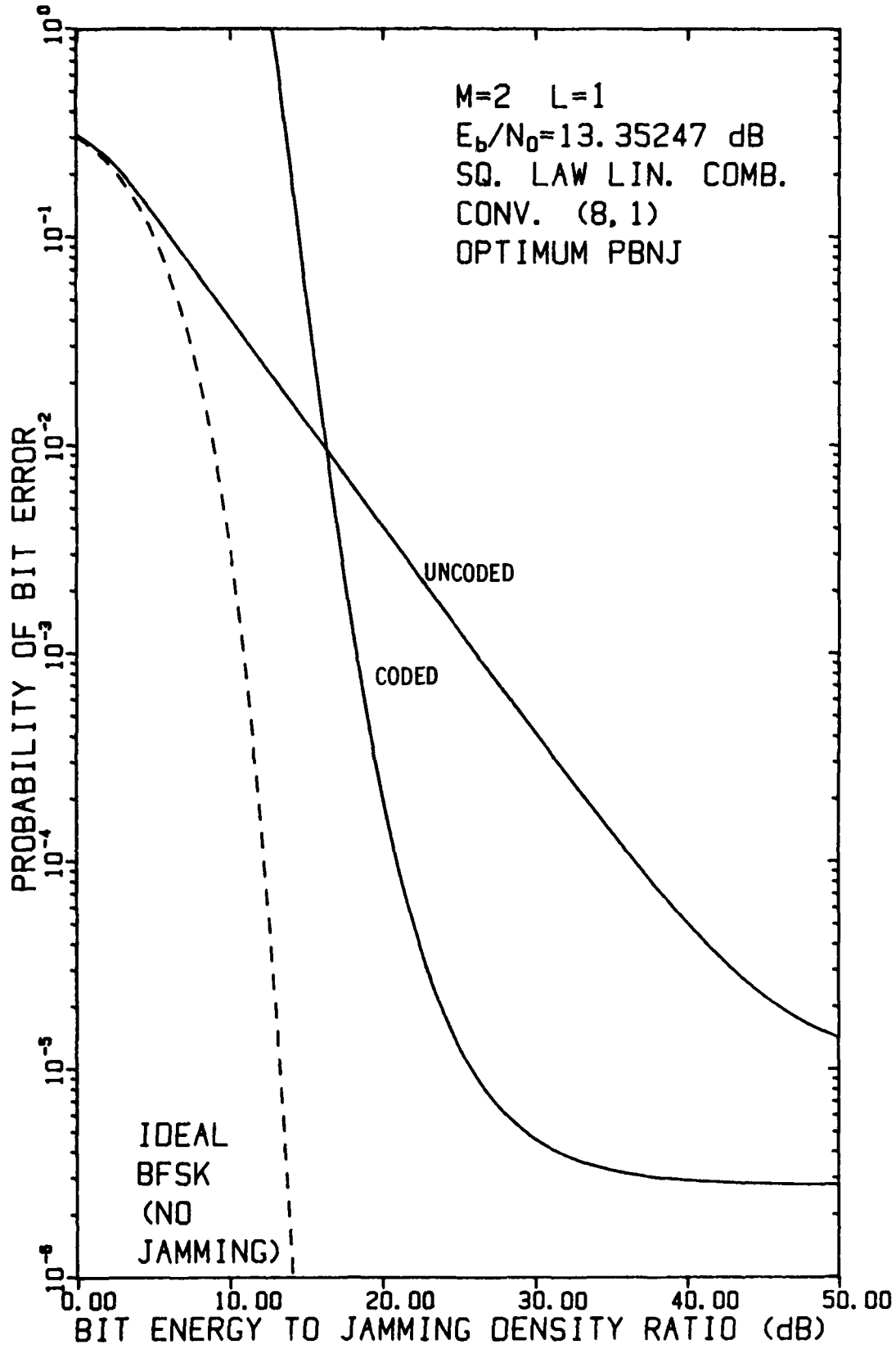

FIGURE 4-61 PERFORMANCE OF FH/BFSK WITH CONVOLUTIONAL RATE-1/8 CODE AND L=1 HOP/DIGIT AS A FUNCTION OF E_b/N_J WHEN E_b/N_0 = 13.35247 dB, USING A LINEAR COMBINING DEMODULATOR, IN OPTIMUM PARTIAL-BAND NOISE JAMMING

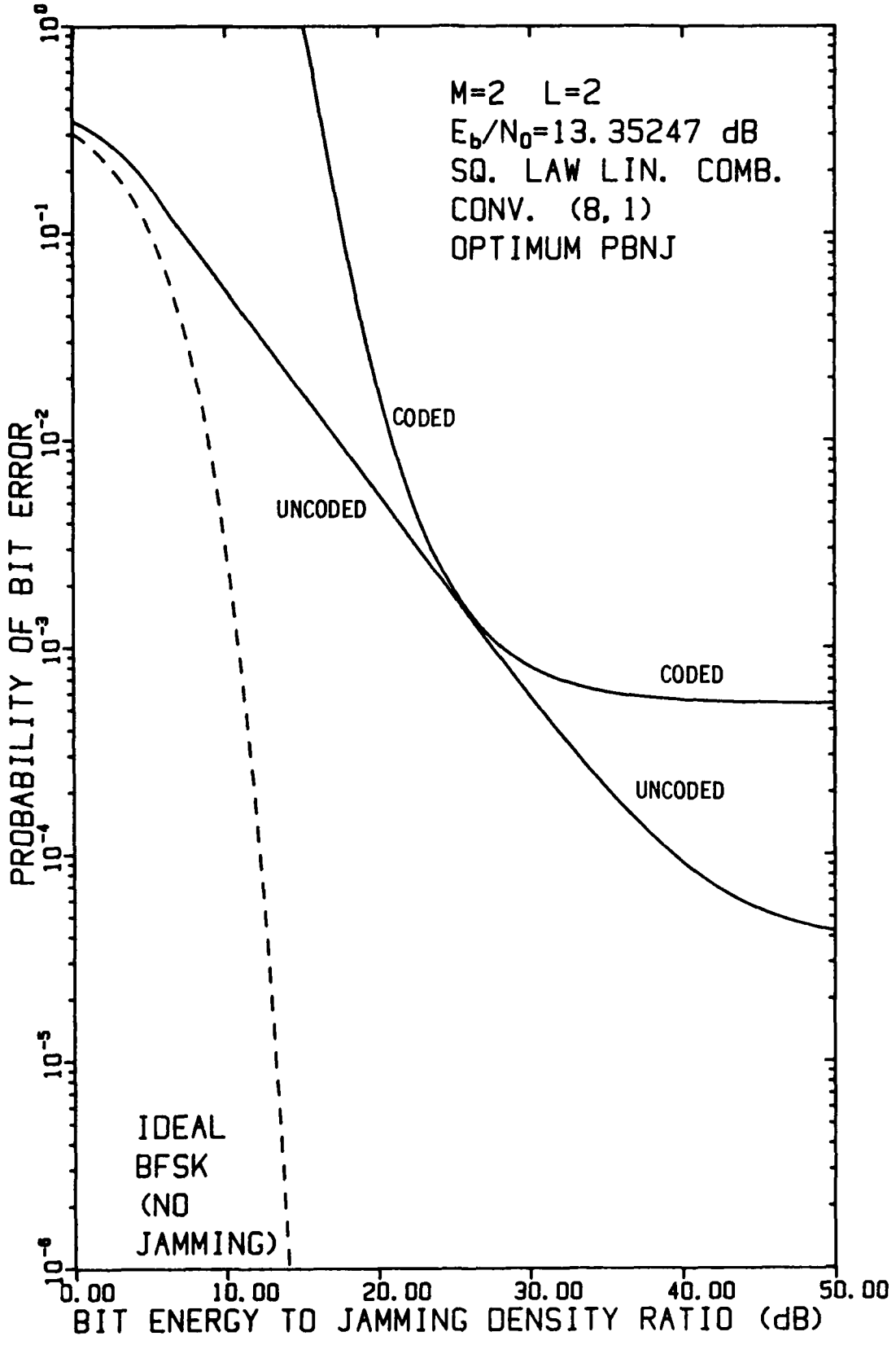

FIGURE 4-62 PERFORMANCE OF FH/BFSK WITH CONVOLUTIONAL RATE-1/8 CODE AND L=2 HOPS/DIGIT AS A FUNCTION OF E_b/N_J WHEN E_b/N_0 = 13.35247 dB, USING A LINEAR COMBINING DEMODULATOR, IN OPTIMUM PARTIAL-BAND NOISE JAMMING

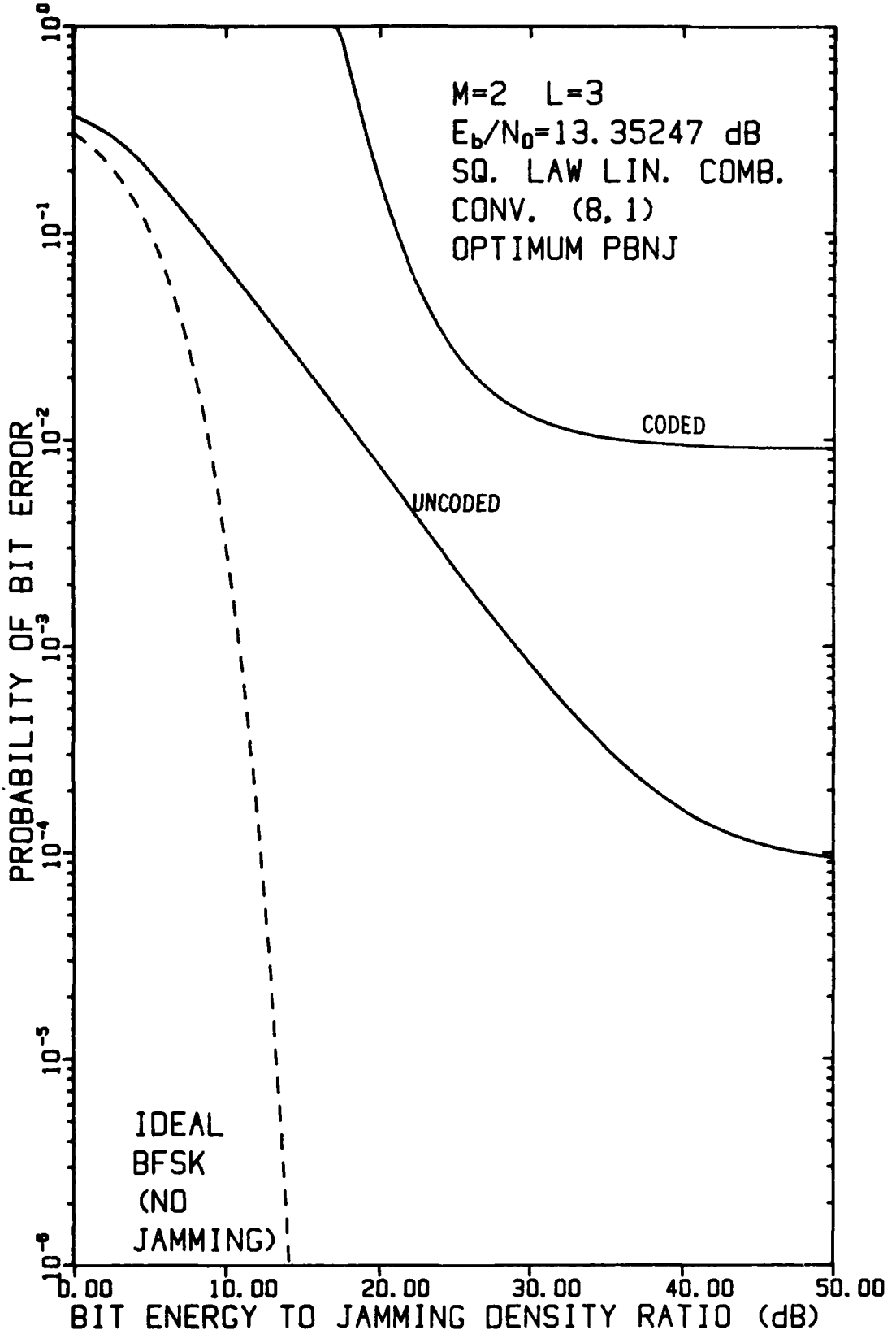

FIGURE 4-63 PERFORMANCE OF FH/BFSK WITH CONVOLUTIONAL RATE-1/8 CODE AND L=3 HOPS/DIGIT AS A FUNCTION OF E_b/N_J WHEN E_b/N_0 = 13.35247 dB, USING A LINEAR COMBINING DEMODULATOR, IN OPTIMUM PARTIAL-BAND NOISE JAMMING

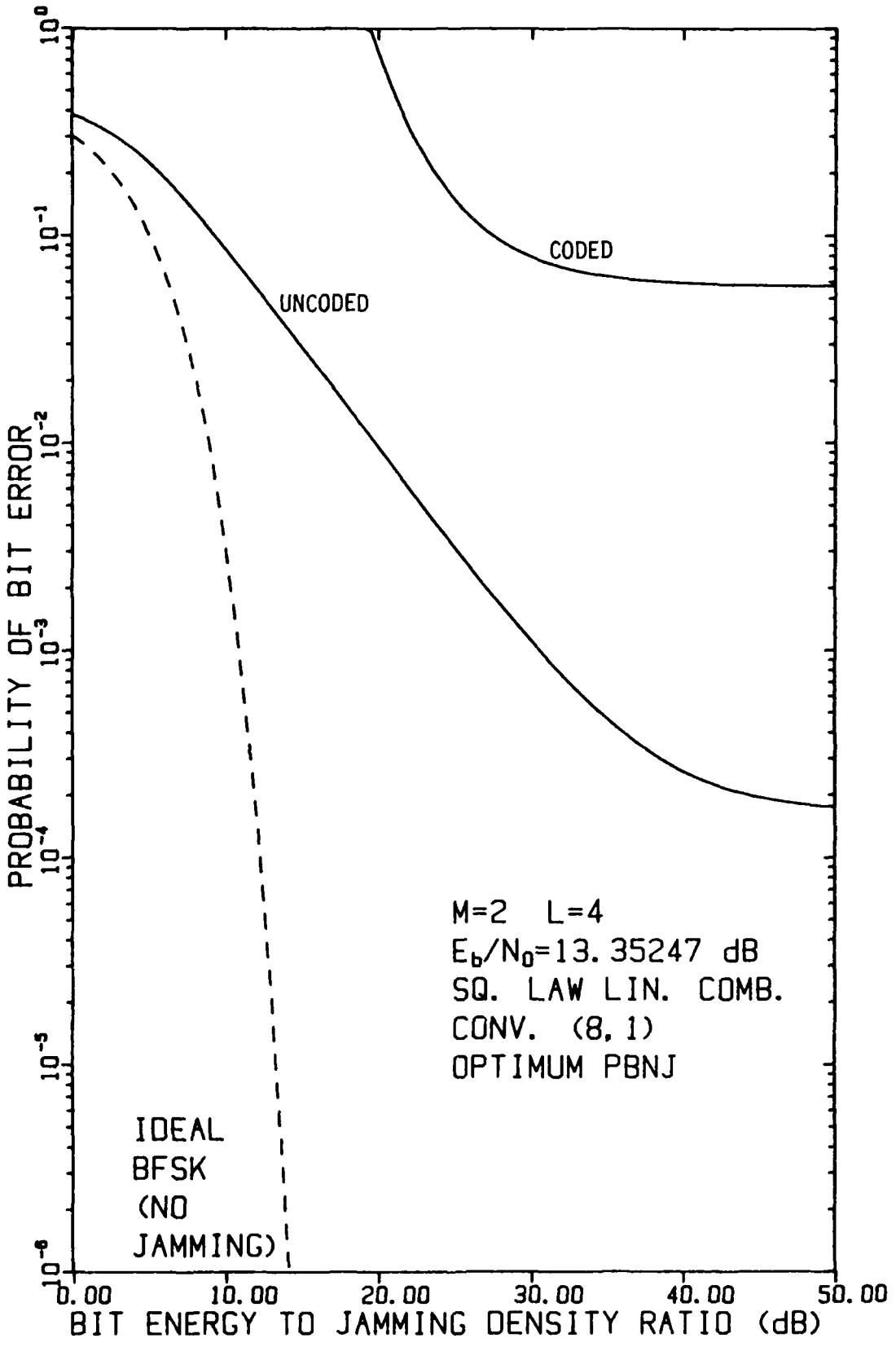

FIGURE 4-64 PERFORMANCE OF FH/BFSK WITH CONVOLUTIONAL RATE-1/8 CODE AND L=4 HOPS/DIGIT AS A FUNCTION OF E_b/N_J WHEN E_b/N_0 = 13.35247 dB, USING A LINEAR COMBINING DEMODULATOR, IN OPTIMUM PARTIAL-BAND NOISE JAMMING

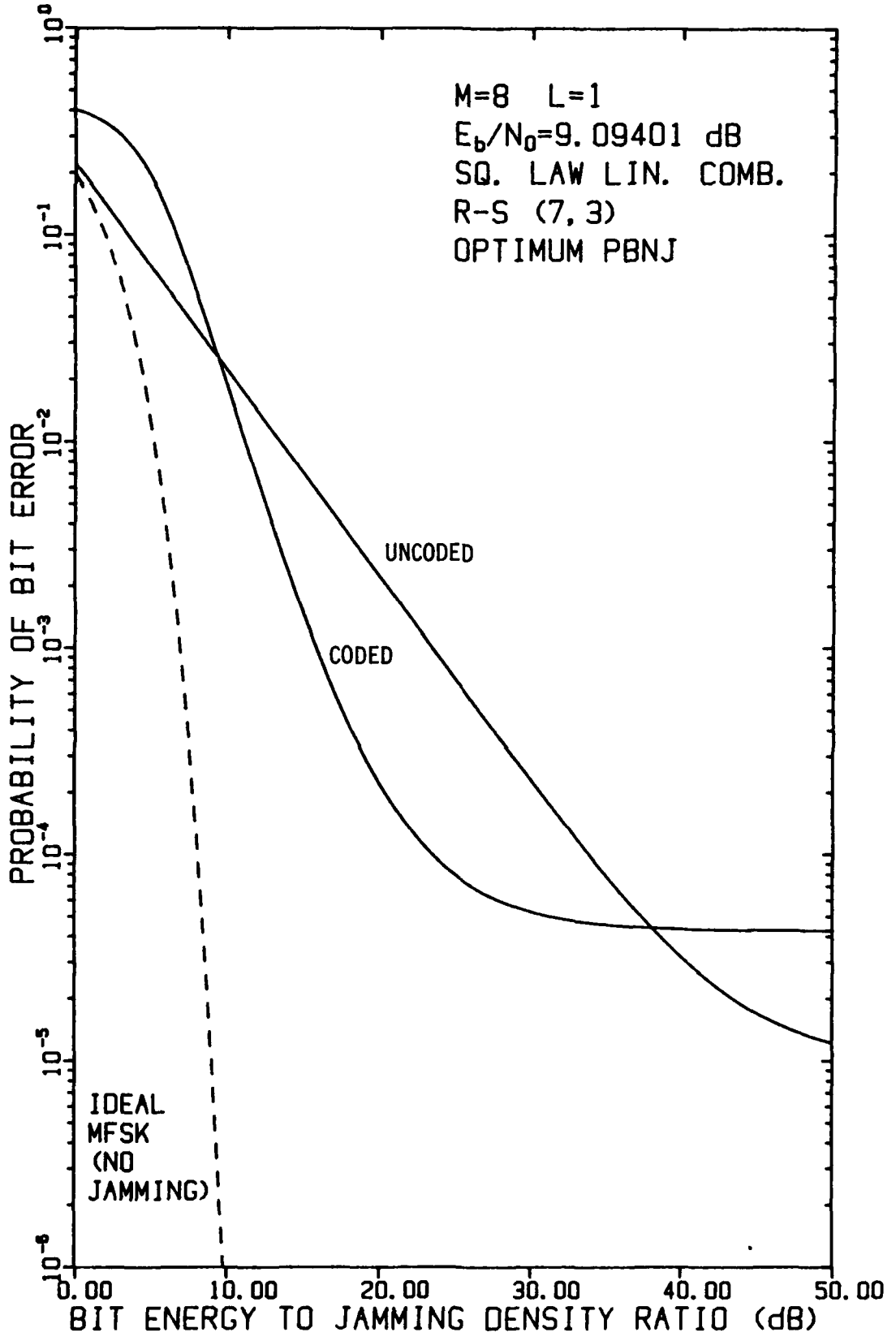

FIGURE 4-65 PERFORMANCE OF FH/MFSK WITH REED-SOLOMON (7,3) CODE AND L=1 HOP/DIGIT AS A FUNCTION OF E_b/N_J WHEN E_b/N_0 = 9.09401 dB, USING A LINEAR COMBINING DEMODULATOR, IN OPTIMUM PARTIAL-BAND NOISE JAMMING

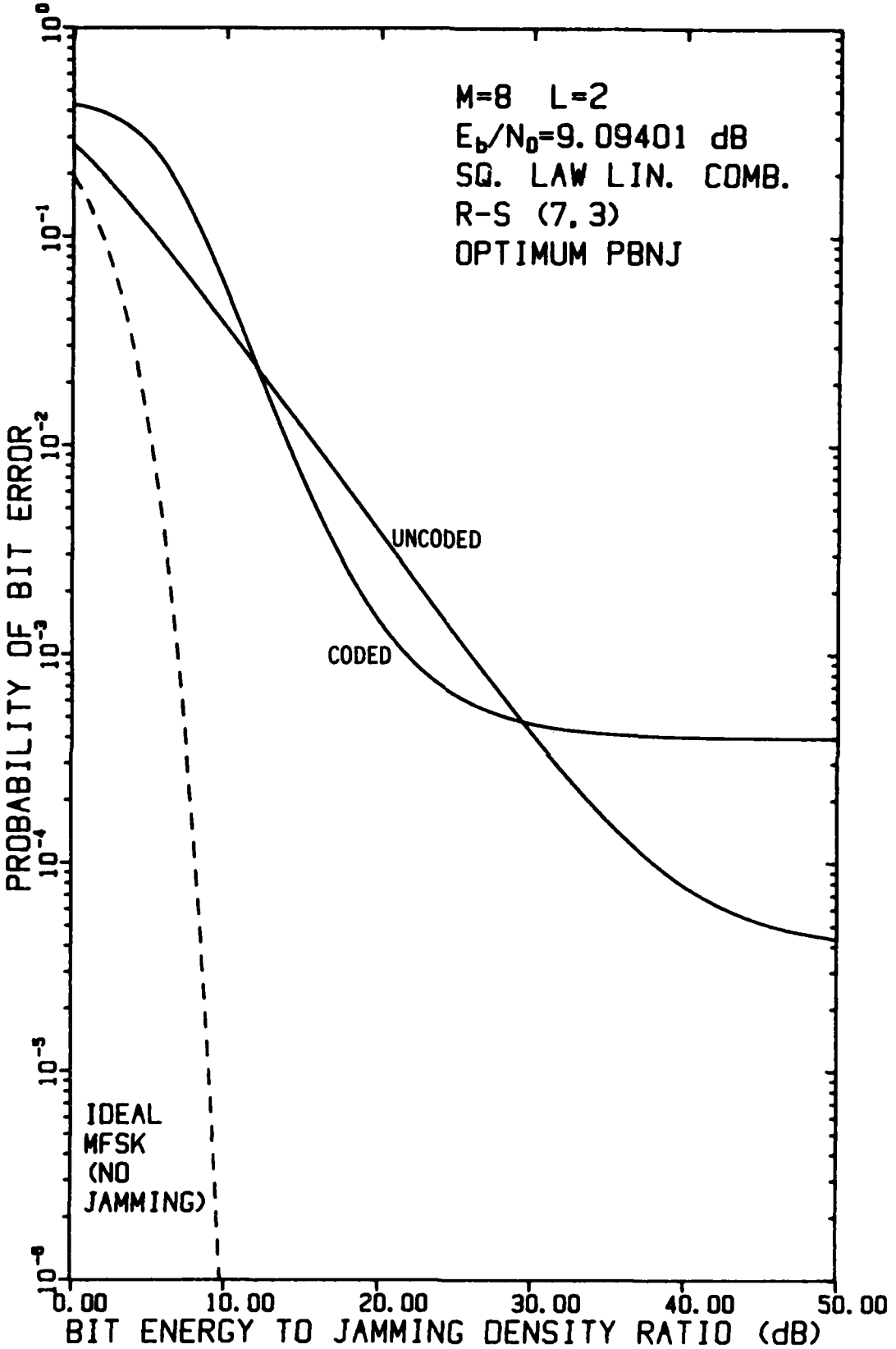

FIGURE 4-66 PERFORMANCE OF FH/MFSK WITH REED-SOLOMON (7,3) CODE AND L=2 HOPS/DIGIT AS A FUNCTION OF E_b/N_J WHEN E_b/N_0 = 9.09401 dB, USING A LINEAR COMBINING DEMODULATOR, IN OPTIMUM PARTIAL-BAND NOISE JAMMING

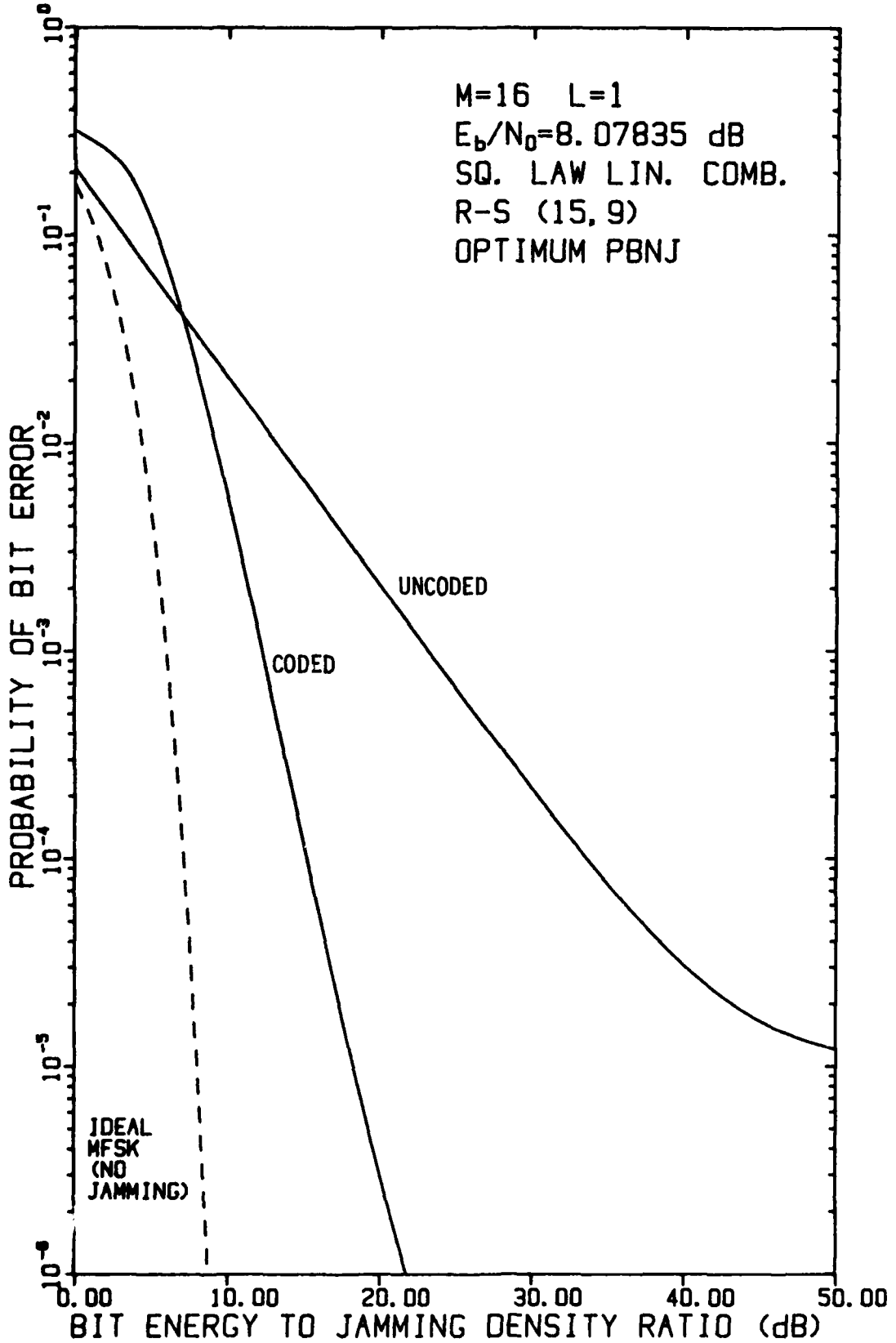

FIGURE 4-67 PERFORMANCE OF FH/MFSK WITH REED-SOLOMON (15,9) CODE AND L=1 HOP/DIGIT AS A FUNCTION OF E_b/N_J WHEN E_b/N_0 = 8.07835 dB, USING A LINEAR COMBINING DEMODULATOR, IN OPTIMUM PARTIAL-BAND NOISE JAMMING

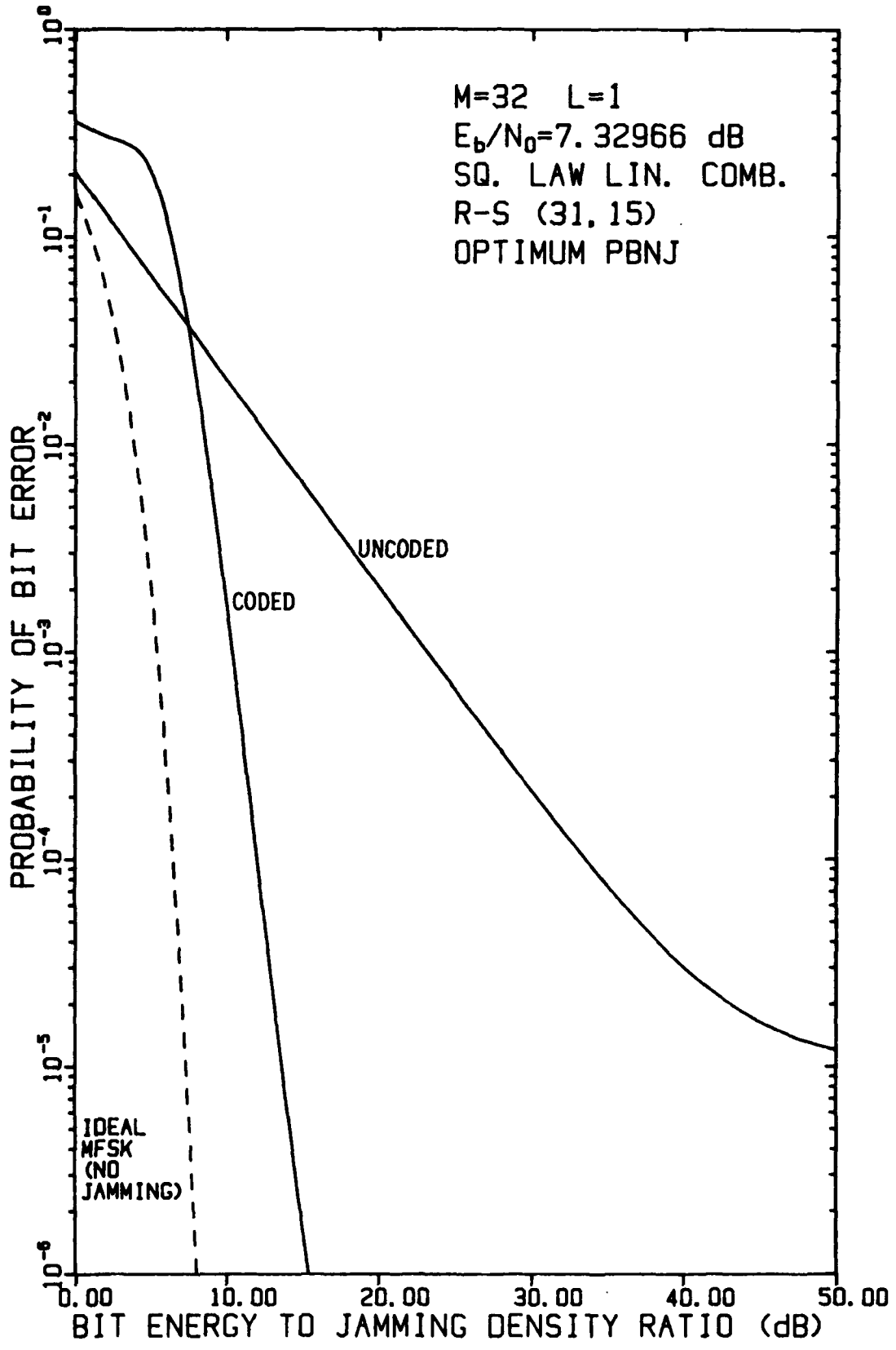

FIGURE 4-68 PERFORMANCE OF FH/MFSK WITH REED-SOLOMON (31,15) CODE AND L=1 HOP/DIGIT AS A FUNCTION OF E_b/N_J WHEN E_b/N_0 = 7.32966 dB, USING A LINEAR COMBINING DEMODULATOR, IN OPTIMUM PARTIAL-BAND NOISE JAMMING

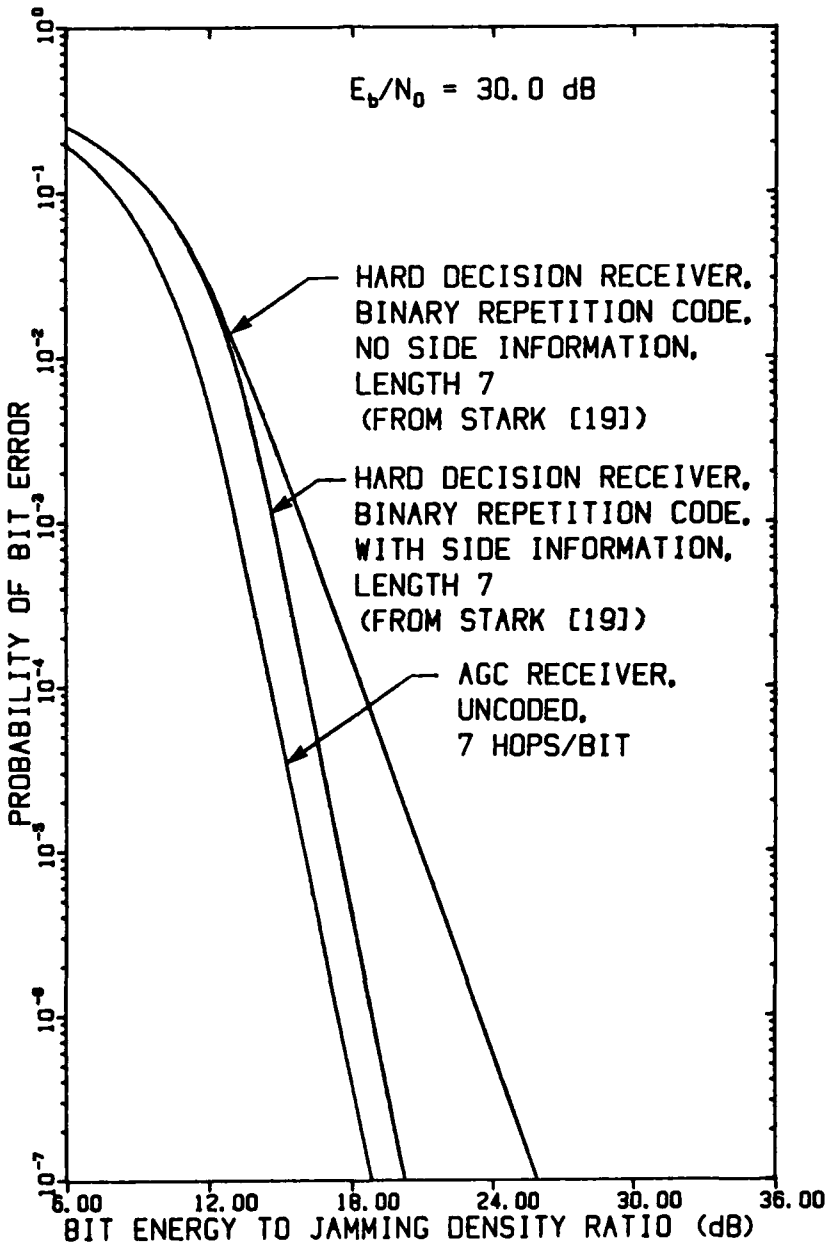

FIGURE 4-69 COMPARISON OF PERFORMANCE OF FH/BFSK AGC RECEIVER WITH L=7 DIVERSITY AND PERFORMANCE OF HARD DECISION RECEIVERS WITH LENGTH-7 BINARY REPETITION CODES

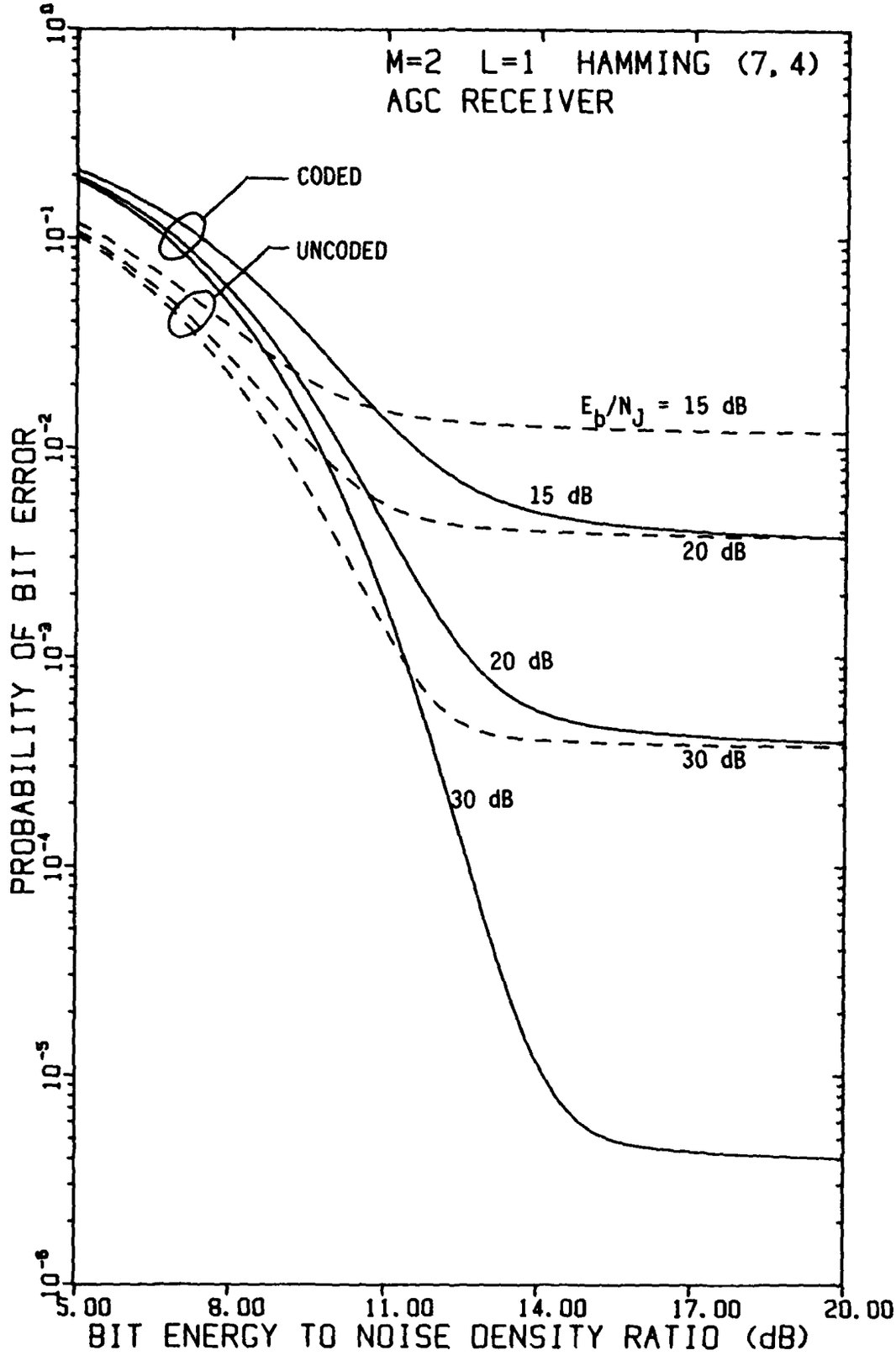

FIGURE 4-70 PERFORMANCE OF FH/BFSK WITH HAMMING (7,4) CODE AND L=1 HOP/DIGIT AS A FUNCTION OF E_b/N_0 WITH E_b/N_J AS A PARAMETER, USING AN AGC DEMODULATOR, IN OPTIMUM PARTIAL-BAND NOISE JAMMING

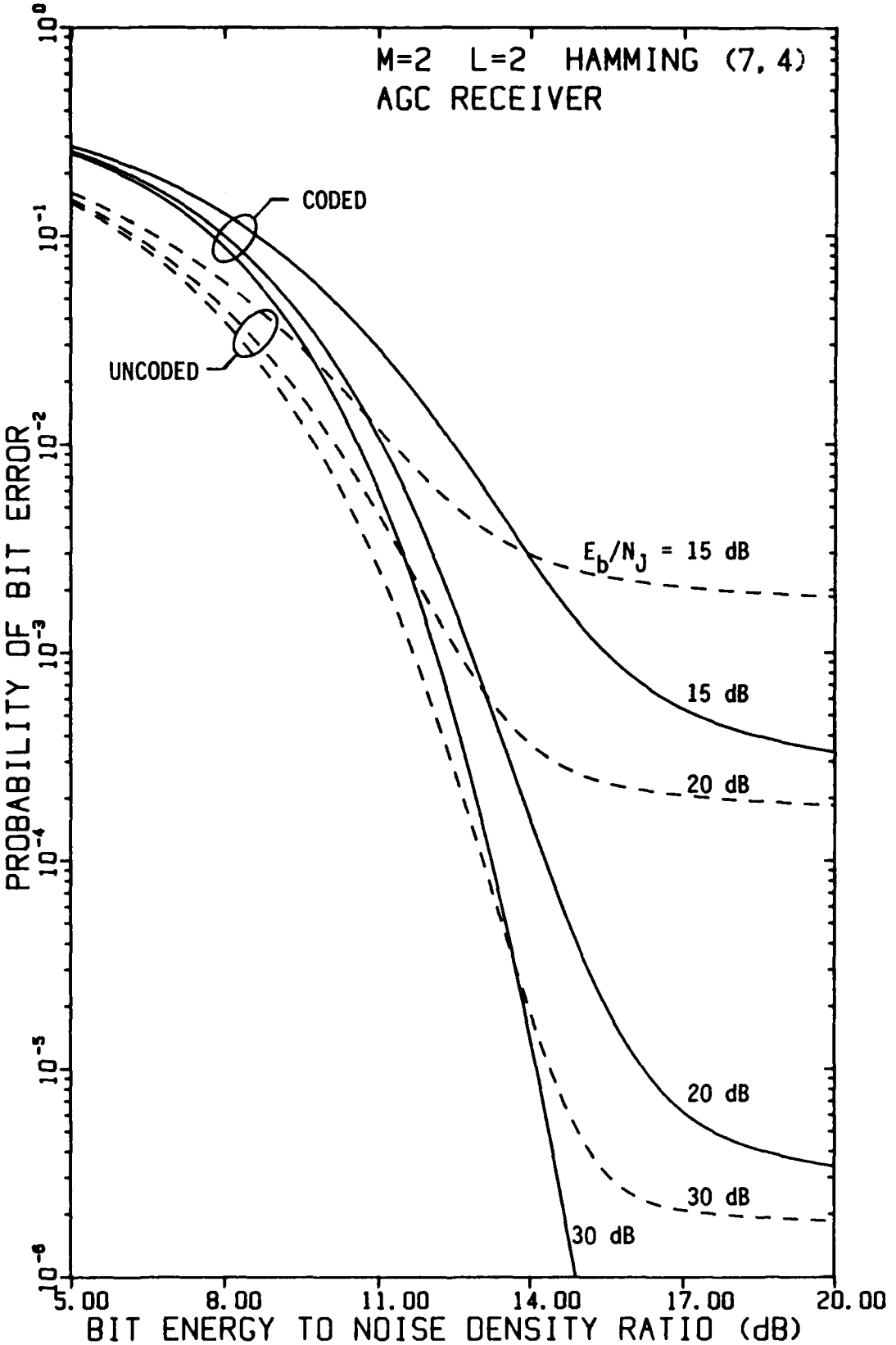

FIGURE 4-71 PERFORMANCE OF FH/BFSK WITH HAMMING (7,4) CODE AND L=2 HOPS/DIGIT AS A FUNCTION OF E_b/N_0 WITH E_b/N_J AS A PARAMETER, USING AN AGC DEMODULATOR, IN OPTIMUM PARTIAL-BAND NOISE JAMMING

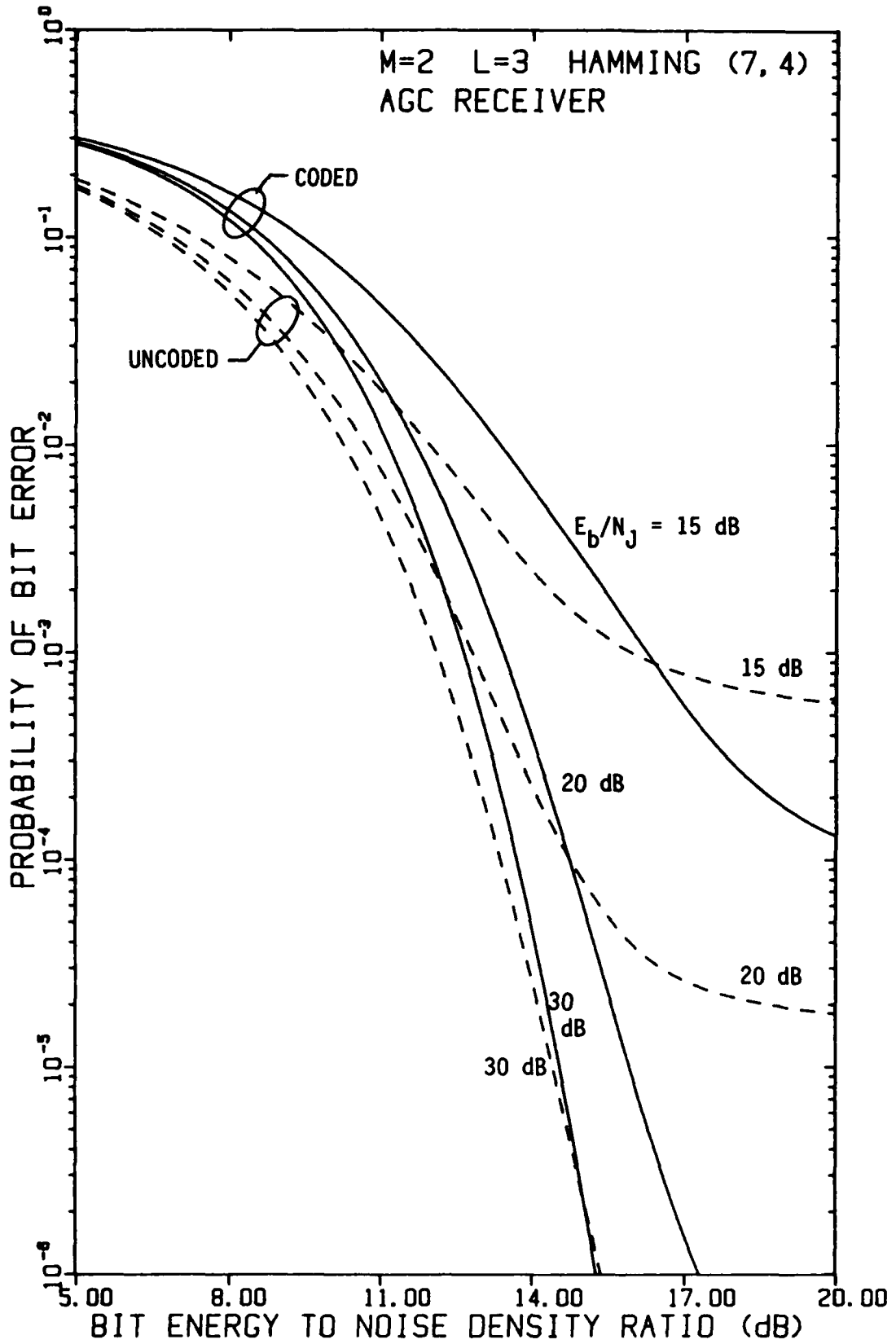

FIGURE 4-72 PERFORMANCE OF FH/BFSK WITH HAMMING (7,4) CODE AND L=3 HOPS/DIGIT AS A FUNCTION OF E_b/N_0 WITH E_b/N_J AS A PARAMETER, USING AN AGC DEMODULATOR, IN OPTIMUM PARTIAL-BAND NOISE JAMMING

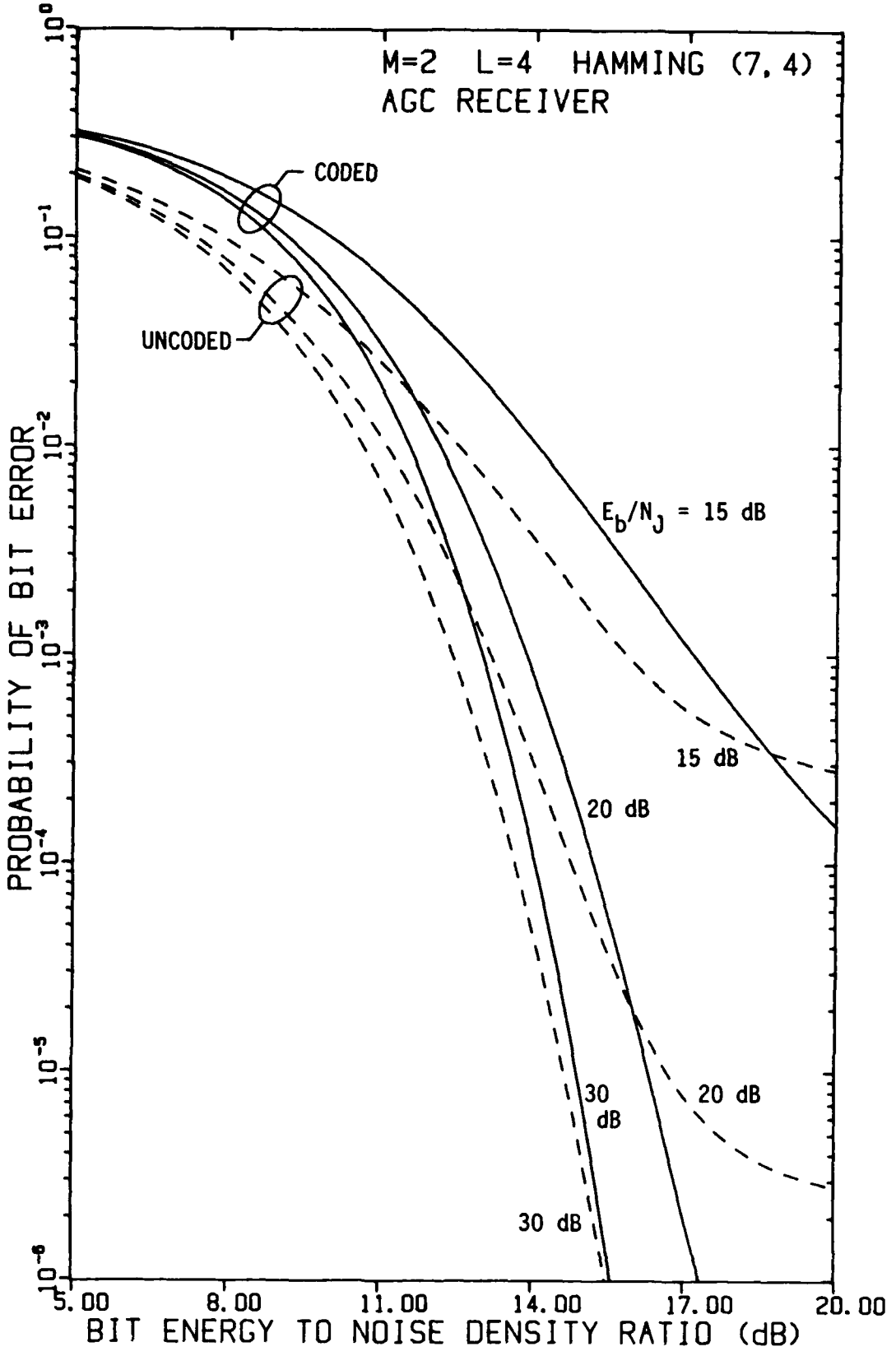

FIGURE 4-73 PERFORMANCE OF FH/BFSK WITH HAMMING (7,4) CODE AND L=4 HOPS/DIGIT AS A FUNCTION OF E_b/N_0 WITH E_b/N_J AS A PARAMETER, USING AN AGC DEMODULATOR, IN OPTIMUM PARTIAL-BAND NOISE JAMMING

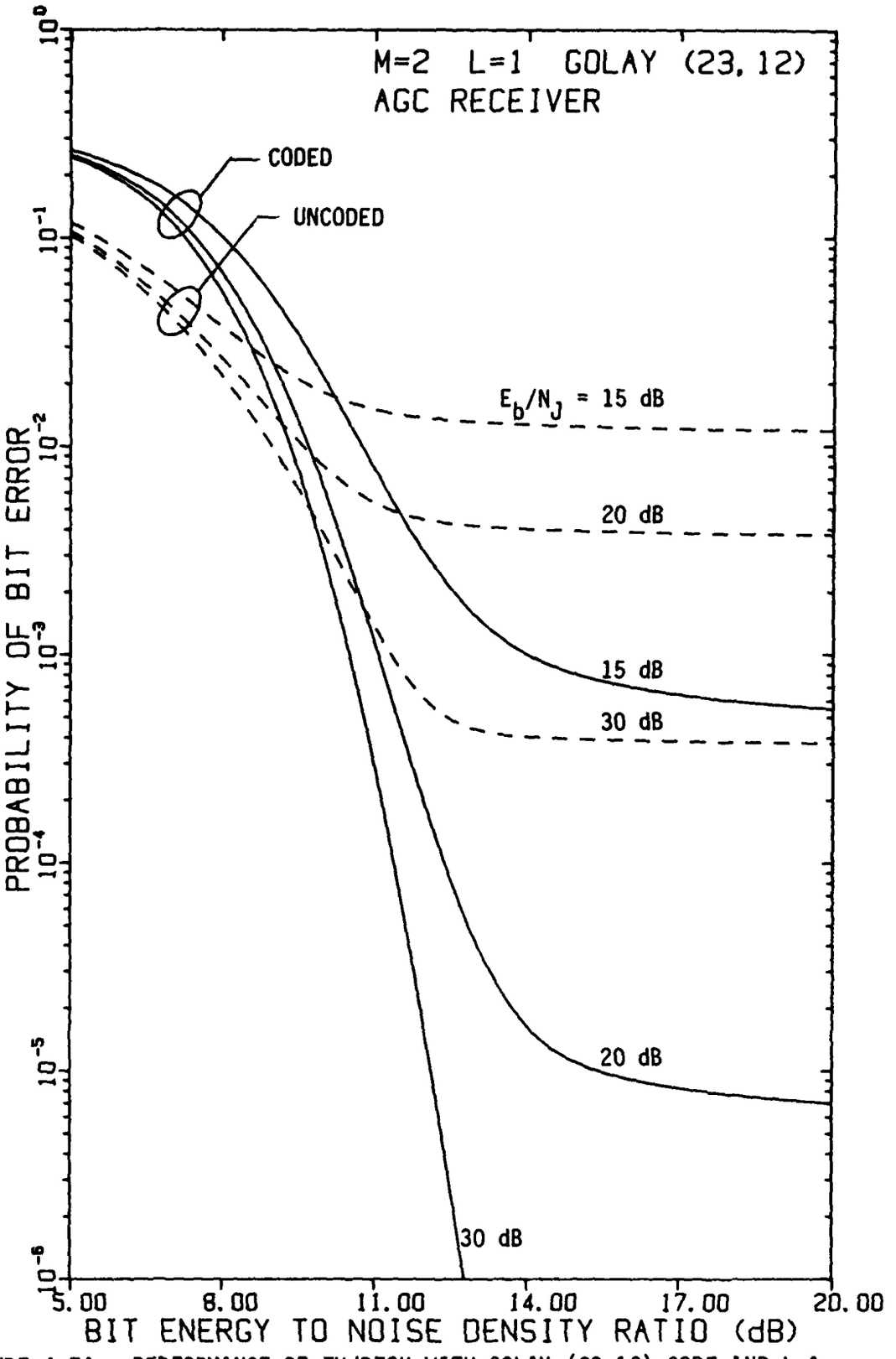

FIGURE 4-74 PERFORMANCE OF FH/BFSK WITH GOLAY (23,12) CODE AND L=1 HOP/DIGIT AS A FUNCTION OF E_b/N_0 WITH E_b/N_J AS A PARAMETER, USING AN AGC DEMODULATOR, IN OPTIMUM PARTIAL-BAND NOISE JAMMING

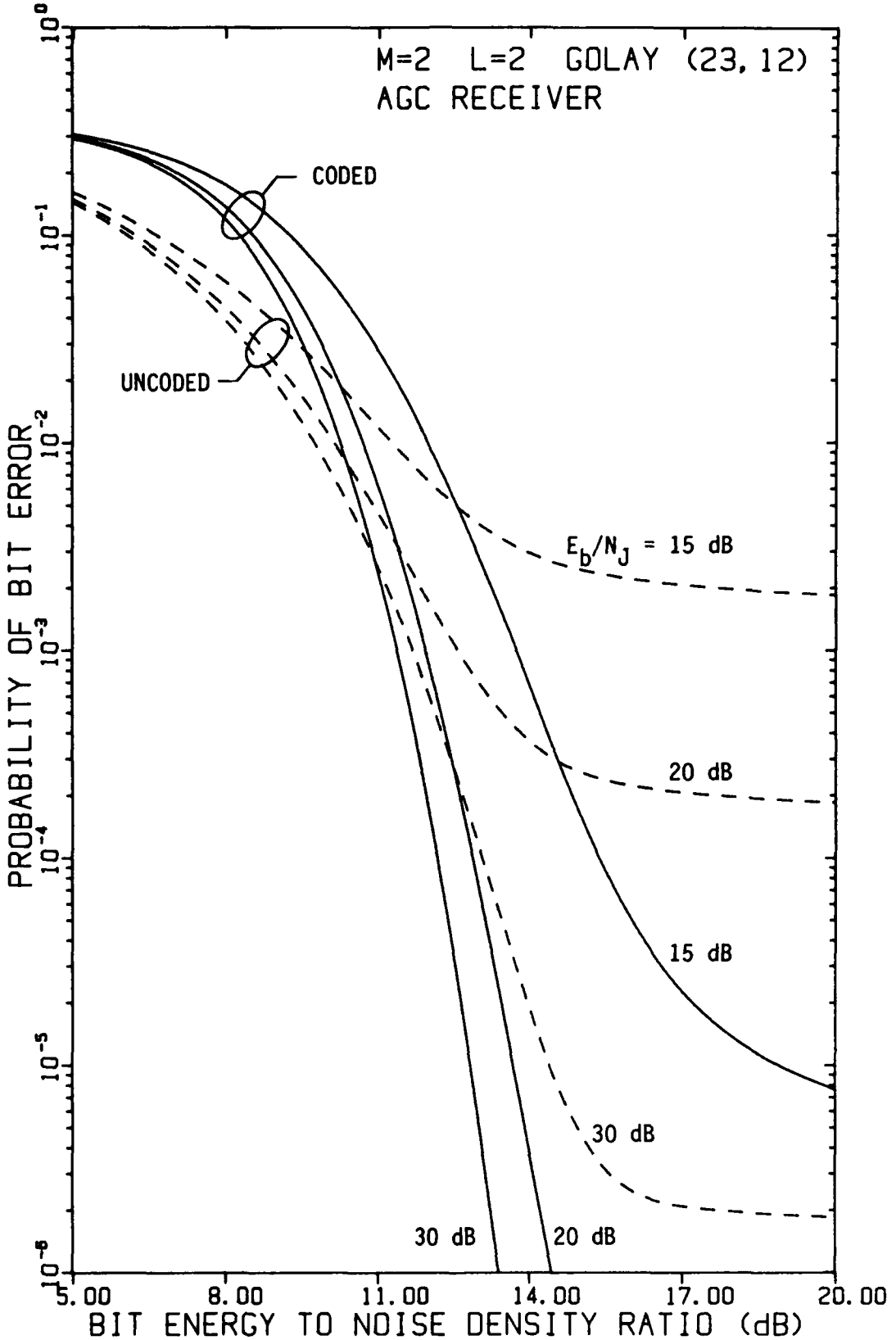

FIGURE 4-75 PERFORMANCE OF FH/BFSK WITH GOLAY (23,12) CODE AND L=2 HOPS/DIGIT AS A FUNCTION OF E_b/N_0 WITH E_b/N_J AS A PARAMETER, USING AN AGC DEMODULATOR, IN OPTIMUM PARTIAL-BAND NOISE JAMMING

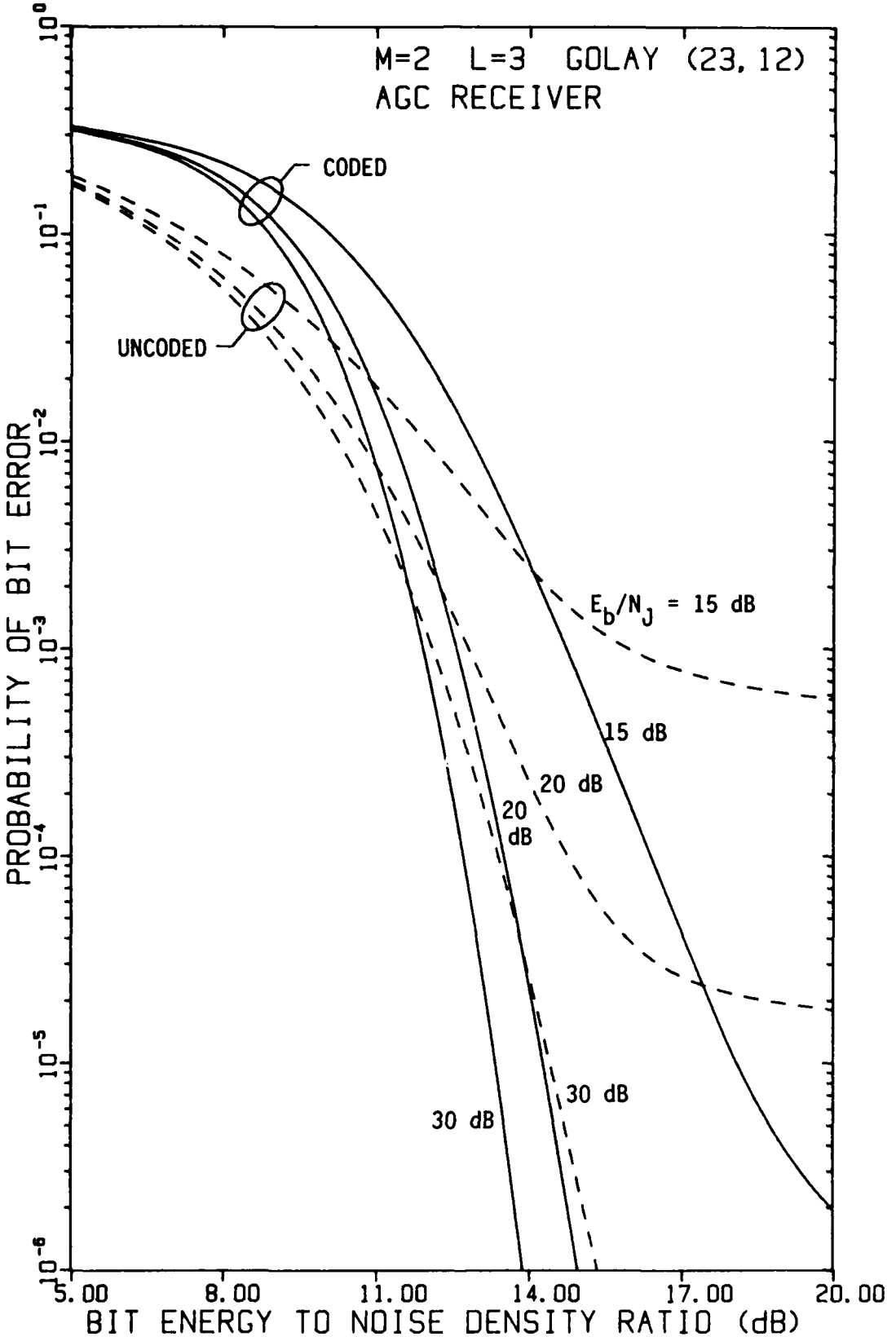

FIGURE 4-76 PERFORMANCE OF FH/BFSK WITH GOLAY (23,12) CODE AND L=3 HOPS/DIGIT AS A FUNCTION OF E_b/N_0 WITH E_b/N_J AS A PARAMETER, USING AN AGC DEMODULATOR, IN OPTIMUM PARTIAL-BAND NOISE JAMMING

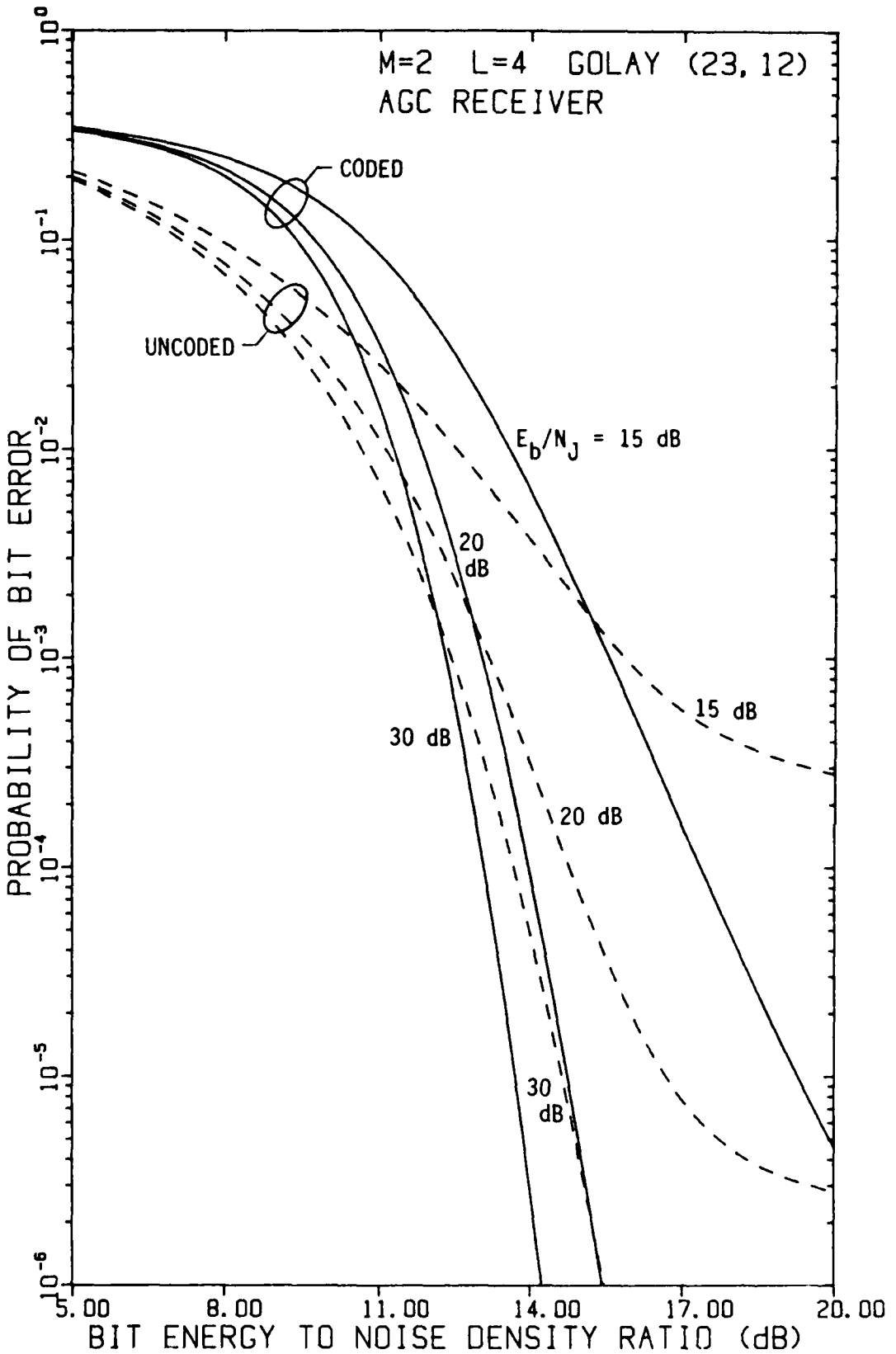

FIGURE 4-77 PERFORMANCE OF FH/BFSK WITH GOLAY (23,12) CODE AND L=4 HOPS/DIGIT AS A FUNCTION OF E_b/N_0 WITH E_b/N_J AS A PARAMETER, USING AN AGC DEMODULATOR, IN OPTIMUM PARTIAL-BAND NOISE JAMMING

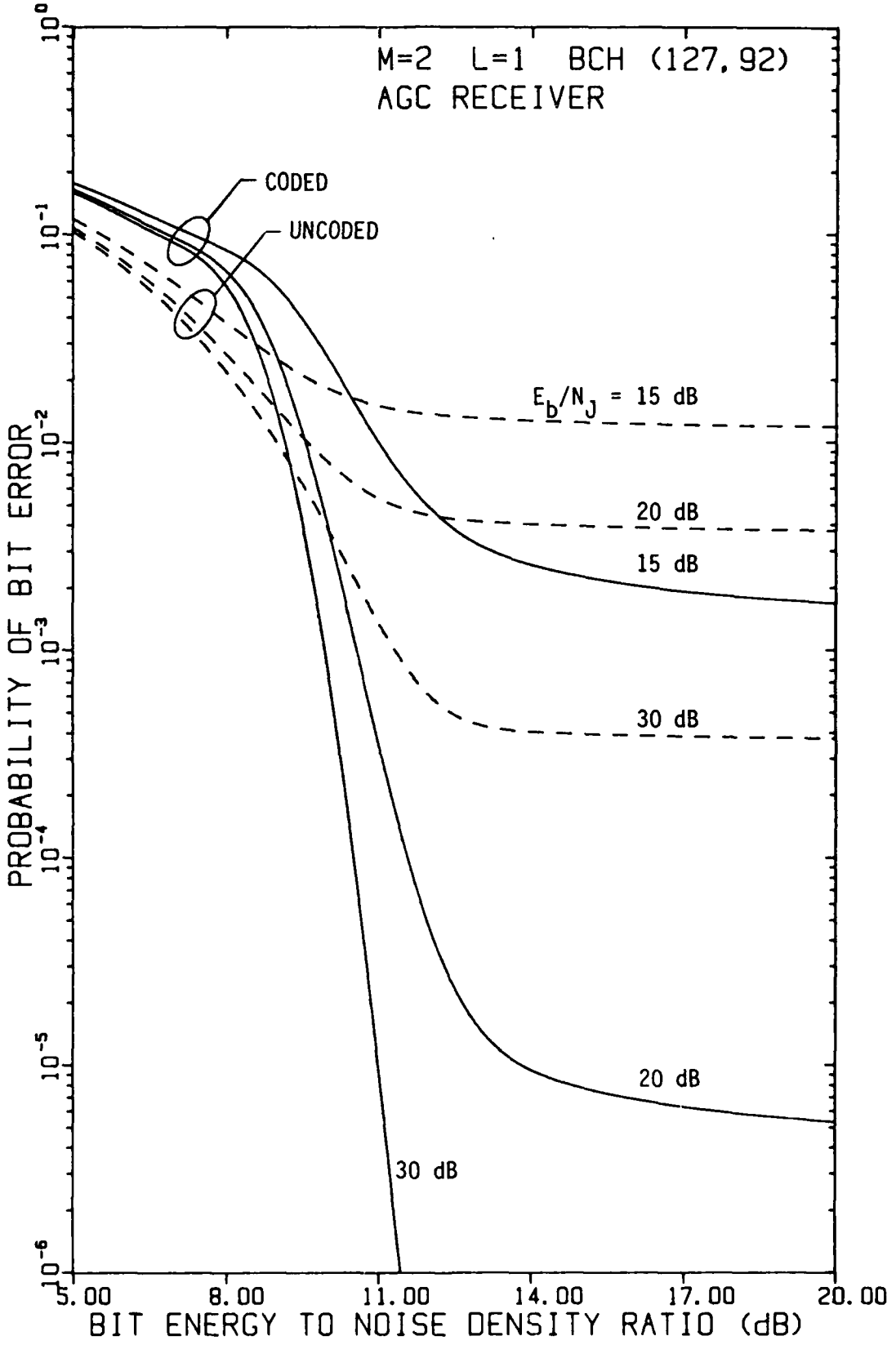

FIGURE 4-78 PERFORMANCE OF FH/BFSK WITH BCH (127,92) CODE AND L=1 HOP/DIGIT AS A FUNCTION OF E_b/N_0 WITH E_b/N_J AS A PARAMETER, USING AN AGC DEMODULATOR, IN OPTIMUM PARTIAL-BAND NOISE JAMMING

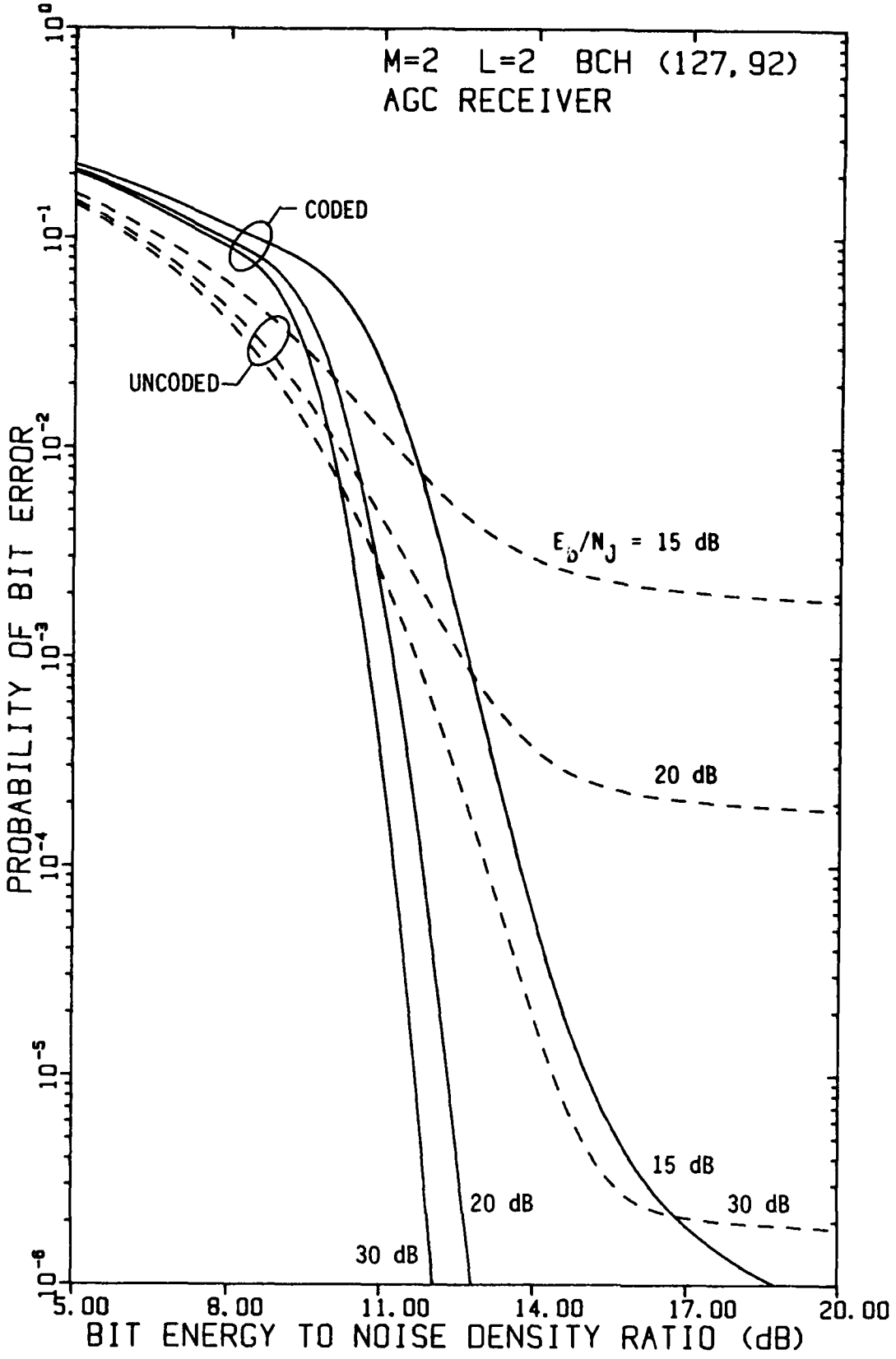

FIGURE 4-79 PERFORMANCE OF FH/BFSK WITH BCH (127,92) CODE AND L=2 HOPS/DIGIT AS A FUNCTION OF E_b/N_0 WITH E_b/N_J AS A PARAMETER, USING AN AGC DEMODULATOR, IN OPTIMUM PARTIAL-BAND NOISE JAMMING

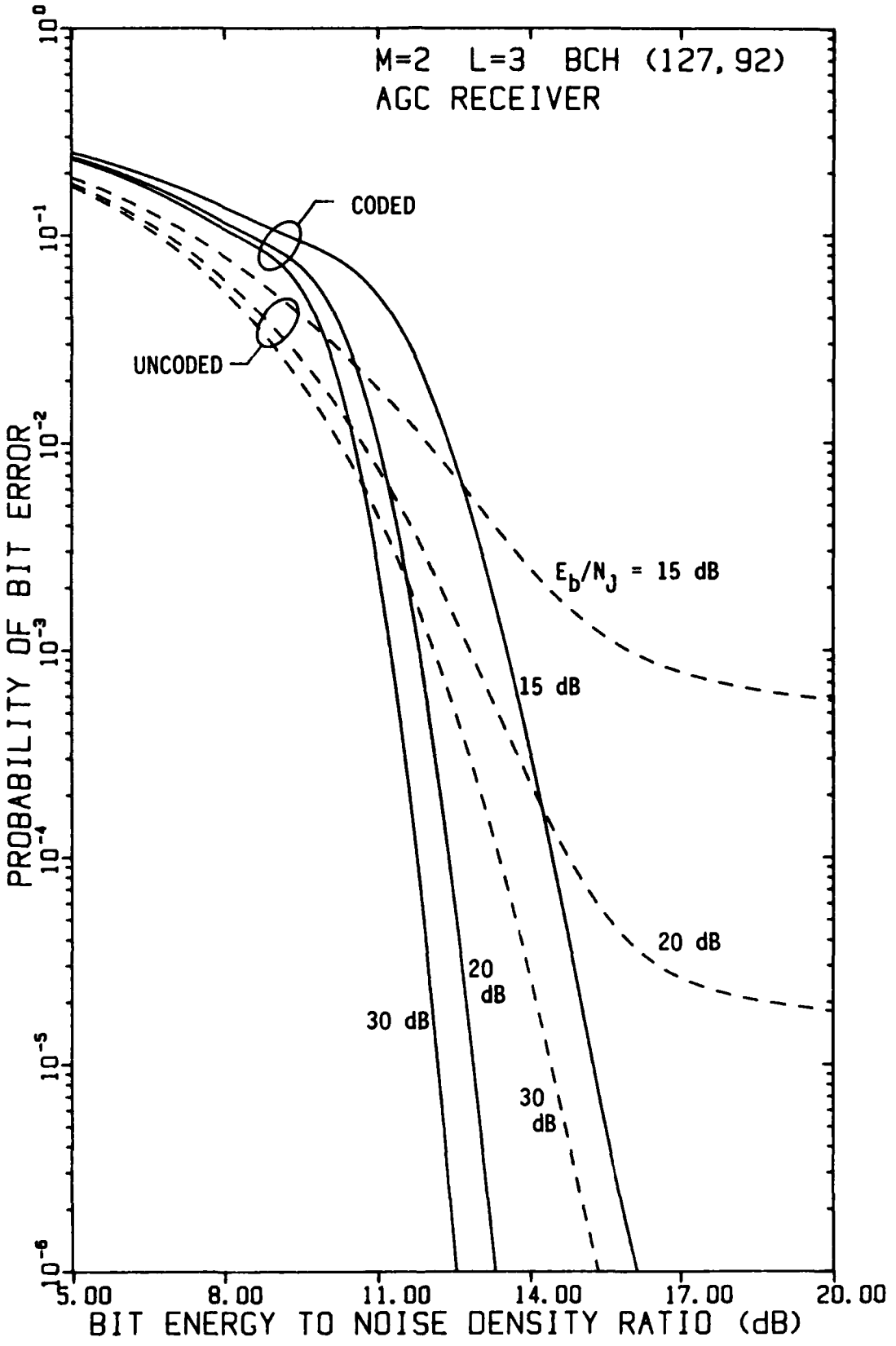

FIGURE 4-80 PERFORMANCE OF FH/BFSK WITH BCH (127,92) CODE AND L=3 HOPS/DIGIT AS A FUNCTION OF E_b/N_0 WITH E_b/N_J AS A PARAMETER, USING AN AGC DEMODULATOR, IN OPTIMUM PARTIAL-BAND NOISE JAMMING

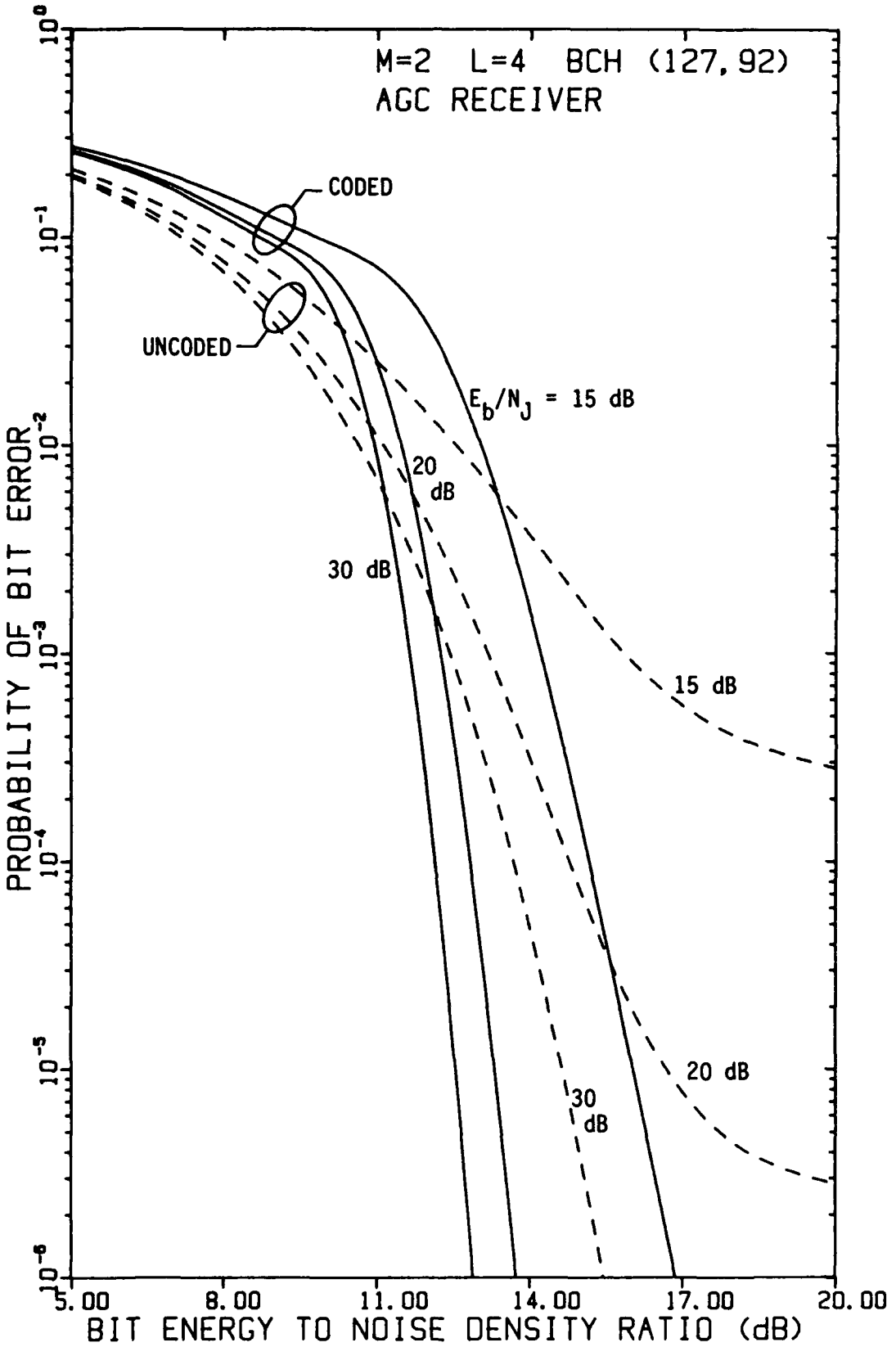

FIGURE 4-81 PERFORMANCE OF FH/BFSK WITH BCH (127,92) CODE AND L=4 HOPS/DIGIT AS A FUNCTION OF E_b/N_0 WITH E_b/N_J AS A PARAMETER, USING AN AGC DEMODULATOR, IN OPTIMUM PARTIAL-BAND NOISE JAMMING

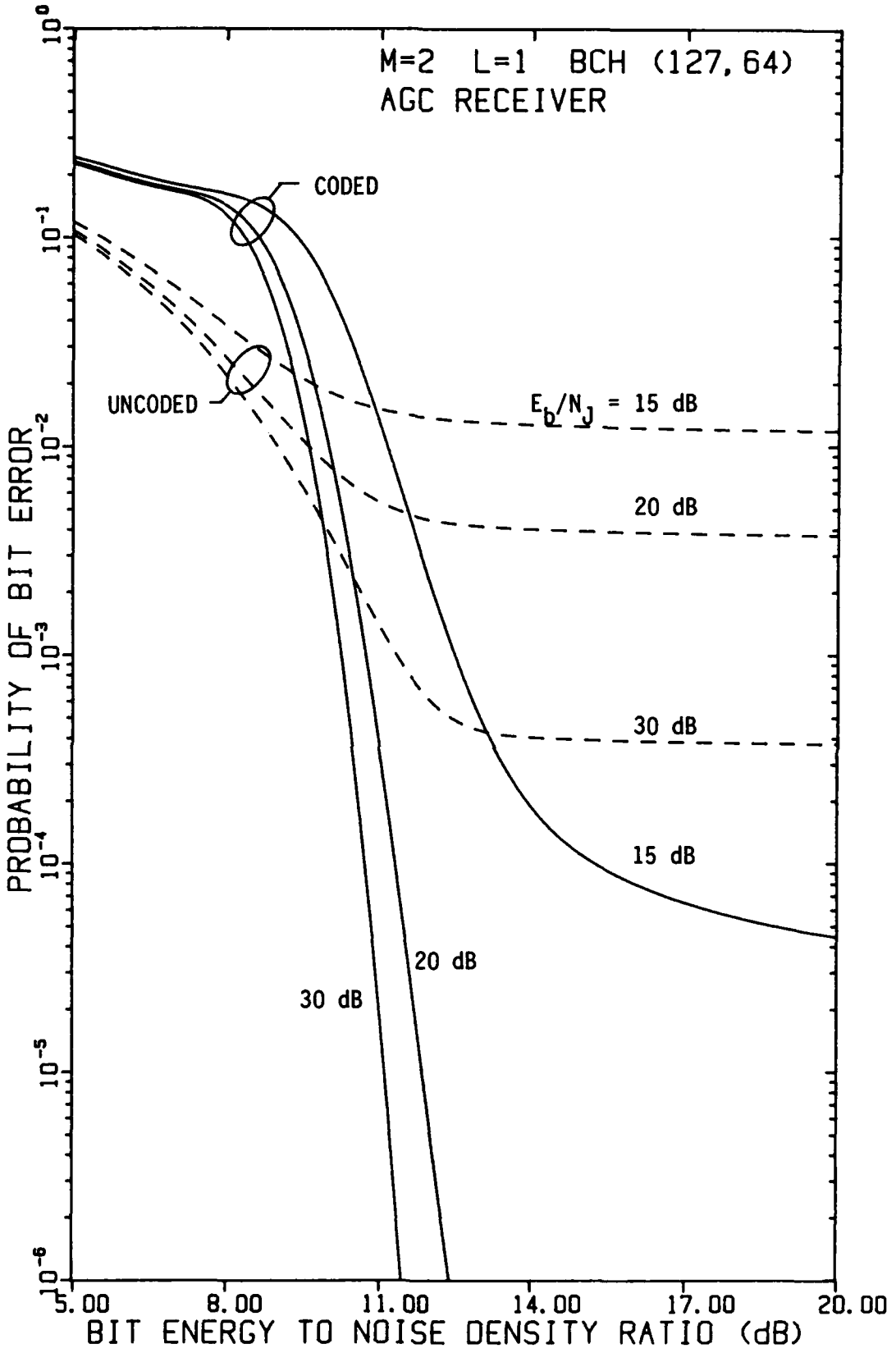

FIGURE 4-82 PERFORMANCE OF FH/BFSK WITH BCH (127,64) CODE AND L=1 HOP/DIGIT AS A FUNCTION OF E_b/N_0 WITH E_b/N_J AS A PARAMETER, USING AN AGC DEMODULATOR, IN OPTIMUM PARTIAL-BAND NOISE JAMMING

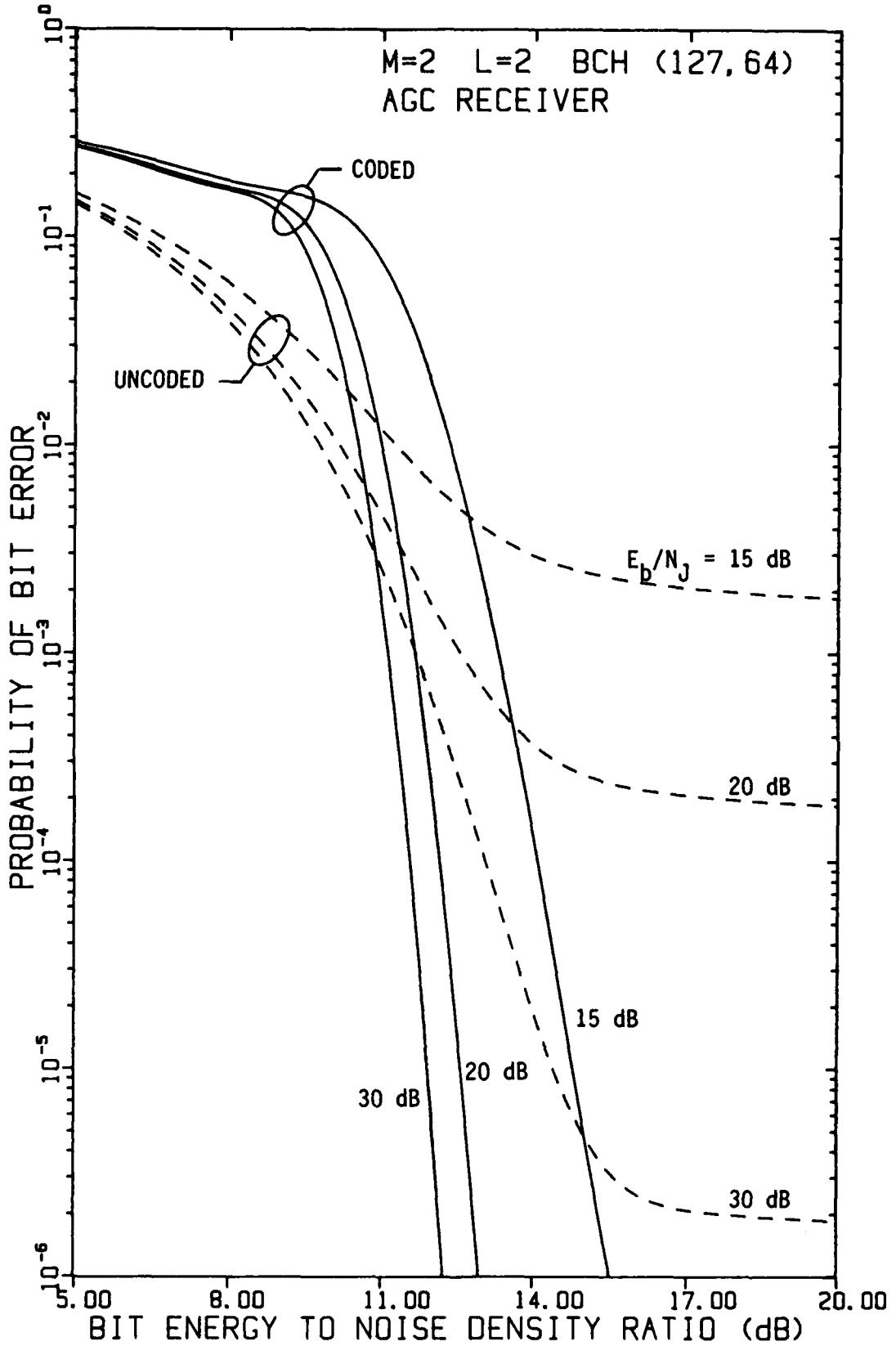

FIGURE 4-83 PERFORMANCE OF FH/BFSK WITH BCH (127,64) CODE AND L=2 HOPS/DIGIT AS A FUNCTION OF E_b/N_0 WITH E_b/N_J AS A PARAMETER, USING AN AGC DEMODULATOR, IN OPTIMUM PARTIAL-BAND NOISE JAMMING

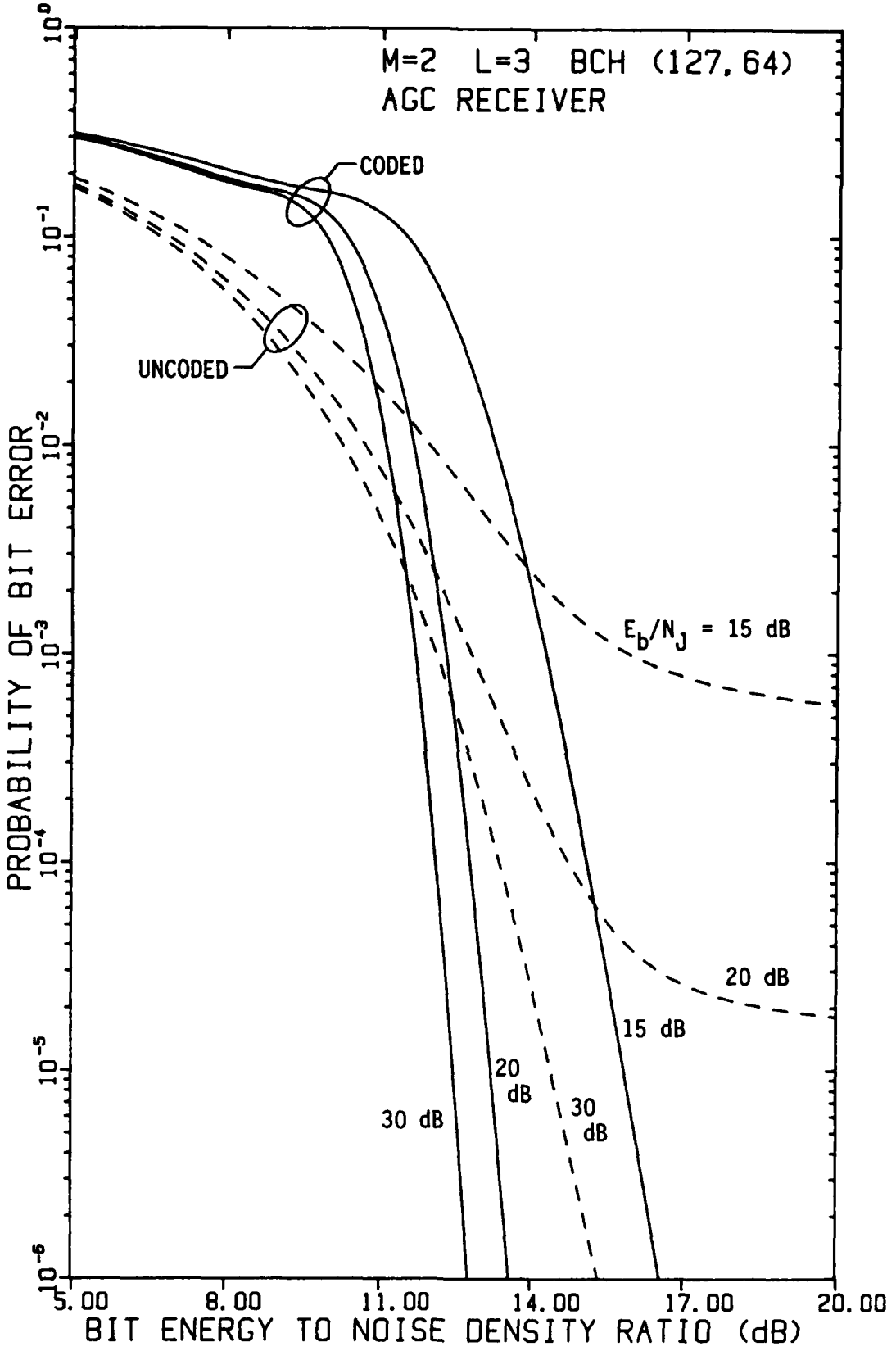

FIGURE 4-84 PERFORMANCE OF FH/BFSK WITH BCH (127,64) CODE AND L=3 HOPS/DIGIT AS A FUNCTION OF E_b/N_0 WITH E_b/N_J AS A PARAMETER, USING AN AGC DEMODULATOR, IN OPTIMUM PARTIAL-BAND NOISE JAMMING

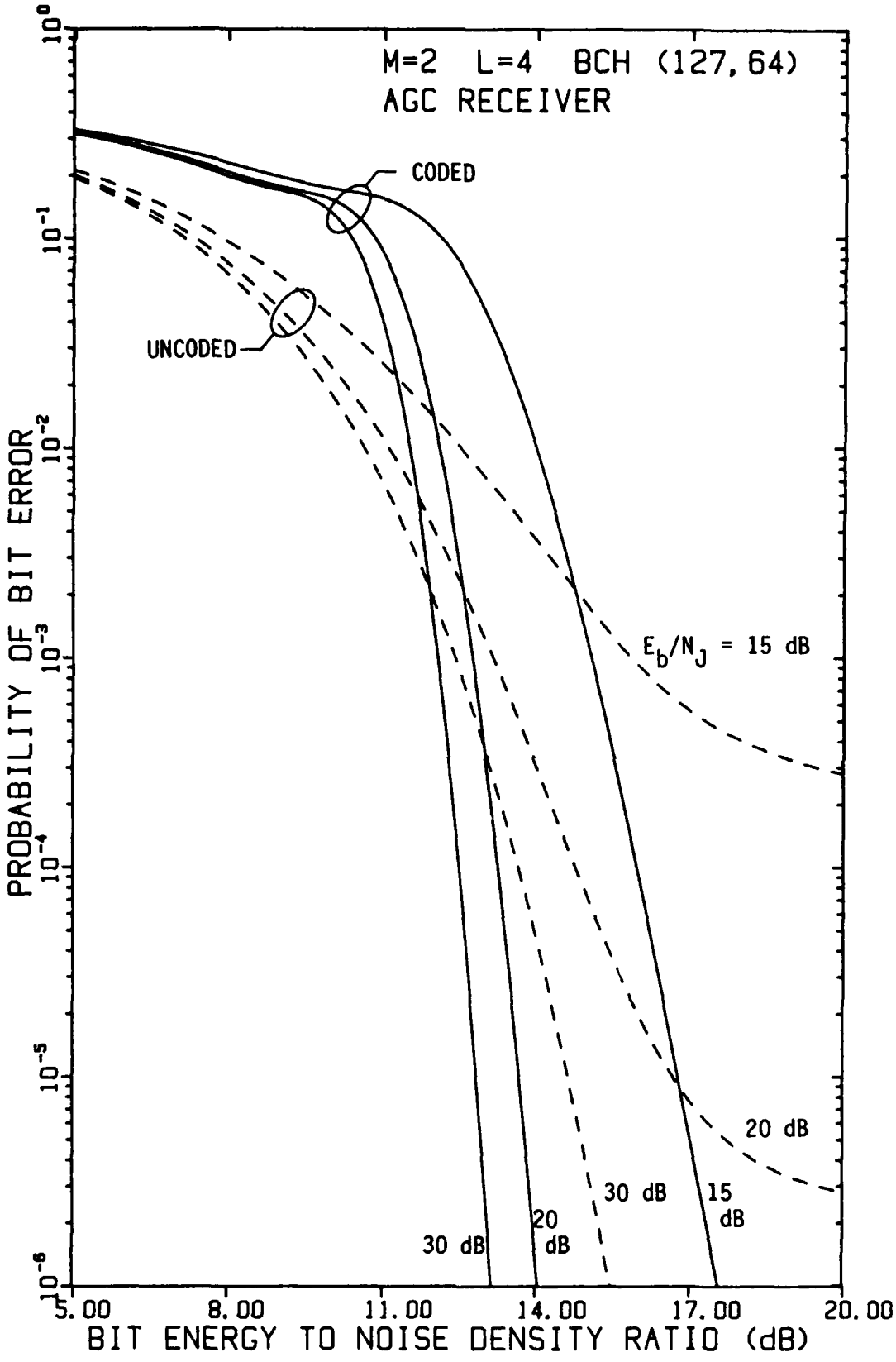

FIGURE 4-85 PERFORMANCE OF FH/BFSK WITH BCH (127,64) CODE AND L=4 HOPS/DIGIT AS A FUNCTION OF E_b/N_0 WITH E_b/N_J AS A PARAMETER, USING AN AGC DEMODULATOR, IN OPTIMUM PARTIAL-BAND NOISE JAMMING

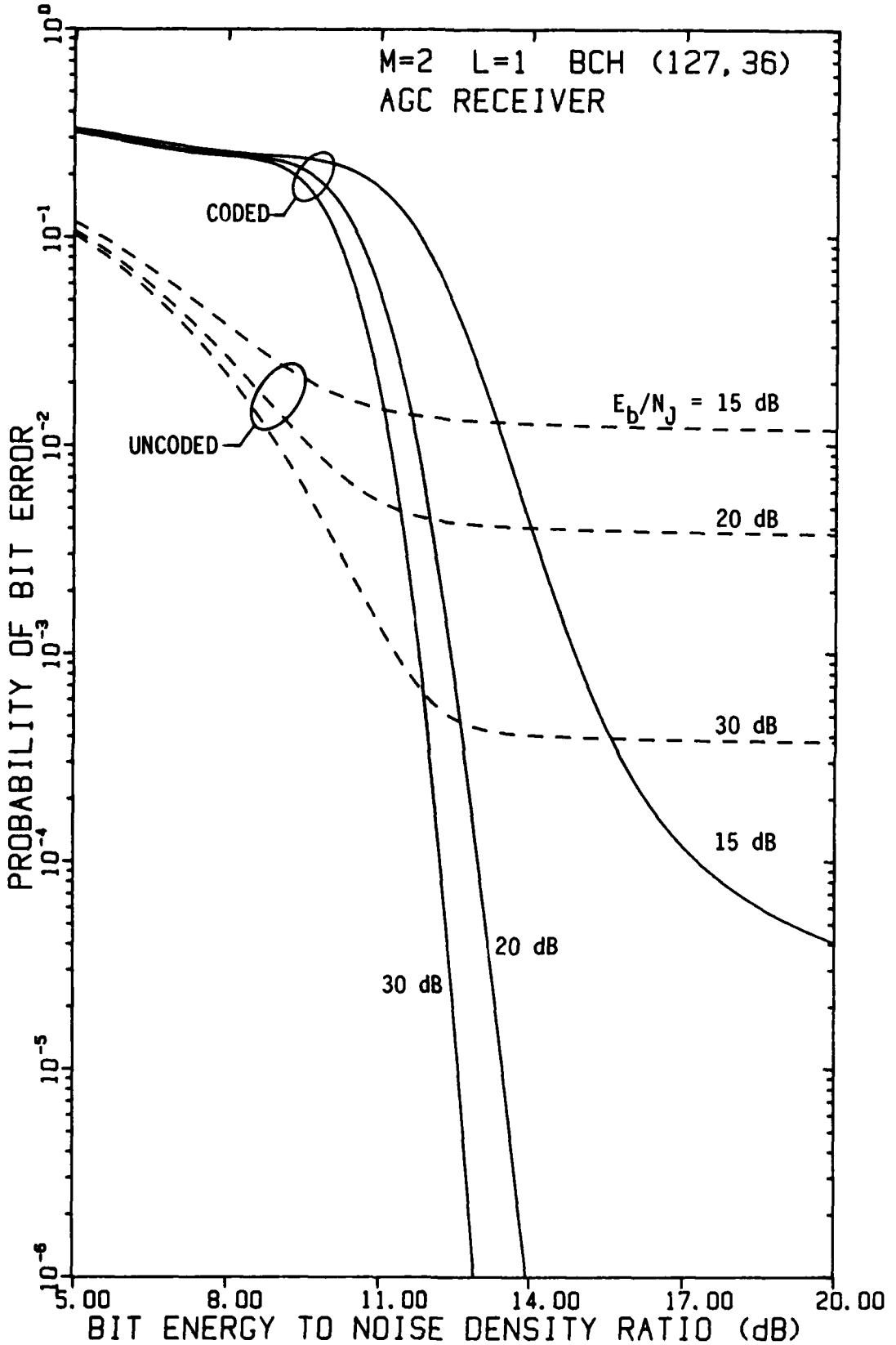

FIGURE 4-86 PERFORMANCE OF FH/BFSK WITH BCH (127,36) CODE AND L=1 HOP/DIGIT AS A FUNCTION OF E_b/N_0 WITH E_b/N_J AS A PARAMETER, USING AN AGC DEMODULATOR, IN OPTIMUM PARTIAL-BAND NOISE JAMMING

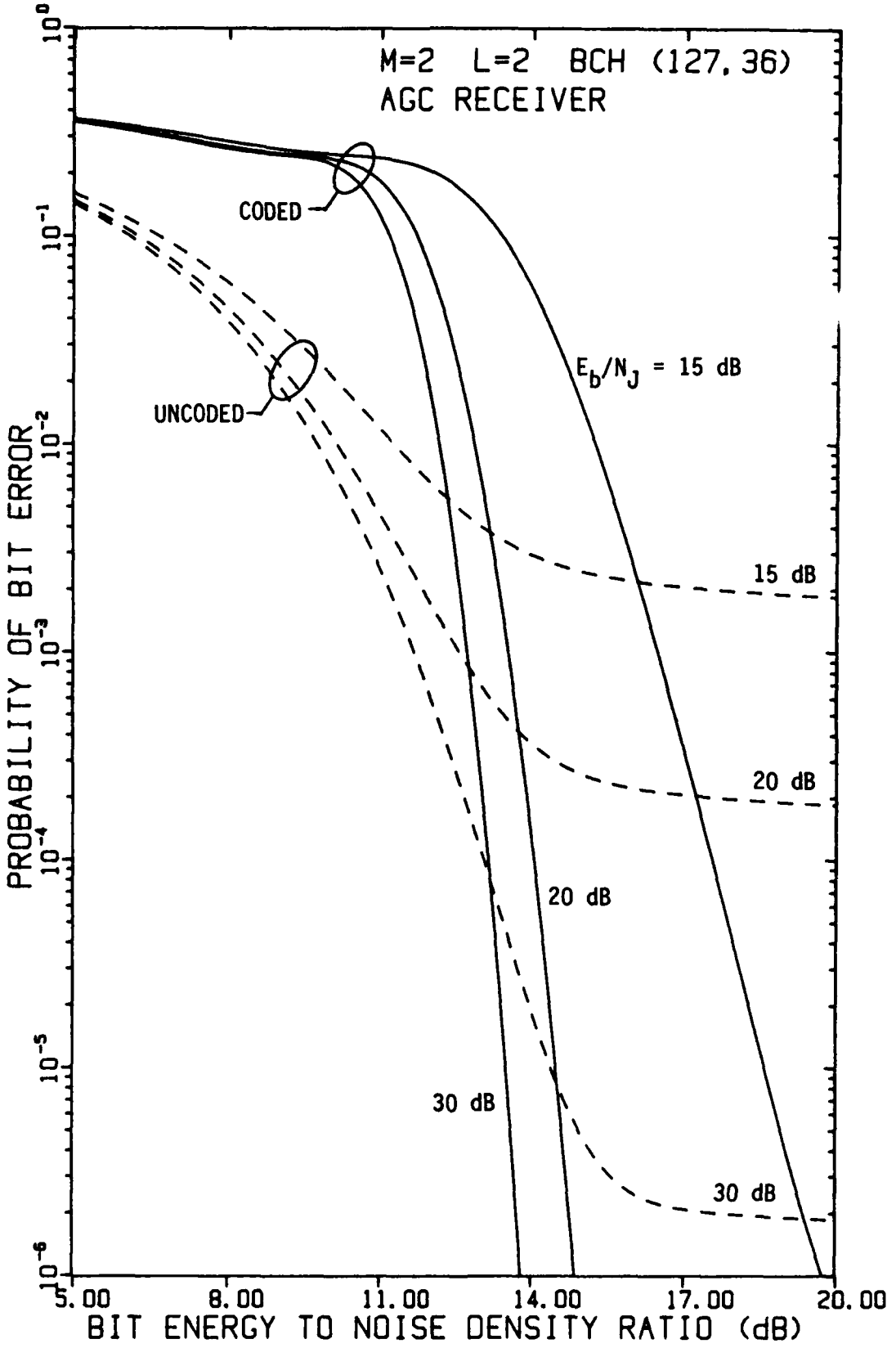

FIGURE 4-87 PERFORMANCE OF FH/BFSK WITH BCH (127,36) CODE AND L=2 HOPS/DIGIT AS A FUNCTION OF E_b/N_0 WITH E_b/N_J AS A PARAMETER, USING AN AGC DEMODULATOR, IN OPTIMUM PARTIAL-BAND NOISE JAMMING

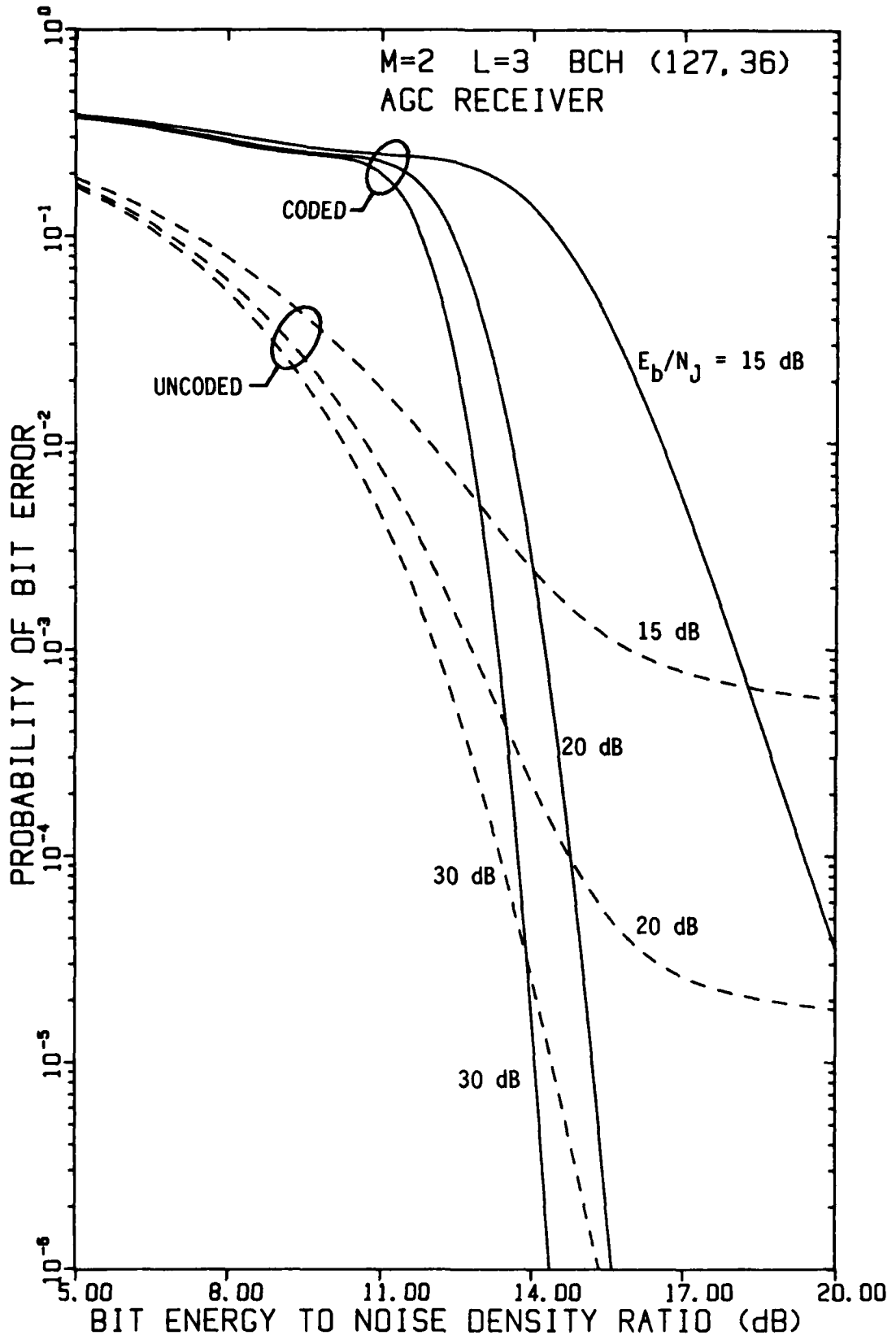

FIGURE 4-88 PERFORMANCE OF FH/BFSK WITH BCH (127,36) CODE AND L=3 HOPS/DIGIT AS A FUNCTION OF E_b/N_0 WITH E_b/N_J AS A PARAMETER, USING AN AGC DEMODULATOR, IN OPTIMUM PARTIAL-BAND NOISE JAMMING

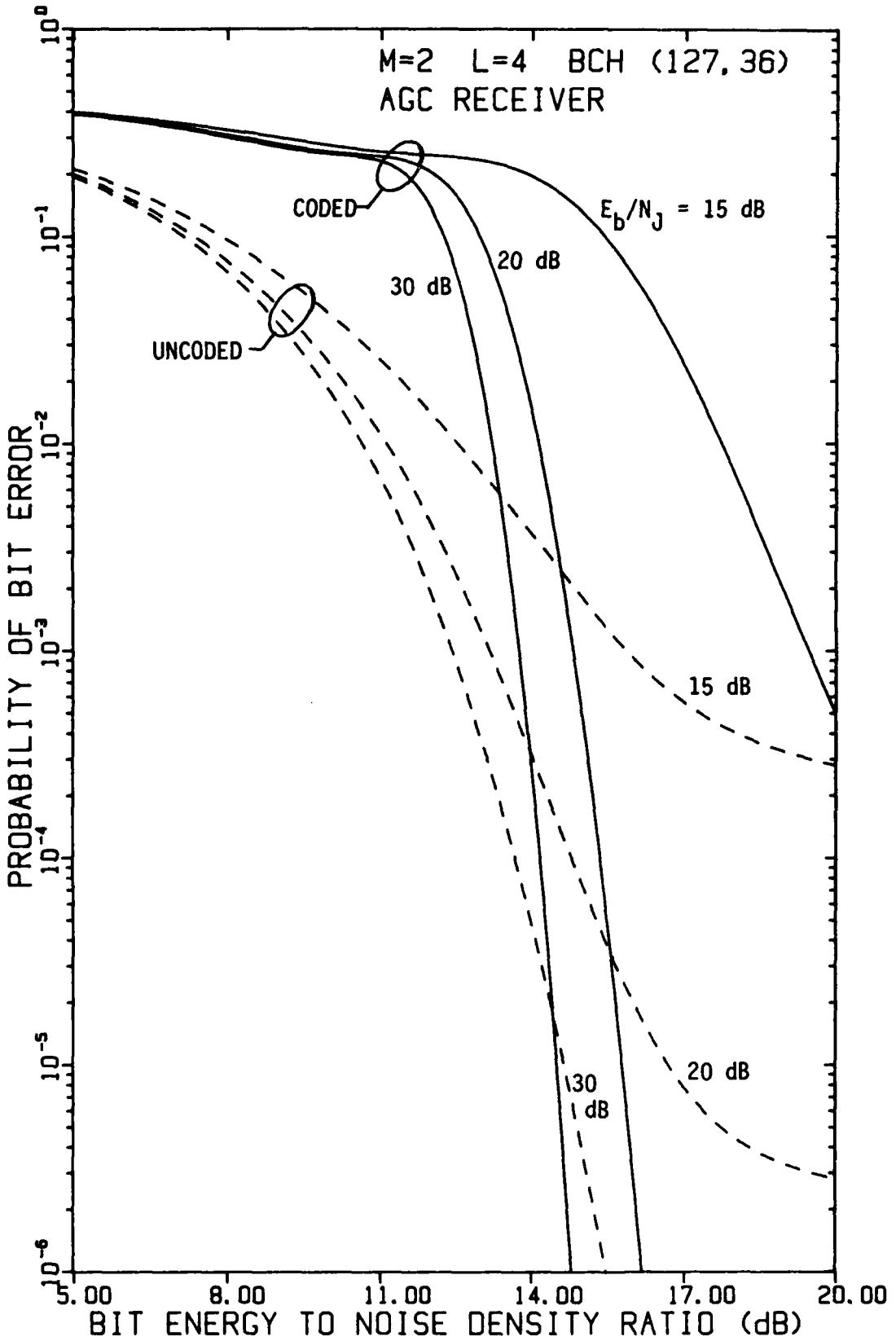

FIGURE 4-89 PERFORMANCE OF FH/BFSK WITH BCH (127,36) CODE AND L=4 HOPS/DIGIT AS A FUNCTION OF E_b/N_0 WITH E_b/N_J AS A PARAMETER, USING AN AGC DEMODULATOR, IN OPTIMUM PARTIAL-BAND NOISE JAMMING

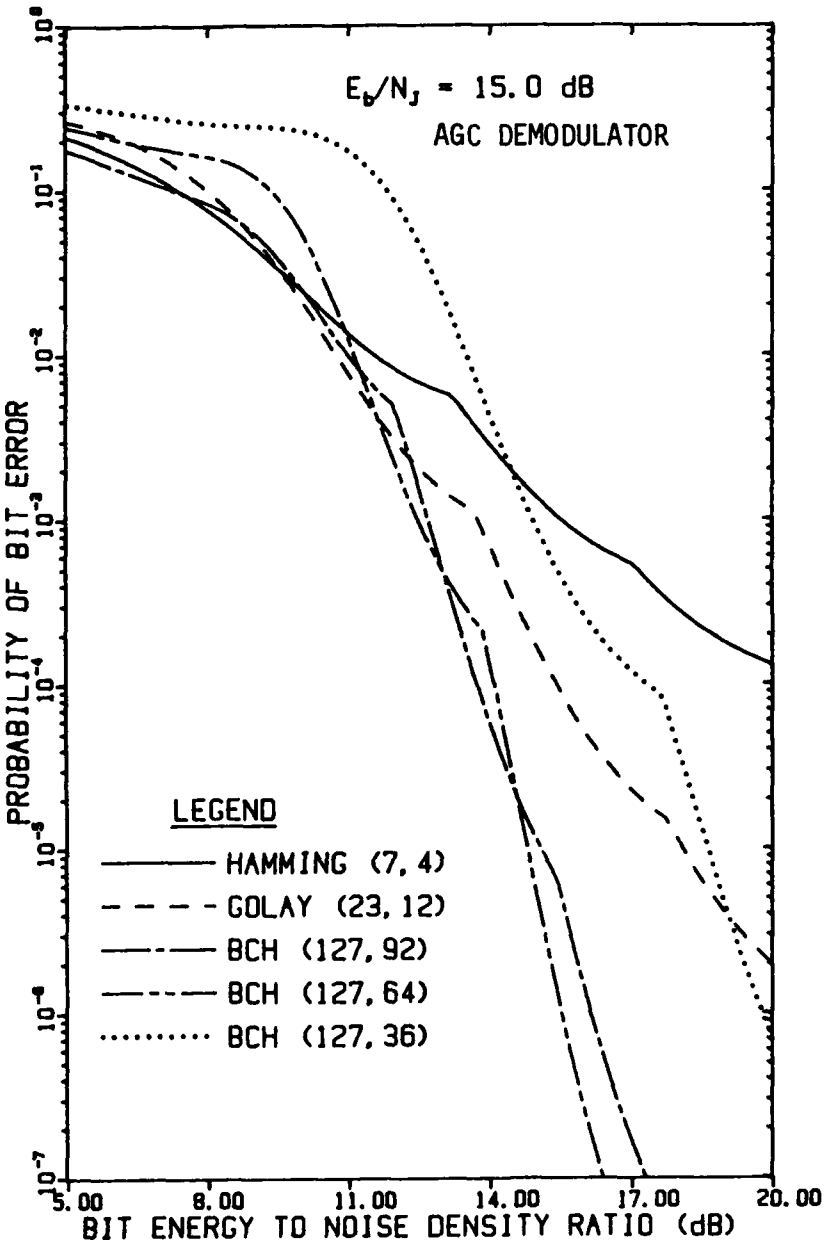

FIGURE 4-90 PERFORMANCE OF BLOCK CODES USING FH/BFSK WITH OPTIMUM DIVERSITY IN WORST-CASE PARTIAL-BAND NOISE JAMMING AS A FUNCTION OF E_b/N_0 WHEN E_b/N_J = 15 dB

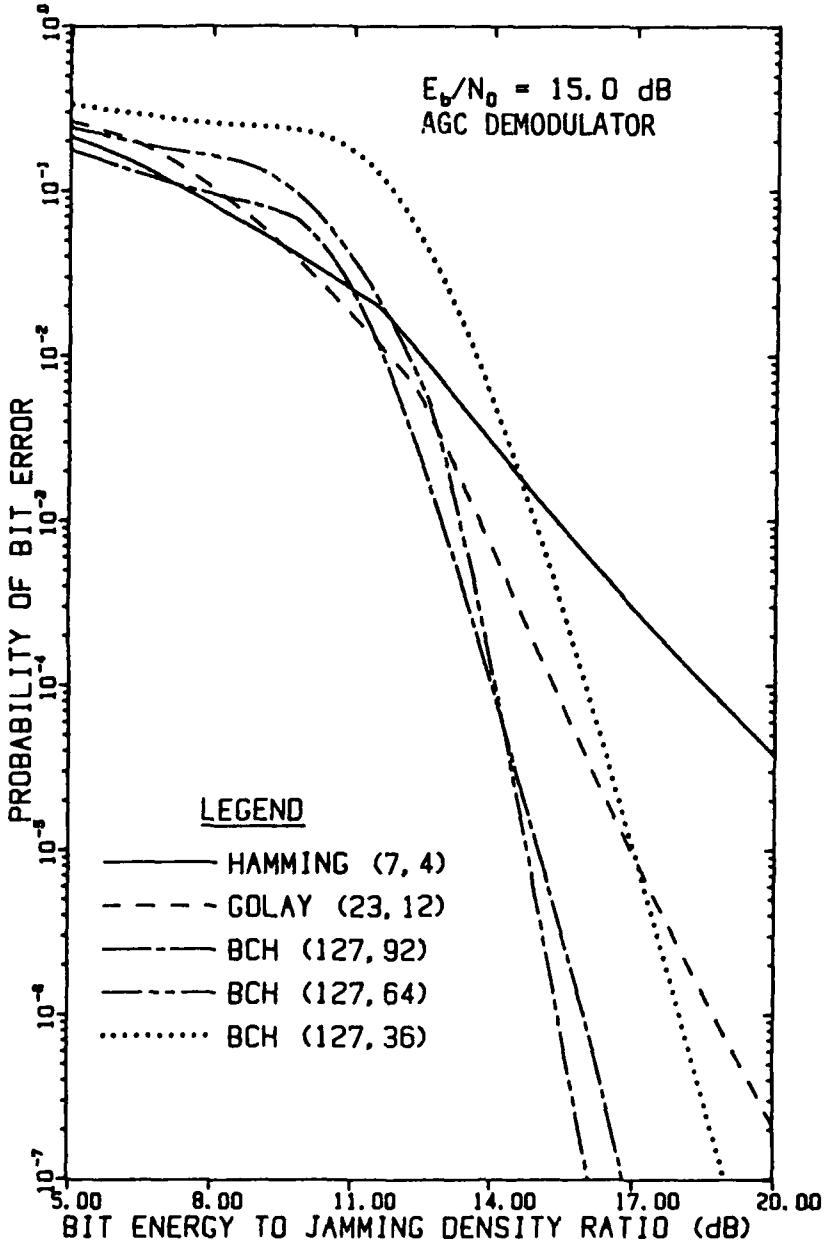

FIGURE 4-91 PERFORMANCE OF BLOCK CODES USING FH/BFSK WITH OPTIMUM DIVERSITY IN WORST-CASE PARTIAL-BAND NOISE JAMMING AS A FUNCTION OF E_b/N_J WHEN E_b/N_0 = 15 dB

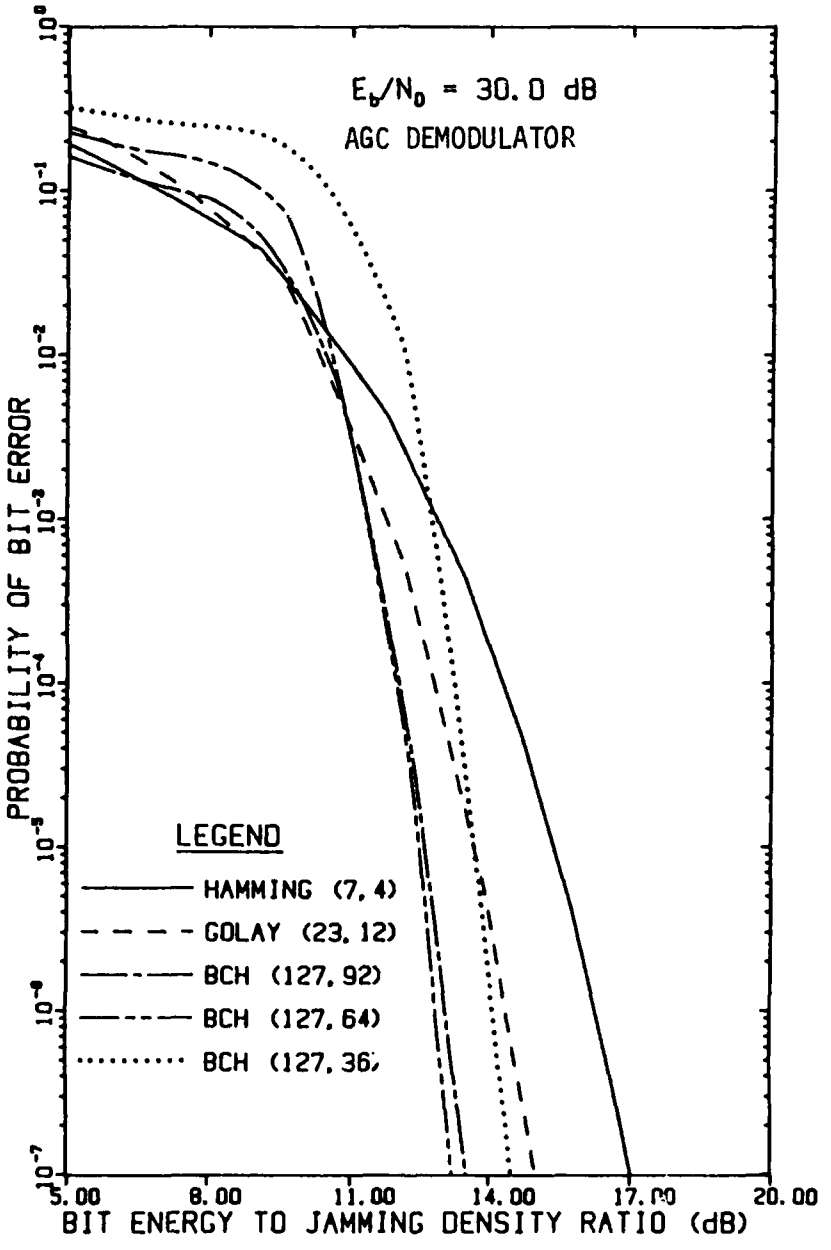

FIGURE 4-92 PERFORMANCE OF BLOCK CODES USING FH/BFSK WITH OPTIMUM DIVERSITY IN WORST-CASE PARTIAL-BAND NOISE JAMMING AS A FUNCTION OF E_b/N_J WHEN E_b/N_0 = 30 dB

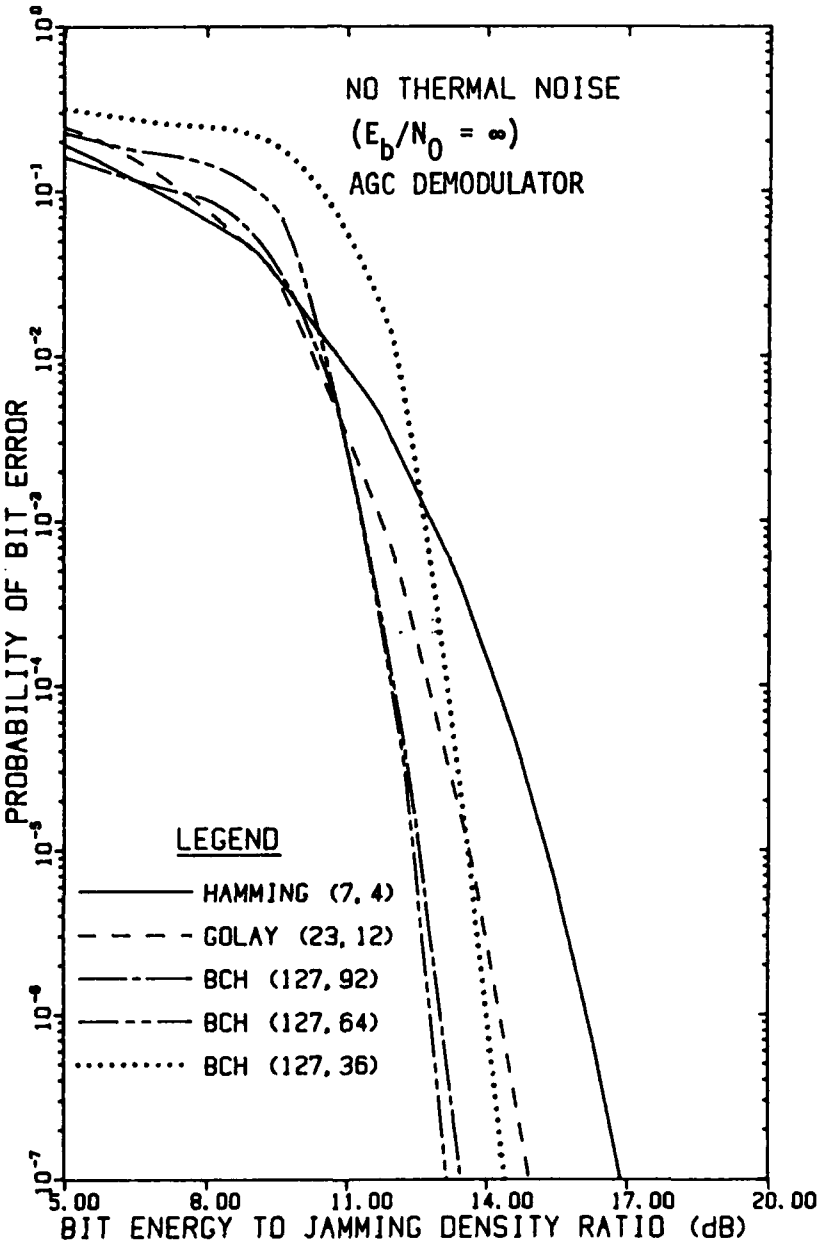

FIGURE 4-93 PERFORMANCE OF BLOCK CODES USING FH/BFSK WITH OPTIMUM DIVERSITY IN WORST-CASE PARTIAL-BAND NOISE JAMMING AS A FUNCTION OF E_b/N_J WHEN $E_b/N_0 = \infty$

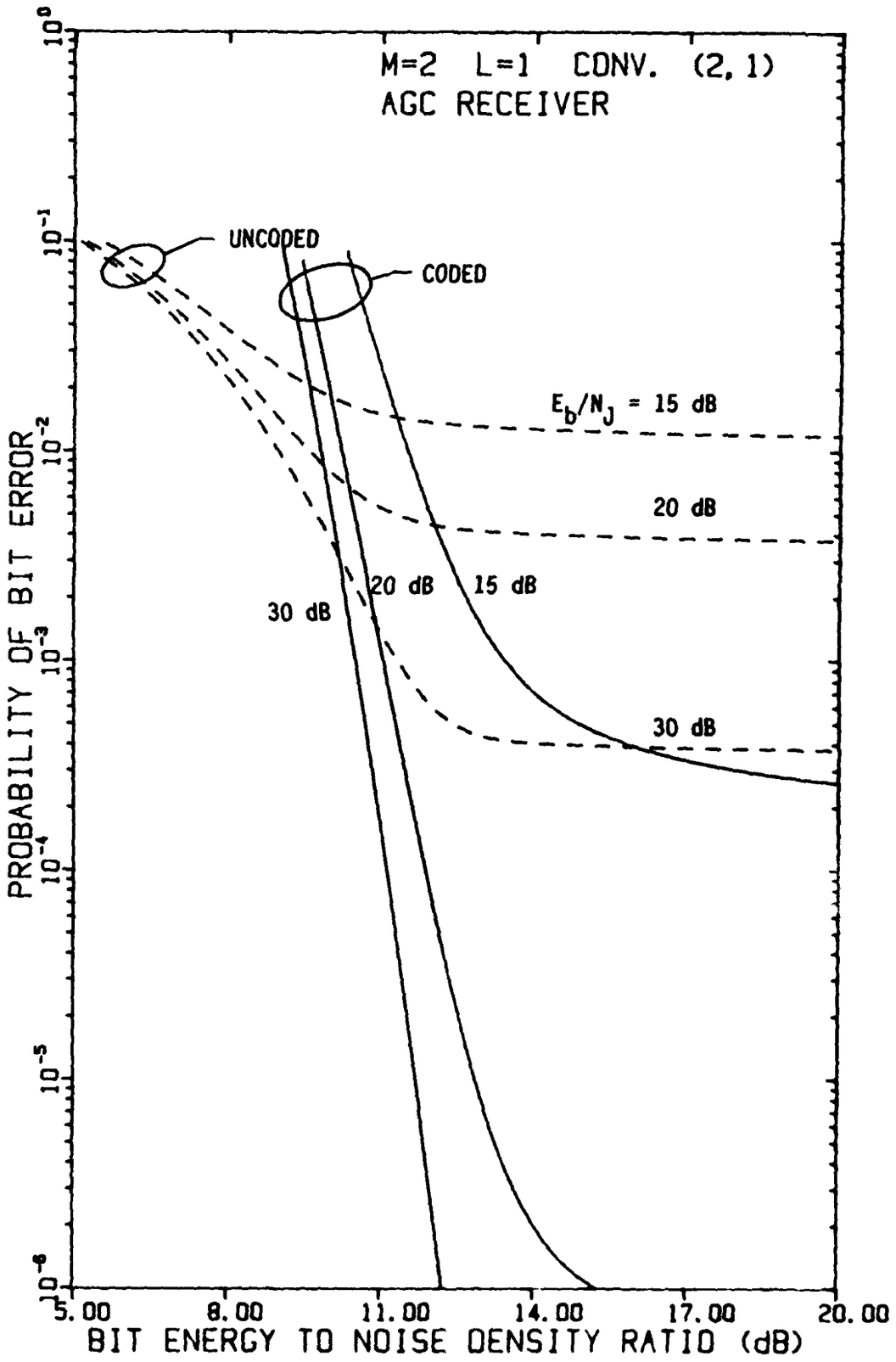

FIGURE 4-94 PERFORMANCE OF FH/BFSK WITH CONVOLUTIONAL RATE-1/2 CODE AND L=1 HOP/DIGIT AS A FUNCTION OF E_b/N_0 WITH E_b/N_J AS A PARAMETER, USING AN AGC DEMODULATOR, IN OPTIMUM PARTIAL-BAND NOISE JAMMING

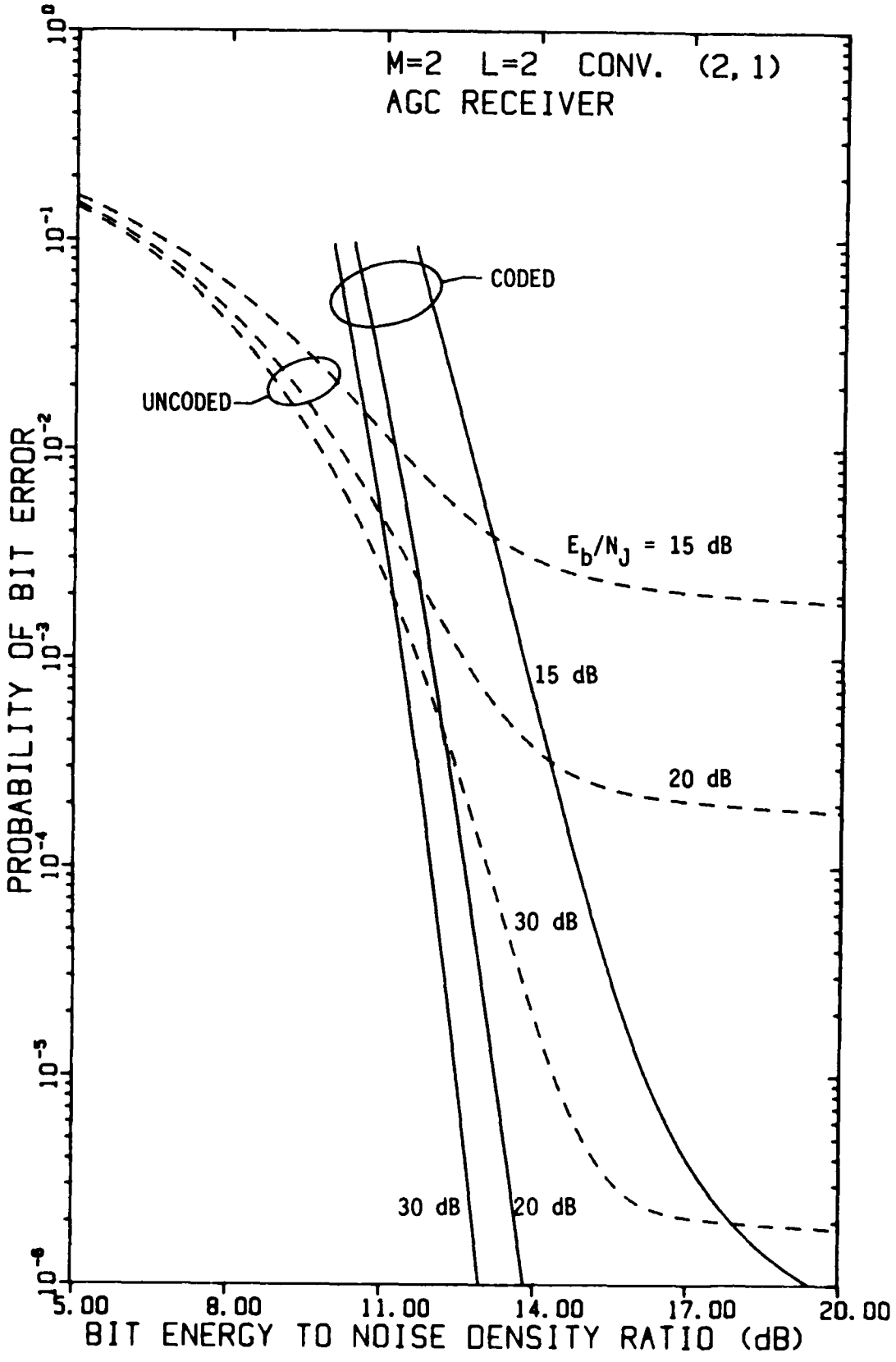

FIGURE 4-95 PERFORMANCE OF FH/BFSK WITH CONVOLUTIONAL RATE-1/2 CODE AND L=2 HOPS/DIGIT AS A FUNCTION OF E_b/N_0 WITH E_b/N_J AS A PARAMETER, USING AN AGC DEMODULATOR, IN OPTIMUM PARTIAL-BAND NOISE JAMMING

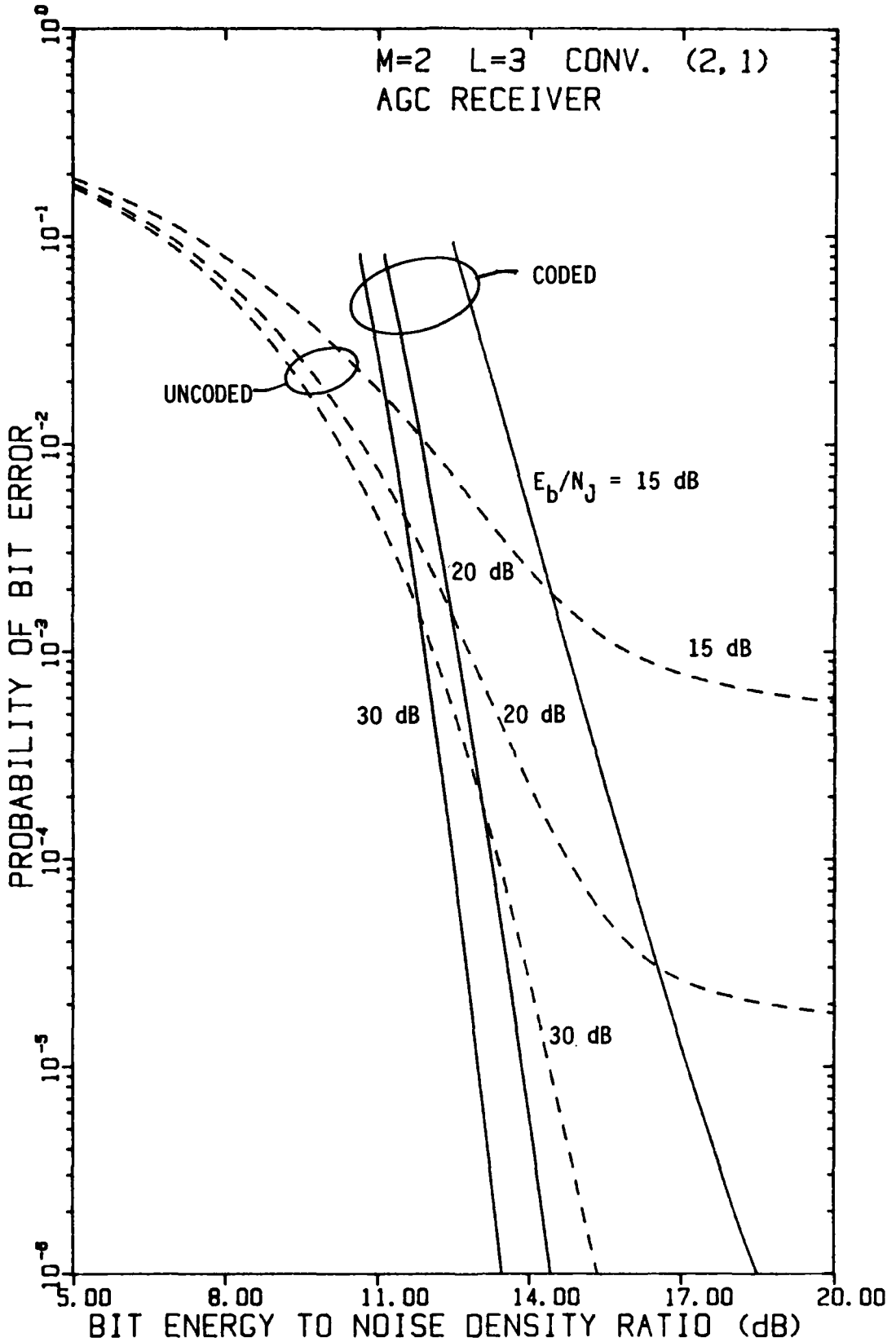

FIGURE 4-96 PERFORMANCE OF FH/BFSK WITH CONVOLUTIONAL RATE-1/2 CODE AND L=3 HOPS/DIGIT AS A FUNCTION OF E_b/N_0 WITH E_b/N_J AS A PARAMETER, USING AN AGC DEMODULATOR, IN OPTIMUM PARTIAL-BAND NOISE JAMMING

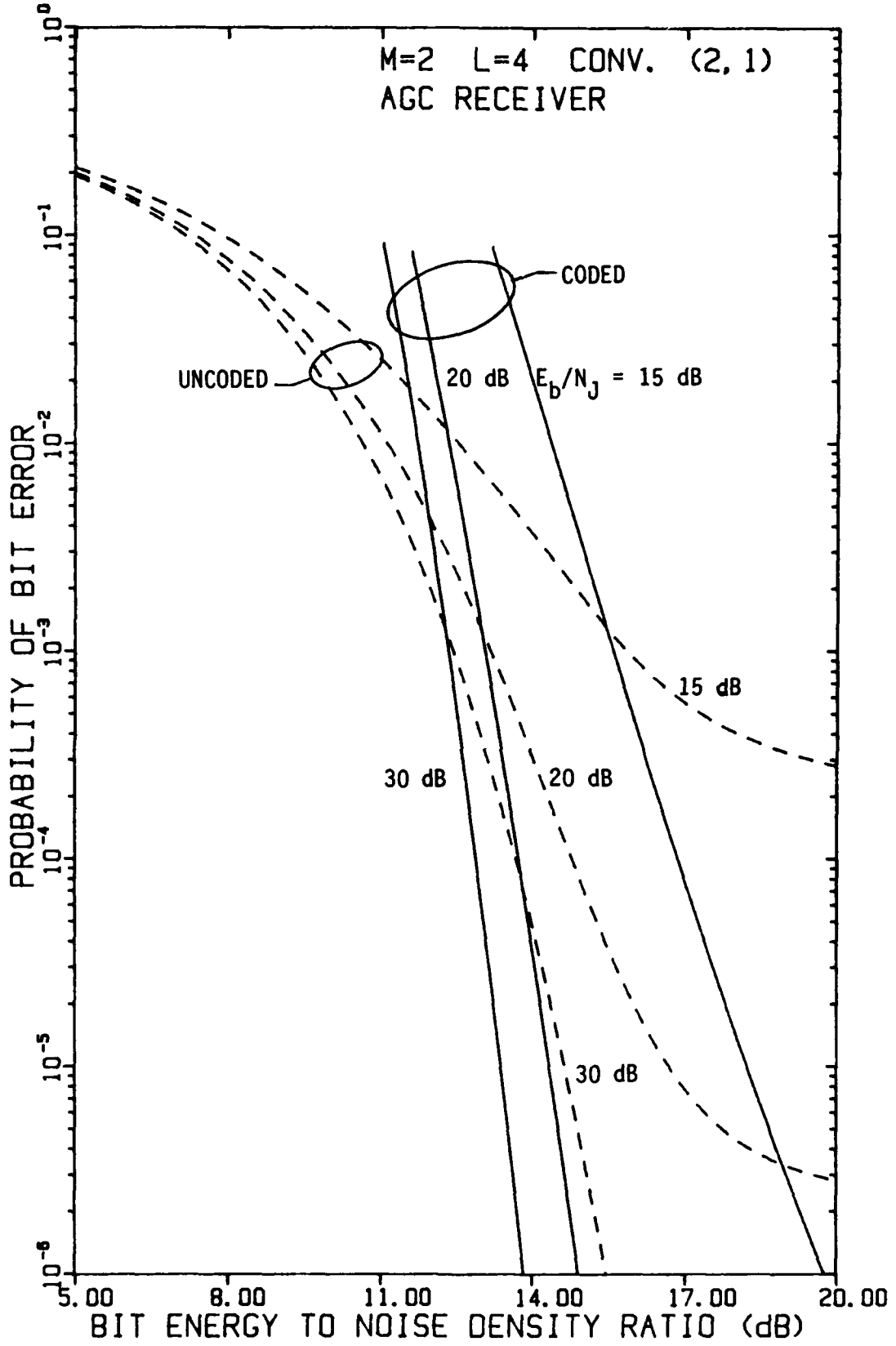

FIGURE 4-97 PERFORMANCE OF FH/BFSK WITH CONVOLUTIONAL RATE-1/2 CODE AND L=4 HOPS/DIGIT AS A FUNCTION OF E_b/N_0 WITH E_b/N_J AS A PARAMETER, USING AN AGC DEMODULATOR, IN OPTIMUM PARTIAL-BAND NOISE JAMMING

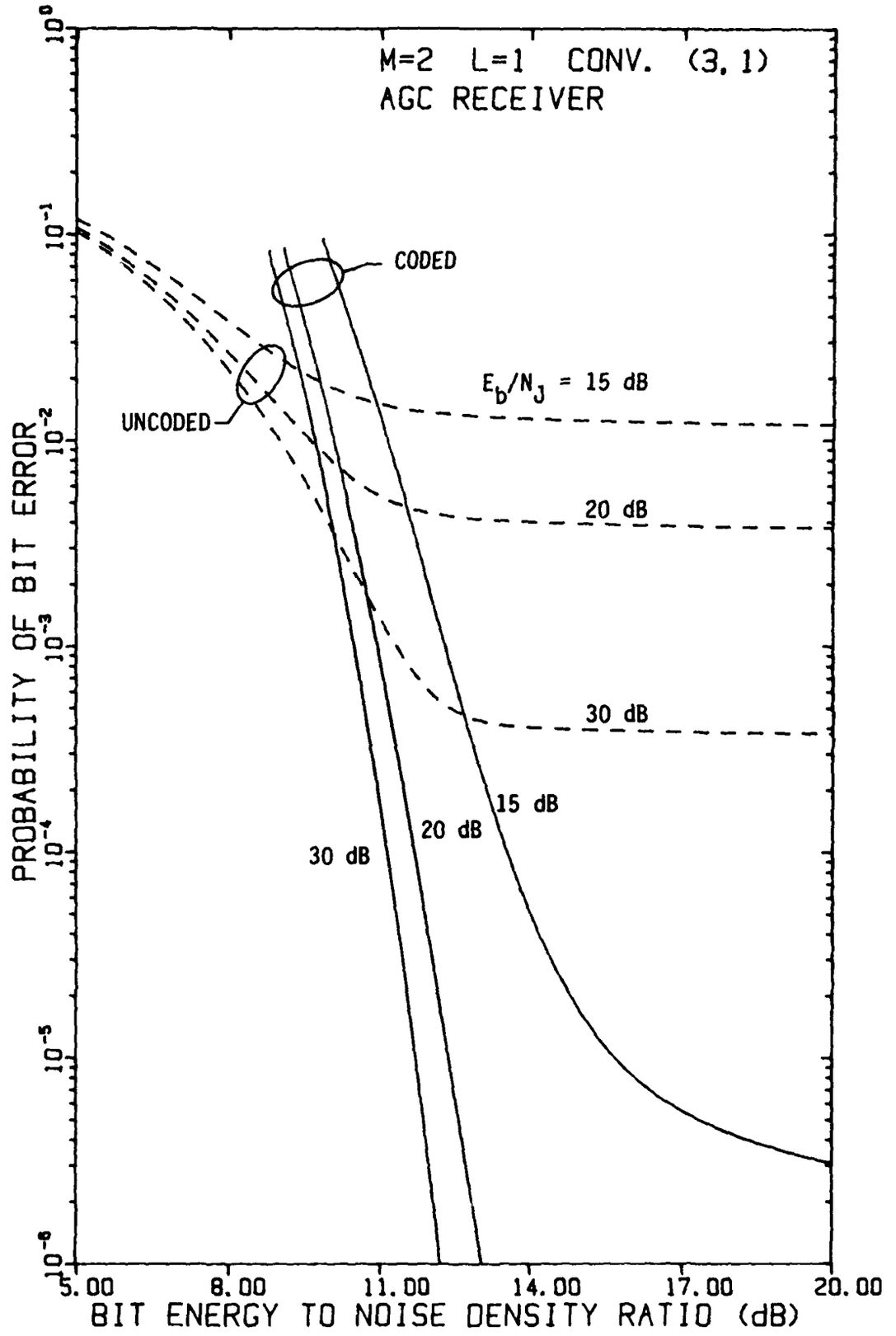

FIGURE 4-98 PERFORMANCE OF FH/BFSK WITH CONVOLUTIONAL RATE-1/3 CODE AND L=1 HOP/DIGIT AS A FUNCTION OF E_b/N_0 WITH E_b/N_J AS A PARAMETER, USING AN AGC DEMODULATOR, IN OPTIMUM PARTIAL-BAND NOISE JAMMING

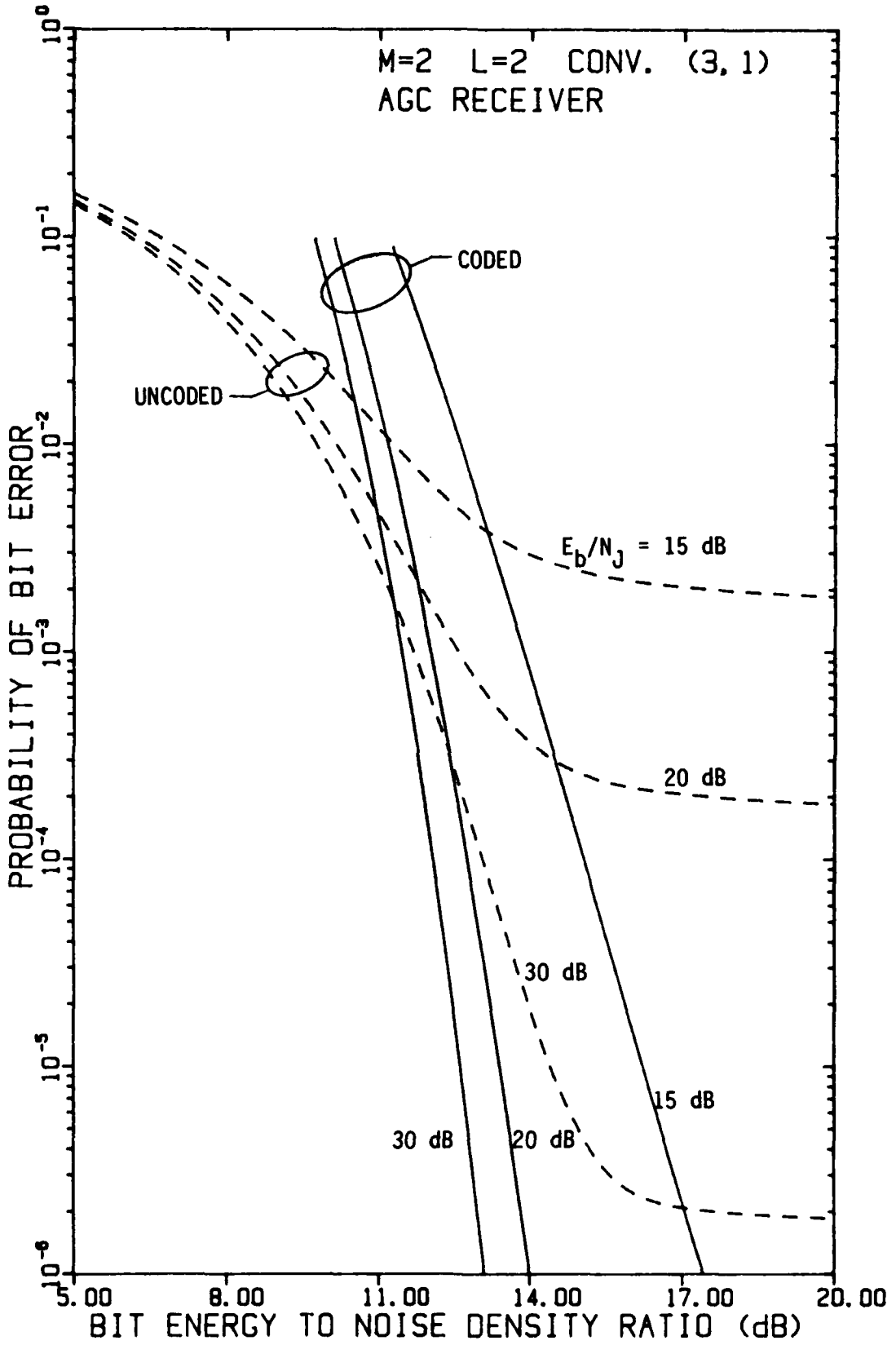

FIGURE 4-99 PERFORMANCE OF FH/BFSK WITH CONVOLUTIONAL RATE-1/3 CODE AND L=2 HOPS/DIGIT AS A FUNCTION OF E_b/N_0 WITH E_b/N_J AS A PARAMETER, USING AN AGC DEMODULATOR, IN OPTIMUM PARTIAL-BAND NOISE JAMMING

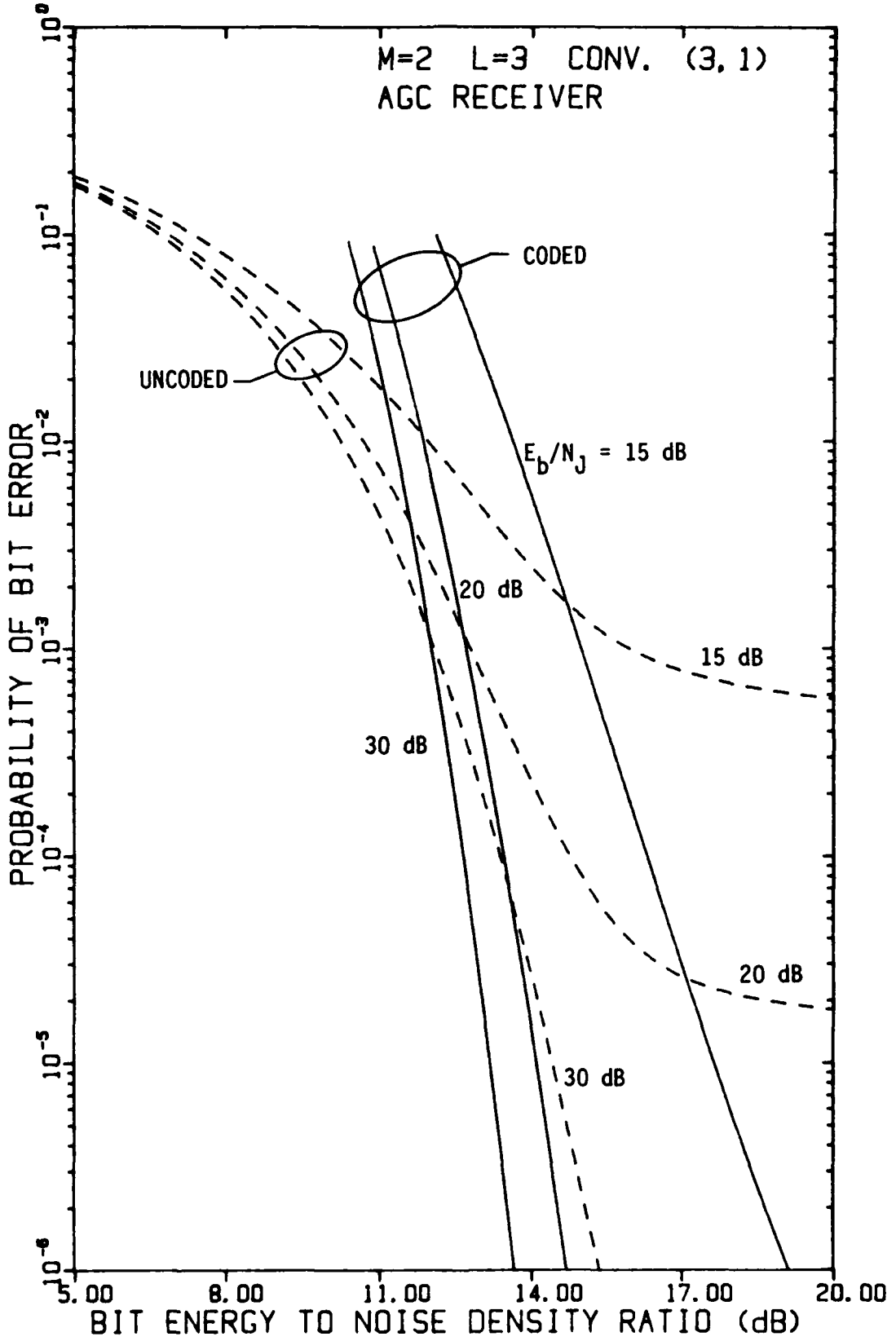

FIGURE 4-100 PERFORMANCE OF FH/BFSK WITH CONVOLUTIONAL RATE-1/3 CODE AND L=3 HOPS/DIGIT AS A FUNCTION OF E_b/N_0 WITH E_b/N_J AS A PARAMETER, USING AN AGC DEMODULATOR, IN OPTIMUM PARTIAL-BAND NOISE JAMMING

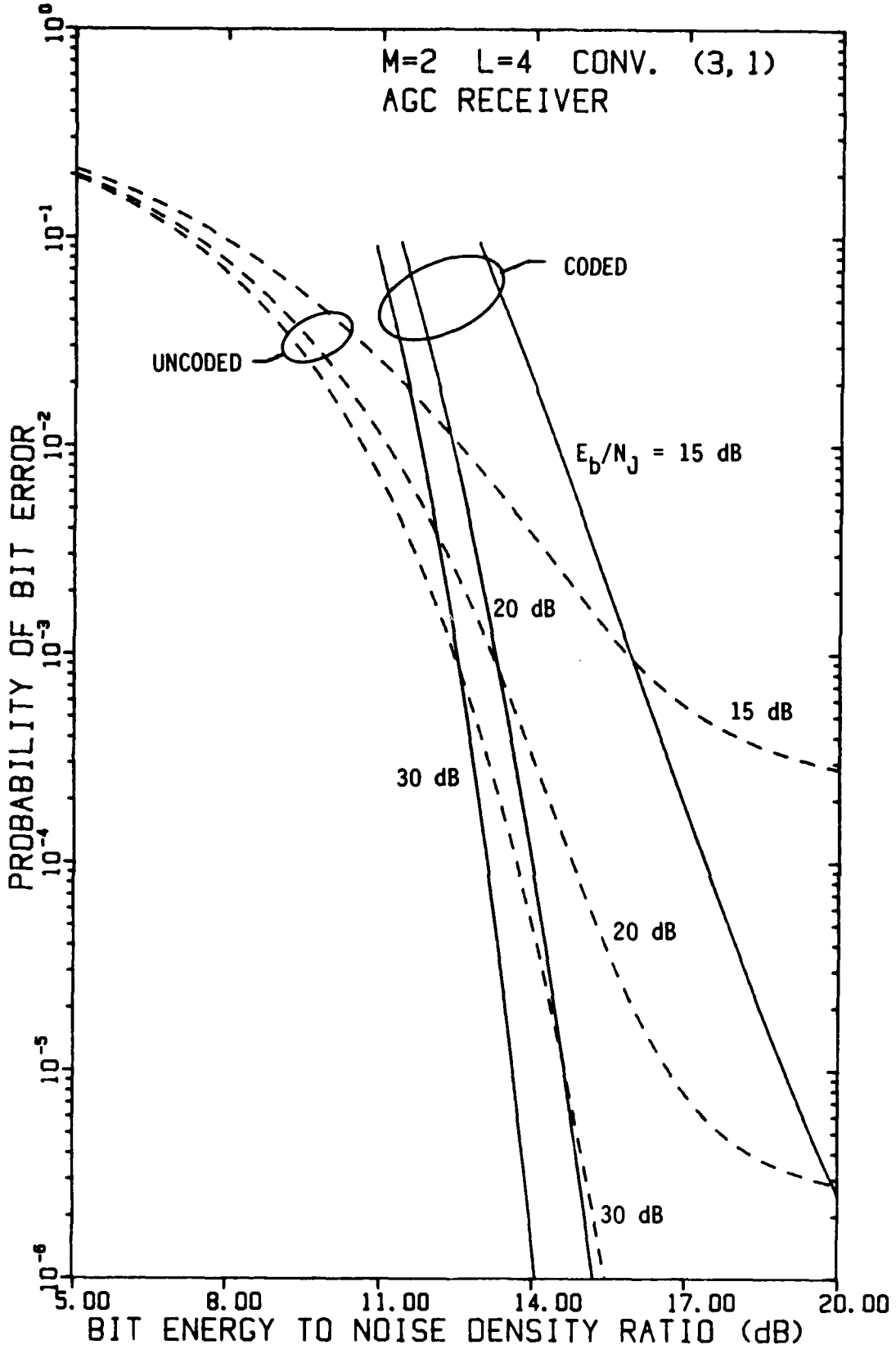

FIGURE 4-101 PERFORMANCE OF FH/BFSK WITH CONVOLUTIONAL RATE-1/3 CODE AND L=4 HOPS/DIGIT AS A FUNCTION OF E_b/N_0 WITH E_b/N_J AS A PARAMETER, USING AN AGC DEMODULATOR, IN OPTIMUM PARTIAL-BAND NOISE JAMMING

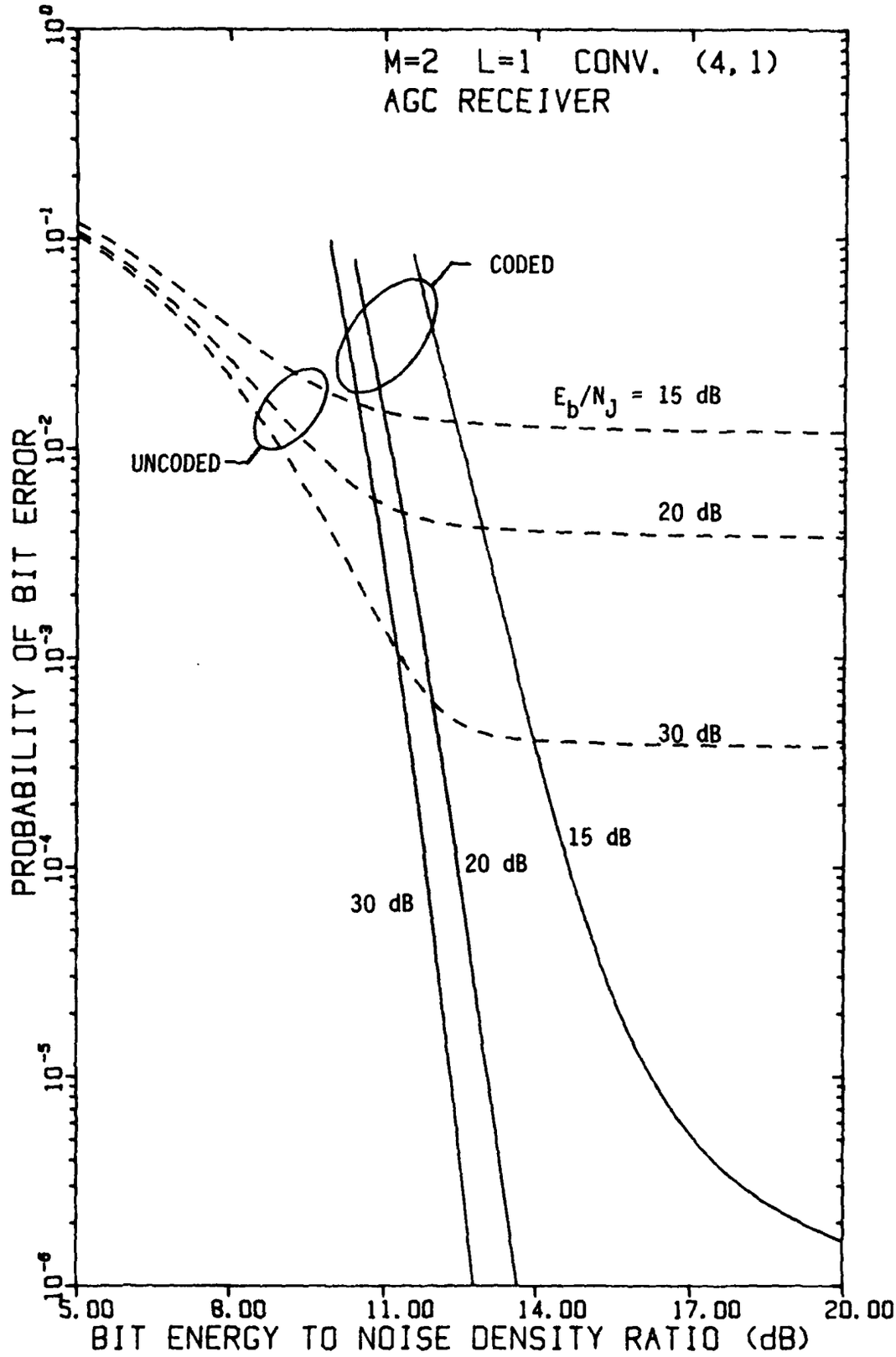

FIGURE 4-102 PERFORMANCE OF FH/BFSK WITH CONVOLUTIONAL RATE-1/4 CODE AND L=1 HOP/DIGIT AS A FUNCTION OF E_b/N_0 WITH E_b/N_J AS A PARAMETER, USING AN AGC DEMODULATOR, IN OPTIMUM PARTIAL-BAND NOISE JAMMING

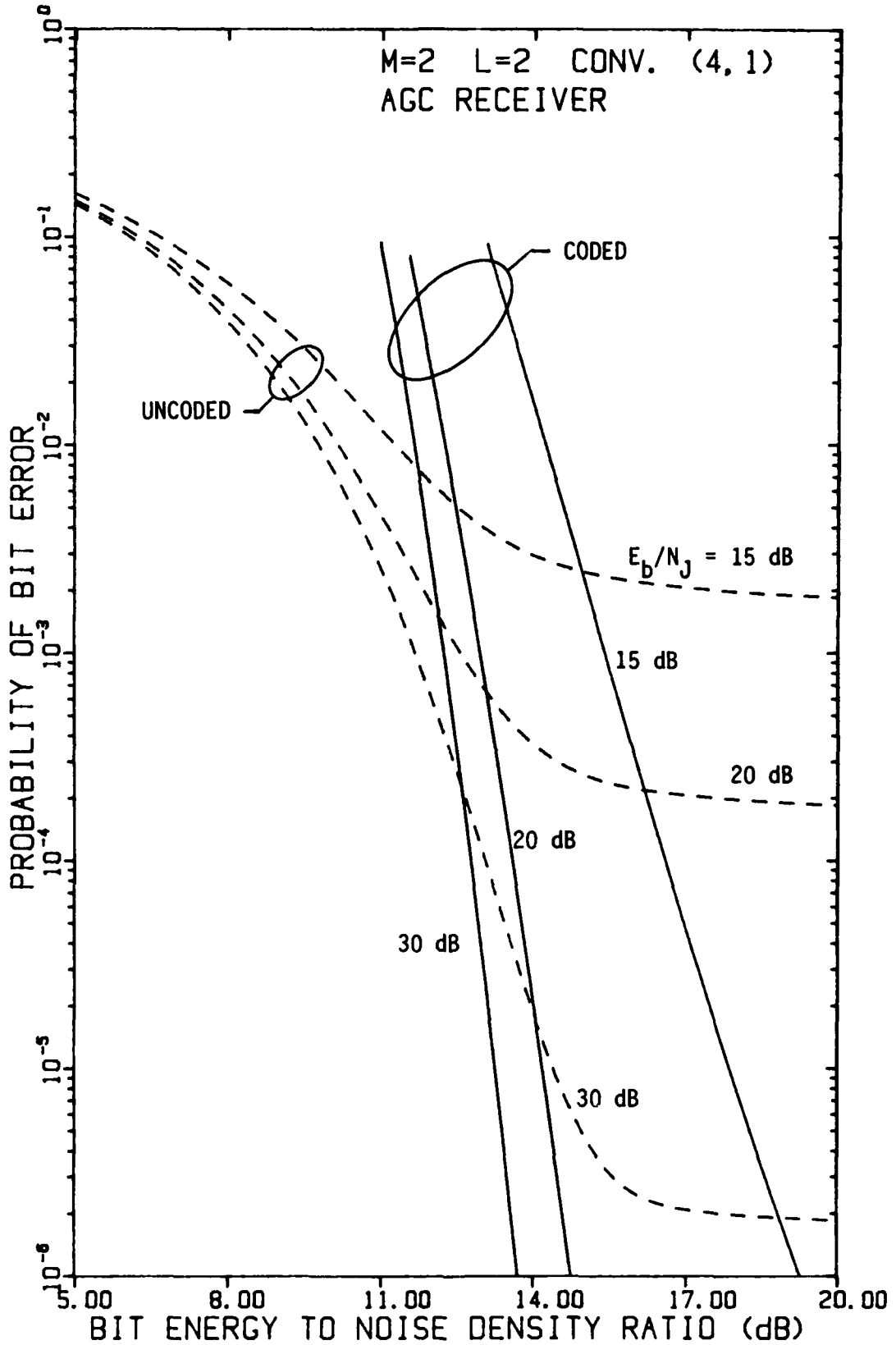

FIGURE 4-103 PERFORMANCE OF FH/BFSK WITH CONVOLUTIONAL RATE-1/4 CODE AND L=2 HOPS/DIGIT AS A FUNCTION OF E_b/N_0 WITH E_b/N_J AS A PARAMETER, USING AN AGC DEMODULATOR, IN OPTIMUM PARTIAL-BAND NOISE JAMMING

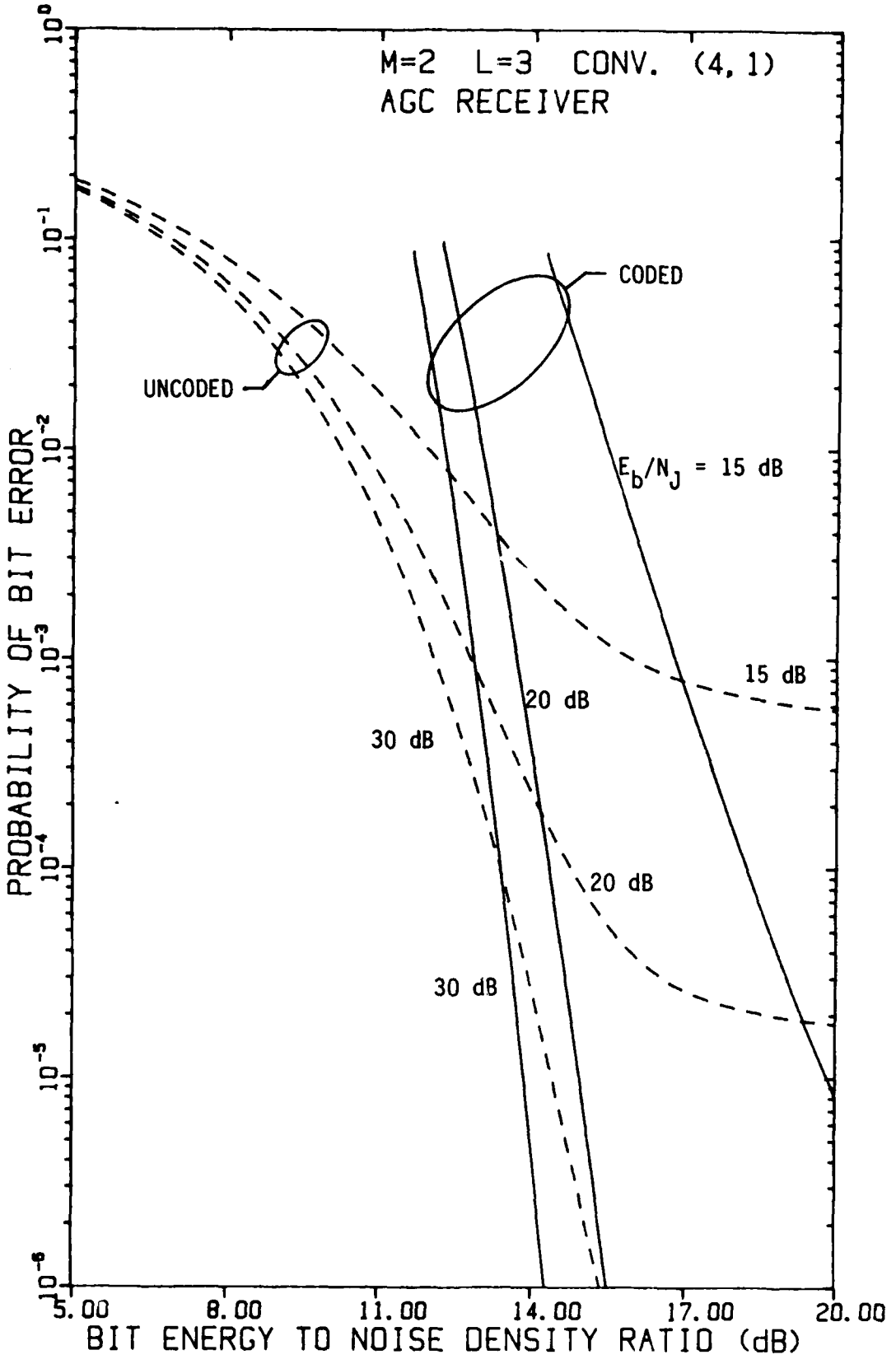

FIGURE 4-104 PERFORMANCE OF FH/BFSK WITH CONVOLUTIONAL RATE-1/4 CODE AND L=3 HOPS/DIGIT AS A FUNCTION OF E_b/N_0 WITH E_b/N_J AS A PARAMETER, USING AN AGC DEMODULATOR, IN OPTIMUM PARTIAL-BAND NOISE JAMMING

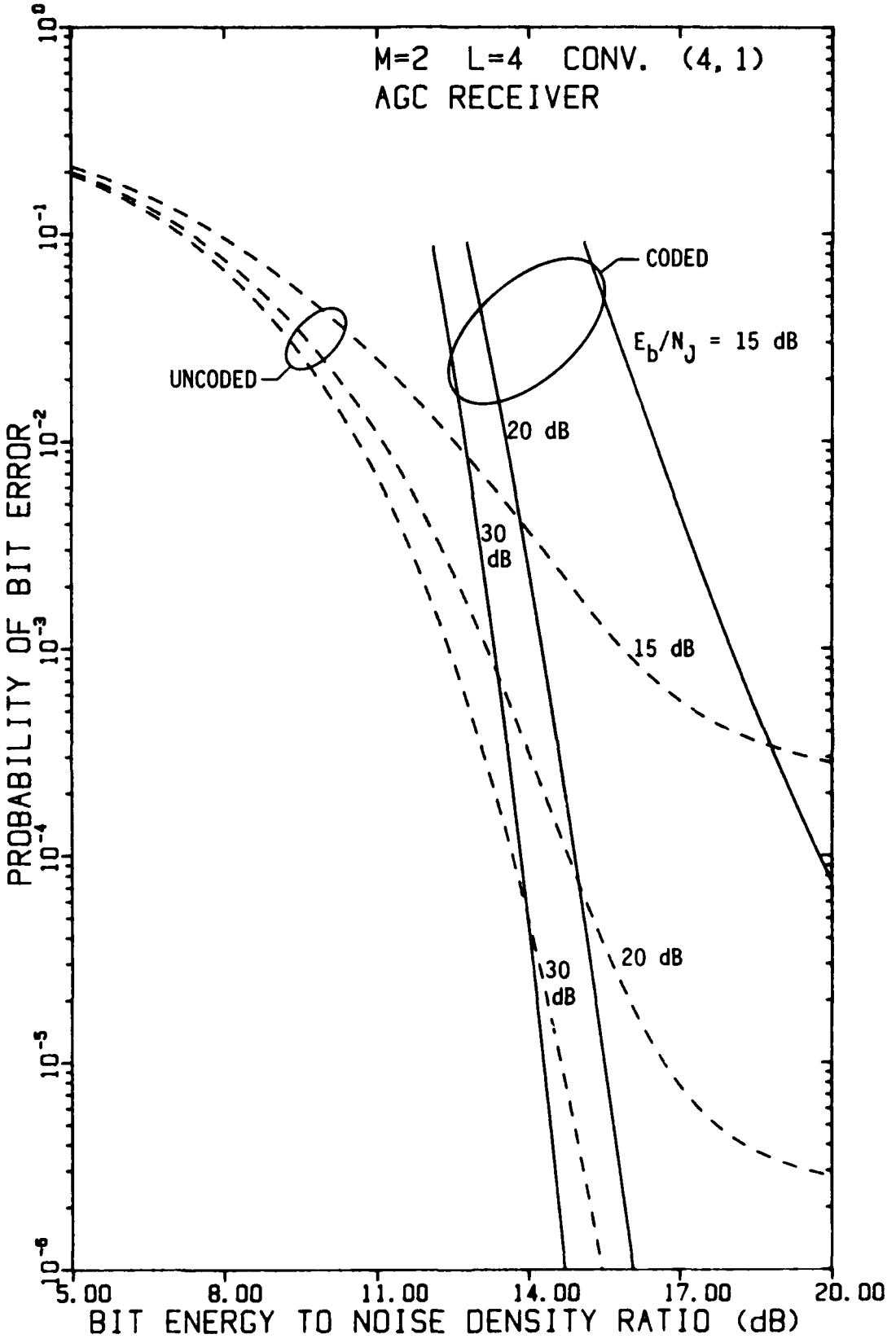

FIGURE 4-105 PERFORMANCE OF FH/BFSK WITH CONVOLUTIONAL RATE-1/4 CODE AND L=4 HOPS/DIGIT AS A FUNCTION OF E_b/N_0 WITH E_b/N_J AS A PARAMETER, USING AN AGC DEMODULATOR, IN OPTIMUM PARTIAL-BAND NOISE JAMMING

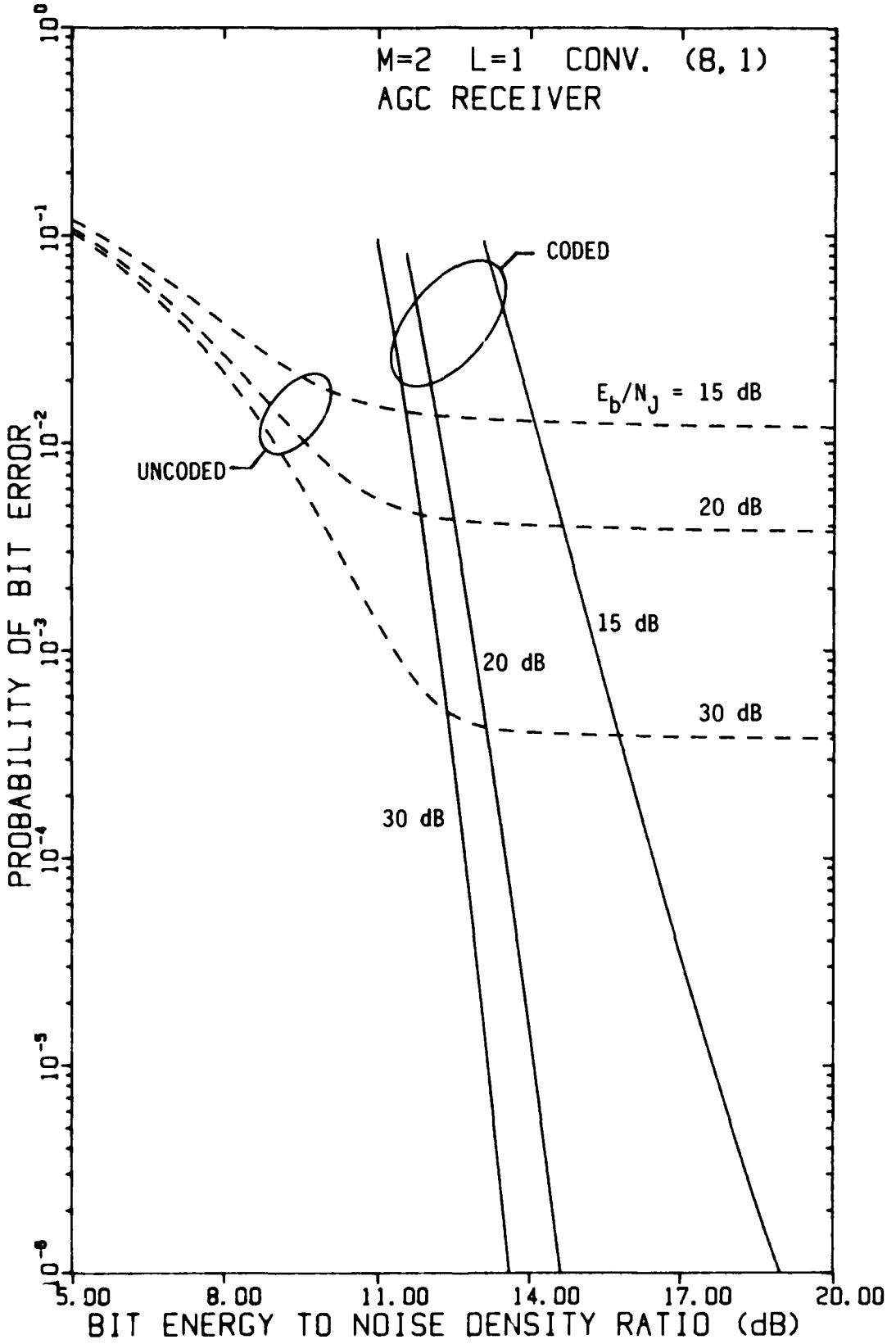

FIGURE 4-106 PERFORMANCE OF FH/BFSK WITH CONVOLUTIONAL RATE-1/8 CODE AND L=1 HOP/DIGIT AS A FUNCTION OF E_b/N_0 WITH E_b/N_J AS A PARAMETER, USING AN AGC DEMODULATOR, IN OPTIMUM PARTIAL-BAND NOISE JAMMING

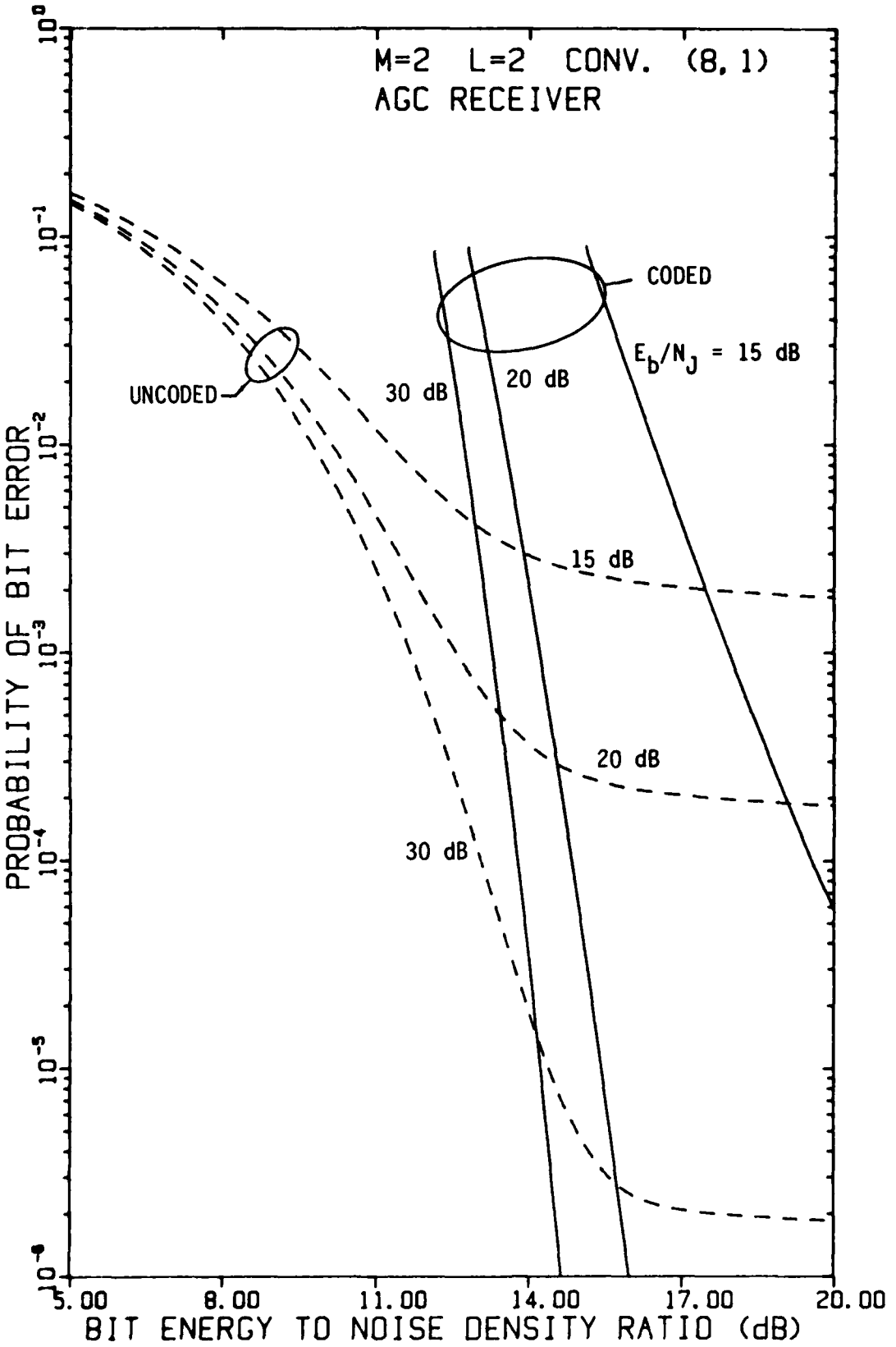

FIGURE 4-107 PERFORMANCE OF FH/BFSK WITH CONVOLUTIONAL RATE-1/8 CODE AND L=2 HOPS/DIGIT AS A FUNCTION OF E_b/N_0 WITH E_b/N_J AS A PARAMETER, USING AN AGC DEMODULATOR, IN OPTIMUM PARTIAL-BAND NOISE JAMMING

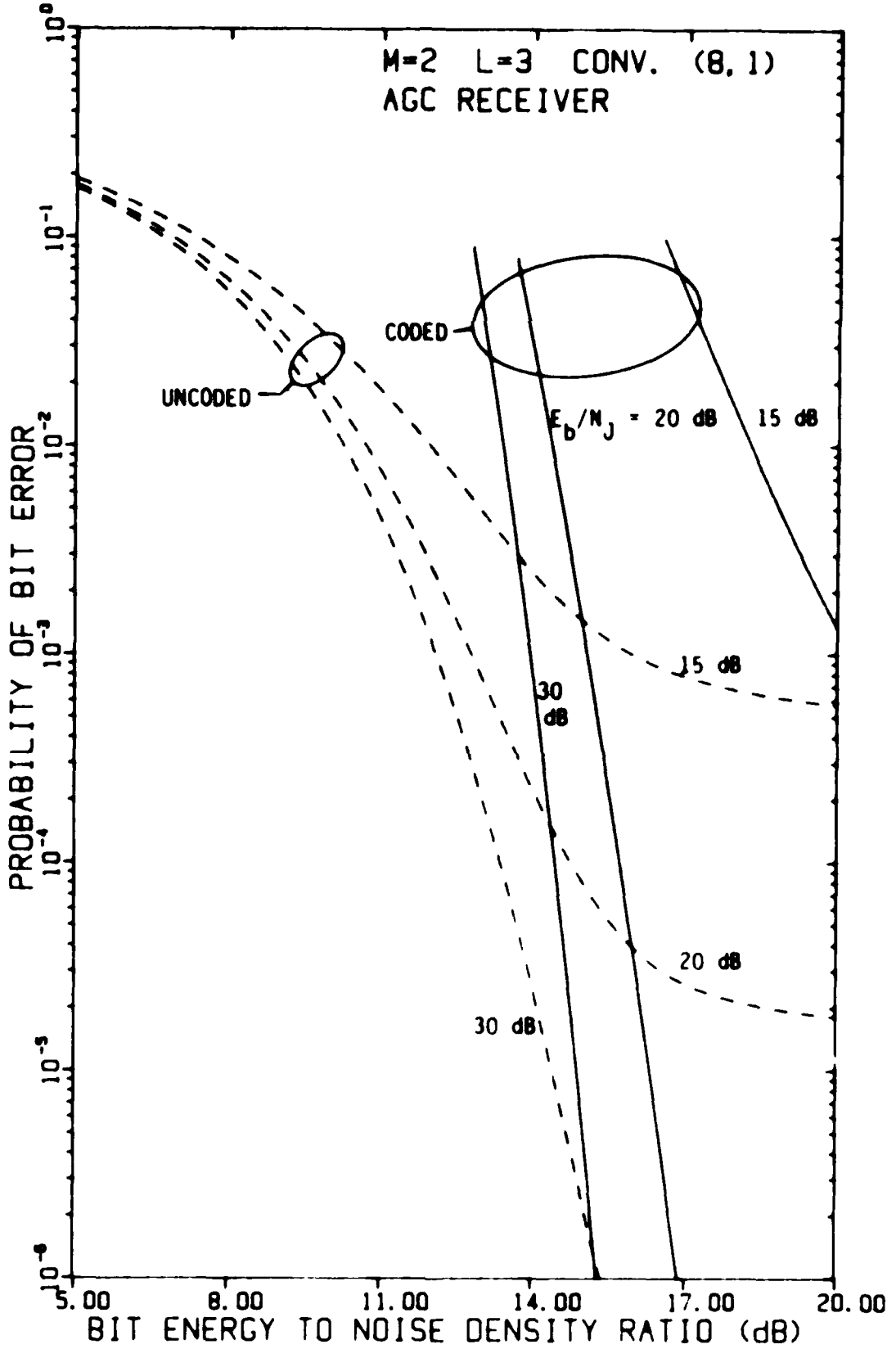

FIGURE 4-108 PERFORMANCE OF FH/BFSK WITH CONVOLUTIONAL RATE-1/8 CODE AND L=3 HOPS/DIGIT AS A FUNCTION OF E_b/N_0 WITH E_b/N_J AS A PARAMETER, USING AN AGC DEMODULATOR, IN OPTIMUM PARTIAL-BAND NOISE JAMMING

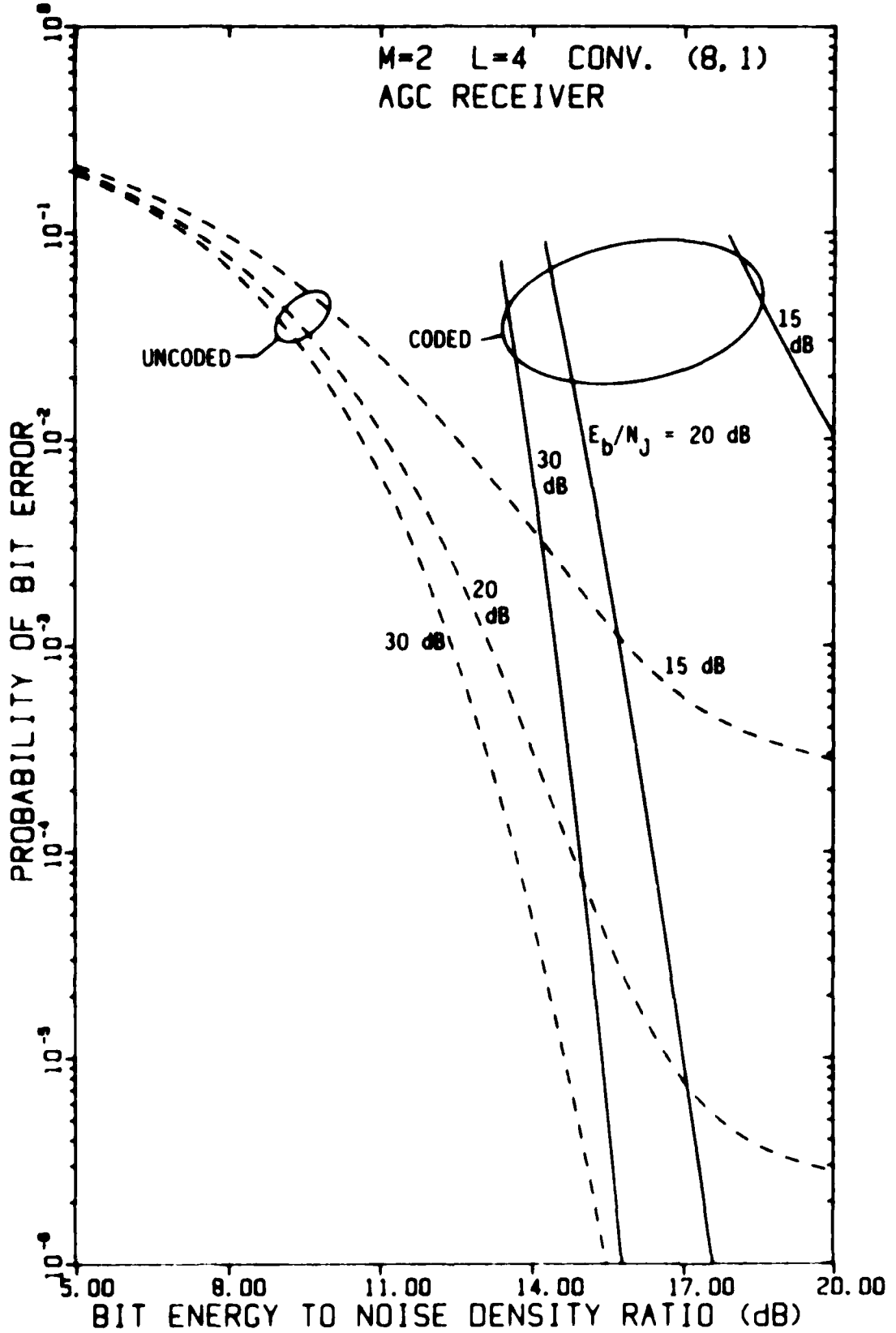

FIGURE 4-109 PERFORMANCE OF FH/BFSK WITH CONVOLUTIONAL RATE-1/8 CODE AND L=4 HOPS/DIGIT AS A FUNCTION OF E_b/N_0 WITH E_b/N_J AS A PARAMETER, USING AN AGC DEMODULATOR, IN OPTIMUM PARTIAL-BAND NOISE JAMMING

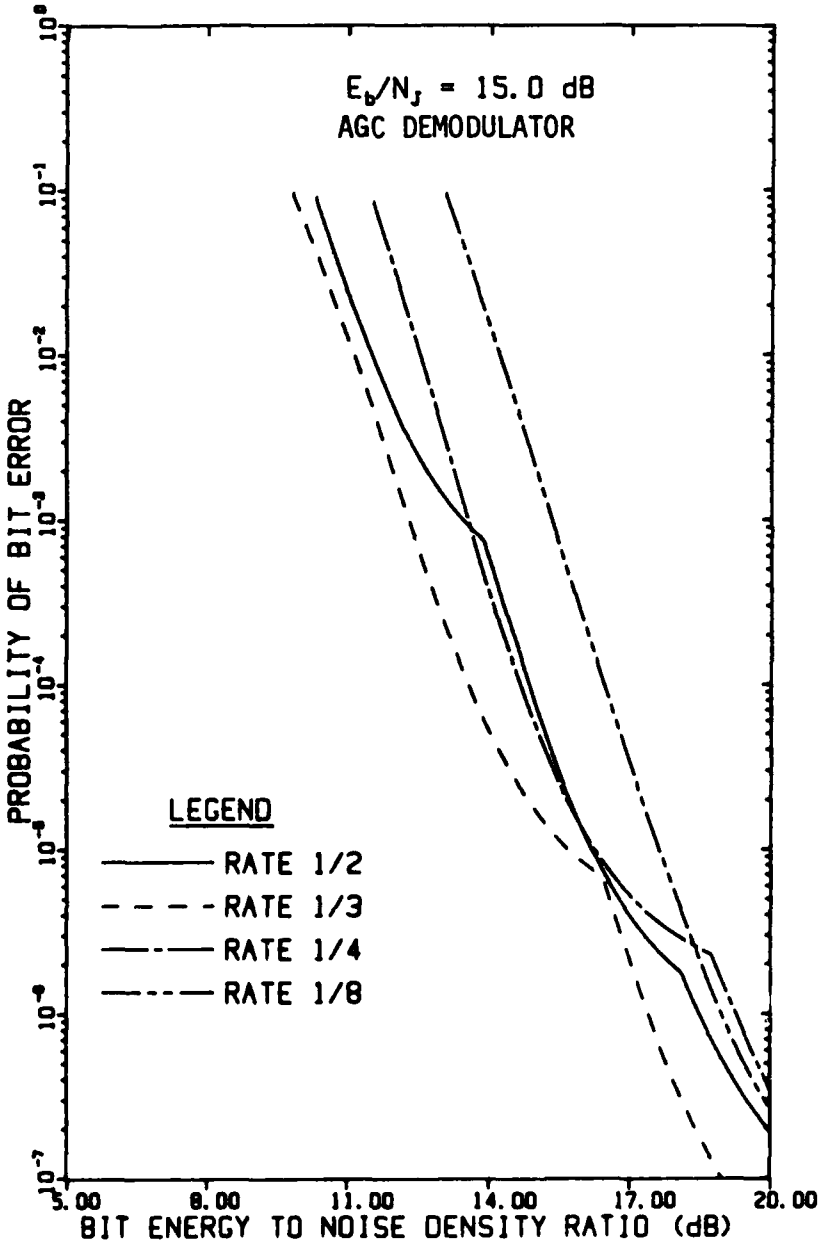

FIGURE 4-110 PERFORMANCE OF CONSTRAINT-LENGTH-7 CONVOLUTIONAL CODES USING OPTIMUM DIVERSITY IN WORST-CASE PARTIAL-BAND NOISE JAMMING AS A FUNCTION OF E_b/N_0 WHEN E_b/N_J = 15 dB

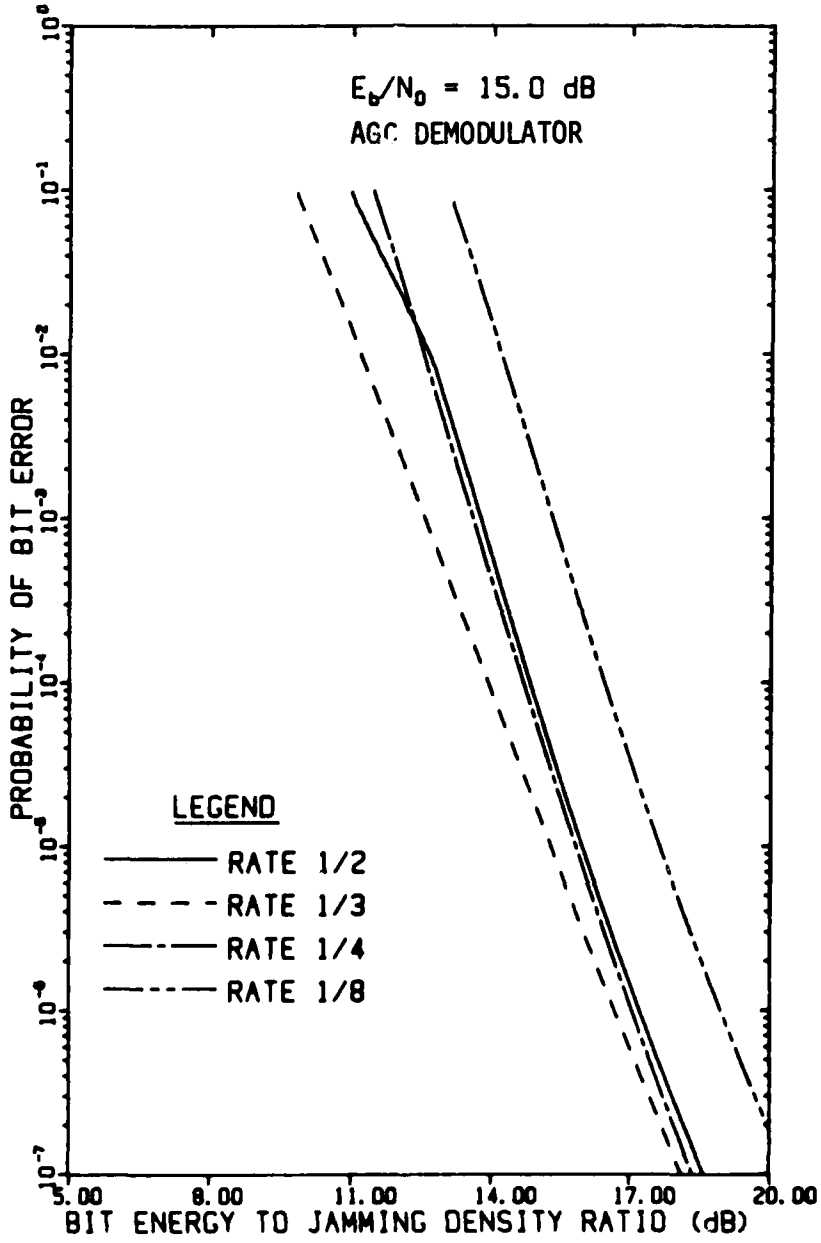

FIGURE 4-111 PERFORMANCE OF CONSTRAINT-LENGTH-7 CONVOLUTIONAL CODES USING FH/BFSK WITH OPTIMUM DIVERSITY IN WORST-CASE PARTIAL-BAND NOISE JAMMING AS A FUNCTION OF E_b/N_J WHEN E_b/N_0 = 15 dB

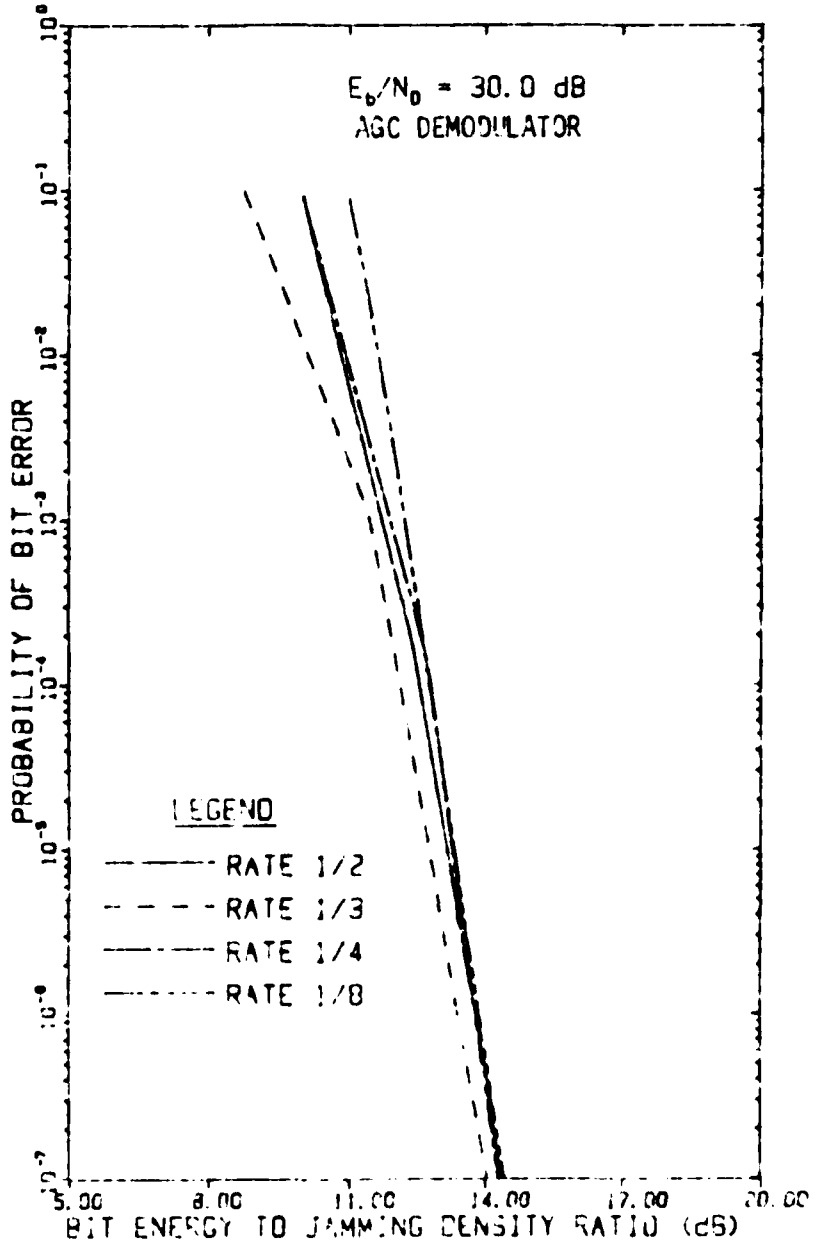

FIGURE 4-112 PERFORMANCE OF CONSTRAINT-LENGTH-7 CONVOLUTIONAL CODES USING FH/BFSK WITH OPTIMUM DIVERSITY IN WORST-CASE PARTIAL-BAND NOISE JAMMING AS A FUNCTION OF E_b/N_J WHEN E_b/N_0 = 30 dB

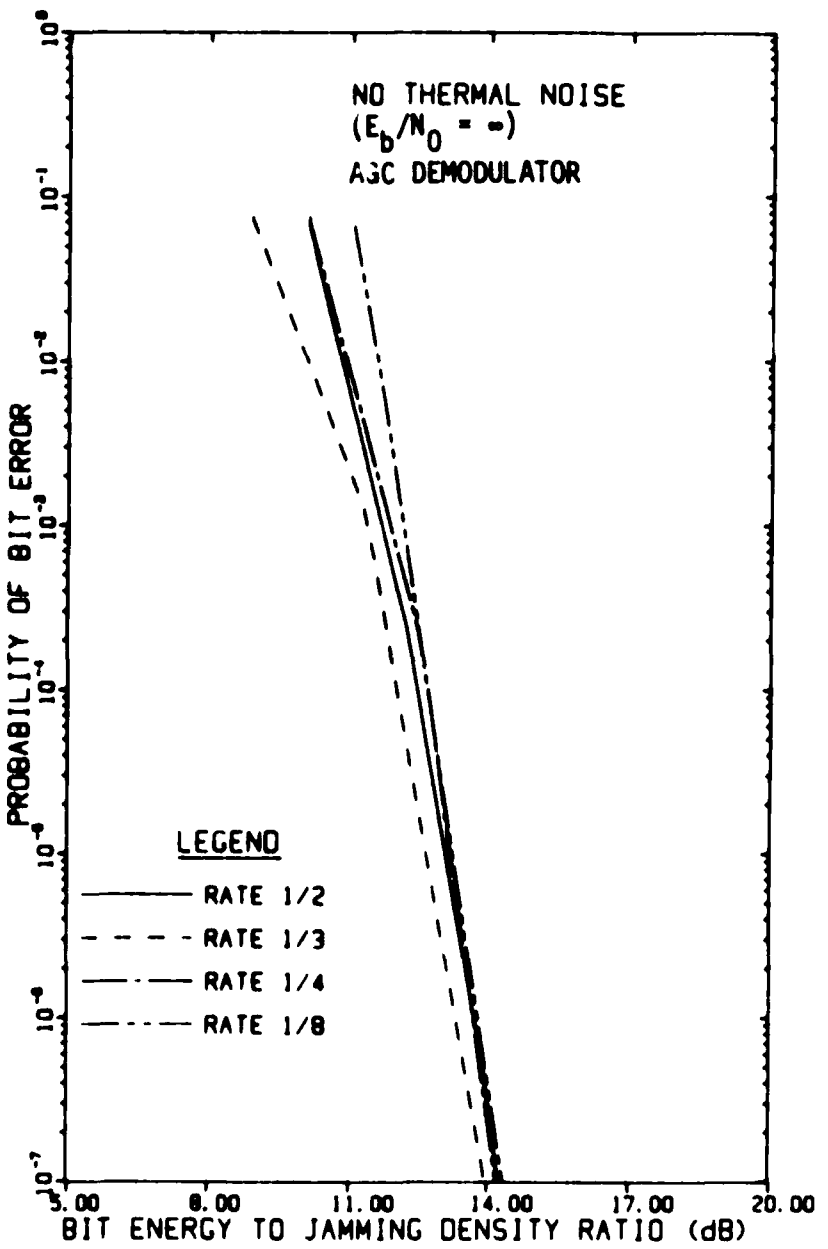

FIGURE 4-113 PERFORMANCE OF CONSTRAINT-LENGTH-7 CONVOLUTIONAL CODES USING FH/BFSK WITH OPTIMUM DIVERSITY IN WORST-CASE PARTIAL-BAND NOISE JAMMING AS A FUNCTION OF E_b/N_J WHEN $E_b/N_0 = \infty$

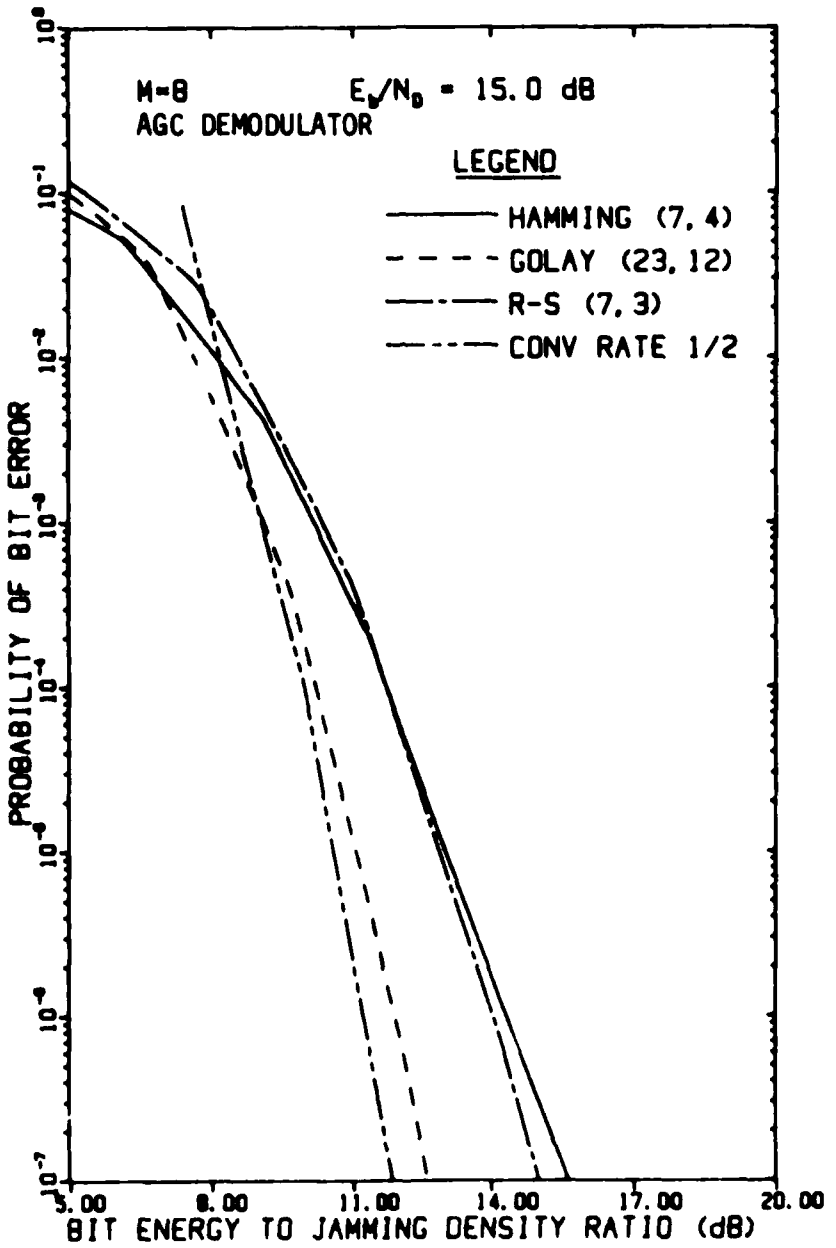

FIGURE 4-114 PERFORMANCE OF SEVERAL CODES WITH FH/8-ARY FSK USING OPTIMUM DIVERSITY IN WORST-CASE PARTIAL-BAND NOISE JAMMING AS A FUNCTION OF E_b/N_J WHEN E_b/N_0 = 15 dB (R-S DENOTES REED-SOLOMON)

5.0 CONCLUSIONS

We have shown the performance of coded L-hop/word FH/MFSK system using optimum diversity in the presence of both worst-case partial-band noise jamming and thermal noise, using both a linear combining demodulator and the nonlinear-combining technique of the adaptive gain control demodulator. Comparisons have been made on the basis of equal energy transmitted per information bit. This implicitly allows the hopping rate R_h to vary as L changes if the bit rate and transmitter power are assumed to be fixed. Furthermore, since the jamming fraction γ is assumed to be continuously variable and not subject to any minimum value, we must assume that the total hopping bandwidth is much greater than the bandwidth of a single hop.

Since the coding parameters are influenced by E_b/N_0 and E_b/N_J, it is very difficult, if not impossible, to evaluate alternative coding schemes by simply scaling performance curves for an uncoded system (unless a very large library of parametric curves should happen to be available). Instead, the analysis must be performed for the entire system of modulation and coding considered as a complete system. We have examined a selection of several codes to illustate the typical analyses which must be conducted in selecting a code for any given application. However, we have made no attempt to pick any one "best" code; such a choice must be made by the system designer who must take into account not only the performance analyses of this report, but also other factors beyond the scope of this effort, such as circuit complexity, size, weight, cost, etc.

The conclusions we draw from this study are as follows:

- The combination of a nonlinear combining technique, M-ary modulation, and forward error control coding is seen to be very effective against worst-case partial-band noise jamming, provided that the code rate is not too low.
- The need for exact analyses including the influence of thermal noise has been shown, particularly with regard to selection of optimum diversity and worst-case jamming fraction.
- For values of E_b/N_0 which are realistic in tactical scenarios, the use of results from a no-thermal-noise analysis may well lead to erroneous choices of system parameters both by the communicator and by the jammer.

REFERENCES

[1] S.W. Houston, "Modulation techniques for communication--Part I: Tone and noise jamming performance of spread-spectrum M-ary FSK, and 2, 4-ary DPSK waveforms," in Proc. IEEE Nat. Aerosp. Electron. Conf., June 10-12, 1975, pp. 51-58.

[2] A.J. Viterbi and I.M. Jacobs, "Advances in coding and modulation for noncoherent channels affected by fading, partial band, and multiple access interference," in Advances in Communication Systems, vol. 4, A.J. Viterbi, Ed. New York: Academic Press, 1975, pp. 279-308.

[3] J.S. Lee and L.E. Miller, "Error performance analyses of differential phase-shift keyed/frequency hopping spread-spectrum communication system in the partial-band jamming environments," IEEE Trans. Commun., vol. COM-30, pp. 943-952, May 1982.

[4] J.S. Lee, R.H. French, and L.E. Miller, "Probability of error analyses of a BFSK frequency-hopping system with diversity under partial-band jamming interference--Part I: Performance of square-law linear combining soft decision receiver," IEEE Trans. Commun., vol. COM-32, pp. 645-653, June 1984.

[5] J.S. Lee, L.E. Miller, and Y.K. Kim, "Probability of error analyses of a BFSK frequency-hopping system with diversity under partial-band jamming interference--Part II: Performance of square-law nonlinear combining soft decision receivers," IEEE Trans. Commun., vol. COM-32, pp. 1243-1250, Dec. 1984.

[6] L.E. Miller, J.S. Lee, and A.P. Kadrichu, "Probability of error analyses of a BFSK frequency-hopping system with diversity under partial-band jamming interference-- rt III: Performance of a square-law self-normalizing soft decision receiver," IEEE Trans. Commun., vol. COM-34, pp. 669-675, July 1986.

[7] J.S. Lee, L.E. Miller, and R.H. French, "The analyses of uncoded performances for certain ECCM receiver design strategies for multihops/symbol FH/MFSK waveforms," IEEE Journal on Selected Areas in Communications, vol. SAC-3, pp. 611-621, Sept. 1985.

[8] G.K. Huth, "Optimization of coded spread spectrum system performance," IEEE Trans. Commun., vol. COM-25, pp. 763-770, Aug. 1977.

[9] B.K. Levitt and J.K. Omura, "Coding tradeoffs for improved performance of FH/MFSK systems in partial band noise," in Nat. Telecommun. Conf. Rec., Nov. 1981, pp. D9.1.1-D9.1.5.

[10] J.K. Omura and B.K. Levitt, "Coded error probability evaluation for antijam communications systems," IEEE Trans. Commun., vol. COM-30, pp. 896-903, May 1982.

[11] H.H. Ma and M.A. Poole, "Error-correcting codes against the worst-case partial-band jammer," IEEE Trans. Commun., vol. COM-32, pp. 124-133, Feb. 1984.

[12] D.J. Torrieri, "Frequency-hopping with multiple frequency-shift-keying and hard decisions," IEEE Trans. Commun., vol. COM-32, pp. 574-582, May 1984.

[13] J.S. Bird and E.B. Felstead, "Antijam performance of fast frequency-hopped M-ary NCFSK--An overview," IEEE Journal on Selected Areas in Communications, vol. SAC-4, pp. 216-233, March 1986.

[14] D.J. Torrieri, "The information-bit error rate for block codes," IEEE Trans. Commun., vol. COM-32, pp. 474-476, April 1984.

[15] J.P. Odenwalder, "Optimal Decoding of Convolutional Codes," Ph.D. dissertation, University of California, Los Angeles, 1970 (University Microfilms no. 70-19,875).

[16] V.K. Bhargava, D. Haccoun, R. Matyas, and P.P. Nuspl, Digital Communications by Satellite. New York: Wiley, 1981.

[17] J.J. Spilker, Jr., Digital Communications by Satellite. Englewood Cliffs, N.J.: Prentice-Hall, 1977.

[18] A.J. Viterbi and J.K. Omura, Principles of Digital Communication and Coding. New York: McGraw-Hill, 1979.

[19] W.E. Stark, "Coding for frequency-hopped spread-spectrum communications with partial-band interference - Part II: Coded performance," IEEE Trans. Commun., vol. COM-33, pp. 1045-1057, Oct. 1985.

[20] J.S. Lee, L.E.Miller, R.H. French, Y.K. Kim, and A.P. Kadrichu, "The optimum jamming effects on frequency-hopping M-ary FSK systems under certain ECCM receiver design strategies," J.S. Lee Associates, Inc., final report on contract N00014-83-C-0312, Oct. 1984 (AD-A147766).

[21] W.W. Peterson and E.J. Weldon, Jr., Error-Correcting Codes, Second Ed. Cambridge, Mass.: MIT Press, 1972.

[22] S. Lin, An Introduction to Error-Correcting Codes. Englewood Cliffs, N.J.: Prentice-Hall, 1970.

[23] J. Conan, "The weight spectra of some short low-rate convolutional codes," IEEE Trans. Commun., vol. COM-32, pp. 1050-1053, Sept. 1984; see also correction in vol. COM-33, p. 570, June 1985.

[24] M. Abramowitz and I. A. Stegun (eds.), Handbook of Mathematical Functions, National Bureau of Standards Applied Mathematics Series 55. Washington, D.C.: Government Printing Office, June 1964, Ninth printing, November 1970.